Gut-Liver Axis on Biotransformation of Environmental Chemicals Polybrominated Diphenyl Ethers (PBDEs)

Yanfei Li

A dissertation
submitted in partial fulfillment of the
requirements for the degree of

Doctor of Philosophy

University of Washington
2018

Reading Committee:
Julia Yue Cui, Chair
Dave L. Eaton
Terrance J. Kavanagh

Program Authorized to Offer Degree:
Department of Environmental and Occupational Health Sciences
School of Public Health

University of Washington

Abstract

Understanding the Role of Gut-Liver Axis on Biotransformation of Environmental Chemicals Polybrominated Diphenyl Ethers (PBDEs)

Yanfei Li

Chair of Supervisory Committee:
Dr. Julia Yue Cui
Department of Environmental and Occupational Health Sciences

Polybrominated diphenyl ethers (PBDEs) are flame retardants that are widely used in plastics, rubbers, textiles, furniture and electronic devices. Worrisome levels of PBDEs have been detected in fatty food, household dust, human blood and breast milk due to their lipophilic and bio-accumulative features. Animal studies, with limited supporting human epidemiology data, have found associations between PBDE exposure and multiple detrimental effects including neurotoxicity, thyroid hormone disorders, and hepatotoxicity such as oxidative stress and cancer. In liver, which is the major organ for xenobiotic biotransformation and nutrient homeostasis, certain PBDE congeners are oxidized by cytochrome P450s (Cyps) to form more toxic metabolites. The gut microbiome has been increasingly recognized as a novel frontier for xenobiotic metabolism, and previous work from our laboratory has demonstrated that lack of a gut microbiome profoundly altered the expression of xenobiotic-processing genes (XPGs) in the liver. However, very little is known regarding the interactions between PBDEs and the gut microbiome, and how such interactions modify the hepatic xenobiotic

biotransformation and intermediary metabolism pathways. Therefore, the goal of my dissertation is to utilize multidisciplinary approaches, including germ-free mice, second generation sequencing (RNA-Seq and microbial 16S rRNA sequencing), targeted proteomics (LC-MS), targeted metabolomics (GC-MS for PBDE phenolics and UPLC-MS/MS for bile acids), as well as bioinformatics, to strategically investigate the effect of PBDEs on the gut microbiome *in vivo*, and further determine how the gut microbiome modulates PBDE-mediated regulation of the hepatic transcriptome and the biotransformation and disposition of PBDEs. To achieve this goal, I exposed nine-week-old male C57BL/6 conventional (CV) and germ-free (GF) mice with vehicle (corn oil, p.o. 10 ml/kg) and the most predominant PBDE congeners, BDE-47 or BDE-99 (100 μmol/kg, p.o.), for four consecutive days. Gut microbiomes were quantified using 16S rRNA sequencing of the large intestinal content (LIC) of CV mice. Both BDE-47 and BDE-99 profoundly decreased the bacterial richness (i.e. α diversity). PBDEs differentially regulated 45 bacterial species, especially an up-regulation of *Akkermansia muciniphila* and *Erysipelotrichacea allobaculum,* which are known to have anti-inflammatory and anti-obesity properties. In livers of GF mice, the major BDE-47 hydroxylated metabolite, 5-OH-BDE-47, was higher as compared to livers of CV mice; whereas 4 minor BDE-47 metabolites and 4 minor BDE-99 metabolites were lower. RNA-Seq of the hepatic transcriptome in CV and GF mice showed that the interactions between gut microbiome and PBDEs not only regulated the protein-coding genes (PCGs), but also long non-coding RNAs (lncRNAs), which are increasingly recognized as novel biomarkers for toxicological responses. The absence of gut microbiome sensitized the liver to BDE-99-mediated transcriptional regulation of both PCGs and

lncRNAs in GF mice. Besides xenobiotic metabolism, the gut microbiome is also important for endogenous functions such as bile acid (BA) homeostasis, which regulates nutrient absorption, and may contribute to obesity, inflammation, and cancer. Targeted metabolomics of 56 BAs in serum, liver, small intestinal content (SIC) and LIC of CV and GF mice showed that PBDEs, especially BDE-99, markedly increased many unconjugated BAs in multiple bio-compartments in a gut microbiota-dependent manner. Therefore, these BAs may serve as secondary signaling molecules to relay toxicological response following PBDE exposure. Taken together, the present study revealed for the first time that there is a novel interaction between the gut microbiome and PBDEs, and this markedly impacts both xenobiotic biotransformation and intermediary metabolism pathways in the host liver. Targeting the "gut-liver axis" may lead to the design of novel probiotic therapies to reduce the toxicities of PBDEs in vulnerable populations.

Table of Contents

List of Figures

List of Tables

List of Abbreviations

Isg15	Interferon-stimulated gene 15
Olfr1033	Olfactory receptor 1033
BDE-47	2, 2', 4, 4'-tetrabromodiphenyl ether
BDE-99	2, 2', 4, 4',5-pentabromodiphenyl ether
Hmgcs1	3-hydroxymethylglutaryl-CoA synthase
PAPS	5'- phosphoadenosine-5'-phosphosulfate
Acsl	Acyl-CoA synthetase
Acot	Acyl-CoA thioesterase
ALT	Alanine aminotransferase
Aox1	Aldehyde oxidase 1
Akr	Aldo-keto reductase
Atrx	Alpha thalassemia/metntal retardation syndrome X-linked homolog
A1bg	Alpha-1-B glycoprotein
αMCA	Alpha-muricholic acid
Alas1	Aminolevulinic acid synthase 1
Asbt	Apical sodium bile acid transporter
AhR	Aryl hydrocarbon receptor
Arid4b	AT-rich interaction domain 4B
Abc	ATP-binding cassette
Bcl6	B cell leukemia/lymphoma 6
BA	Bile acid
Baat	Bile acid CoA: animo acid N-acyltransferase
Bal	Bile acid-CoA ligase
Bsep	Bile salt export pump
Bshs	Bile salt hydrolases
BAM	Binary alignment/map
BSA	Bovine serum albumin
Ccl5	C-C motif chemokine ligand 5
Camk2b	Calcium/calmodulin dependent protein kinase II beta
Caln1	Calneuron 1 or calcium-binding protein
Cel	Carboxyl ester lipase
Ces4a	Carboxylesterase 4A
Cpa	Carboxypeptidase
CDCA	Chenodeoxycholic acid
Clic3	Chloride intracellular channel 3
CA	Cholic acid
Chka	Choline kinase alpha
Ctrb1	Chymotrypsinogen B1

Ciart	Circadian associated repressor of transcription
Ccdc141	Coiled-coil domain containing 141
Col5a1	Collagen type V alpha 1 chain
cDNA	Complementary DNA
CAR	constitutive androstane receptor
CV	Conventional
CO	Corn oil
Cdkn1a	Cyclin-dependent kinase inhibitor 1A
Crip2	Cysteine-rich intestinal protein 2
Cyps	Cytochrome P450s
Dbp	D site albumin promoter binding protein
Dct	Dopachrome tautomerase
DPGs	Drug-processing Genes
Elovl	Elongation of very long chain fatty acids
Epha2	Ephrin type-A receptor A2
Egfr	Epidermal growth factor receptor
Errfl1	ERBB receptor feedback inhibitor 1
EROD	Ethoxyresorufin-O-deethylase
Eif4ebp3	Eukaryotic translation initiation factor 4E binding protein 3
FDR	False discovery rate adjusted
Fam222a	Family with sequence similarity genes
FXR	Farnesoid-X-receptor
Fgf	Fibroblast growth factor
Fgfr	Fibroblast growth factor receptor
Flywch2	FLYWCH family member 2
Fpgs	Folylpolyglutamyl synthetase
Foxa2	Forkhead box A2
FPKM	Fragments per kilobase of transcript per million mapped reads
GCMS	Gas chromatography mass spectroscopy
Gmds	GDP-mannose 4,6-dehydratase
GF	Germ-free
Got1	Glutamic-oxaloacetic transaminase 1
Gst	Glutathione S-transferases
Gclc	Glutathione-cysteine ligase
Gadd45g	Growth arrest and DNA damage 45g
Gbp2	Guanylate binding protein 2
Guca1a	Guanylate cyclase activator 1A
H&E	Haemotoxylin & Eosin
Hes1	Hairy and enhancer of split-1
Hsp90aa1	Heat shock protein 90 alpha family class A member 1

Hmox1	Heme oxygenase 1
Hbb-bt	Hemoglobin, beta adult t chain
HISAT	Hierarchical Indexing for Spliced Alignment of Transcripts
HDL	High-density lipoprotein
H2-Ab1	Histocompatibility 2, class II antigen A, beta 1
Hdac5	Histone deacetylase 5
OH-BDEs	Hydroxylated metabolites
Hcn3	Hyperpolarization-activated cyclic nucleotide-gated channel
Igip	IgA inducing protein
IPA	Indole-3-propionate acid
IPA	Ingenuity Pathway Analysis
Id3	Inhibitor of DNA biding 3
IACUC	Institutional Animal Care and Use Committee
Cib3	Integrin binding protein 3
Ifi27l2b	Interferon alpha-inducible protein 27 like 2B
LIC	Large intestinal content
Lgals4	Lectin, galactoside-binding soluble 4
Lect1	Leukocyte cell derived chemotaxin 1
Leng8	Leukocyte receptor cluster member 8
Lcn2	Lipocalin 2
LCA	Lithocholic acid
LncRNAs	Long non-coding RNAs
LOAEL	Lowest-observed-adverse-effect level
Lypd8	Ly6/PLAUR domain containing 8
Loxl4	Lysyl oxidase-like 4
Mups	Major urinary proteins
Dmbt1	Malignant brain tumors 1
Med24	Mediator complex subunit 24
Meig1	Meiosis expressed gene 1
Ms4a6d	Membrane-spanning 4-domains subfamily A member 6D
Mt	Metallothionein
Map1lc3a	Microtubule associated protein 1 light chain 3 alpha
Mrpl	Mitochondrial ribosomal proteins
Mapk8ip3	Mitogen-activated protein kinase 8 interacting protein 3
Mmd2	Monocyte to macrophage differentiation associated 2
Smad9	Mothers against decapentaplegic homolog 9
Mrp4	Multidrug resistance related protein 4
Mafg	Musculoaponeurotic fibrosarcoma oncogene homolog G
Mypop	Myb related transcription factor
Mycl	MYCL proto-oncogene

Ndrg1	N-myc downstream regulated gene 1
NHANES	National Health and Nutrition Examination Survey
Ngfr	Nerve growth factor receptor
Nedd4l	Neural precursor cell expressed, developmentally down-regulated gene 4-like
Npas2	Neuronal PAS domain protein 2
Nnmt	Nicotinamide N-methyltransferase
NAFLD	Nonalcoholic fatty liver disease
HNF-4α	Nuclear factor 4 alpha
Nfil3	Nuclear factor interleukin 3
Oas	Oligoadenylate synthases
Oatp1b2	Organic anion transporting polypeptide 1b2
Ost	Organic solute transporter
Orm3	Orosomucoid 3
Por	P450 oxidoreductase
Pnlip	Pancreatic lipase
Pnliprp1	Pancreatic lipase protein 1
PAVIS	Peak annotation and visualization
Ppig	Peptidylprolyl isomerase G
PPARα	Peroxisome proliferator-activated receptor alpha
Ethe1	Persulfide dioxygenase
Phospho1	Phosphoethanolamine/phosphocholine phosphatase
Plcb3	Phospholipase C beta 3
Plscr1	Phospholipid scramblase 1
Pir	Pirin, Iron-binding nuclear protein
Phip	Pleckstrin homology domain interacting protein
PBDEs	Polybrominated Diphenyl Ethers
Pkd2	Polycystin 2
Prpf39	Pre-mRNA processing factor
PXR	Pregnane X receptor
PCN	Pregnenolone-16-carbonitrile
Prap1	Proline rich acidic protein 1
Ptgds	Prostaglandin D2 synthase
Prss2	Protease serine 2
PCGs	Protein-coding genes
qPCR	Quantitative polymerase chain reaction
Rad51b	RAD51 homolog b
Rab26os	Ras related oncogene family member
Reg3b	Regenerating islet-derived 3 beta
Rfx4	Regulated regulatory factor X4

Rgs16	Regulator of G-protein signaling 16
Rbp2	Retinol binding protein 2
Rock1	Rho-associated protein kinase 1
Robo1	Roundabout guidance receptor 1
STRING	Search Tool for the Retrieval of Interacting Genes/Proteins
Szt2	Seizure threshold 2
SAM	Sequencing alignment/map
Serpina3c	Serine peptidase inhibitor member 3C
Serpina9	Serine peptidase inhibitor member 9
Serpinh1	Serpin family H member 1
Saa2	Serum amyloid A2
Sesn2	Sestrin 2
SHP	Small heterodimer partner
SIC	Small intestinal content
Snora7a	Small nucleolar RNA 7A
Snhg	Small nucleolar RNA host gene 11
Ntcp	Sodium taurocholate cotransporting polypeptide
Slco	Solute carrier organic anions
Smpd3	Sphingomyelin phosphodiesterase 3
SE	Standard error
Stbd1	Starch-binding domain 1
Samd9l	Sterile alpha motif domain containing 9 like
Sults	Sulfotransferases
Socs2	Suppressor of cytokine signaling 2
Ttc39c	Tetratricopeptide repeat-containing protein
TSS	Transcription start site
TTS	Transcriptional termination site
TGF-β	Transforming growth factor beta
Tsc22d1	Transforming growth factor beta-stimulated clone 22 homolog
Tm7sf2	Transmembrane 7 superfamily member 2
Tff	Trefoil factor 2
Try5	Trypsin 5
Tubb2b	Tubulin beta 2B class IIb
Ugp2	UDP-glucose pyrophosphorylase 2
Ugts	UDP-glucuronosyl transferases
UTR	Untranslated region
Upf3b	Up-frameshift suppressor 3 homolog B
Vtcn1	V-set domain containing T cell activation inhibitor 1
Wfdc2	WAP four-disulfide core domain 2
Zfp	Zinc-finger protein

Acknowledgements

I am grateful to my advisor, Dr. Julia Yue Cui, for her guidance and endless support of my PhD studies. Throughout the three and half years in Julia's lab since the lab was initially set up, Julia has been endlessly patient and encouraging me to do work that I didn't think I was capable of. I've learned so much from her. I'd like to thank other members of my dissertation committee, Dave Eaton, Terry Kavanagh, Tom Burbacher, and Ken Thummel for their thoughtful comments on my research.

I am grateful to the past and present members of the Cui laboratory, especially Dr. Sunny Lihua Cheng, Joseph Dempsey, and Soowan Lee who all spent many hours helping me with animal work and lab experiments. I also would like to thank Dr. Theo Bammler for his guidance and advice on my projects. In addition, I would like to thank my fellow graduate students, especially Dr. Shirley Chang, Rachel Chang, Julie Park, and Dr. David Scoville, who have provided me with assistance, support, and advice. I would also like to extend special thanks to our collaborators for their work and advice for my projects.

I would like to thank my family, and friends for supporting me through this challenging quest. A special thank you goes to my husband Jingjing for providing me with support and encouragement, and my daughter for bringing me so many pleasant surprises to my life in Seattle. Finally, this work would not have been possible without funding from the National Institute of Health (NIH) grants [GM111381, ES019487, and ES025708], and the University of Washington Center for Exposures, Diseases, Genomics, and Environment [P30 ES0007033], as well as the Sheldon D. Murphy Endowment.

CHAPTER 1: Introduction

Polybrominated diphenyl ethers (PBDEs)

PBDEs are a class of brominated flame retardants used in a wide variety of consumer products such as textiles, carpets, polyurethane foams, furniture, electronic devices and building materials. The general chemical structure of PBDEs is shown in **Fig 1.1**, which

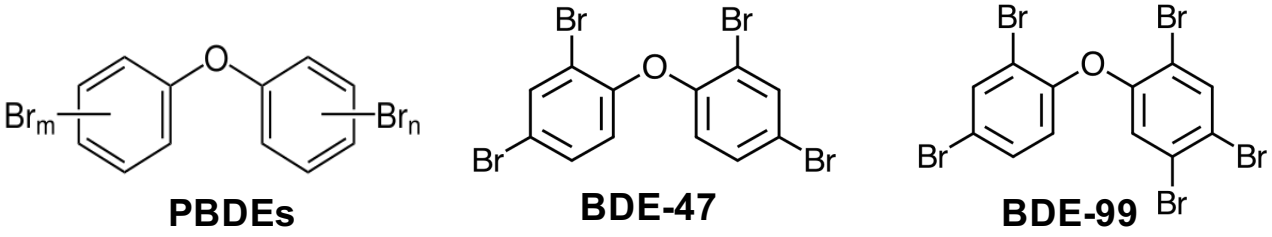

Figure 1.1 General chemical structures of PBDEs (m+n = 1 to 10), BDE-47 and BDE-99.

contains a central biphenyl structure surrounded by up to 10 bromine atoms. Depending on the number and position of bromine atoms, there are 209 possible PBDE congeners (ranging from mono- to decabromodiphenyl ethers). PBDEs are highly lipophilic, and thus their solubility in water is low, especially for the higher brominated compounds. The commercially produced PBDEs consist predominantly of penta-, octa-, and decabromodiphenyl ether mixtures. Although the production of pentaBDE and octaBDE ceased in 2004 and decaBDE was also phased out years later in 2013, human exposures to PBDEs continues due to their highly persistent and bio-accumulative nature in the environment. PBDEs have been reported to exhibit neurotoxicity, thyroid hormone disorders, and hepatotoxicity in animal studies, leading to growing public concerns about their use (Darnerud, 2003).

PBDEs have been detected in air, soil, sediments, birds, marine species, fish, and human tissues, as well as blood and breast milk (Darnerud et al., 2001; Frederiksen et al., 2009). The widespread contamination of the environment by PBDEs and the detection of them in wildlife and in human tissues have raised great concerns for their potential adverse health effects to humans and the environment. Diet and house dust appear to be the major sources of PBDE exposure in the general population (Costa and Giordano, 2007). Among food, fish has the highest content of PBDEs, followed by meat and dairy products (Schecter et al., 2004). According to a *US EPA* 2010 report, the adult daily intake dose of total PBDEs is estimated to be 7.1 ng/kg body weight (which is equivalent to 31.0 ng/g lipid weight, assuming a body fat proportion of 25%); whereas for children, the estimated intakes of total PBDEs are higher at 47.2 ng/kg/day for ages 1-5, 13.0 ng/kg/day for ages 6-11, and 8.3 ng/kg/day for ages 12-19 (EPA 2010 May, https://cfpub.epa.gov/ncea/risk/recordisplay.cfm?deid=210404). PBDE levels in breast milk, cord blood and placentas are generally higher in North America than in other regions, such as Asia, Europe, Oceania and Africa (Frederiksen et al., 2009; Tang and Zhai, 2017). Analysis of 2,062 human serum samples from the National Health and Nutrition Examination Survey (NHANES) 2003-2004 detected PBDEs in nearly all participants, with BDE-47 [geometric mean 20.5 ng/g lipid] and BDE-99 [5.0 ng/g lipid] among the highest serum concentration of PBDE congeners measured (Sjodin et al., 2008). BDE-47 and BDE-99 are also the predominant congeners detected in seafood and breast milk, which raises concerns for potential adverse effects for newborns and children (Darnerud, 2003; Guvenius et al., 2003; Lind et al., 2003; Schecter et al., 2003; Darnerud and Risberg, 2006; Hooper et al., 2007; Abdallah and Harrad, 2011).

Therefore, my dissertation focuses on these two most predominant PBDE congeners, BDE-47 and BDE-99.

Because of the lack of consensus on the levels of BDE-47 and BDE-99 that are considered to be toxic to humans, a reference dose (RfD) of 0.1 μg/kg body weight per day was suggested for both BDE-47 and BDE-99 (*USEPA 2010*). For BDE-47, the RfD of 0.1 μg/kg body weight was derived from a benchmark dose lower confidence limit ($BMDL_{1SD}$) of 0.35 mg/kg body weight per day, based on the changes in habituation ratios in adult mice (Eriksson et al., 2001), with application of a total uncertain factor of 3,000 to account for interspecies variability, human variability, extrapolation from a single dose (on postnatal day 10) to chronic exposure and for database deficiencies. For BDE-99, the RfD of 0.1 μg/kg body weight was derived from a $BMDL_{1SD}$ of 0.29 mg/kg body weight per day, based on the effects on spontaneous motor behavior in mice (Viberg et al., 2004), with application of a total uncertain factor of 3,000 to account for interspecies variability, human variability, extrapolation from a single dose (on postnatal day 10) to chronic exposure and for database deficiencies (*USEPA 2010*). In this dissertation, the adult male mice were orally administered a low dose (5 mg/kg body weight, which is equivalent to 10 μmol/kg) or a high dose (50 mg/kg body weight, which is equivalent to 100 μmol/kg) of BDE-47 or BDE-99 for four consecutive days and the tissues were collected on the fifth day. These doses are relatively higher than those of environmental exposure to humans. However, these doses are still relevant to assess the exposure risk to humans because of the highly persistent and bio-accumulative potential of PBDEs in breast-fed infants and children. According to the literature, the

concentrations of BDE-47 in human plasma from the United States range from 10 to 511 ng/g of lipid weight (lwt), with an average of 50 ng/g lipid (Petreas et al., 2003). The blood concentration of BDE-99 in the general U.S. populations ranges from 2.46 to 241 ng/g lwt, with an average of 11.6 ng/g lipid (Fitzgerald et al., 2012). In human breast milk, the mean BDE-47 and BDE-99 are approximately 27.8 ng/g lwt and 5.7ng/g lwt (Frederiksen et al., 2009). There is a significant gap between human bio-monitoring data and health assessment of PBDEs in humans and animals. Using these doses and dosing regimen, which are similar to those used in adult mice to induced cytochrome P450s (Pacyniak et al., 2007), we could compare our results with previous literature to characterize the effect of PBDEs on hepatic enzymes. Meanwhile, to make sure there are no off-target effects from liver injury, I quantified the serum alanine aminotransferase (ALT) from all treatment groups and performed Hematoxylin & Eosin (H&E) staining of liver histological sections collected from the high dose group. The results indicated the serum ALT levels were all within the normal range and there were no apparent liver injuries sustained by the high dose group. Therefore, we performed all the downstream experiments in the high dose group to maximally capture the effects induced by PBDEs through the gut-liver axis.

Toxicokinetics and toxicodynamics of BDE-47 and BDE-99

The toxicokinetics of BDE-47 have been studied in rats and mice orally dosed with ^{14}C-labelled BDE-47 (Orn and Klasson-Wehler, 1998; de Wit, 2002). The results indicated that BDE-47 was efficiently absorbed from the gastrointestinal tract (≥80%), and accumulated in adipose tissue, liver, adrenal, ovary, lung and brain. There were

marked species differences in regards to the metabolism and excretion of BDE-47. In rats, 86% of the administered dose (approximately 14.6 mg/kg body weight via a single gavage dose) was retained after 5 days with the highest concentrations found in adipose tissue; 14% of the administered dose was excreted in feces, with less than 0.5% excreted in urine. Of the amount excreted, 79% was the parent compound and 21% was as metabolites. The parent compound of BDE-47 was detected in all tissues analyzed, whereas five hydroxylated metabolites of BDE-47 were only detected in liver at low concentrations. In mice, 47% of the administered dose was retained in the body after 5 days, 20% was excreted in feces and 33% in urine. Of the amount excreted, 15% was the parent compound and 85% was metabolites. Mice appeared to have a higher rate of biotransformation and subsequent urinary excretion of BDE-47, compared with rats. The radioactivity was about 3 times higher in adipose tissue, relative to liver in rats, whereas the adipose and liver concentrations were similar in mice.

Studies of BDE-99 in several strains of rats suggest that absorption varies between 60 and 90%. The study (Hakk et al., 2002) with ^{14}C-labelled BDE-99, which was given as a single oral dose of 8 mg/kg to groups of conventional and bile-duct-cannulated male Sprague-Dawley rats, indicated that over 50% of the dose was retained at 72 h and preferably accumulated in adipose tissue, followed by adrenals, gastrointestinal tract and skin. Fecal elimination is the major route of elimination of BDE-99 in rats, evidenced by over 43% of the administered dose excreted via feces, 3.6% via bile and less than 1% via urine at 72 h. Of the amount excreted, more than 90% was parent BDE-99. In addition, small amounts of mono- and di-hydroxylated metabolites of penta-

and tetraBDE were detected in feces, suggesting the gut microbiome or intestinal epithelial enzymes are capable of oxidizing BDE-99 *in vivo*. In this dissertation, I will mainly focus on the role of gut microbiome in the biotransformation of PBDEs.

In studies with mice, gender differences in elimination were observed for both BDE-47 and BDE-99, in that male mice appeared to have higher urinary excretion than female mice. This has been suggested to be due to the higher levels of major urinary proteins (Mups) in male mice that bind to PBDEs for their elimination (Staskal et al., 2006). The half-life of tetra- to hexa-PBDEs has been shown to range from 20 to 120 days in rodents, with an increase proportional to the degree of bromination (Hakk et al., 2002). For humans, the half-life of lower brominated PBDE congeners were estimated to be much longer, with 1.8 years for BDE-47 and 2.9 years for BDE-99 (Costa and Giordano, 2007). The biotransformation and excretion of BDE-47 is species-dependent, in which mice have a faster biotransformation and excretion than rats. Male mice appeared to have higher urinary excretion of BDE-47 and BDE-99 than female mice. Formation of hydroxylated and debrominated metabolites of BDE-47 and BDE-99 has been demonstrated in rats and mice. In addition, the methoxylated PBDE congeners have been found in fish and seals, which may be formed by *in vivo* methylation of hydroxylated PBDE metabolites, or by microbial transformation (Darnerud et al., 2001). Microbial degradation is thought to be an important process to modify PBDE contamination in the environment. PBDEs can be reductively debrominated by anaerobic or aerobic microbes (Tokarz et al., 2008; Qiu et al., 2012; Zhang et al., 2013; Xu et al., 2014; Yang et al., 2017b). However, most studies have been done *in vitro*

with individual bacterial strains. Little is known about the microbial communities involved in PBDE anaerobic degradation *in vivo*, as well as how PBDEs affect microbes involved in diverse biological functions *in vivo*.

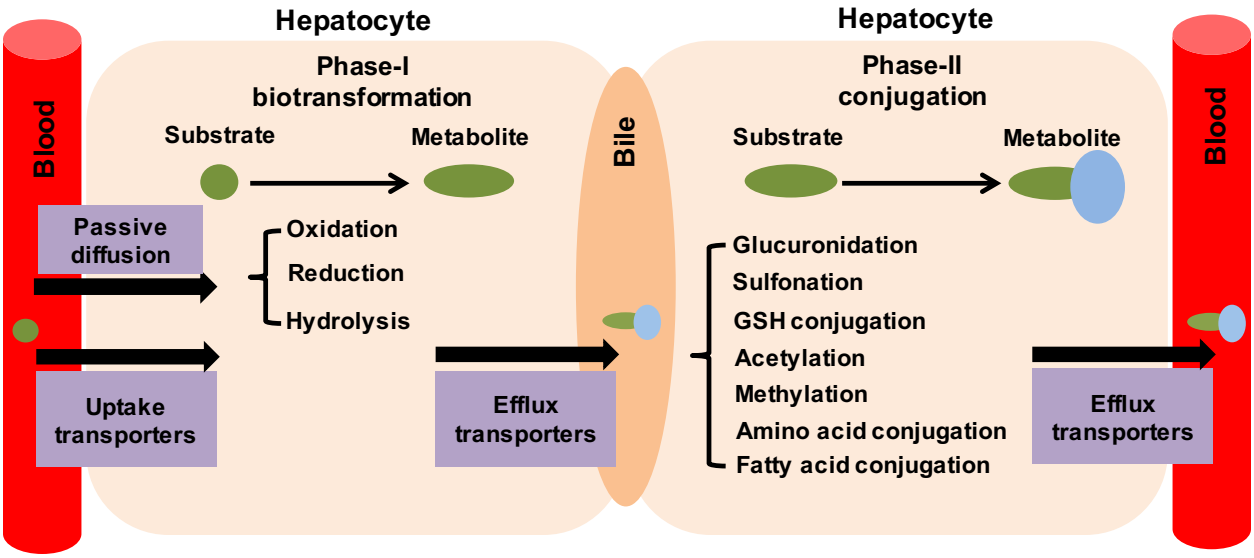

Figure 1.2 Biotransformation of xenobiotics in liver. (from Cui, J. Y. & Li, C. Y. (2018) Regulation of Xenobiotic Metabolism in the Liver. Comprehensive Toxicology, Third Edition. Vol. 2, pp. 168-214)

As shown in **Figure 1.2**, the phase-I xenobiotic-biotransformation enzymes perform oxidation, reduction, and hydrolysis reactions to add a small function group to the substrates and slightly increase the water-solubility; and phase-II enzymes catalyze various conjugation reactions to further increase their elimination (Aleksunes and Klaassen, 2012). Uptake and efflux transporters are also important in modulating the absorption, disposition, and excretion of chemicals (Klaassen and Aleksunes, 2010). It is well known that the expression of xenobiotic-processing genes (XPGs) is regulated by xenobiotic-sensing transcription factors such as the aryl hydrocarbon receptor (AhR), constitutive androstane receptor (CAR/Nr1i3), and pregnane X receptor (PXR/Nr1i2) (Klaassen and Slitt, 2005; Aleksunes and Klaassen, 2012).

Regarding the pharmacodynamics of PBDEs, PBDE exposure can regulate the expression and/or activity of certain xenobiotic-processing genes. BDE-47 and BDE-99 have been shown to be activators of CAR and PXR in both rodent livers and human hepatocytes, leading to induced expression of genes important in xenobiotic metabolism (Pacyniak et al., 2007; Sueyoshi et al., 2014). BDE-99 has also been shown to activate AhR-signaling, leading to induced expression of CYP1A and Ugt1ab in zebrafish liver cells (Yang et al., 2016b). Thus, activation of these transcription factors by PBDEs may alter the expression of many DPGs and influence the pharmacokinetics of co-administered drugs or other chemicals, resulting in drug-drug interactions or adverse drug reactions. PBDEs have been shown to up-regulate both phase-I and phase-II xenobiotic-metabolizing enzymes. Rats exposed to pentaBDEs showed up-regulated expression of CYP1A1 and CYP1A2 as indicated by the increased activity of liver microsomal ethoxyresorufin-*O*-deethylase (EROD) (von Meyerinck et al., 1990). Higher UGT activity was also observed in rats exposed to PBDE mixtures at a concentration of 100 μmol/kg bw for 14 days (Hallgren et al., 2001).

In liver, BDE-47 and BDE-99 were oxidized predominantly by human CYP2B6 to hydroxylated metabolites (OH-BDEs) (Erratico et al., 2012; Erratico et al., 2013; Feo et al., 2013; Gross et al., 2015). The OH-BDEs have been identified in blood samples of women and children who were environmentally exposed to PBDEs (Qiu et al., 2009), as well as in blood, bile, urine, and feces of rodents after exposure to BDE-47, BDE-99, or PBDE mixtures (Orn and Klasson-Wehler, 1998; Hakk et al., 2002; Malmberg et al.,

2005; Chen et al., 2006; Marsh et al., 2006; Staskal et al., 2006). The OH-BDEs are considered more potent and toxic than their parent compounds in disrupting Ca^{2+} homeostasis, altering neuronal viability, and competing with thyroxine for binding to human transthyretin (Meerts et al., 2000; Canton et al., 2005; Hamers et al., 2006; Dingemans et al., 2011). The OH-BDEs are substrates for phase-II conjugation enzymes such as UDP-glucuronosyl transferases (Ugts) and sulfotransferases (Sults) *in vitro* (Erratico et al., 2015). Transporters are also important for PBDE disposition. Uptake transporters bring various chemicals into hepatocytes for biotransformation, whereas efflux transporters export chemicals out of hepatocytes for elimination into urine or bile. Previous studies have shown that BDE47 and BDE-99 were transported to hepatocytes by the human uptake transporters SLCO/OATP1B1, OATP1B3, and OATP2B1 (Pacyniak et al., 2010) and by the mouse transporters Slco/Oatp1a4, Oatp1b2, and Oatp2b1 (Pacyniak et al., 2011). The efflux of water-soluble conjugates of hydroxylated PBDEs likely occurs via efflux transporters, which has yet to be determined.

Additionally, numerous *in vitro* studies in multiple cell types have shown that PBDEs can induce oxidative stress, which may lead to DNA damage, and apoptosis (He et al., 2008; Costa et al., 2015). For example, the pentaBDE mixture DE-71 and BDE-47 increased the production of reactive oxygen species (ROS) in human neutrophil granulocytes (Reistad and Mariussen, 2005). BDE-47 was also reported to cause oxidative stress and apoptosis in human neuroblastoma cells, in hippocampal neurons, and human fetal liver hematopoietic cells (He et al., 2008; Shao et al., 2008). BDE-99 has been shown

to induce apoptosis in human astrocytoma cells (Madia et al., 2004). A study of pentaBDE mixture DE-71 in neurons and astrocytes have demonstrated the neurotoxicity of DE-71 is modulated by intracellular GSH levels, which are major components of the cellular antioxidant defense mechanism. Moreover, cells that were collected from glutamate cysteine ligase modifier subunit knockout mice ($Gclm^{-/-}$) with significantly lower levels of GSH than wild-type mice were more susceptible to DE-71 toxicity. Consistently, *in vivo* exposure of mice to BDE-47 (10 mg/kg, on PND 10) caused an increase of oxidative stress in cerebellum and hippocampus (Giordano et al., 2008). However, the mechanisms involved in PBDE-induced oxidative stress and mitochondrial dysfunction, leading to apoptotic cell death, have not been elucidated. One potential mechanism is that the antioxidant transcription factor nuclear factor E2-related factor (Nrf2) may play a critically protective role in the regulation of PBDE-mediated cellular defense responses. Nrf2 is a well-known redox-sensitive transcriptional factor that translocates to the nucleus where it binds to antioxidant response element (ARE) and activates downstream genes (Motohashi and Yamamoto, 2004). Nrf2 regulates many XPGs, especially phase-II detoxification and antioxidant enzymes, such as glutathione S-transferase (GST), NAD(P)H: quinone oxidoreductase 1 (NQO1), heme oxygenase-1 (HO-1) and UDP-glucuronosyltransferase (UGT), as well as transporters gene such as multidrug resistance-associated protein (MRP)(Klaassen and Slitt, 2005; Shen and Kong, 2009). Induction of these enzymes in cells is well known to confer resistance against carcinogen, reactive metabolites or reactive oxygen species by enhancing their elimination. It is suggested that BDE-47 activated oxidative stress response pathway and stimulated the expression of redox-sensitive genes and

augmentation of intracellular GSH through the activation of Nrf2 in human extravillous trophoblast cell line (Park and Loch-Caruso, 2014). Therefore, although this dissertation is mainly focusing on the effect of PBDEs on hepatic xenobiotic-processing genes through CAR/PXR, other pathways such as oxidative stress or Nrf2 pathways may also contribute to XPG regulation in our research model.

Gut Microbiome

Studies have found that the enterohepatic circulation of PBDEs is affected by variation in gut microbial populations, leading to increased residence time in the body and toxicity (Meijer et al., 2006). Exposure to environmental toxicants or drugs can modify the gut microbiome composition and functionality, and this may interfere with the pharmacokinetics/toxicokinetics of other chemicals co-administered chemicals. The gut microbiome contains a wide spectrum of microorganisms which reside in the gastrointestinal tract and play an important role in nutrient absorption, host intermediary metabolism, and xenobiotic biotransformation (Shreiner et al., 2015; Fu and Cui, 2017). Disruptions in the composition of gut microbial communities and altered interactions between microbiota-host interactions have been linked to several diseases, such as cancer, nonalcoholic fatty liver disease (NAFLD), and insulin resistance (Dumas et al., 2006), as well as allergies, inflammatory bowel disorders, obesity, and diabetes (Wikoff et al., 2009; Jumpertz et al., 2011). For example, obese patients have an increased *Firmicutes/Bacteriodetes* ratio in their feces (Ley et al., 2005; Turnbaugh et al., 2006; Duncan et al., 2008) and have reduced bacterial diversity (Turnbaugh and Gordon, 2009; Turnbaugh et al., 2009). Germ-free (GF) mice are protected from obesity (Rabot

et al., 2010), and colonization of GF mice with feces from obese human results in increased total body and fat mass as well as obesity-associated metabolic phenotypes (Ridaura et al., 2013). The gut microbiome, serving as an “internal environment”, can directly biotransform xenobiotics utilizing their own microbial enzymes, or produce microbial metabolites that enter the enterohepatic circulation to interact with the host receptors and modify hepatic biotransformation indirectly. Gut microbiomes may communicate with distinct xenobiotic sensors to regulate xenobiotic metabolism. For instance, the secondary bile acid lithocholic acid (LCA), which is exclusively produced by intestinal bacteria, is an activator of mouse and human PXR (Staudinger et al., 2001; Kliewer et al., 2002). The microbial metabolite of the essential amino acid tryptophan, indole-3-propionate acid (IPA), is also a novel PXR activator in mouse intestine. IPA improves gut barrier permeability and reduces metabolic endotoxins and host inflammation through PXR (Venkatesh et al., 2014). Using GF mice, our laboratory has observed a marked decrease in the expression and activity of Cyp3a as compared to conventional (CV) mice, whereas conventionalization of GF mice restored to control levels Cyp3a mRNA, protein and enzyme activities (Selwyn et al., 2015b). However, it is unclear how and to what extent gut microbiome-mediated modulation of DPGs will affect PXR-signaling and hepatic biotransformation of PBDEs. Therefore, in my dissertation I used both CV and GF mice to study the role of the gut microbiome in modulation PBDE-mediated effects.

In addition to xenobiotic biotransformation, the gut microbiome plays an essential role in intermediary metabolism. In the intestine, gut microbiota convert primary BAs into

secondary BAs via dehydroxylation, deconjugation, and epimerization reactions (Chiang, 2009). The intestinal microbiota contains enzymes that metabolize BAs; for example, bile salt hydrolases (Bshs), which are widely present in intestinal bacteria, remove glycine or taurine from conjugated BAs. The bacteria *Clostridia* bacteria contain hydroxysteroid dehydrogenases and 7-dehydratases, which produce BA intermediates and secondary BAs (Ridlon et al., 2006). Ninety-five percent of BAs undergo reabsorption from the intestinal lumen via active transport and recirculate to liver via the portal blood (Chiang, 2003) (**Fig. 1.3**). BAs function as signaling molecules and not

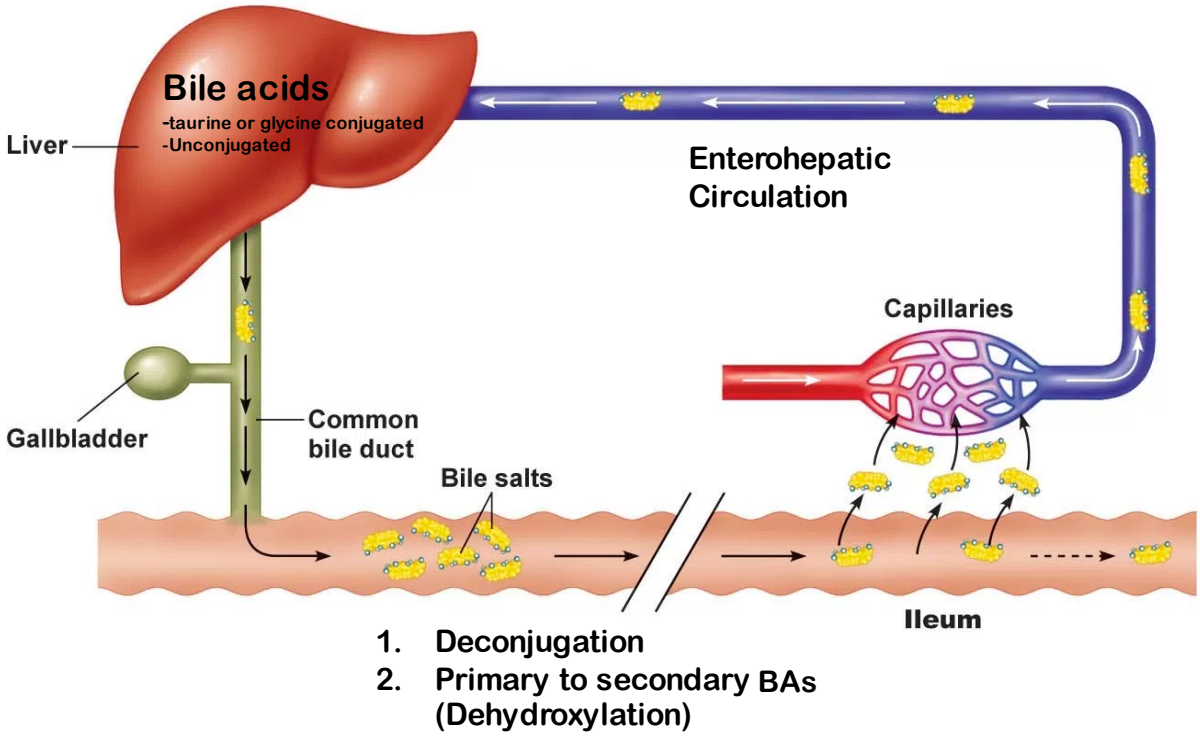

Figure 1.3 Gut-liver axis on bile acid metabolism. (Figure modified based on https://hackyourgut.com/2017/02/28/bile-flow-bacteria-and-chronic-inflammation/)

only regulate their own biosynthesis, but also communicate with distinct host receptors to regulate many physiological pathways in xenobiotic biotransformation and

intermediary metabolism (Chiang, 2003). Clinically, many therapeutic drugs have been shown to produce cholestatic liver injury by elevating hepatic BA levels (Padda et al., 2011). In laboratory animals, activation of the xenobiotic sensor, CAR, by its activators, phenobarbital and TCPOBOP, led to decreased BA levels in mouse liver, but increased fecal excretion of muricholic acids (Sberna et al., 2011; Lickteig et al., 2016). Lack of gut microbiota in GF mice resulted in higher BA concentrations in serum, liver, bile, and ileum than that in CV mice (Selwyn et al., 2015c). However, very little is known regarding to what extent environmental chemicals such as PBDEs may modulate the host BA homeostasis, and whether gut microbiota is involved in this process.

Long non-coding RNAs (lncRNAs)

Recently, lncRNAs are increasing recognized as novel biomarkers and key regulators of toxicological response (Dempsey and Cui, 2016). LncRNAs are transcribed from mammalian genome, are >200 nucleotides in length and generally lack protein coding capacity. They play pivotal roles in the regulation of genomic integrity, imprinting, mRNA processing, cell differentiation and development (Guttman et al., 2009; Loewer et al., 2010; Guttman et al., 2011; Hung et al., 2011; Parasramka et al., 2016). Specifically, lncRNAs frequently serve as the co-modulators of transcription factors to regulate gene expression (Lan et al., 2016). LncRNAs may serve as scaffolds to transport transcription factors to their promoter region, resulting in transcriptional activation or repression. LncRNAs can also function as ‘decoys’ or ‘molecular sinks’ to bind with chromatin regulatory proteins thereby inhibiting their function (Wang and Chang, 2011; Dempsey and Cui, 2016). Some lncRNAs act in *cis* to activate the transcription of the

neighboring genes, whereas others in *trans* may exhibit suppressive functions (Zhou et al., 2015).

Regarding the involvement of lncRNAs in human diseases, aberrant lncRNA expression has been reported in cancer and metabolic disorders (Wapinski and Chang, 2011; Bhan and Mandal, 2014). LncRNAs have been found to regulate cellular cholesterol metabolism (Lan et al., 2016), lipid metabolism and BA homeostasis (Li et al., 2015). Regarding environmental chemicals, altered expression of lncRNAs has been reported for polycyclic aromatic hydrocarbons (Gao et al., 2016), benzene (Bai et al., 2014), cadmium (Zhou et al., 2015), and bisphenol A (Kumamoto and Oshio, 2013). In blood samples obtained from humans exposed to benzene, the lncRNAs NR_045623 and NR_028291 were up-regulated with increasing levels of benzene exposure (Bai et al., 2014). Rats treated with cadmium showed increased expression of ENST000004144355 in a dose-dependent manner, implicating that lncRNAs may serve as novel biomarkers for DNA damage and repair in cadmium toxicity (Zhou et al., 2015). However, there is little information regarding the mechanisms of lncRNAs involved in the toxification/detoxification following xenobiotic exposure of PBDEs, and hepatic lncRNA expression is regulated by the gut microbiome.

Dissertation Outline

The *overall goal* of this dissertation is to characterize the interactions between the gut microbiome and the environmental chemicals PBDEs on host hepatic xenobiotic biotransformation and intermediary metabolism in liver. The *objective* of this

dissertation is to utilize multidisciplinary approaches to strategically investigate the gut-liver axis on the biotransformation of PBDEs, and the regulation of the hepatic transcriptome by PBDE-gut microbiome interactions. My *central hypothesis* is that PBDE-gut microbiome interactions markedly regulate the expression of hepatic xenobiotic-processing genes (XPGs), the activities of drug-metabolizing enzymes, as well as the production of endogenous intermediary metabolites such as bile acids.

Chapter 1: Introduction.

Chapter 2: The gut microbiome is a novel frontier for xenobiotic metabolism, serving as an internal environment to modify the bioavailability, efficacy, and toxicity of chemicals from the external environment. PBDEs are among the most abundant and persistent environmental contaminants in the human population, and especially the BDE-47 and BDE-99 congeners are prevalent in seafood and human breast milk at worrisome levels. Very little is known about the potential interactions between the gut microbiome and PBDEs. In this chapter, I used a GF mouse model, PBDE targeted metabolomics, RNA-Seq, and LC-MS/MS-based targeted proteomics, to strategically investigate how the gut microbiome modifies PBDE-mediated regulation of the hepatic XPGs, and characterize how the lack of a gut microbiome modifies the hepatic hydroxylation of PBDEs.

Chapter 3: In addition to xenobiotic metabolism, the gut microbiome also plays an essential role in the metabolism of bile acids (BAs), which are important signaling molecules implicated in obesity and diabetes, inflammation, and cancer. Pharmacological activation of the major xenobiotic-sensing nuclear receptor, pregnane

X receptor (PXR) by its prototypical (rodent-specific) agonist pregnenolone-16α-carbonitrile (PCN) has been shown to decrease the activity of the rate-limiting enzyme for BA synthesis in rodent liver. PBDEs have also been shown to activate PXR in rodent liver and human hepatocytes. However, very little is known regarding the effect of PBDEs on BA homeostasis. In this chapter, I utilized bacterial metagenomics (16S rRNA sequencing of large intestinal contents [LIC]), targeted proteomics (LC-MS/MS of BA-processing genes), and targeted metabolomics (LC-MS/MS of 56 BAs), to characterize the effect of PBDEs on the composition of the gut microbiome composition and the production of microbial metabolites that are involved in BA homeostasis.

Chapter 4: LncRNAs are increasingly recognized as novel regulators and biomarkers for chemical-mediated toxicities. However very little is known regarding the regulation of lncRNAs following the toxic exposure to PBDEs in the liver, which is the major organ for xenobiotic biotransformation. Therefore, in this chapter I analyzed RNA-Seq data collected from both CV and GF mice to capture the hepatic transcriptome of both lncRNAs and PCGs responsive to PBDE exposure. The goal of the chapter is to unveil and compare the common and unique PBDE-target genes and signaling pathways in response to PBDE and gut microbiome mediated effects. Another goal of this chapter is to identify distinct lncRNAs as novel biomarkers for PBDEs exposure, which may also facilitate future mechanistic studies of lncRNAs in gene expression during toxicological responses.

To address my research goals, I have developed three related hypotheses and specific aims to test these hypotheses.

Specific Aims and Hypotheses

Chapter 2

Specific Aim: Determine the necessity of gut microbiome on host hepatic biotransformation of PBDEs.

Hypothesis: Gut microbiome interacts with hepatic xenobiotic biotransformation enzymes to modulate the hepatic biotransformation of PBDEs.

Chapter 3

Specific Aim: Characterize the effect of PBDEs on gut microbiome composition and function, as well as on the production of microbial metabolites that modulate bile acid homeostasis.

Hypothesis: Oral exposure to PBDEs causes dysbiosis and aberrant regulation of BA homeostasis.

Chapter 4

Specific Aim: Explore novel biomarkers for PBDEs and gut microbiome interactions

Hypothesis: Gut microbiome not only modifies the PBDE-mediated hepatic expression of protein-coding genes, but also modulates the expression of lncRNAs, which may serve as novel biomarkers for PBDEs exposure.

CHAPTER 2: Novel Interactions between Gut Microbiome and Host Drug-processing Genes: Modification of Hepatic Metabolism of PBDEs

This chapter was published in Journal of Drug Metabolism & Disposition on 2017/09.

The authors of the manuscript are:

Cindy Yanfei Li, Soowan Lee, Sara Cade, Li-Jung Kuo, Irvin R. Schultz, Deepak K. Bhatt, Bhagwat Prasad, Theo K. Bammler, and Julia Yue Cui

Department of Environmental & Occupational Health Sciences, University of Washington, Seattle, WA 98105 (C. Y. L, S. L, T. K. B, J. Y. C); Pacific Northwest National Laboratory, Sequim, WA 98382 (S. C, L. K, I. R. S); Department of Pharmaceutics, University of Washington, Seattle, WA 98105 (D. K. B, B. P).

ABSTRACT

The gut microbiome is a novel frontier in xenobiotic metabolism. Polybrominated diphenyl ethers (PBDEs), especially BDE-47 and BDE-99, are among the most abundant and persistent environmental contaminants that produce a variety of toxicities. Little is known about how the gut microbiome affects the hepatic metabolism of PBDEs and the PBDE-mediated regulation of drug-processing genes (DPGs) *in vivo*. The goal of this study was to determine the role of gut microbiome in modulating the hepatic biotransformation of PBDEs. Nine-week-old male C57BL/6J conventional (CV) or germ free (GF) mice were treated with vehicle, BDE-47 or BDE-99 (100 μmol/kg) for four days. Following BDE-47 treatment, GF mice had higher level of 5-OH-BDE-47 but lower levels of 4 other metabolites in liver than CV mice; whereas following BDE-99 treatment, GF

mice had lower levels of 4 minor metabolites in liver than CV mice. RNA-Seq demonstrated that the hepatic expression of DPGs was regulated by both PBDEs and enterotypes. Under basal condition, the lack of gut microbiome up-regulated the *Cyp2c* subfamily but down-regulated the *Cyp3a* subfamily. Following PBDE exposure, certain DPGs were differentially regulated by PBDEs in a gut microbiome-dependent manner. Interestingly, the lack of gut microbiome augmented PBDE-mediated up-regulation of many DPGs, such as Cyp1a2 and Cyp3a11 in mouse liver, which was further confirmed by targeted metabolomics. The lack of gut microbiome also augmented the Cyp3a enzyme activity in liver. In conclusion, our study has unveiled a novel interaction between gut microbiome and the hepatic biotransformation of PBDEs.

INTRODUCTION

The liver is a major organ for the metabolism and excretion of xenobiotics. Many genes encoding drug-metabolizing enzymes or transporters (together called drug-processing genes [DPGs]) are highly expressed in liver. Drug metabolizing enzymes include phase-I enzymes that perform oxidation, reduction, and hydrolysis reactions; and phase-II enzymes that catalyze various conjugation reactions (Aleksunes and Klaassen, 2012; Li et al., 2016b). Uptake transporters bring various chemicals into hepatocytes for biotransformation, whereas efflux transporters export chemicals out of hepatocytes for elimination into urine or bile (Klaassen and Aleksunes, 2010). The expression of DPGs is regulated by xenobiotic-sensing transcription factors such as the aryl hydrocarbon receptor (AhR), constitutive androstane receptor (CAR/Nr1i3), and pregnane X receptor (PXR/Nr1i2) (Klaassen and Slitt, 2005; Cui et al., 2009; Aleksunes

and Klaassen, 2012; Cui and Klaassen, 2016; Li et al., 2016b; Park et al., 2016). Activation of these transcription factors by drugs or other xenobiotics alters the expression of DPGs, which may influence the pharmacokinetics of co-administered drugs or other chemicals, resulting in drug-drug interactions or drug-food reactions.

Polybrominated diphenyl ethers (PBDEs) are widely used as flame retardants and persistently present in the environment due to their lipophilic and bio-accumulative properties. Accumulating evidence have shown the adverse effects of PBDEs on laboratory animals, including thyroid hormone disorders (Zhou et al., 2002), neurotoxicity (Madia et al., 2004), hepatic oxidative stress (Fernie et al., 2005), and carcinogenesis (National Toxicology, 1986). Among all 209 known PBDE congeners, BDE-47 and BDE-99 are the most predominant congeners detected in humans (Sjodin et al., 2001; Schecter et al., 2003; Hites, 2004). BDE-47 and BDE-99 are also activators of CAR and PXR in both rodents and human hepatocytes, leading to induced expression of genes important in xenobiotic metabolism and disposition (Pacyniak et al., 2007; Sueyoshi et al., 2014). Studies incubating BDE-47 and BDE-99 with rat or human microsomes have demonstrated that PBDEs are first biotransformed to hydroxylated metabolites (OH-BDEs) by cytochrome P450 enzymes (Hamers et al., 2008; Lupton et al., 2009; Stapleton et al., 2009; Dong et al., 2010; Erratico et al., 2010; Erratico et al., 2011; Feo et al., 2013). OH-BDEs have been identified in blood samples of women and children who were environmentally exposed to PBDEs (Qiu et al., 2009), and in blood, bile, urine, and feces of rodents after exposure to BDE-47, BDE-99, or PBDE mixtures (Orn and Klasson-Wehler, 1998; Hakk et al., 2002; Malmberg et al., 2005; Chen et al., 2006; Marsh et al., 2006; Staskal et al., 2006). The OH-BDEs are potentially more

potent and toxic than their parent compounds in disrupting Ca^{2+} homeostasis, altering neuronal viability, and competing with thyroxine for binding to human transthyretin (Meerts et al., 2000; Canton et al., 2005; Hamers et al., 2006; Dingemans et al., 2011). The OH-BDEs are then further metabolized by phase-II enzymes such as UDP-glucuronosyl transferases (Ugts) and sulfotransferases (Sults) before elimination (Erratico et al., 2015).

The gut microbiome is recognized as an additional regulator of DPGs in liver. Profound differences have been reported in the expression patterns of DPGs between CV and GF mice (Bjorkholm et al., 2009; Toda et al., 2009; Selwyn et al., 2015a; Selwyn et al., 2015b; Selwyn et al., 2015d). Alterations in the gut microbiome by either diet or other environmental factors have been suggested to contribute to inter-individual variations in drug response and altered expression of DPGs. This in turn may also change the composition of gut microbiota and ultimately exaggerate the adverse effects of the initial insults (Klaassen and Cui, 2015; Nayak and Turnbaugh, 2016). Therefore, classification of the human gut microbiome into distinct “enterotypes”, defined by their bacterial composition, has been proposed to serve as a new research paradigm to better understand the interplay between microbial variation and human diseases (Arumugam et al., 2011; Knights et al., 2014; Nayak and Turnbaugh, 2016).

Despite the known importance of hepatic DPGs and gut microbiome in xenobiotic biotransformation, very little is known regarding the potential contribution of the liver-gut-bacteria axis on hepatic PBDE metabolism and disposition *in vivo*. The goals of the present study were to: 1) investigate how gut microbiome modifies the PBDE-mediated regulation of the hepatic DPGs; 2) how the lack of gut microbiome modifies the hepatic

hydroxylation of PBDEs. To accomplish these goals, we used GF mouse models, PBDE targeted metabolomics, RNA-Seq, and LC-MS/MS-based targeted proteomics, to strategically investigate the novel interactions between gut microbiome and host DPGs, and their effect on the metabolism of the major PBDE congeners BDE-47 and BDE-99 in liver.

MATERIALS AND METHODS

Chemicals. BDE-47 (2, 2', 4, 4'-tetrabromodiphenyl ether) was purchased from Chem Service, Inc. (West Chester, PA). BDE-99 (2, 2', 4, 4',5-pentabromodiphenyl ether) was purchased from AccuStandard, Inc. (New Haven, CT). The phosphate-buffered saline (PBS, 10x, pH 7.4) was purchased from Thermo Fisher Scientific (Grand Island, NY). Synthetic heavy labeled peptides (Supplementary Table 1S) were obtained from Thermo Fisher Scientific (Rockford, IL). Ammonium bicarbonate (98% purity) and Pierce™ Trypsin protease (MS-grade) were purchased from Thermo Fisher Scientific (Rockford, IL). Chloroform, ethyl ether, Optima MS-grade acetonitrile, methanol and formic acid were purchased from Fischer Scientific (Fair Lawn, NJ). All other chemicals and reagents, unless indicated otherwise, were purchased from Sigma-Aldrich (St. Louis, MO).

Animals. Eight-week-old male C57BL/6J CV mice were purchased from the Jackson Laboratory (Bar Harbor, ME), and were acclimated to the animal facility at the University of Washington for one-week prior to experiments. The initial breeding colony of GF mice in C57BL/6 background was established with mice purchased from the National

Gnotobiotic Rodent Resource Center (University of North Carolina, Chapel Hill). All mice were housed according to the Association for Assessment and Accreditation of Laboratory Animal Care International guidelines, and studies were approved by the Institutional Animal Care and Use Committee (IACUC) at the University of Washington. CV and GF mice were exposed to the same diet (laboratory autoclaved rodent diet [LabDiet #5010]), water (non-acidified autoclaved water), and bedding (autoclaved Enrich-N'Pure). All chemical solutions were sterilized using the Steriflip Vacuum-driven Filtration System with a 0.22 μm Millipore Express Plus Membrane (EMD Millipore, Temecula, CA). All gavage needles and syringes were sterilized by autoclave. At 9-weeks of age, CV mice (n=5 per group) were randomly allocated for the treatment of vehicle (corn oil, 10ml/kg), BDE-47 (10 μmol/kg and 100 μmol/kg), or BDE-99 (10 μmol/kg and 100 μmol/kg) via oral gavage once daily for 4 days. Livers were collected 24 hours after the last dosing on the 5^{th} day and immediately frozen in liquid nitrogen. Based on the highest induction of Cyp2b10 and Cyp3a11 mRNAs in CV mice, age-matched GF mice (n= 3 or 4 per group) were treated with vehicle (corn oil, 10ml/kg), BDE-47 (100 μmol/kg) or BDE-99 (100 μmol/kg) following the same procedure (as shown in Fig. 1). Due to the potential variations caused by the estrous cycle in adult female mice, only male livers were used for this study. All tissues were immediately frozen in liquid nitrogen and stored at -80 °C until further analysis.

Serum alanine aminotransferase (ALT) quantification and Haemotoxylin & Eosin (H&E) staining. Serum samples were analyzed by standard enzymatic-colorimetric assays using ALT kits according to the manufacturer's protocol (Pointe Scientific, Inc.

Canton, MI). H&E staining of liver sections collected from CV and GF mice treated with corn oil, BDE-47, or BDE-99 was performed at the Histology and Imaging Core Facility (HIC) at University of Washington. Representative slides were shown (x100).

Total RNA isolation. Total RNA was isolated from frozen tissues using RNA-Bee reagent (Tel-Test Inc., Friendswood, TX) according to the manufacturer's protocol. RNA concentrations were quantified using NanoDrop 1000 Spectrophotometer (Thermo Scientific, Waltham, MA) at 260 nm. Integrity of total RNA samples was evaluated by formaldehyde-agarose gel electrophoresis with visualization of 18S and 28S rRNA bands under ultraviolet light, and by Agilent 2100 Bioanalyzer (Agilent Technologies Inc. Santa Clara, CA). Samples with RNA Integrity Numbers above 8.0 were used for RNA-sequencing.

Quantification of gene expression by RT-qPCR. Total RNA was transcribed to cDNA using a High Capacity cDNA Reverse Transcription Kit (Applied Biosystems, Foster City, CA). The cDNAs were amplified by PCR using SsoAdvanced Universal SYBR Green Supermix in a BioRad CFX384 Real-Time PCR Detection System (Bio-Rad, Hercules, CA). The PCR primers were synthesized by Integrated DNA Technologies (Coralville, IA). The primers for β-actin were GGCCAACCGTGAAAAGATGA (Forward) and CAGCCTGGATGGCTACGTACA (Reverse), for Cyp1a2 were GACATGGCCTAACGTGCAG (Forward) and GGTCAGAAAGCCGTGGTTG (Reverse), for Cyp2b10 were AAGGAGAAGTCCAACCAGCA (Forward) and CTCTGCAACATGGGGGTACT (Reverse), and for Cyp3a11 were

ACAAACAAGCAGGGATGGAC (Forward) and GGTAGAGGAGCACCAAGCTG (Reverse). The ddCq values were calculated for each target gene and were normalized to the expression of the housekeeping gene β-actin.

Complementary DNA library preparation and RNA-sequencing. The complementary DNA (cDNA) libraries were constructed from total RNA samples using an Illumina TruSeq Stranded mRNA kit (Illumina, San Diego, CA). Briefly, 1.25 μg of total RNA was used as the RNA input. The mRNAs were selected from the total RNAs by purifying the poly-A containing molecules using poly-T primers. The RNA fragmentation, first and second strand cDNA syntheses, end repair, adaptor ligation, and PCR amplification were performed according to the manufacturer's protocol. The cDNA libraries were validated for integrity and quantity using an Agilent 2100 Bioanalyzer (Agilent Technologies, Santa Clara, CA) before sequencing. The cDNA libraries were sequenced on an Illumina HiSeq2000 sequencer using a 50 bp paired-end multiplexing strategy with 5 samples per lane at Dr. Nickerson's Sequencing Facility at the UW Genome Sciences Department.

RNA-Seq data analysis. FASTQ files were de-multiplexed and concatenated per sample for downstream analysis. Quality control of all FASTQ files was performed using FastQC (http://www.bioinformatics.babraham.ac.uk/projects/fastqc/). RNA-Seq reads from FASTQ files were mapped to the reference genome (NCBI GRCm38/mm10) using Hierarchical Indexing for Spliced Alignment of Transcripts (HISAT) (version 0.1.6 beta) (Kim et al., 2015). SAM (sequencing alignment/map) files were converted to

binary format using Samtools (version 1.2) (Li et al., 2009a). The output files in BAM (binary alignment/map) format were analyzed by Cufflinks (version 2.2.1) to estimate the transcript abundance (Trapnell et al., 2010). The mRNA abundance was expressed as FPKM (fragments per kilobase of transcript per million mapped reads). Differential expression analysis was performed using Cuffdiff. The differentially expressed genes were defined as FDR (false discovery rate adjusted p-value) <0.05 in at least one of the chemical-treated groups as compared to the vehicle-treated group of the same enterotypes of mice, as well as genes that were differentially expressed by the lack of gut microbiome under the same treatment. The RNA-Seq generated an average of 70 million reads per sample, and more than 80% of the reads were mapped to the mouse reference genome (NCBI GRCm38/mm10). The data discussed in this publication have been deposited in NCBI's Gene Expression Omnibus and are accessible through GEO Series accession number GSE101650.

Extraction and quantification of PBDE hydroxylated metabolites. The extraction and measurement of OH-BDEs was modified from the methods described by Hovander et al. (Hovander et al., 2000). Briefly, liver samples were first homogenized with 4-volumes of deionized water and then spiked with the surrogate, 4-OH-PCB-159. Next, the homogenates were denatured by adding 6 M HCl and 2-propanol. After 5-min at RT, the mixture was extracted with hexane/methyl *tert*-butyl ether (MTBE; 1:1 v/v). The organic extract was volume reduced and the phenolic fraction (containing the OH-BDEs) was separated from neutral compounds by adding a solution of potassium hydroxide (0.5 M in 50% ethanol). The aqueous layer, which contains phenolic compounds, was

acidified with 2 M HCl and then extracted with hexane/MTBE mix (9:1 v/v). The hexane/ether extract, which now contained the phenolic compounds, was dried over ~ 2 g of sodium sulfate for 1 hour, then volume reduced to 2 ml and mixed with 200 µl of diazomethane for derivatization. After overnight incubation at RT, the derivatized extract was further cleaned using an acid silica gel column. The columns were prepared with 2 g of acid silica, 1 g of neutral silica, and a top layer of sodium sulfate. Prior to sample loading, the column was exhaustively rinsed with dichloromethane and hexane. After loading, the samples were eluted from the column with 40 mL of dichloromethane. Afterwards, the dichloromethane extract was evaporated and then solvent exchanged with hexane and subsequently evaporated to approximately 100 µL in volume and spiked with an internal standard (BDE-166) for analysis. Quantification of OH-BDEs in the hexane extract was by gas chromatography mass spectroscopy (GCMS) in the negative chemical ionization (NCI) mode using an Agilent 7890B / 5977A GCMS system. Calibration curves were made using authentic OH-BDE standards.

LC/MS-MS protein quantification. The procedure is similar as published in a prior paper with few modifications (Selwyn et al., 2015a). Briefly, the membrane proteins of the mouse livers were isolated using the Mem-PER plus membrane protein extraction kit (Pierce Biotechnology, Rockford, IL). The total membrane protein concentration was quantified using a bicinchoninic acid (BCA) kit, followed by digestion using an in-solution trypsin digestion kit (Pierce Biotechnology, Rockford, IL). Eighty µl of the tissue extract (2 mg/ml total protein) was mixed with 10 µl DTT (250 mM), 20 µl of 0.2 mg/ml bovine serum albumin, 10 µl of 10 mg/ml human serum albumin and 40 µl ammonium

bicarbonate buffer (100 mM, pH 7.8), and incubated at 95°C for 5 min (denaturation and reduction). Subsequently, 20 µl iodoacetamide (500 mM) was added and the sample was incubated for 30 min at ambient temperature in the dark (alkylation). Ice-cold methanol (0.5 ml), chloroform (0.1 ml) and water (0.4 ml) were added to each sample. After centrifugation at 16,000 *x g* for 5 min at 4°C, the upper and lower layer were removed and the pellet was washed with ice-cold methanol (0.5 ml) and centrifuged at 8,000 *x g* for 5 min at 4°C. The pellet was resuspended with 40 µl 50 mM ammonium bicarbonate buffer. Trypsin (20 µl) was added at 1:80 trypsin: protein ratio (w/w) and samples were incubated for 18 h at 37°C. Trypsin digestion was stopped by adding 10 µl of chilled quenching solvent (80% acetonitrile with 0.5% formic acid) and 30 µl heavy peptide internal standard, samples were centrifuged for 5 min at 4,000*xg* and 4°C, and supernatant was collected in LC-MS/MS vials. The stable isotope-labeled heavy peptides were used as internal standards (Thermo Fisher Scientific, Rockford, IL). LC-MS/MS consisted of an Acquity LC (Waters Technologies, Milford, MA) coupled to an AB Sciex Triple Quadrupole 6500 MS system (Framingham, MA). One to three surrogate peptides per protein were designed for the quantification of selected proteins (Supplemental Table 1) according to a previously published protocol (Vrana et al., 2017) (QPrOmics; www.qpromics.uw.edu/qpromics/assay/). The peptide separation was achieved on an Acquity UPLC column (HSS T3 1.8 µm, 2.1x100 mm, Waters, Hertfordshire, UK). Mobile phase A (water with formic acid 0.1%; v/v) and mobile phase B (acetonitrile with formic acid 0.1%; v/v) were used with a flow rate of 0.3 ml/min in a gradient manner. Peak integration and quantification were performed using Analyst (Version 1.6, Mass Spectrometry Toolkit v3.3, Framingham, MA, USA). A robust

strategy was used to ensure optimal reproducibility when quantifying these proteins, for example, ion suppression was addressed by using heavy peptide. Bovine serum albumin (BSA) was used as an exogenous internal standard, which was added to each sample to correct for protein loss during processing and digestion efficiency. In total, three-step data normalization was used; first average light peak areas for specific peptide daughter fragments were divided by corresponding average heavy peak areas. This ratio was further divided by BSA light/heavy area ratio. Data were further normalized to average quality control values (pooled representative sample). The protein abundance data are expressed as the mean (normalized to total protein) of the three biological replicates with standard error (SE).

Preparation of crude membrane and microsomal fractions (for enzyme activities). For isolation of crude membranes, livers were homogenized in Sucrose-Tris (ST) buffer (0.25 M sucrose, 10 mM Tris-HCl, pH 7.4) containing protease inhibitors (1:100, Sigma-Aldrich Corp., St. Louis, MO), and centrifuged at 100,000 x *g* for 60 min at 4°C. The resulting pellet constituted the crude membrane fraction and was re-suspended in ST buffer. For isolation of microsomes, homogenates were first centrifuged at 10,000 x *g* for 20 min at 4°C. The supernatant was then centrifuged at 100,000 x *g* for 60 min. ST buffer was used to re-suspend the microsomal pellet. Protein concentration was determined using the Qubit Protein Assay Kit (Thermo Fisher Scientific, Grand Island, NY).

Enzyme activity of Cyp1a, Cyp2b and Cyp3a in mouse liver microsomes. The Cyp1a, Cyp2b, and Cyp3a enzyme activities in liver microsomes from CV and GF mice were determined using a P450-Glo^{TM} Screening system (Promega, Madison, WI) as described previously . Briefly, a luminogenic P450-Glo^{TM} substrate (100 μM Luciferin-ME for Cyp1a, 3 μM Luciferin-2B6 for Cyp2b, or 3 μM Luciferin-IPA for Cyp3a) was incubated at 37°C with 10 μg of liver microsomal protein, control membrane, or positive P450 enzyme for 10 min. The reactions were initiated by adding the NADPH-regeneration system and incubated for 10 min. At the end of the incubation, an equal volume of the luciferin detection reagent (50 μl) was added at room temperature, and luminescence was quantified 20 min later using a Glomax^{TM} 96 Microplate Luminometer (Promega Corporation, Madison, WI). The magnitude of the light signal is dependent on and directly proportional to the amount of luciferin product generated by the P450 reaction.

Clustering analysis. A hierarchical clustering dendrogram (Ward's minimum variance method, distance scale) of the differentially expressed DPGs was generated based on their standardized mean FPKM values, using JMP Genomics software (SAS Institute, Inc., Cary, NC).

Statistical analysis. RNA-Seq data are expressed as mean FPKM ± S.E. Genes with mean FPKM value per treatment group lower than 1 in all groups were defined as not expressed in liver. Asterisks (*) represent significant differences between corn oil- and PBDE-treated groups of the same enterotypes of mice. Pounds (#) represent significant

differences between CV and GF mice under the same treatment. The mean FPKM and fold change of differentially regulated DPGs by gut microbiome or by PBDEs were summarized in Supplemental Table 2 and 3.

RESULTS

Dose-response of PBDE exposure on hepatic gene expression

To determine at which dose PBDEs produce more changes in DPG expression in livers of CV mice, CV mice were treated with vehicle, a low dose (10 μmol/kg), or a high dose (100 μmol/kg) of BDE-47 or BDE-99 as described in Fig. 1A (upper panel). The mRNAs of phase-I drug-metabolizing enzymes Cyp1a2 (prototypical AhR-target gene), Cyp2b10 (prototypical CAR-target gene), and Cyp3a11 (prototypical PXR-target gene) were quantified in livers of CV mice using RT-qPCR. As shown in Fig. 1B, Cyp1a2, Cyp2b10, and Cyp3a11 mRNAs were all up-regulated by BDE-47 and BDE-99 only at the high dose. Therefore, the high dose of PBDEs were selected for the GF mice treatment to compare the effect of the lack of gut microbiota on the regulation of DPGs in liver (Fig. 1A, lower panel).

Serum ALT and liver histology after PBDE exposure

To ensure that the doses used in this study did not produce any off-target effects due to liver injuries, serum ALT and liver histology were performed as shown in Supplemental Fig. 1. Serum ALT levels were within the normal range [between 4 and 36 IU/L at 37°C] in all treatment groups of CV and GF mice (Supplemental Fig. 1A). Consistent with the serum ALT data, H&E staining showed no apparent hepatic injuries

in livers of CV and GF mice treated with corn oil, BDE-47 or BDE-99 (Supplemental Fig. 1B).

Hydroxylated metabolites of PBDEs in livers of CV and GF mice

Sixteen hydroxylated metabolites of BDE-47 and BDE-99 were measured by PBDE targeted metabolomics (GC-MS-NCI) in livers of CV and GF mice treated with corn oil, BDE-47 (100 μmol/kg) or BDE-99 (100 μmol/kg) (Fig. 2). Total hepatic levels of PBDE hydroxylated metabolites were similar between CV and GF mice treated with the same PBDE congener (Fig. 2A). However, at equal molar dose, the total hydroxylated metabolites of BDE-99 were higher than those of BDE-47 in CV mice, whereas this difference was not observed in GF mice. This suggests that the bioavailability of BDE-99 is higher than BDE-47, which may be due to a combination of the host and microbiota effects, including different substrate specificities of the host transporters or P450s, or different microbial biotransformation pathways in gut microbiome that influence the absorption of the two PBDE congeners. Alternatively, this may also suggest that BDE-99 is more readily hydroxylated than BDE-47 due to substrate specificities and/or levels of preferred P450s.

Regarding individual hydroxylated metabolites of PBDEs (Fig. 2B), low levels of PBDE hydroxylated metabolites were detected in livers of CV mice treated with corn oil. These PBDE metabolites are likely a result of a background exposure to PBDEs from diet, bedding, and other environmental factors within the animal facility. Control GF mice appeared to have higher levels of many PBDE metabolites, although statistical significance was not achieved (Fig. 2B top panel). Following BDE-47 treatment (Fig. 2B

middle panel), 12 out of 16 PBDE hydroxylated metabolites were detected in livers of CV and GF mice. The major hydroxylated metabolite of BDE-47 was 5-OH-BDE-47 in livers of both CV and GF mice, with a higher level observed in GF conditions. Four minor BDE-47 metabolites were decreased in livers of GF mice as compared to livers of BDE-47 treated CV mice, including 4'-OH-BDE-17, 2'-OH-BDE-28, 3-OH-BDE-47, and 4'-OH-BDE-49. There was no difference for 6-OH-BDE-47 between BDE-47 treated CV and GF mice. Unexpectedly, although mice were treated exclusively with BDE-47 which contains 4 bromine atoms, there were low levels of other tetraBDEs (2'-OH-BDE-68 and 2'-OH-BDE-75) and also pentaBDEs (6-OH-BDE-85, 5'-OH-BDE-99, 4'-OH-BDE-101 and 4'-OH-BDE-103) detected in livers of BDE-47-treated CV and/or GF mice. Among these, 2'-OH-BDE-75, 6-OH-BDE-85, and 4'-OH-BDE-101 were increased in livers of GF mice compared with livers of BDE-47-treated CV mice. These hydroxylated tetraBDE and pentaBDE metabolites may come from the diet or other environmental sources. Following BDE-99 treatment (Fig. 2B bottom panel), 13 out of 16 hydroxylated PBDE metabolites were detected in livers of CV and GF mice. The major hydroxylated metabolite of BDE-99 was 5'-OH-BDE-99 in livers of both CV and GF mice, and it remained unchanged between CV and GF conditions. Four minor BDE-99 hydroxylated metabolites were decreased in livers of GF mice as compared to livers of BDE-99 treated CV mice, including 4'-OH-BDE-49, 6-OH-BDE-85, 4'-OH-BDE-101, and 4'-OH-BDE-103. There was no difference for 6'-OH-BDE-99 between BDE-99 treated CV and GF mice. In addition, very low amounts of tetraBDEs (4'-OH-BDE-17, 5-OH-BDE-47, 6-OH-BDE-47, 2'-OH-BDE-68, 2'-OH-BDE-75) and pentaBDEs (3-OH-BDE-100 and 5'-OH-BDE-100) were detected in livers of BDE-99 treated CV and GF mice. Chemical

structures of individual BDE-47 and BDE-99 metabolites, especially the major metabolite and the metabolites that were altered in GF condition, were plotted using ChemDoodle and are shown in Fig. 3. In summary, the lack of gut microbiota modifies the bioavailability and the hepatic metabolism of PBDEs. Divergent regulatory patterns were observed regarding individual hydroxylated PBDE metabolites between CV and GF conditions, indicating the involvement of multiple P450s that are divergently regulated by gut microbiota in PBDE hepatic oxidative metabolism.

To determine the role of the gut microbiome on hepatic transcriptome that is likely to be involved in PBDE metabolism and disposition, the expression of various phase-I (Cyp1, 2, and 3 family members, which are critically involved in xenobiotic metabolism) and phase-II drug metabolizing enzymes (Ugts, Sults, and Gsts), as well as transporters (Slco and Abcc family members) was examined. Only DPGs that were differentially expressed by PBDEs or by the lack of gut microbiome are shown in Figures 4-7. DPGs were plotted separately to better visualize the fold changes, and plotted together to compare the absolute abundance within the same family/subfamily.

Regulation of hepatic Cyp1 and Cyp2a-c genes by BDE-47 and BDE-99 in CV and GF mice

For the Cyp1 family, both Cyp1a1 and Cyp1a2 were differentially regulated by PBDEs (Fig. 4A), whereas Cyp1b1 remained unchanged (data not shown). Cyp1a2 was the predominant Cyp1 isoform that was much more abundantly expressed in the liver as compared to Cyp1a1. Under basal conditions, Cyp1a1 mRNA remained unchanged between CV and GF mice, whereas the lack of gut microbiome lead to a

moderate increase in the constitutive expression of Cyp1a2 mRNA (1.62-fold). In livers of CV mice, BDE-47 did not alter Cyp1a1 mRNA expression, but up-regulated Cyp1a2 mRNA (2.26-fold); whereas in livers of GF mice, BDE-47 did not alter the mRNAs of Cyp1a1 or Cyp1a2. In livers of CV mice, BDE-99 did not alter the mRNAs of Cyp1a1 or 1a2, however, it markedly increased the mRNAs of both Cyp1a1 (2.22-fold) and 1a2 (2.45-fold) in livers of GF mice, suggesting that the lack of gut microbiome augmented BDE-99 mediated up-regulation of Cyp1a1 and Cyp1a2 mRNAs in mouse liver.

For the Cyp2a subfamily, Cyp2a4, 2a5, and 2a22 were differentially regulated by PBDEs in liver, among which Cyp2a5 mRNA was the highest expressed isoform in all treatment groups (Fig. 4B). Lack of gut microbiome had no effect on the basal expression of these Cyp2a isoforms. In livers of CV mice, BDE-47 markedly increased the mRNAs of Cyp2a4 (2.87-fold) and 2a5 (2.86-fold); whereas in livers of GF mice, BDE-47 also increased the mRNAs of Cyp2a4 (3.47-fold) and 2a5 (3.10-fold), with higher fold-increase in Cyp2a4 mRNA as compared to BDE-47 treated CV mice. Cyp2a22 mRNA was not altered by BDE-47 in livers of CV mice, but was up-regulated by BDE-47 in livers of GF mice as compared to GF control group (1.62-fold), suggesting that the lack of gut microbiome augmented BDE-47-mediated up-regulation of Cyp2a22 in mouse liver. In livers of CV mice, BDE-99 increased the Cyp2a5 mRNA (3.82-fold) and tended to increase Cyp2a4 mRNA (3.58-fold, although a statistical significance was not achieved), but slightly decreased the mRNA of Cyp2a22 (15.75%). In livers of GF mice, the mRNA fold-increases were much greater for BDE-99-mediated up-regulation of Cyp2a4 (10.09-fold) and 2a5 (10.23-fold), whereas Cyp2a22 mRNA remained unchanged. In summary, BDE-99 had a more prominent effect than BDE-47 on the up-

regulation of Cyp2a4 and Cyp2a5 mRNAs in GF condition; lack of gut microbiome augmented BDE-47 mediated up-regulation of Cyp2a4 and Cyp2a22; and also augmented BDE-99-mediated up-regulation of Cyp2a4 and 2a5 in mouse liver.

For the Cyp2b subfamily, Cyp2b9, 2b10, and 2b13 were differentially regulated by PBDEs in liver and all of them were lowly expressed under basal conditions in CV mice. The lack of gut microbiome resulted in a constitutive increase in the basal mRNA expression of Cyp2b9 (2.59-fold) and 2b13 (3.69-fold) (Fig. 4B). In livers of CV mice, BDE-47 up-regulated the mRNAs of both Cyp2b10 (18.84-fold) and 2b13 (14.38-fold), and such up-regulation was also observed in livers of GF mice (22.41-fold for Cyp2b10 and 12.71-fold for Cyp2b13). The BDE-47 mediated up-regulation of Cyp2b13 was greater in livers of GF mice as compared to BDE-47 treated CV mice. Interestingly, BDE-47 decreased Cyp2b9 mRNA in CV conditions (45.20%) but this pattern was reversed in GF conditions as evidenced by a 3.22-fold increase in Cyp2b9 mRNA in livers of BDE-47 treated GF mice. In livers of CV mice, BDE-99 markedly increased the mRNAs of Cyp2b10 (29.40-fold) and Cyp2b13 (22.22-fold), and such up-regulation was also observed in livers of GF mice (53.56-fold for Cyp2b10 and 10.08-fold for Cyp2b13). The BDE-99 mediated up-regulation of Cyp2b10 was greater in GF mice as compared to BDE-99 treated CV mice. BDE-99 did not alter the Cyp2b9 mRNA in CV or GF conditions as compared to the control group of the same enterotype. In summary, the lack of gut microbiome increased the basal expression of Cyp2b9 and 2b13 mRNAs, and reversed the BDE-47-mediated regulatory pattern of Cyp2b9 mRNA; BDE-99 appeared to have a more prominent effect than BDE-47 on the mRNA expression of Cyp2b10, which is the highest expressed Cyp2b isoform under treatment conditions; the

lack of gut microbiome augmented BDE-47 mediated up-regulation of Cyp2b9 and Cyp2b13, and also augmented BDE-99 mediated up-regulation of Cyp2b10 in mouse liver.

For the Cyp2c subfamily, 12 Cyp2c members (Cyp2c29, Cyp2c37, Cyp2c38, Cyp2c39, Cyp2c40, Cyp2c50, Cyp2c54, Cyp2c55, Cyp2c67, Cyp2c68, Cyp2c69 and Cyp2c70) were differentially regulated by PBDEs in liver, among which Cyp2c29 mRNA was the highest expressed isoform under basal and treatment conditions, followed by Cyp2c50, and Cyp2c37 and 2c54 at similar levels (Fig. 4C). Under basal conditions, the lack of gut microbiome led to a constitutive increase in the basal mRNA expression of Cyp2c40 (2.38-fold), Cyp2c50 (1.61-fold), Cyp2c54 (1.96-fold), Cyp2c67 (1.99-fold), Cyp2c68 (1.81-fold), Cyp2c69 (2.77-fold), and Cyp2c70 (2.15-fold); whereas other Cyp2c isoforms remained unchanged (Fig. 4C). In livers of CV mice, BDE-47 up-regulated the mRNAs of most Cyp2c isoforms, including Cyp2c29 (3.22-fold), Cyp2c37 (2.50-fold), Cyp2c39 (2.21-fold), Cyp2c50 (2.56-fold), Cyp2c54 (2.52-fold), and Cyp2c55 (13.45-fold). The BDE-47 mediated up-regulation was also observed in livers of GF mice (3.00-fold for Cyp2c29, 2.51-fold for Cyp2c37, 2.23-fold for Cyp2c50, 1.87-fold for Cyp2c54, and 15.88-fold for Cyp2c55). Compared to BDE-47 treated CV mice, BDE-47 treated GF mice had higher hepatic levels of Cyp2c37 and 2c54, indicating a augmentation effect of BDE-47 due to lack of gut microbiota. In livers of CV mice, BDE-99 increased the mRNAs of Cyp2c29 (3.44-fold), Cyp2c37 (2.73-fold), Cyp2c39 (2.51-fold), Cyp2c50 (2.70-fold), Cyp2c54 (2.73-fold), and Cyp2c55 (18.68-fold). The BDE-99 mediated up-regulation was also observed in livers of GF mice (3.13-fold for Cyp2c29, 3.91-fold for Cyp2c37, 3.74-fold for Cyp2c50, 2.91-fold for Cyp2c54, and 52.83-fold for

Cyp2c55). BDE-99 slightly down-regulated the mRNAs of Cyp2c40 (14.74%) and Cyp2c69 (8.90%) in livers of CV mice, and such down-regulation was also observed in livers of GF mice (22.37% for Cyp2c40 and 31.11% for Cyp2c69). The lack of gut microbiome augmented the BDE-99 mediated mRNA increase in Cyp2c37, 2c40, 2c50, 2c54, and 2c55, as compared to BDE-99 treated CV mice. In summary, the lack of gut microbiome increased the basal expression of many Cyp2c isoforms; BDE-99 appeared to have a more prominent effect than BDE-47 on the mRNA expression of Cyp2c37, 2c50, 2c54, and 2c55; and the lack of gut microbiome augmented PBDE mediated up-regulation of many Cyp2c isoforms in mouse livers.

Regulation of hepatic Cyp2d, Cyp2e1, Cyp2g1, Cyp2j9 and Cyp2r1 genes by BDE-47 and BDE-99 in CV and GF mice

For the Cyp2d subfamily, eight Cyp2d family members (Cyp2d9, Cyp2d10, Cyp2d11, Cyp2d12, Cyp2d13, Cyp2d26, Cyp2d34, and Cyp2d40) were differentially regulated by PBDEs in liver (Fig. 5A). Among these Cyp2d isoforms, Cyp2d9, 2d10, and 2d26 were the most abundantly expressed in general. The lack of gut microbiome had no effect on the basal expression of these Cyp2d isoforms. In livers of CV mice, BDE-47 had minimal effect on the mRNA expression of Cyp2d9, 2d10, 2d11, 2d12, 2d26, 2d34 and 2d40, but markedly decreased Cyp2d13 mRNA (42.66%); whereas in livers of GF mice, BDE-47 decreased Cyp2d40 mRNA (26.47%). Compared to BDE-47 treated CV mice, BDE-47 treated GF mice had lower hepatic expression of Cyp2d9, 2d11, and 2d12. In livers of CV mice, BDE-99 down-regulated the mRNAs of Cyp2d11 (12.08%), Cyp2d13 (40.34%), and Cyp2d34 (12.12%). BDE-99 also down-regulated Cyp2d11 (35.58%)

and Cyp2d34 (17.86%) in livers of GF mice, but reversed the down-regulation pattern for Cyp2d13, evidenced by a 1.59-fold mRNA increase in GF conditions. In addition, in livers of GF mice, BDE-99 decreased the mRNAs of Cyp2d9 (28.10%), 2d10 (27.41%), 2d12 (29.47%), 2d26 (45.16%), and 2d40 (54.63%). The lack of gut microbiome augmented BDE-99 mediated down-regulation of Cyp2d11, 2c12, 2d34, and 2d40, but also augmented the BDE-99 mediated up-regulation of Cyp2d13. In summary, the lack of gut microbiome had no effect on the basal expression of Cyp2d isoforms; whereas PBDEs tended to down-regulate certain Cyp2d isoforms in either CV or GF conditions, except for Cyp2d13 which was up-regulated in livers of BDE-99 treated GF mice. BDE-99 in general had a more prominent effect than BDE-47 on the regulation of most Cyp2d isoforms.

For the Cyp2e1, Cyp2g1, Cyp2j9, and Cyp2r1 genes, under basal conditions, the lack of gut microbiome increased the mRNAs of Cyp2e1 (1.67-fold) and Cyp2g1 (2.33-fold), but decreased Cyp2j9 mRNA (62.55%). In livers of CV mice, BDE-47 markedly increased Cyp2g1 mRNA (3.25-fold) and decreased Cyp2j9 mRNA (64.05%), but had no effect on Cyp2e1 and Cyp2r1. In livers of GF mice, BDE-47 had minimal effect on the mRNA expression of Cyp2e1, Cyp2g1, Cyp2j9, and Cyp2r1. No difference was observed for their mRNA abundances between BDE-47 treated CV and GF mice. In livers of CV mice, BDE-99 increased the mRNAs of Cyp2g1 (4.49-fold) and Cyp2r1 (1.61-fold), and tended to increase their mRNAs in GF mice, although a statistical significance was not achieved. Interestingly, BDE-99 decreased Cyp2j9 mRNA in CV conditions (48.87%) but this pattern was reversed in GF conditions as evidenced by an increase in its mRNA (2.36-fold).

Regulation of hepatic Cyp3a genes by BDE-47 and BDE-99 in CV and GF mice

For the Cyp3a subfamily, eight Cyp3a family members (Cyp3a11, Cyp3a13, Cyp3a16, Cyp3a25, Cyp3a41a, Cyp3a41b, Cyp3a44, and Cyp3a59) were differentially regulated by PBDEs in liver, among which Cyp3a11 mRNA was the highest expressed isoform (Fig. 5B). Under basal conditions, the lack of gut microbiome led to a dramatic decrease of most Cyp3a isoforms, including Cyp3a11 (89.69%), Cyp3a16 (91.13%), Cyp3a41a (89.82%), Cyp3a41b (89.96%), Cyp3a44 (87.75%), and Cyp3a59 (56.16%). In livers of CV mice, BDE-47 increased the mRNAs of Cyp3a11 (1.55-fold), Cyp3a16 (1.57-fold), Cyp3a41a (1.48-fold), and Cyp3a41b (1.46-fold), and such up-regulation was further increased in GF conditions (6.78-fold for Cyp3a11, 7.87-fold for Cyp3a16, 7.12-fold for Cyp3a41a, and 7.12-fold for Cyp3a41b). In livers of GF mice, BDE-47 also increased the mRNAs of Cyp3a44 (6.63-fold) and Cyp3a59 (2.74-fold), indicating the augmentation effect of GF conditions in BDE-47 mediated transcriptional regulation. In livers of CV mice, BDE-99 increased the mRNAs of Cyp3a13 (2.33-fold) and Cyp3a59 (1.50-fold), whereas the lack of gut microbiota augmented the BDE-99 mediated mRNA increase of Cyp3a11 (10.96-fold), 3a16 (10.54-fold), 3a25 (3.48-fold), 3a41a (9.34-fold), 3a41b (9.34-fold), 3a44 (8.53-fold), and Cyp3a59 (6.42-fold). In summary, the lack of gut microbiome resulted in a constitutive decrease in the basal mRNA expression of most Cyp3a isoforms, and also augmented PBDE-mediated transcriptional increase of many Cyp3a isoforms in mouse liver.

Regulation of hepatic Ugts by BDE-47 and BDE-99 in CV and GF mice

For the Ugt family, Ugt2b1, Ugt2b5, Ugt2b34, Ugt2b35, Ugt2b36, Ugt2b37, Ugt2b38, UDP-glucose 6-dehydrogenase (Ugdh), and UDP-glucose pyrophosphorylase 2 (Ugp2) were differentially regulated by PBDEs in liver (Fig. 6A). Ugdh and Ugp2 are enzymes involved in the synthesis of cosubstrates for phase-II glucuronidation reaction. Ugp2 catalyzes the synthesis from glucose-1-phosphate to UDP-glucose, and Ugdh converts UDP-glucose to UDPGA, which is the cosubstrate for UDP-glucuronidation. Lack of gut microbiome had minimal effect on the basal expression of these genes. In livers of CV mice, BDE-47 increased the mRNAs of Ugt2b1 (1.61-fold), Ugt2b5 (1.34-fold), Ugt2b34 (1.38-fold), and Ugt2b35 (1.37-fold), and the up-regulation of Ugt2b34 and Ugt2b35 were also observed in GF mice (1.76-fold for Ugt2b34 and 1.77-fold for Ugt2b35). BDE-47 also increased Ugdh mRNA in livers of GF mice (1.82-fold). In livers of CV mice, BDE-99 increased the mRNAs of Ugt2b34 (1.85-fold), Ugt2b35 (1.79-fold), and Ugt2b37 (1.25-fold); whereas in livers of GF mice, BDE-99 markedly increased the mRNAs of Ugt2b1 (2.60-fold), 2b5 (2.40-fold), 2b34 (3.60-fold), 2b35 (3.94-fold), 2b36 (2.40-fold), 2b38 (2.63-fold), Ugdh (4.91-fold), and Ugp2 (2.05-fold), and tended to increase Ugt2b37 (statistical significance was not achieved). Under BDE-99 treated conditions, the lack of gut microbiome lead to a greater fold increase of the mRNAs of Ugt2b1, 2b35, 2b38, as well as Ugdh and Ugp2, suggesting that it augmented BDE-99-mediated up-regulation of these genes in mouse liver.

Regulation of hepatic Sults by BDE-47 and BDE-99 in CV and GF mice

For the Sult family, Sult1a1, Sult1b1, Sult1c2, Sult1d1, Sult1e1, Sult2a1, Sult2a2, Sult2a7, Sult5a1, and 3'- Phosphoadenosine 5'-phosphosulfate synthase 2 (Papss2)

were differentially regulated by PBDEs in liver, among which Sult1a1 mRNA was the highest expressed isoform (Fig. 6B). Papss2 catalyzes the synthesis of 5'-phosphoadenosine-5'-phosphosulfate (PAPS), the sulfate donor for all Sulfation reactions. Under basal conditions, the lack of gut microbiome increased the mRNAs of Sult1a1 (1.57-fold) and Sult1b1 (1.74-fold), but decreased Papss2 mRNA (54.13%). In livers of CV mice, BDE-47 increased the mRNAs of Sult1c2 (1.62-fold) and Sult5a1 (1.74-fold); whereas in livers of GF mice, BDE-47 increased the mRNAs of Sult1c2 (2.52-fold), Sult2a1(24.13-fold), and Sult2a2 (25.39-fold). Compared to BDE-47 treated CV mice, BDE-47 treated GF mice had higher levels of Sult1a1, 1b1, 1d1, 1e1, and 2a2. In livers of CV mice, BDE-99 increased the mRNAs of Sult1c2 (2.20-fold), Sult1d1 (1.68-fold), and Sult2a7 (2.38-fold); whereas in livers of GF mice, BDE-99 increased the mRNAs of Sult1c2, Sult1d1, Sult1e1, and Papss2 (2.70-fold for Sult1c2, 4.17-fold for Sult1d1, 15.48-fold for Sult1e1, and 3.12-fold for Papss2), but decreased the mRNA of Sult2a1 (99.64%). Compared to BDE-99 treated CV mice, BDE-99 treated GF mice had higher levels of Sult1a1, 1b1, 1d1, 1e1, and Papss2. In summary, the lack of gut microbiome increased the basal expression of Sult1a1 and Sult1b1, but decreased Papss2; the lack of gut microbiome augmented BDE-47 mediated up-regulation of Sult2a2, and augmented BDE-99 mediated up-regulation of Sult1d1, Sult1e1, and Papss2 in mouse livers.

Regulation of hepatic Gsts by BDE-47 and BDE-99 in CV and GF mice

For the Gst family, Gsta1, Gsta2, Gsta4, Gstk1, Gstm1-m7, Gstp1, Gstp2, Gstt2, Gstt3, Gstz1, and Gclc were differentially regulated by PBDEs in liver, among which

Gstm1 was the highest expressed isoform (Fig. 7A). Under basal conditions, the lack of gut microbiome increased the basal mRNAs of Gstm2 (1.76-fold) and Gstm6 (1.45-fold). In livers of CV mice, BDE-47 markedly increased the mRNAs of Gsta1 (3.04-fold), Gsta2 (1.48-fold), Gsta4 (1.69-fold), Gstm1 (2.03-fold), Gstm2 (1.49-fold), Gstm3 (2.86-fold), Gstm4 (1.96-fold), Gstp1 (1.71-fold), and Gstp2 (1.72-fold), and Gstt3 (1.86-fold). In livers of GF mice, BDE-47 also increased the mRNAs of many Gst isoforms (4.55-fold for Gsta1, 2.82-fold for Gsta2, 2.20-fold for Gsta4, 2.54-fold for Gstm1, 5.24-fold for Gstm3, 2.16-fold for Gstm4, and 2.56-fold for Gstt3). However, the BDE-47 mediated mRNA increase in Gstm2, Gstp1, and Gstp2 was gut microbiota-dependent. Conversely, BDE-47 mediated mRNA increase in Gsta2, m3, and t3 was augmented by lack of gut microbiota. In livers of CV mice, BDE-99 up-regulated Gsta1 (4.14-fold), Gstm2 (1.97-fold), Gstm3 (4.12-fold), Gstm4 (1.74-fold), Gstt3 (1.98-fold), and such up-regulation was also observed in GF mice (19.15-fold for Gsta1, 3.25-fold for Gstm2, 18.41-fold for Gstm3, 3.12-fold for Gstm4, and 3.19-fold for Gstt3). In GF mice, BDE-99 also up-regulated the mRNAs of Gsta2 (4.93-fold), Gstm1 (3.84-fold), and Gclc (2.70-fold), but down-regulated the mRNAs of Gstk1 (31.12%) and Gstz1 (32.33%). The lack of gut microbiota augmented the BDE-99 mediated mRNA increase in Gsta1, Gsta2, Gstm2, Gstm3, Gstt3, and Gclc, and the mRNA decrease in Gstk1 and Gstz1. In summary, the lack of gut microbiome increased the basal expression of Gstm2 and Gstm6; lack of gut microbiome augmented BDE-47 mediated up-regulation of Gsta2, Gstm3, and Gstt3, and augmented BDE-99 mediated up-regulation of Gsta1, Gsta2, Gstm2, Gstm3, Gstt3, and Gclc.

Regulation of hepatic uptake transporters by BDE-47 and BDE-99 in CV and GF mice

For the solute carrier organic anions (Slco) uptake transporters, Slco1a1, Slco1a4, Slco1b2, and Slco2a1 were differentially regulated in liver, among which Slco1b2 was the highest expressed isoform (Fig. 7B). The lack of gut microbiome had no effect on the basal mRNAs of these Slco isoforms. In livers of CV mice, BDE-47 had minimal effect on the mRNAs of Slco1a1, 1a4, 1b2, and 2a1; whereas in livers of GF mice, BDE-47 increased Slco1a4 mRNA (1.74-fold). BDE-99 also did not affect the mRNAs of these Slco transporters in liver of CV mice, however, in livers of GF mice, BDE-99 increased the mRNAs of Slco1a4 (3.11-fold) and Slco1b2 (2.69-fold), but slightly decreased Slco2a1 (20.72%). In summary, lack of gut microbiota augmented PBDE-mediated (and especially BDE-99 mediated) transcriptional changes of these hepatic uptake transporters.

Regulation of hepatic efflux transporters by BDE-47 and BDE-99 in CV and GF mice

For the ATP-binding cassette (Abc) efflux transporters, Abcb1a, Abcb1b, Abcc2, Abcc3, Abcc4, and Abcc10 were differentially regulated in liver, among which Abcc3 was the highest expressed isoform (Fig. 7B). Under basal conditions, the lack of gut microbiome decreased the constitutive mRNA expression of Abcb1a (41.23%) and Abcc10 (57.60%). BDE-47 increased the mRNAs of Abcb1b (1.32-fold), Abcc3 (1.42-fold), and Abcc4 (1.82-fold), but decreased Abcc10 mRNA (53.27%) in liver, all in a gut microbiome dependent manner. In livers of CV mice, BDE-99 increased Abcc4 mRNA

(2.43-fold), and such up-regulation was also observed in GF mice (3.91-fold). Conversely, BDE-99 decreased Abcc10 mRNA in CV conditions (44.81%) and this pattern was reversed in GF conditions as evidenced by an increase in its mRNA (2.21-fold) by BDE-99 treatment. The lack of gut microbiota also augmented the BDE-99 mediated increase in the mRNAs of Abcc2 (2.97-fold) only in livers of GF mice. In summary, the lack of gut microbiome decreased the basal mRNAs of Abcb1a and Abcc10; the BDE-47 mediated up-regulation of Abcb1b, Abcc3, and Abcc4 depended on the presence of gut microbiota, whereas the lack of gut microbiome augmented BDE-99 mediated up-regulation of Abcc2, and reversed BDE-99 mediated regulatory pattern on the expression of Abcc10 in mouse liver.

As shown in Fig. 8, a two-way hierarchical clustering dendrogram of the mean FPKM values revealed 4 distinct patterns of the 86 DPGs that were differentially expressed and summarized in Figures 1 through 7. PBDEs appeared to have a more prominent effect than enterotypes in modulating the expression of these genes, evidenced by a greater separation between vehicle-treated vs. PBDE-treated groups and CV control vs. GF control groups, BDE-99 appeared to have a more prominent effect than BDE-47 in the differential expression of these DPGs. Genes in Pattern I (39 DPGs) were sensitized to BDE-99 mediated differential regulation due to the lack of gut microbiota. Genes in Pattern II (12 DPGs) were sensitized to BDE-47 mediated differential regulation due to lack of gut microbiota. Genes in Pattern III (14 DPGs) were affected more by enterotypes, because they were in general up-regulated in livers of GF mice under both basal and PBDE-treated conditions. Conversely, Genes in Pattern IV (21 DPGs) were in general down-regulated in livers of GF mice. For example, many Cyp3a

and Cyp2d subfamily members were down-regulated in GF mice under both control and PBDE-treated conditions (Fig. 8). In summary, both PBDEs (to a greater extent) and enterotypes (to a lesser extent) regulate the expression of DPGs in liver. The gut microbiome-dependent effect and germ free augmentation effect are summarized in Table 1, which is complimentary to Figure 8 as it displays the differentially regulated DPGs per category (namely Phase-I, Phase-II, and transporters), and also highlights three distinct regulatory patterns, namely 1) genes that were regulated by gut microbiota under basal conditions (category A); 2) genes that were regulated by PBDEs in a gut microbiome-dependent manner (category B); and 3) genes that were regulated by PBDEs in the absence of gut microbiome (category C). Information between Figure 8 and Table 1 can be cross-referenced, for example, genes in pattern I (Fig. 8) were up-regulated to a greater extent by BDE-99 due to lack of gut microbiome. The majority of these genes also belong category C in Table 1 (augmentation effect due to lack of gut microbiome), including Cyp1a1, Cyp1a2, Cyp2a4, Cyp2a5, Cyp2b10, Cyp2cs, Ugt2bs, Slco1a4, Slco1b2, Abcc10 and etc. Similarly, genes in pattern II (Fig. 8) were up-regulated to a greater extent by BDE-47 effect due to lack of gut microbiome, and they were also shown in category C of Table 1, including Cyp2a22, Sult2a2, Cyp2b13, Cyp2b9 and etc. Genes in Pattern III (Fig. 8) were affected more by enterotype and were generally up-regulated in livers of GF mice. These genes were shown in category A of Table 1, such as Cyp2c40, Cyp2c69, Cyp2c67, Cyp2c68, Cyp2e1, Gstm6, and Sult1a1. Genes in Pattern IV (Fig. 8) were in general down-regulated in livers of GF mice, such as Gstp1, Gstp2, and Sult5a1, and these genes also belong to category B of Table 1 (gut microbiome-dependent effect).

LC-MS/MS proteomic quantification of Cyp1a2 and Cyp3a11 in CV and GF mouse livers

The hepatic Cyp1a2 and Cyp3a11 proteins in CV and GF mice were further quantified by a LC-MS/MS proteomic approach as described in Materials and Methods. These two proteins were quantified based on either their importance in drug-processing or availability of surrogate peptides. As shown in Fig. 9A, Cyp1a2 protein was not altered by BDE-47, however, it was increased by BDE-99 in both CV and GF mice, with a greater effect observed in GF conditions (1.70-fold in CV mice, 3.09-fold in GF mice). Compared to BDE-99 treated CV mice, the lack of gut microbiome augmented BDE-99 mediated up-regulation of Cyp1a2 protein expression in GF mouse livers (1.62-fold). Consistent with the literature (Selwyn et al., 2015d), the constitutive level of Cyp3a11 protein was down-regulated by the lack of gut microbiome (decreased 91.27%). Interestingly, in livers of GF mice, both BDE-47 and BDE-99 up-regulated or restored Cyp3a11 protein level, with a greater effect observed for BDE-99 (6.05-fold by BDE-47, and 10.00-fold by BDE-99). However, the increased Cyp3a11 protein in GF mice under BDE-47 treatment was still lower than its vehicle control level in CV mice (43.10% lower). As for BDE-99 effect, there was no significant difference between CV and GF mice. These observations suggested that at the given dose, BDE-99 is more effective than BDE-47 in up-regulating Cyp3a11 protein expression under GF conditions (Fig. 9A).

Enzyme activities of Cyp1a, Cyp2b, and Cyp3a in CV and GF mouse livers

Because the importance of Cyp1, Cyp2 and Cyp3 enzymes in xenobiotic metabolism and their dramatic changes induced by PBDE in CV and GF mice, the enzyme activities of Cyp1a, Cyp2b, and Cyp3a were quantified in CV and GF mice treated with corn oil, BDE-47 or BDE-99 (Fig. 9B). Under control conditions, Cyp1a enzyme activity increased 1.68-fold in GF mice, and this was consistent with the basal mRNA increase of Cyp1a2 (Fig. 4A). Although Cyp1a2 mRNA was up-regulated by BDE-47 in livers of CV mice (Fig. 4A), Cyp1a2 protein and Cyp1a activity was not altered by BDE-47 in livers of CV mice. The discrepancies of Cyp1a2 mRNA, protein and activity by BDE-47 could be due to post-transcriptional modification such as the production of microRNAs, which are known to simultaneously inhibit mRNA translation into protein. In livers of CV mice, Cyp1a2 mRNA also tended to be up-regulated by BDE-99, followed by the increased expression of Cyp1a2 protein (Fig. 9A). However, Cyp1a activity was not altered by BDE-99 in livers of CV mice, suggesting the presence of post-translational modification that regulate protein degradation. In livers of GF mice, Cyp1a2 mRNA and protein were both up-regulated by BDE-99. However, Cyp1a activity was decreased by both BDE-47 (24.13%) and BDE-99 (68.18%) in livers of GF mice, suggesting that there may be extensive post-translational down-regulation of Cyp1a gene expression to prevent the induction of Cyp1a activity in GF conditions.

Under control conditions, Cyp2b enzyme activity increased 1.64-fold in GF mice, and this correlates with the basal mRNA increase in Cyp2b9 and 2b13, but not Cyp2b10 (Fig. 4B). In livers of CV mice, Cyp2b10 mRNA was up-regulated by both BDE-47 and BDE-99 (Fig. 4B). Expectedly, Cyp2b enzyme activity was increased by BDE-99 (3.26-fold), and tended to be increased by BDE-47 (although a statistical significance was not

achieved) (Fig. 9B). In livers of GF mice, Cyp2b enzyme activity was increased by BDE-47 (2.51-fold), and this correlates with a greater fold-increase in the mRNAs of Cyp2b9 and Cyp2b13 in BDE-47 treated GF mice, but not with the Cyp2b10 data which were equally up-regulated by BDE-47 between CV and GF conditions (Fig. 4B). Therefore, surprisingly, the major Cyp2b isoform Cyp2b10 did not appear to contribute to the PBDE-mediated increase in Cyp2b enzyme activities, and the minor Cyp2b isoforms Cyp2b9 and 2b13 may be more important in contributing the overall increase in the Cyp2b enzyme activities following PBDE exposure.

Regarding Cyp3a enzyme activities, in livers of CV mice, Cyp3a11 mRNA was moderately up-regulated by BDE-47 (Fig. 5B), however, its protein and enzyme activity was not altered by PBDEs, suggesting the involvement of post-transcriptional modification mechanisms that may suppress the expression and activity of Cyp3a11. In livers of GF mice, consistent with the mRNA and proteomic data (Fig. 5B and Fig. 9A), Cyp3a activity was markedly decreased by the lack of gut microbiome in the control group (79.57%). Following PBDE exposure, consistent with mRNA and proteomics data, the lack of gut microbiota markedly augmented PBDE-mediated increase in Cyp3a enzyme activities (BDE-47: 6.78-fold increase; BDE-99: 6.08-fold increase) (Fig. 9B).

DISCUSSION

The present study has unveiled a novel interaction between the gut microbiome and host DPGs on the metabolism of BDE-47 and BDE-99 in CV and GF mice. A systematic comparison of the hepatic DPGs expression between CV and GF mice has revealed three notable findings: 1) under basal condition, the lack of gut microbiome

displays divergent regulatory patterns on DPGs expression, with a marked up-regulation of Cyp2c genes (e.g. Cyp2c40, Cyp2c50, Cyp2c54, Cyp2c67, Cyp2c68, Cyp2c69 and Cyp2c70), and a marked down-regulation of Cyp3a genes (e.g. Cyp3a11, Cyp3a16, Cyp3a41a, Cyp3a41b, Cyp3a44, and Cyp3a59); 2) the lack of gut microbiome abolishes PBDE-mediated up- or down-regulation of certain DPGs as observed in CV mice, suggesting that the expression of these DPGs is gut microbiome dependent. For example, the up-regulation of Ugt2b1, Ugt2b5, Sult5a1, Gstp1, Gstp2, Abcb1b, Abcc3 and Abcc4 by BDE-47 is only observed with the presence of gut microbiome in livers of CV mice but not in GF mice. Similarly, the down-regulation of Abcc10 by BDE-47 is only observed in CV mice but not in GF mice; 3) the lack of gut microbiome potentiates PBDE-mediated alterations on some DPGs expression in mouse liver. For example, many Cyp2 family members (such as Cyp2a5, Cyp2b10, Cyp2c37, Cyp2c50, Cyp2c54, and Cyp2c55) are up-regulated by BDE-99 in livers of both CV and GF mice, with a much greater fold-change observed in GF condition (Table. 1).

Intestinal microbiota can regulate certain host DPGs (Selwyn et al., 2015d). In this study, the lack of gut microbiome up-regulates Cyp1a2, Cyp2b9, Cyp2c40, Cyp2c50, Cyp2c54, Cyp2c67, Cyp2c68, Cyp2c69, Sult1a1, and Sult1b1, but down-regulates Cyp3a11, Cyp3a16, Cyp3a44, and Cyp3a59 in livers of GF mice, which are consistent with previous reports in adult male GF mice by RNA-Seq (Selwyn et al., 2015a; Selwyn et al., 2015d). The observations of up-regulated Cyp2b9 and Cyp2b13 and down-regulated Cyp3a subfamily by the lack of gut microbiome are also consistent with findings from two other groups (Bjorkholm et al., 2009; Toda et al., 2009; Selwyn et al., 2015b). Although previous study has shown decreased Cyp1a2, Cyp2b9, and Cyp2b13

mRNAs in GF mice as compared to CV mice (Toda et al., 2009), in the present study, these genes appeared to be up-regulated in livers of GF mice. Toda et al also showed decreased mRNAs of Sult1d1 and Abcc3 in GF mice (Toda et al., 2009), however, in the present study the mRNA levels of Sult1d1 and Abcc3 remained the same in GF and CV mice. These discrepancies are likely due to differences in the strain of mice (IQI GF mice vs C57BL/6J GF mice) and experimental conditions. Additionally, the observations of up-regulated Cyp2g1, and down-regulated Cyp2j9, Cyp3a41b, Papss2 and Abcc10 by the lack of gut microbiome has not been reported previously.

The present study has added new knowledge to the existing paradigm regarding the role of gut microbiome in xenobiotic metabolism. It is known that PBDEs can modulate the expression of the prototypical target genes of CAR (mouse Cyp2b10 and human CYP2B6) and PXR (mouse Cyp3a11 and human CYP3A4) in mouse liver and human hepatocyptes (Erratico et al., 2012; Sueyoshi et al., 2014). The present study provides the first evidence showing that the lack of gut microbiome can modify PBDE-mediated alterations on DPGs expression in mouse liver. For example, the lack of gut microbiome abolishes BDE-47 mediated up-regulation of Cyp1a2, Ugt2b1, Ugt2b5, Sult5a1, Gstp1, Gstp2, Abcc3, and Abcc4, and down-regulation of Cyp2d13 and Abcc10 in GF mice. Similarly, the lack of gut microbiome also abolishes BDE-99 mediated up-regulation of Cyp2a22, Cyp2c39, Cyp2g1, Cyp2r1, Cyp3a13, and Sult2a7 in GF mice. Interestingly, the lack of gut microbiome can also potentiate PBDE mediated alterations, evidenced by a greater fold change observed in GF conditions. Many DPGs that were minimally or moderately regulated by PBDEs in the livers of CV mice were markedly altered by PBDEs with the absence of gut microbiome in GF mice.

These genes include Cyp2a22 and Cyp3a11 by BDE-47, Cyp3a59, Ugt2b35, Ugdh, Sult1d1, and Sult1e1 by BDE-99, as well as Cyp3a16, Cyp3a41a, Cyp3a41b, Cyp3a44, Gsta2, Gstt3 and Slco1a4 by both BDE-47 and BDE-99. The augmentation effect of the lack of gut microbiome seemed to be more prominent for BDE-99. For example, the lack of gut microbiome potentiates BDE-99 mediated up-regulation of over half of DPGs as shown in this study, including phase I gene family (Cyp1 to Cyp3), phase II gene families (Ugts, Sults and Gsts), as well as transporters (Slco1a4, Slco1b2, Abcb1a, Abcc2 and Abcc10).

The present study has provided critical information on the *in vivo* hepatic metabolism of BDE-47 and BDE-99 in CV and GF mice, with a primary focus on the hydroxylated PBDE metabolites. Accumulated evidence have demonstrated that PBDEs are first biotransformed to hydroxylated metabolites in mammals (Hamers et al., 2008; Lupton et al., 2009; Stapleton et al., 2009; Dong et al., 2010; Erratico et al., 2010). Almost 20 OH-BDE metabolites have been identified in rat blood after exposure to a mixture of tetra- to decaBDEs. In the present study, sixteen hydroxylated metabolites of PBDEs were measured by PBDE targeted metabolomics (GC-MS-NCI) in livers of CV and GF mice treated with BDE-47 or BDE-99. 12 out of 16 measured OH-BDEs were detected in livers of CV and GF mice treated with BDE-47. The major hydroxylated metabolite of BDE-47 was 5-OH-BDE-47 in livers of both CV and GF mice, with a higher level observed in GF conditions. The findings of six hydroxylated BDE-47 metabolites in the present study, namely 5-OH-BDE-47, 4'-OH-BDE-49, 3-OH-BDE-47, and 6-OH-BDE-47, 4'-OH-BDE-17, and 2'-OH-BDE-28, are consistent with previous in vitro studies which incubated BDE-47 with phenobarbital-induced rat liver microsomes or recombinant

human CYPs (Hamers et al., 2008; Erratico et al., 2013; Feo et al., 2013). Following BDE-99 treatment, 13 out of 16 measured OH-BDEs were detected in livers of CV and GF mice. The major hydroxylated metabolite of BDE-99 was 5'-OH-BDE-99 in livers of both CV and GF mice. The findings of hydroxylated BDE-99 metabolites, namely 5'-OH-BDE-99, 6'-OH-BDE-99, and 4'-OH-BDE-101, are consistent with previous studies which incubated BDE-99 with rat liver microsomes (Stapleton et al., 2009; Erratico et al., 2011). In human blood, 5-OH-BDE-47 and 5'-OH-BDE-99 are also reported being the two most abundant metabolites of BDE-47 and BDE-99, respectively. The mean concentrations of BDE-47 and BDE-99 are 60 ± 29 ng/g lipid and 19 ± 8.6 ng/g lipid in human fetal and maternal blood samples from the United States (Qiu et al., 2009). However, the present study did not measure 4-OH-BDE-90 and 2,4,5-TBP as observed in previous report, due to the lack of corresponding standards. Compared with prior in vitro and in vivo studies, the present study is the first study to introduced gut microbiome as key determinants of the biotransformation of BDE-47 and BDE-99.

The present study has suggested the involvement of multiple DPGs in the biotransformation of BDE-47 and BDE-99 with the absence of gut microbiome. Evidence from human or rat microsomes and recombinant human CYP enzymes has demonstrated that BDE-47 and BDE-99 are initially oxidized to hydroxylated metabolites (OH-BDEs) by various CYPs, particularly by CYP2A2 and CYP3A1 in rats, and CYP2B6 in humans (Erratico et al., 2011; Feo et al., 2013). The lack of gut microbiome increased the major metabolite of BDE-47 in livers of GF mice, but decreased the other four minor metabolites, suggesting the involvement of multiple Cyps in the biotransformation of BDE-47. For example, the lack of gut microbiome up-regulated the

expression of Cyp2b9, Cyp2b13 and many Cyp2c subfamily members, which could contribute to the increased formation of the major BDE-47 metabolite; whereas the lack of gut microbiome significantly down-regulated Cyp3a enzymes (such as Cyp3a11, Cyp3a16, Cyp3a41a, Cyp3a41b, Cyp3a44 and Cyp3a59) in livers of GF mice, which may be responsible for the decreased four minor BDE-47 metabolites. Conversely, the lack of gut microbiome not only affects the biotransformation of PBDEs through the baseline expression levels of these enzymes, it also modulates how these PBDEs and their metabolites in turn affect the expression of these and other drug metabolizing enzymes.

The Promega P450-Glo assay used in the present study provides a highly sensitive and selective substrate for each specific CYP enzyme (CYP1 to 3) in liver microsomes (Cali et al., 2006; Hrycay and Bandiera, 2009; Cali et al., 2012). Although it was initially designed for human samples, it has been widely used in the mouse studies as shown in the prior publications (Sekiya and Suzuki, 2011; Lee et al., 2013; Selwyn et al., 2015a). For example, the CYP1A1 activity was measured in mouse with C57BL/6 background using the P450-Glo CYP1A1 assay (containing Luciferin-CEE substrate)(Lee et al., 2013). The CYP1A2 activity was measured in mouse embryonic fibroblasts, defined transcription factor-induced hepatocyte-like cells, and mouse primary hepatocyte using P450-Glo CYP1A2 (containing Luciferin-ME substrate)(Lim et al., 2016). The Cyp3a activity was measured in germ-free mice and mouse hepatocyte using the P450-Glo CYP3A4 assay (containing Luciferin-IPA) (Sekiya and Suzuki, 2011; Selwyn et al., 2015a). The recombinant human P450 isoforms have shown that CYP2B6 was the predominant isoform that could metabolize Luciferin-2B6 to luciferin, and CYP3A4 was

the predominant isoform that could metabolize Luciferin-IPA to luciferin. According to NCBI Homologene database, the mouse Cyp2b and Cyp3a are sequence homologs of the corresponding human P450s within the same families, and the human P450s are not sequence homologs of the mouse P450s of other families such as Cyp1a, Cyp2a, or Cyp2c. Therefore, the substrates used in this study are most likely substrates for the mouse P450s of the same family as humans. However, it is possible that the CYP2B substrates can be metabolized by multiple mouse Cyp2b isoforms other than Cyp2b10.

Because there lacks a systematical comparison of PBDE exposure in humans at various groups such as newborns and children, elderly, adults, and occupational workers who are at a high risk of PBDE exposure. The low dose used in the present study was based on the exposure to PBDEs in newborns because these data are readily available (Frederiksen et al., 2009). This human-relevant dose is one of the examples that represent one of the most vulnerable populations. In the present study, the mice were dosed with 5 mg/kg and 50 mg/kg of PBDEs, which are calculated based on the potential exposure for infants, who are more vulnerable to adverse drug reactions than adults. The dose estimation is based on the fact that BDE-47 and -99 in human breast milk are approximately 27.8ng/g liquid weight (lw) and 5.7ng/g lw (Frederiksen et al., 2009). Assuming newborns weigh 5kg on average, and consumes 960 g per day, the 1-day human exposure of BDE-47 and BDE-99 in newborns is approximately 5.337 mg/kg (10.2 umol/kg) and 1.094 mg/kg (1.8 umol/kg), respectively. Therefore, the low dose is actually within the range of acute to sub-chronic exposure in the newborn vulnerable populations, whereas the high dose represents the dose of choice across species. Results from the National Health and Nutrition Examination

Survey have shown that the adult intake dose of total PBDEs was estimated to be 7.7 ng/kg body weight/day, and children's estimated intakes were higher at 49.3 ng/kg/day for ages 1-5, 14.4 ng/kg/day for 6-11, and 9.1 ng/kg/day for 12-19 (Lorber, 2008). Therefore, the acute low doses of PBDEs used in the present study (4 consecutive days) are similar to newborn sub-chronic exposure in humans (approximately 3 months), whereas the acute high doses of PBDEs considered an extrapolation of 10 across different species. These doses are similar to what have been used in adult mice to induce Cyps (Pacyniak et al., 2007).

In conclusion, we report a novel interaction between the gut microbiome and host hepatic DPGs *in vivo*. Most notably, the lack of gut microbiome augmented BDE-99 mediated up-regulation of many DPGs and also impacts the hydroxylation of PBDEs. Using GF mice as a research model, the present study is the first to characterize the effect of the gut microbiome on the host metabolism of the environmental PBDEs. However, there are some limitations to this study. Future studies are needed to systematically determine the distribution of PBDEs and quantify the blood and lipid metabolome profiles of PBDEs. Future studies are also needed to determine members of the gut microbiota that have the most significant effect on host DPGs expression involved in PBDE metabolism.

Figure 1

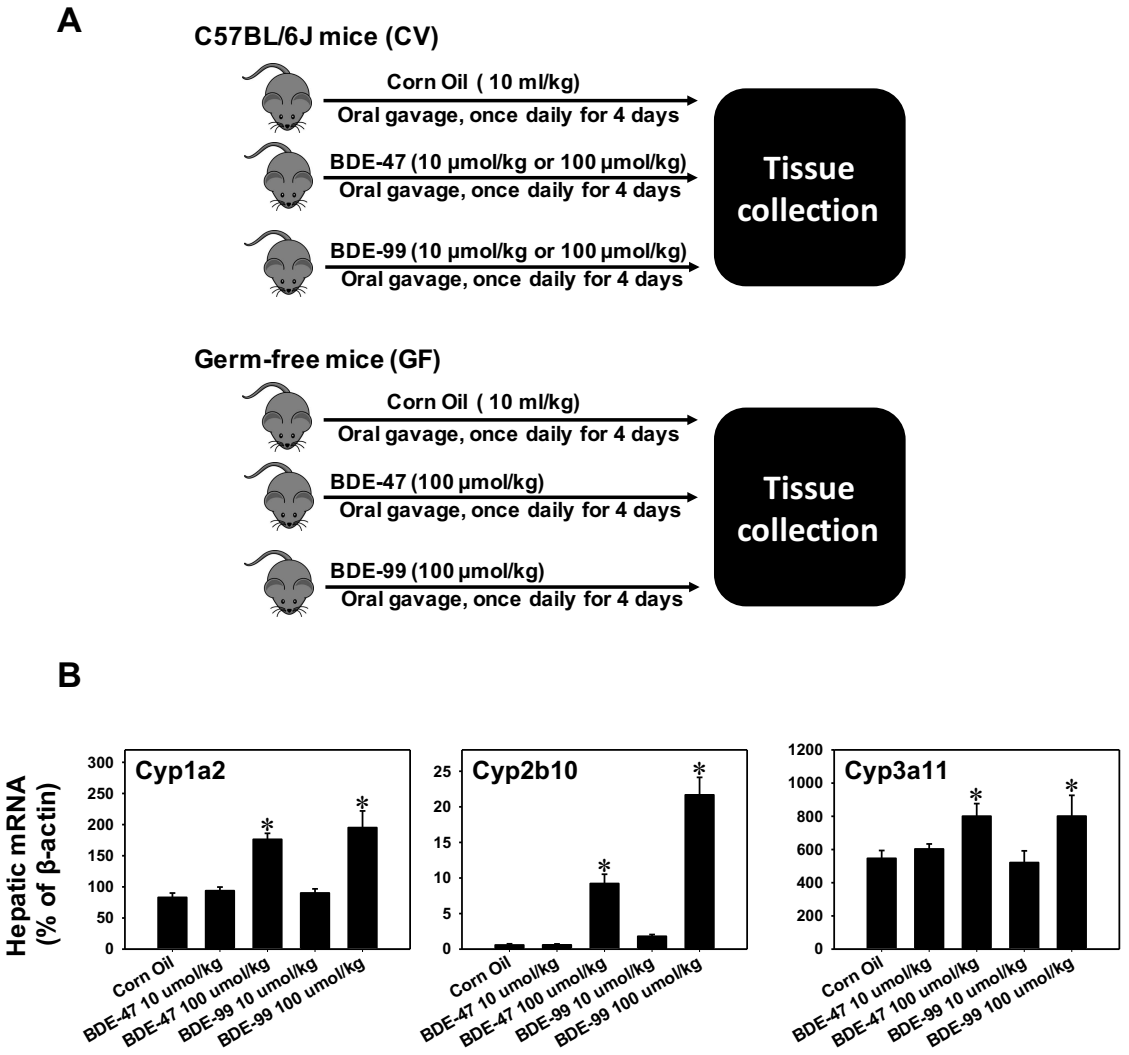

Figure 1. (A) A diagram illustrating the experimental design and dosing regimen of mice. Briefly, 9-week-old C57BL/6J CV mice were treated with vehicle (corn oil, 10ml/kg, oral gavage), BDE-47 (10 μmol/kg or 100 μmol/kg, oral gavage) or BDE-99 (10 μmol/kg or 100 μmol/kg, oral gavage) once daily for 4 days (n=5 per group). Tissues were collected 24h after the final dose. Age-matched GF mice were treated with vehicle (corn oil, 10ml/kg, oral gavage), BDE-47 (100 μmol/kg, oral gavage) or BDE-99 (100 μmol/kg, oral gavage) following the same procedure (n= 3 or 4 per group). **(B)** RT-qPCR quantification of mRNAs of the prototypical AhR-target gene Cyp1a2, the prototypical CAR-target gene Cyp2b10, and the prototypical PXR-target gene Cyp3a11 in liver of CV mice treated with corn oil, BDE-47 (10 or 100 μmol/kg) or BDE-99 (10 or 100 μmol/kg). Data are expressed as percentage of the housekeeping gene β-actin (n= 5 per group). Asterisks (*) indicate statistically significant differences between corn oil- and PBDE-treated groups in liver ($p<0.05$).

Figure 2

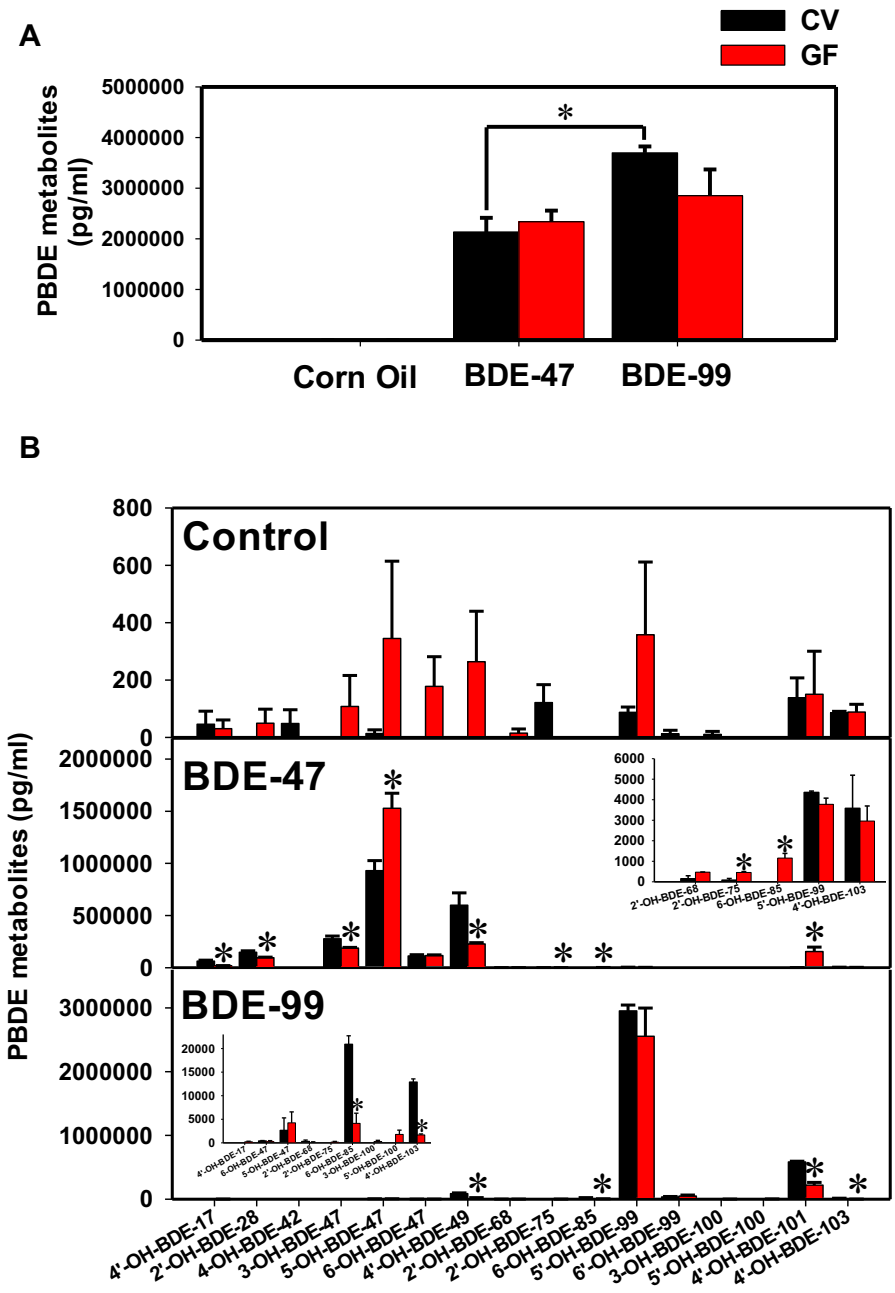

Figure 2. Concentrations of hydroxylated PBDE metabolites (pg/ml, mean ± standard error) in livers of CV and GF mice treated with corn oil, BDE-47 (100 μmol/kg) or BDE-99 (100 μmol/kg). (**A**) The total hepatic levels of hydroxylated PBDE metabolites in CV and GF mice treated with corn oil, BDE-47 (100 μmol/kg) or BDE-99 (100 μmol/kg). Asterisks (*) represent statistically significant differences between comparison groups. (**B**) Concentrations of individual hydroxylated metabolites of BDE-47 and BDE-99 in livers of CV and GF mice treated with corn oil, BDE-47 (100 μmol/kg) or BDE-99 (100 μmol/kg). Asterisks (*) represent statistically significant differences between CV and GF mice.

Figure 3

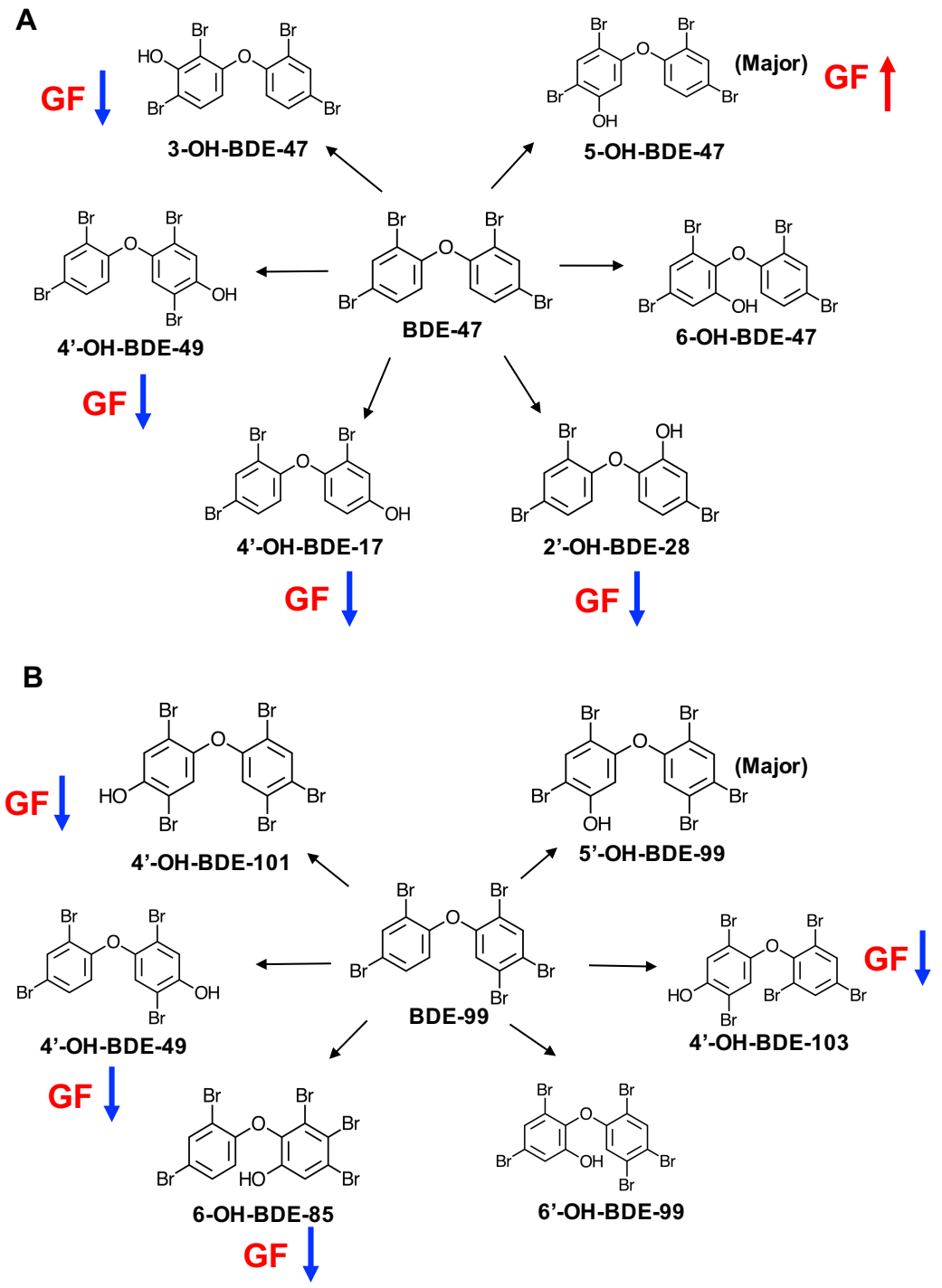

Figure 3. Chemical structures (plotted by ChemDoodle) of hydroxylated metabolites of BDE-47 (**A**) and BDE-99 (**B**) in livers of CV and GF mice treated with corn oil, BDE-47(100 μmol/kg) or BDE-99 (100 μmol/kg). The major hydroxylated metabolite of BDE-47 or BDE-99 was labeled. Compared to CV mice, the up-regulated (red arrow) or down-regulated (blue arrow) individual metabolite in GF conditions were highlighted.

Figure 4

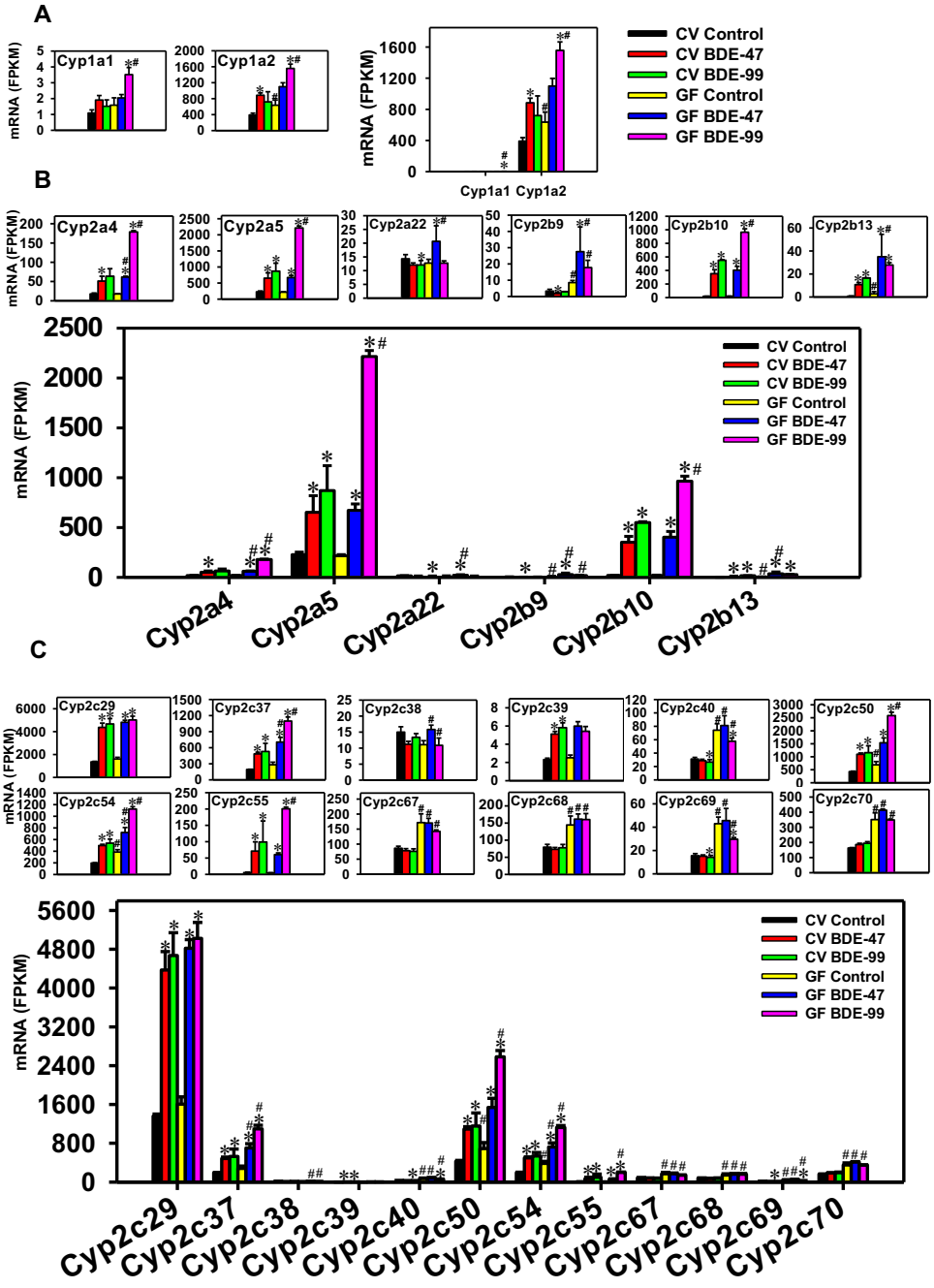

Figure 4. Regulation of Phase-I Cyp1 (**A**), Cyp2a and Cyp2b (**B**), and Cyp2c (**C**) drug-metabolizing enzymes by BDE-47 or BDE-99 in livers of CV and GF mice. Only Cyps that were differentially expressed by PBDEs or by lack of gut microbiota were shown. Genes in the same family were grouped together in the same figure to quantitatively compare the mRNA abundance, and were also presented individually to better visualize the mRNA fold-changes by BDE-47 or BDE-99 in CV and GF mice. Asterisks (*) represent statistically significant differences between corn oil- and PBDE-treated groups of the same enterotypes of mice (FDR-adjusted p value <0.05). Pounds (#) represent statistically significant differences between CV and GF mice under the same treatment.

Figure 5

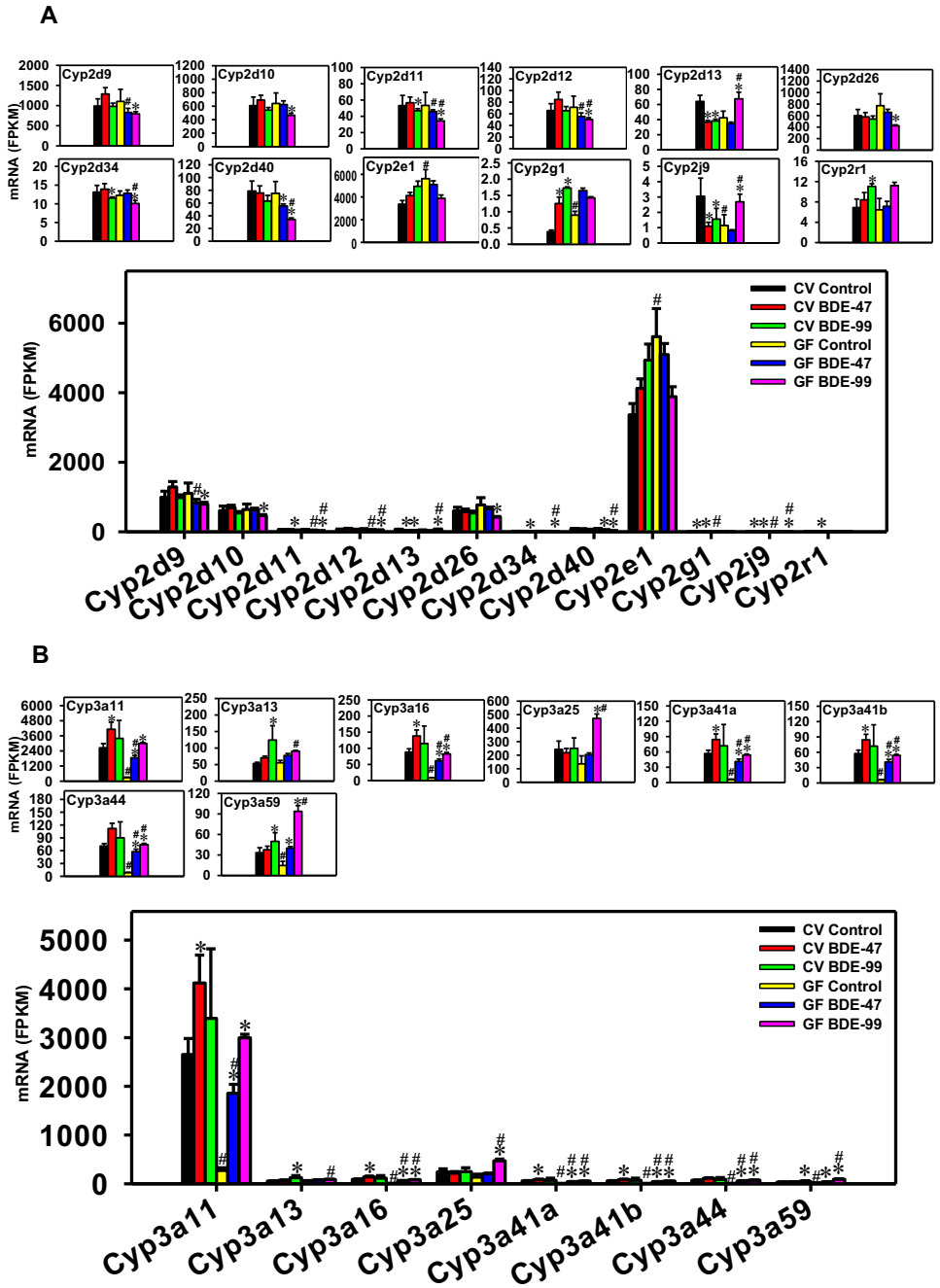

Figure 5. Regulation of Phase-I Cyp2d, Cyp2e1, Cyp2g1, Cyp2j9, Cyp2r1 (**A**), and Cyp3a (**B**) drug-metabolizing enzymes by BDE-47 or BDE-99 in livers of CV and GF mice. Only Cyps that were differentially expressed by PBDEs or by lack of gut microbiota were shown. Genes in the same family were grouped together in the same figure to quantitatively compare the mRNA abundance, and were also presented individually to better visualize the mRNA fold-changes by BDE-47 or BDE-99 in CV and GF mice. Asterisks (*) represent statistically significant differences between corn oil- and PBDE-treated groups of the same enterotypes of mice (FDR-adjusted p value <0.05). Pounds (#) represent statistically significant differences between CV and GF mice under the same treatment.

Figure 6

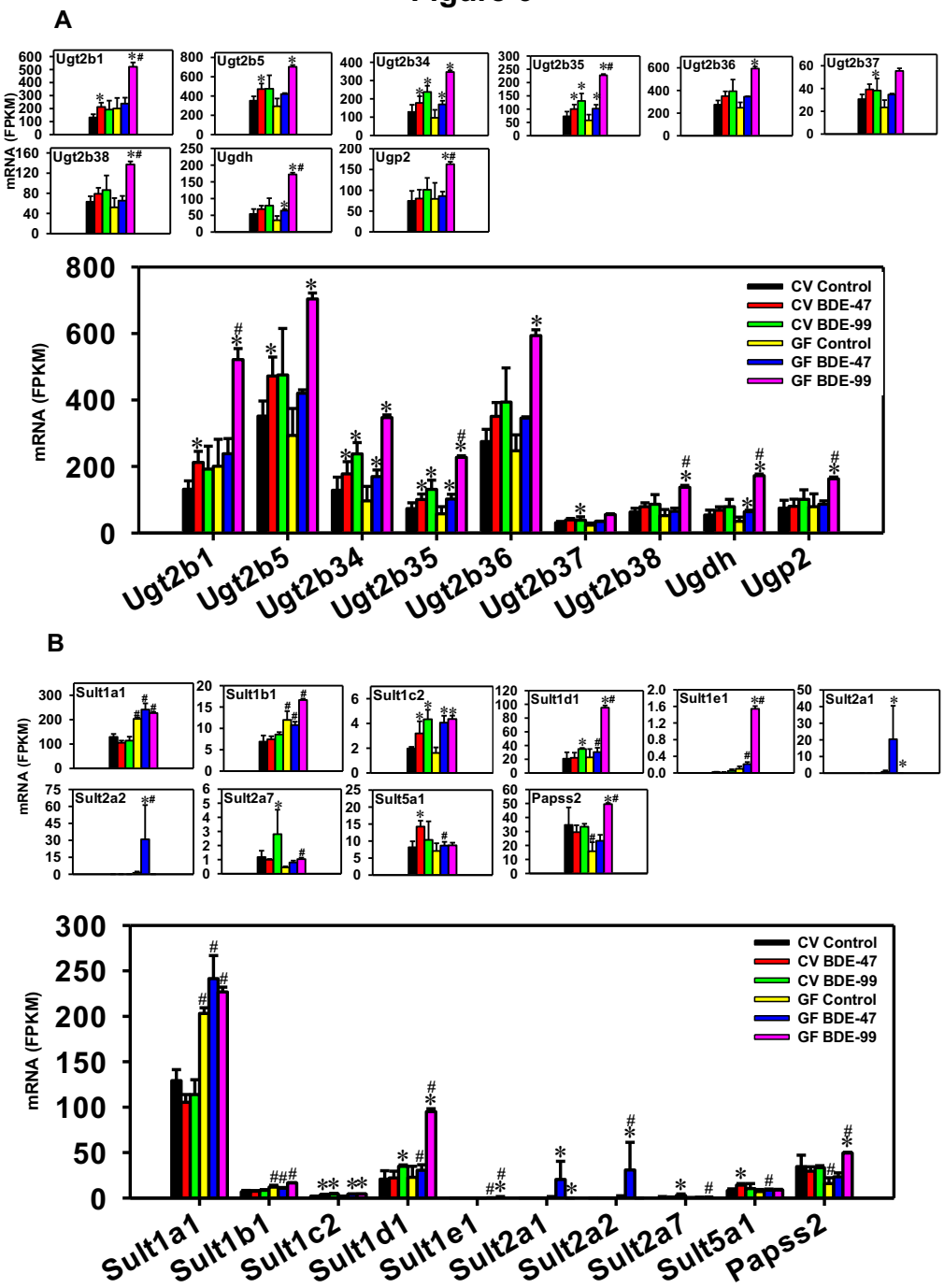

Figure 6. Regulation of Phase-II Ugts (**A**) and Sults (**B**) by BDE-47 or BDE-99 in livers of CV and GF mice. Only DPGs that were differentially expressed by PBDEs or by lack of gut microbiota were shown. Genes in the same family were grouped together in the same figure to quantitatively compare the mRNA abundance, and were also presented individually to better visualize the mRNA fold-changes by BDE-47 or BDE-99 in CV and GF mice. Asterisks (*) represent statistically significant differences between corn oil- and PBDE-treated groups of the same enterotypes of mice (FDR-adjusted p value <0.05). Pounds (#) represent statistically significant differences between CV and GF mice under the same treatment.

Figure 7

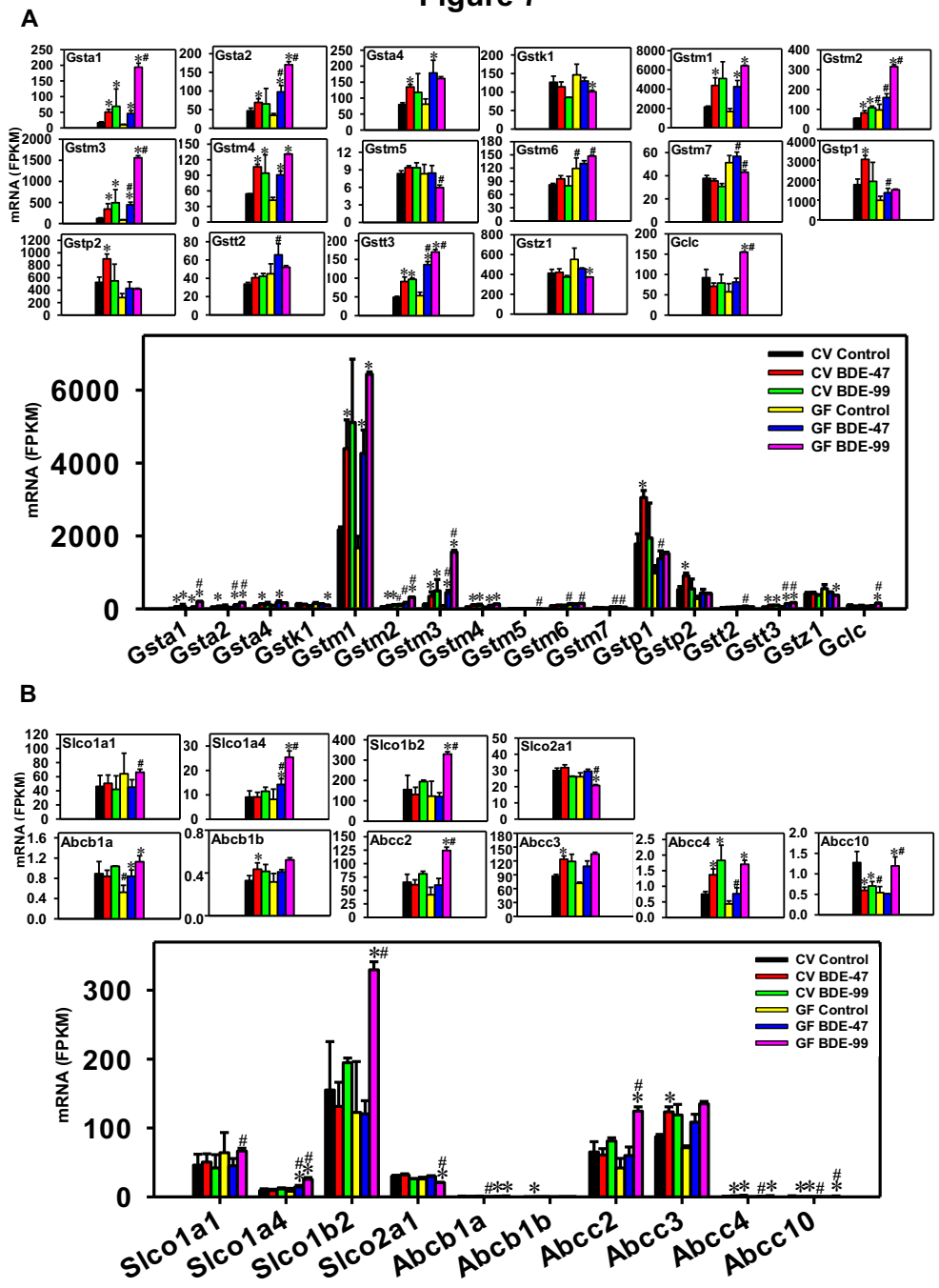

Figure 7. Regulation of Phase-II Gsts (**A**), as well as transporters in the Slco and Abc families (**B**) by BDE-47 or BDE-99 in livers of CV and GF mice. Only DPGs that were differentially expressed by PBDEs or by lack of gut microbiota were shown. Genes in the same family were grouped together in the same figure to quantitatively compare the mRNA abundance, and were also presented individually to better visualize the mRNA fold-changes by BDE-47 or BDE-99 in CV and GF mice. Asterisks (*) represent statistically significant differences between corn oil- and PBDE-treated groups of the same enterotypes of mice (FDR-adjusted p value <0.05). Pounds (#) represent statistically significant differences between CV and GF mice under the same treatment.

Figure 8

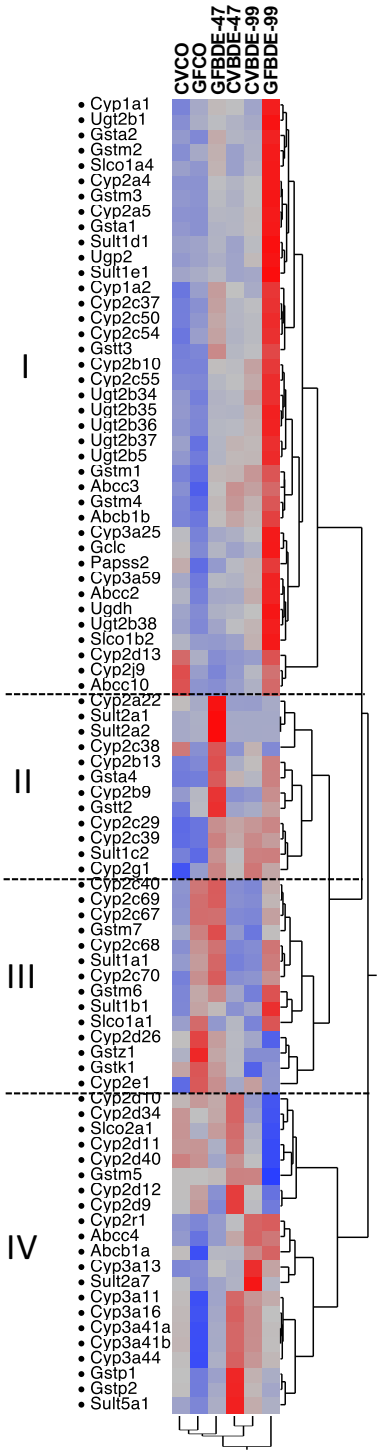

Figure 8. Two-way hierarchical clustering dendrogram of critical DPGs that were differentially regulated by PBDEs or by the lack of gut microbiome in livers of CV and GF mice. Red color represents up-regulation and blue color represents down-regulation.

Figure 9

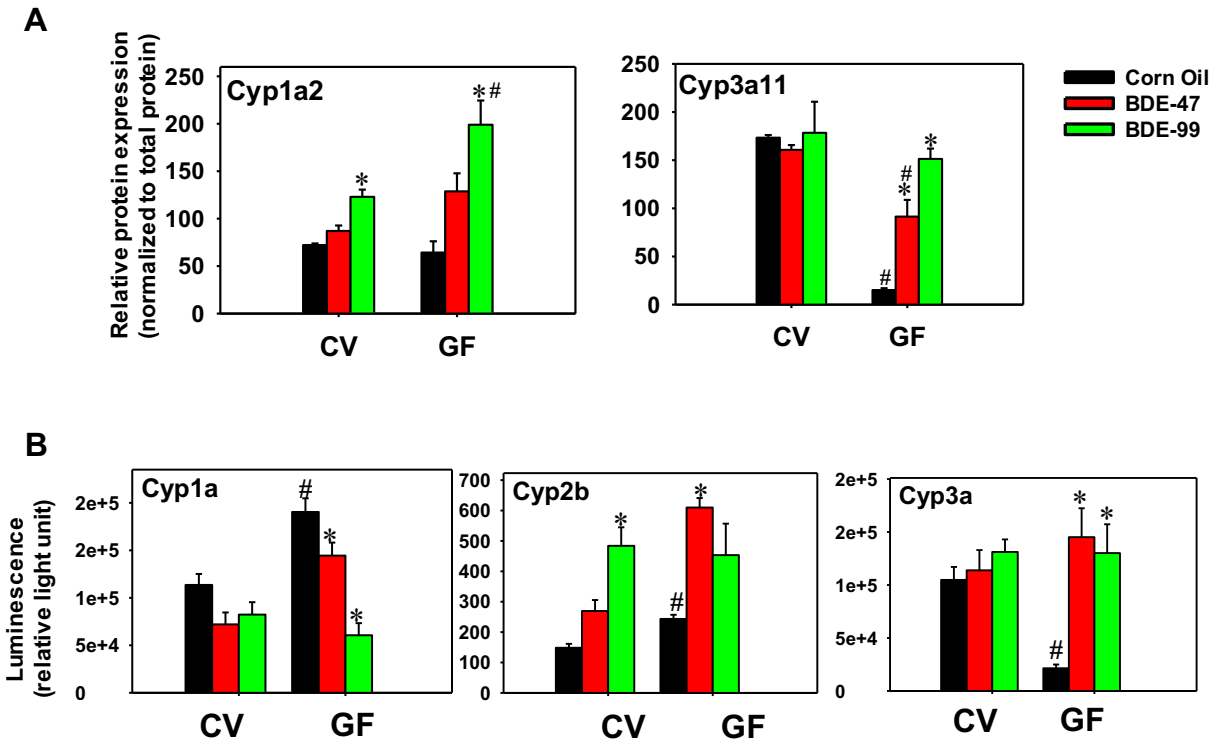

Figure 9. (A) UPLC-MS quantification of Cyp1a2 and Cyp3a11 protein levels in livers of CV and GF mice treated with corn oil, BDE-47 (100 μmol/kg) or BDE-99 (100 μmol/kg). **(B)** Enzyme activities of Cyp1a, Cyp2b and Cyp3a in livers of CV or GF using the Promega P450-Glo™ CYP1A, CYP2B and CYP3A Assays. Asterisks (*) represent statistically significant differences between corn oil- and PBDE-treated groups of the same enterotypes of mice ($p<0.05$). Pounds (#) represent statistically significant differences between CV and GF mice under the same treatment ($p<0.05$).

Supplemental Figure 1

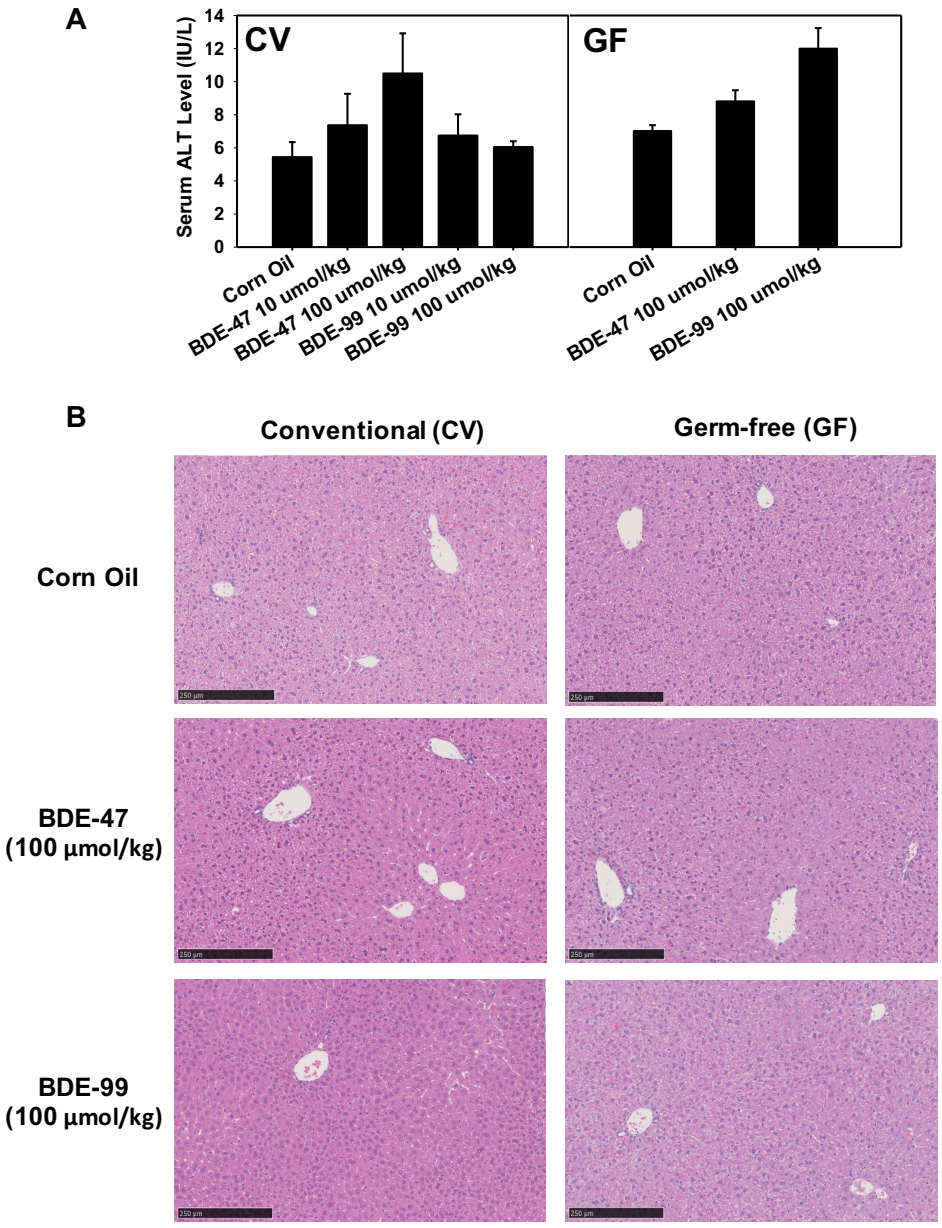

Supplemental Figure 1. (A) Serum Alanine Aminotransferase (ALT) quantification in CV and GF mice treated with corn oil, BDE-47 or BDE-99 at various doses. Serum ALT is expressed as mean IU/L ± standard error of mean (S.E.M). (B) Haemotoxylin & Eosin staining of livers from CV and GF mice treated with corn oil, BDE-47 (100 µmol/kg) or BDE-99 (100 µmol/kg) (x100).

Table 1. DPGs that were differentially regulated by the lack of gut microbiome and by PBDEs in livers of CV and GF mice treated with corn oil, BDE-47 (100 μmol/kg) or BDE-99 (100 μmol/kg). CVCO, Corn Oil-treated Conventional mice, GFCO, Corn Oil-treated Germ free mice.

Category	Treatment	Phase I	Phase II	Transporters
A. Genes that were differentially regulated by gut microbiome (CVCO vs GFCO)	Corn Oil	Cyp1a2, Cyp2b9, Cyp2b13, Cyp2c (2c40, 2c50, 2c54, 2c67, 2c68, 2c69, 2c70), Cyp2e1, Cyp2g1, Cyp2j9, Cyp3a (3a11, 3a16, 3a41a, 3a41b, 3a44, 3a59)	Sult1a1, Sult1b1, Papss2, Gstm2, Gstm6	Abcb1a, Abcc10
B. Genes that were differentially regulated by PBDEs only in CV mice (gut microbiome dependent effect)	BDE-47	Cyp1a2, Cyp2c39, Cyp2d13, Cyp2g1, Cyp2j9	Ugt2b1, Ugt2b5, Sult5a1, Gstm2 Gstp1, Gstp2	Abcb1b, Abcc3, Abcc4, Abcc10
	BDE-99	Cyp2a22, Cyp2c39, Cyp2g1, Cyp2r1, Cyp3a13	Ugt2b37, Sult2a7	
C. Genes that were differentially regulated by PBDEs preferably in GF mice (augmentation effect due to the lack of gut microbiome)	BDE-47	Cyp2a4, Cyp2a22, Cyp2b9, Cyp2b13, Cyp2c37, Cyp2c54, Cyp3a11, Cyp3a16, Cyp3a41a, Cyp3a41b, Cyp3a44	Sult2a2, Gsta2, Gstm3, Gstt3	Slco1a4
	BDE-99	Cyp1a1, Cyp1a2, Cyp2a4, Cyp2a5, Cyp2b10, Cyp2c (2c37, 2c40, 2c50, 2c54, 2c55, 2c69), Cyp2d (2d11, 2d12, 2d13, 2d34, 2d40), Cyp2j9, Cyp3a (3a16, 3a25, 3a41a, 3a41b, 3a44, 3a59)	Ugt2b1, Ugt2b35, Ugt2b38, Ugdh, Ugp2, Sult1d1, Sult1e1, Papss2, Gsta1, Gsta2, Gstm2, Gstm3, Gstt3, Gclc	Slco1a4, Slco1b2, Slco2a1, Abcc2, Abcc10

Supplemental Table 1 – Optimized LC-MS/MS parameters for analysis of surrogate peptides of mouse drug-metabolizing enzymes Cyp1a2 and Cyp3a11. DP: declustering potential, CE: Collision energy and RT-retention time. Terminal K and R residues were labeled with ^{13}C and ^{15}N.

Protein	Peptide sequence	Light/Heavy	Parent ion (m/z)	Daughter ion (m/z)	DP (V)	CE (eV)	RT (min)
Cyp1a2	FLTNNNSAID(K)	Light	618.8	976.5	66.2	29	18.6
			618.8	875.4	66.2	29	18.6
			618.8	761.4	66.2	29	18.6
		Heavy	622.8	984.5	66.2	29	18.6
			622.8	883.4	66.2	29	18.6
			622.8	769.4	66.2	29	18.6
	VMLFGLG(K)	Light	432.8	765.4	52.7	17.4	16.8
			432.8	634.4	52.7	17.4	16.8
			432.8	521.3	52.7	17.4	16.8
		Heavy	436.8	773.4	52.7	17.4	16.8
			436.8	642.4	52.7	17.4	16.8
			436.8	529.3	52.7	17.4	16.8
	NSIQDITSALF(K)	Light	668.9	894.5	69.9	25.9	10.5
			668.9	779.5	69.9	25.9	10.5
			668.9	568.3	69.9	25.9	10.5
		Heavy	672.9	902.5	69.9	25.9	10.5
			672.9	787.5	69.9	25.9	10.5
			672.9	572.3	69.9	25.9	10.5
Cyp3a11	LQDEIDEALPN(K)	Light	692.9	1143.6	85	29	12.5
			692.9	899.5	85	29	12.5
			692.9	786.4	85	29	12.5
		Heavy	696.9	1151.6	85	29	12.5
			696.9	794.4	85	29	12.5
Bovine serum albumin (BSA)	AEFVEVT(K)	Light	461.8	722.4	70	25.8	10.8
			461.8	476.3	70	25.8	10.8
			461.8	575.3	70	25.8	10.8
		Heavy	465.8	730.4	70	25.9	10.8
			465.8	484.3	70	25.9	10.8
			465.8	583.4	70	25.9	10.8

Supplemental Table 2. Average FPKM values and standard errors for DPGs that were differentially regulated by PBDEs or by enterotypes from RNA-Seq.

Genes	Category	CVCO	s.e.	CVBDE47	s.e.	CVBDE99	s.e.	GFCO	s.e.	GFBDE47	s.e.	GFBDE99	s.e.
Cyp1a1	Phase I	1.09	0.20	1.91	0.29	1.51	0.41	1.58	0.46	2.04	0.21	3.51	0.45
Cyp1a2	Phase I	391.96	44.93	884.13	58.82	719.69	252.70	635.10	130.15	1098.82	98.74	1557.19	108.28
Cyp2a4	Phase I	17.80	2.30	51.16	12.44	63.80	19.38	17.73	0.66	61.55	2.12	178.85	3.27
Cyp2a5	Phase I	227.48	25.65	651.65	167.32	869.87	249.35	216.37	10.84	671.54	64.42	2214.54	60.40
Cyp2a22	Phase I	14.28	1.55	12.04	0.76	12.03	1.67	12.74	1.39	20.64	5.69	12.73	0.83
Cyp2b9	Phase I	3.29	1.11	1.80	0.85	2.87	0.15	8.54	1.28	27.51	15.20	17.72	4.49
Cyp2b10	Phase I	18.72	1.45	352.58	57.93	550.29	8.35	18.00	4.28	403.26	56.66	963.99	50.05
Cyp2b13	Phase I	0.75	0.16	10.73	1.75	16.58	0.05	2.76	1.92	35.05	19.44	27.80	2.03
Cyp2c29	Phase I	1358.95	41.58	4370.67	381.61	4671.23	469.56	1605.94	149.43	4820.12	180.39	5023.44	331.18
Cyp2c37	Phase I	193.49	4.46	484.33	30.88	529.16	151.28	280.93	48.12	704.26	88.19	1097.83	74.38
Cyp2c38	Phase I	14.98	1.68	11.18	0.93	13.37	1.17	11.06	1.24	15.80	1.37	10.87	2.26
Cyp2c39	Phase I	2.31	0.16	5.11	0.29	5.82	0.53	2.52	0.29	5.99	0.49	5.42	0.52
Cyp2c40	Phase I	31.17	2.41	28.77	1.97	26.57	3.78	74.28	9.59	81.17	14.66	57.66	4.77
Cyp2c50	Phase I	428.37	18.40	1094.53	48.36	1155.31	268.69	690.14	123.18	1537.97	188.07	2583.09	128.07
Cyp2c54	Phase I	197.33	4.94	497.79	20.44	538.88	68.84	386.07	40.27	721.67	85.91	1124.85	40.02
Cyp2c55	Phase I	5.29	1.44	71.18	28.12	98.82	64.68	3.80	1.51	60.33	5.37	200.72	4.68
Cyp2c67	Phase I	86.29	6.83	78.28	6.76	75.96	8.48	171.48	29.38	170.33	15.63	142.56	4.70
Cyp2c68	Phase I	79.52	8.20	73.29	5.37	77.77	9.74	144.31	26.17	161.41	15.16	160.21	17.51
Cyp2c69	Phase I	15.52	1.79	15.08	1.10	14.14	1.61	43.04	5.62	45.67	10.44	29.65	1.47
Cyp2c70	Phase I	163.19	2.40	186.35	7.91	194.20	10.70	351.01	44.65	413.47	7.32	349.02	5.75
Cyp2d9	Phase I	989.42	176.76	1286.08	158.88	980.33	78.66	1102.76	299.52	828.56	103.00	792.92	54.41
Cyp2d10	Phase I	607.44	128.67	690.92	71.80	541.79	38.30	640.74	155.53	623.36	54.81	465.12	30.33
Cyp2d11	Phase I	53.17	12.52	56.61	7.03	46.75	2.58	53.34	16.09	45.75	2.17	34.36	2.45
Cyp2d12	Phase I	65.64	11.69	84.59	12.78	65.10	7.41	71.12	19.29	55.31	6.20	50.17	3.29
Cyp2d13	Phase I	64.03	8.18	36.71	2.03	38.20	2.35	42.44	8.76	34.58	2.11	67.50	8.83
Cyp2d26	Phase I	598.42	107.28	578.12	74.99	539.59	53.48	772.39	207.59	655.98	52.65	423.57	15.26
Cyp2d34	Phase I	13.13	1.80	13.91	1.51	11.54	0.32	12.27	1.17	12.81	0.89	10.08	0.81
Cyp2d40	Phase I	78.85	15.75	75.74	11.22	63.17	8.76	75.15	18.71	55.25	3.25	34.10	2.45
Cyp2e1	Phase I	3362.01	323.90	4122.52	274.33	4936.22	461.03	5611.13	808.69	5093.98	321.62	3883.34	286.75
Cyp2g1	Phase I	0.38	0.05	1.25	0.20	1.73	0.03	0.90	0.12	1.65	0.08	1.43	0.03
Cyp2j9	Phase I	3.05	1.18	1.10	0.25	1.56	0.70	1.14	0.71	0.80	0.06	2.69	0.50
Cyp2r1	Phase I	6.88	1.69	8.41	1.42	11.05	0.53	6.44	2.24	7.13	0.98	11.23	0.63
Cyp3a11	Phase I	2650.58	328.62	4119.00	572.44	3393.70	1426.97	273.31	52.72	1854.17	185.95	2994.30	72.10
Cyp3a13	Phase I	53.24	3.74	70.47	5.06	124.03	43.48	55.29	7.45	77.39	6.05	90.14	3.07
Cyp3a16	Phase I	88.04	10.42	138.11	18.59	114.66	54.11	7.81	1.13	61.45	5.30	82.33	4.44
Cyp3a25	Phase I	243.23	61.21	218.09	31.57	250.25	77.40	135.64	59.83	204.05	12.91	471.74	32.52
Cyp3a41a	Phase I	56.71	6.61	84.17	10.97	71.95	41.81	5.77	1.04	41.06	4.95	53.88	1.98
Cyp3a41b	Phase I	57.49	6.53	84.17	10.97	71.95	41.81	5.77	1.04	41.06	4.95	53.88	1.98
Cyp3a44	Phase I	70.69	5.76	111.66	12.23	89.84	37.46	8.66	0.53	57.46	5.80	73.93	2.90
Cyp3a59	Phase I	33.31	7.34	37.59	5.21	49.89	12.58	14.60	6.13	39.99	2.32	93.73	8.45

Genes	Category	CVCO	s.e.	CVBDE47	s.e.	CVBDE99	s.e.	GFCO	s.e.	GFBDE47	s.e.	GFBDE99	s.e.
Ugt2b1	Phase II	131.71	24.72	212.08	33.52	191.94	68.91	200.54	81.29	238.35	45.63	521.31	33.15
Ugt2b5	Phase II	351.46	45.27	472.00	57.26	475.38	139.52	293.53	80.82	419.95	10.51	703.66	17.99
Ugt2b34	Phase II	128.43	39.38	177.76	36.49	237.90	33.90	96.47	43.66	169.83	19.70	346.89	8.42
Ugt2b35	Phase II	73.11	17.52	100.44	16.62	131.08	27.65	57.68	21.63	101.86	14.60	227.49	4.69
Ugt2b36	Phase II	275.05	36.81	350.55	41.71	393.74	102.83	247.31	47.63	345.49	3.69	593.76	17.40
Ugt2b37	Phase II	30.73	4.08	39.25	4.64	38.28	10.56	23.42	6.41	34.66	0.90	55.44	2.31
Ugt2b38	Phase II	63.16	10.87	78.91	11.97	86.40	28.88	52.18	18.20	65.37	9.38	137.20	6.11
Ugdh	Phase II	53.81	14.78	68.26	10.31	78.98	21.88	35.07	12.80	63.78	4.46	172.16	5.30
Ugp2	Phase II	74.58	23.86	80.16	21.16	101.28	28.46	79.21	38.63	86.11	10.64	162.70	5.73
Sult1a1	Phase II	129.10	12.15	105.33	8.48	113.90	16.26	203.16	6.23	241.49	25.39	226.81	5.18
Sult1b1	Phase II	6.89	1.43	7.44	0.71	8.56	0.55	11.96	2.06	10.77	0.77	16.64	0.30
Sult1c2	Phase II	1.97	0.13	3.20	0.98	4.34	0.77	1.62	0.45	4.07	0.56	4.35	0.28
Sult1d1	Phase II	20.84	9.18	22.16	7.39	34.92	1.53	22.80	12.09	30.45	6.16	95.12	3.18
Sult1e1	Phase II	0.02	0.00	0.01	0.01	0.05	0.04	0.10	0.06	0.21	0.05	1.54	0.07
Sult2a1	Phase II	0.03	0.00	0.01	0.01	0.01	0.01	0.84	0.76	20.38	20.07	0.00	0.00
Sult2a2	Phase II	0.04	0.02	0.03	0.02	0.01	0.01	1.22	1.15	30.86	30.33	0.03	0.02
Sult2a7	Phase II	1.18	0.45	0.99	0.05	2.80	1.73	0.45	0.07	0.79	0.13	1.04	0.10
Sult5a1	Phase II	8.17	1.75	14.23	1.73	10.34	5.46	7.09	2.25	8.66	1.10	8.74	0.76
Papss2	Phase II	34.62	12.57	29.50	4.93	33.37	2.14	15.88	6.39	23.33	4.24	49.56	0.75
Gsta1	Phase II	16.64	3.04	50.54	8.84	68.91	55.57	10.13	1.76	46.04	8.78	193.95	12.62
Gsta2	Phase II	46.67	7.28	69.27	10.14	65.13	41.69	34.63	4.86	97.54	17.09	170.69	8.38
Gsta4	Phase II	79.81	5.52	134.76	7.95	118.01	58.75	81.07	16.34	178.75	39.76	161.34	5.71
Gstk1	Phase II	126.44	16.44	114.05	13.33	85.31	0.59	146.40	28.80	129.71	9.49	100.84	4.01
Gstm1	Phase II	2164.30	83.33	4393.48	790.27	5111.82	1735.97	1675.81	314.18	4264.18	642.48	6435.67	63.64
Gstm2	Phase II	54.97	0.52	82.04	11.81	108.17	8.31	96.89	28.36	159.32	19.38	315.24	9.39
Gstm3	Phase II	119.71	15.43	342.75	127.73	493.32	309.24	84.61	6.98	443.57	62.22	1558.04	50.20
Gstm4	Phase II	54.12	0.40	106.27	4.98	94.16	35.17	42.00	5.36	90.75	7.46	130.86	0.52
Gstm5	Phase II	8.35	0.49	9.38	0.32	9.36	0.86	8.33	1.59	8.45	1.29	5.95	0.44
Gstm6	Phase II	82.23	3.05	95.75	7.08	79.76	21.56	119.26	23.77	130.40	6.24	147.11	1.88
Gstm7	Phase II	37.78	2.52	35.54	1.78	30.77	2.43	51.35	6.12	56.82	3.69	43.01	1.95
Gstp1	Phase II	1779.56	278.93	3050.83	194.72	1941.65	958.66	984.02	204.51	1370.70	218.00	1517.70	35.96
Gstp2	Phase II	525.78	85.16	903.40	76.97	549.05	269.83	281.98	62.71	429.54	104.61	418.79	12.09
Gstt2	Phase II	33.74	1.81	40.68	4.06	42.13	3.20	44.95	10.85	65.61	12.23	52.15	1.73
Gstt3	Phase II	48.89	2.63	90.87	12.22	96.99	3.07	53.25	9.14	136.14	8.37	169.77	6.63
Gstz1	Phase II	412.49	38.08	420.78	35.95	373.20	15.17	551.25	113.77	457.81	8.11	373.02	1.81
Gclc	Phase II	92.19	20.38	70.81	8.07	78.88	21.32	57.29	20.30	81.33	9.29	154.83	1.12
Slco1a1	Transporters	46.21	15.70	50.54	11.86	42.06	19.18	64.14	29.20	45.18	10.56	66.35	4.23
Slco1a4	Transporters	9.10	2.53	9.16	1.89	11.47	1.68	8.17	4.17	14.25	2.37	25.41	2.62
Slco1b2	Transporters	155.06	70.43	131.28	35.09	194.67	6.93	122.65	73.85	120.61	18.99	329.73	11.62
Slco2a1	Transporters	29.88	1.52	31.72	1.77	26.19	0.36	26.11	2.40	29.52	1.20	20.70	0.59
Abcb1a	Transporters	0.89	0.24	0.84	0.12	1.04	0.01	0.52	0.14	0.84	0.12	1.13	0.12
Abcb1b	Transporters	0.33	0.05	0.44	0.06	0.42	0.06	0.32	0.08	0.41	0.02	0.52	0.02
Abcc2	Transporters	65.28	14.86	60.79	9.09	81.07	4.55	41.97	13.94	59.92	12.47	124.44	6.27
Abcc3	Transporters	87.27	3.48	123.51	7.24	118.86	15.44	71.51	2.63	108.41	11.49	135.10	3.51
Abcc4	Transporters	0.75	0.08	1.37	0.19	1.83	0.49	0.44	0.09	0.76	0.19	1.70	0.13
Abcc10	Transporters	1.28	0.27	0.60	0.08	0.70	0.11	0.54	0.15	0.51	0.00	1.19	0.22

Supplemental Table 3. Fold change and FDR-adjusted p value for DPGs that were differentially regulated by PBDEs or by enterotypes under basal and PBDE-treated conditions. (Data are expressed as ratios of the FPKM from RNA-Seq).

Gene Symbol	GFCO vs CVCO	p value	CVBDE47 vs CVCO	p value	CVBDE99 vs CVCO	p value	GFBDE47 vs GFCO	p value	GFBDE99 vs GFCO	p value	GFBDE47 vs CVBDE47	p value	GFBDE99 vs CVBDE99	p value
Cyp1a1	1.45	0.59	1.75	0.35	1.39	0.93	1.29	0.21	2.22	0.00	1.07	0.88	2.33	0.00
Cyp1a2	1.62	0.03	2.26	0.00	1.84	0.09	1.73	0.19	2.45	0.03	1.24	0.27	2.16	0.01
Cyp2a4	1.00	0.03	2.87	0.04	3.58	0.26	3.47	0.00	10.09	0.00	1.20	0.00	2.80	0.00
Cyp2a5	0.95	0.56	2.86	0.00	3.82	0.00	3.10	0.00	10.23	0.00	1.03	0.69	2.55	0.00
Cyp2a22	0.89	0.60	0.84	0.06	0.84	0.02	1.62	0.01	1.00	0.10	1.71	0.00	1.06	0.59
Cyp2b9	2.59	0.00	0.55	0.00	0.87	0.12	3.22	0.00	2.08	0.08	15.25	0.00	6.18	0.00
Cyp2b10	0.96	0.53	18.84	0.00	29.40	0.00	22.41	0.00	53.56	0.00	1.14	0.40	1.75	0.04
Cyp2b13	3.69	0.01	14.38	0.00	22.22	0.01	12.71	0.00	10.08	0.00	3.27	0.00	1.68	0.54
Cyp2c29	1.18	0.26	3.22	0.00	3.44	0.01	3.00	0.00	3.13	0.00	1.10	0.55	1.08	0.94
Cyp2c37	1.45	0.07	2.50	0.00	2.73	0.00	2.51	0.00	3.91	0.00	1.45	0.03	2.07	0.00
Cyp2c38	0.74	0.66	0.75	0.36	0.89	0.60	1.43	0.29	0.98	0.38	1.41	0.04	0.81	0.04
Cyp2c39	1.09	0.54	2.21	0.02	2.51	0.02	2.38	0.07	2.15	0.52	1.17	0.18	0.93	0.10
Cyp2c40	2.38	0.00	0.92	0.23	0.85	0.00	1.09	0.74	0.78	0.00	2.82	0.00	2.17	0.00
Cyp2c50	1.61	0.03	2.56	0.00	2.70	0.00	2.23	0.01	3.74	0.00	1.41	0.09	2.24	0.02
Cyp2c54	1.96	0.00	2.52	0.00	2.73	0.00	1.87	0.05	2.91	0.00	1.45	0.04	2.09	0.01
Cyp2c55	0.72	0.53	13.45	0.00	18.68	0.00	15.88	0.00	52.83	0.00	0.85	0.68	2.03	0.00
Cyp2c67	1.99	0.00	0.91	0.96	0.88	0.56	0.99	0.87	0.83	0.10	2.18	0.00	1.88	0.00
Cyp2c68	1.81	0.01	0.92	0.98	0.98	0.99	1.12	0.90	1.11	0.92	2.20	0.00	2.06	0.00
Cyp2c69	2.77	0.00	0.97	0.97	0.91	0.01	1.06	0.61	0.69	0.00	3.03	0.00	2.10	0.00
Cyp2c70	2.15	0.00	1.14	0.28	1.19	0.52	1.18	0.78	0.99	0.36	2.22	0.00	1.80	0.00
Cyp2d9	1.11	0.29	1.30	0.15	0.99	0.83	0.75	0.10	0.72	0.02	0.64	0.04	0.81	0.24
Cyp2d10	1.05	0.37	1.14	0.38	0.89	0.58	0.97	0.49	0.73	0.02	0.90	0.73	0.86	0.28
Cyp2d11	1.00	0.96	1.06	0.86	0.88	0.03	0.86	0.07	0.64	0.00	0.81	0.00	0.73	0.01
Cyp2d12	1.08	0.83	1.29	0.46	0.99	0.58	0.78	0.27	0.71	0.00	0.65	0.04	0.77	0.00
Cyp2d13	0.66	0.18	0.57	0.00	0.60	0.02	0.81	0.17	1.59	0.01	0.94	0.69	1.77	0.00
Cyp2d26	1.29	0.12	0.97	0.85	0.90	0.61	0.85	0.20	0.55	0.00	1.13	0.53	0.78	0.12
Cyp2d34	0.93	0.08	1.06	0.43	0.88	0.01	1.04	0.40	0.82	0.01	0.92	0.44	0.87	0.00
Cyp2d40	0.95	0.42	0.96	0.81	0.80	0.27	0.74	0.03	0.45	0.00	0.73	0.06	0.54	0.00
Cyp2e1	1.67	0.05	1.23	0.28	1.47	0.50	0.91	0.43	0.69	0.05	1.24	0.31	0.79	0.52
Cyp2g1	2.33	0.01	3.25	0.00	4.49	0.00	1.84	0.14	1.59	0.49	1.32	0.14	0.82	0.12
Cyp2j9	0.37	0.03	0.36	0.00	0.51	0.02	0.70	0.37	2.36	0.02	0.73	0.27	1.73	0.00
Cyp2r1	0.94	0.84	1.22	0.18	1.61	0.04	1.11	0.80	1.74	0.12	0.85	0.61	1.02	0.76
Cyp3a11	0.10	0.00	1.55	0.03	1.28	0.60	6.78	0.00	10.96	0.00	0.45	0.00	0.88	0.78
Cyp3a13	1.04	0.45	1.32	0.07	2.33	0.00	1.40	0.32	1.63	0.22	1.10	0.47	0.73	0.02
Cyp3a16	0.09	0.00	1.57	0.03	1.30	0.65	7.87	0.00	10.54	0.00	0.44	0.00	0.72	0.00
Cyp3a25	0.56	0.12	0.90	0.96	1.03	0.89	1.50	0.14	3.48	0.00	0.94	0.97	1.89	0.00
Cyp3a41a	0.10	0.00	1.48	0.01	1.27	0.39	7.12	0.00	9.34	0.00	0.49	0.00	0.75	0.00
Cyp3a41b	0.10	0.00	1.46	0.01	1.25	0.39	7.12	0.00	9.34	0.00	0.49	0.00	0.75	0.00
Cyp3a44	0.12	0.00	1.58	0.44	1.27	0.15	6.63	0.00	8.53	0.00	0.51	0.00	0.82	0.01
Cyp3a59	0.44	0.01	1.13	0.16	1.50	0.02	2.74	0.00	6.42	0.00	1.06	0.25	1.88	0.00
Ugt2b1	1.52	0.07	1.61	0.01	1.46	0.15	1.19	0.58	2.60	0.00	1.12	0.38	2.72	0.00

Gene Symbol	GFCO vs CVCO	p value	CVBDE47 vs CVCO	p value	CVBDE99 vs CVCO	p value	GFBDE47 vs GFCO	p value	GFBDE99 vs GFCO	p value	GFBDE47 vs CVBDE47	p value	GFBDE99 vs CVBDE99	p value
Ugt2b5	0.84	0.89	1.34	0.05	1.35	0.27	1.43	0.18	2.40	0.00	0.89	0.80	1.48	0.10
Ugt2b34	0.75	0.57	1.38	0.04	1.85	0.02	1.76	0.04	3.60	0.00	0.96	0.89	1.46	0.11
Ugt2b35	0.79	0.69	1.37	0.04	1.79	0.02	1.77	0.04	3.94	0.00	1.01	0.70	1.74	0.01
Ugt2b36	0.90	0.82	1.27	0.10	1.43	0.20	1.40	0.27	2.40	0.00	0.99	0.78	1.51	0.08
Ugt2b37	0.76	0.17	1.28	0.74	1.25	0.01	1.48	0.24	2.37	0.75	0.88	0.89	1.45	0.07
Ugt2b38	0.83	0.39	1.25	0.31	1.37	0.44	1.25	0.45	2.63	0.01	0.83	0.27	1.59	0.00
Ugdh	0.65	0.31	1.27	0.09	1.47	0.10	1.82	0.03	4.91	0.00	0.93	0.98	2.18	0.00
Ugp2	1.06	0.61	1.07	0.44	1.36	0.22	1.09	0.73	2.05	0.02	1.07	0.45	1.61	0.02
Sult1a1	1.57	0.03	0.82	0.50	0.88	0.48	1.19	0.81	1.12	0.58	2.29	0.00	1.99	0.00
Sult1b1	1.74	0.01	1.08	0.37	1.24	0.33	0.90	0.47	1.39	0.56	1.45	0.02	1.94	0.00
Sult1c2	0.82	0.83	1.62	0.02	2.20	0.00	2.52	0.00	2.70	0.00	1.27	0.11	1.00	0.70
Sult1d1	1.09	0.55	1.06	0.44	1.68	0.02	1.34	0.25	4.17	0.00	1.37	0.03	2.72	0.00
Sult1e1	4.56	1.00	0.68	1.00	2.22	1.00	2.13	1.00	15.48	0.00	14.34	0.05	31.83	0.00
Sult2a1	29.74	0.14	0.50	1.00	0.47	1.00	24.13	0.00	0.00	0.00	1443.11	0.20	0.23	1.00
Sult2a2	34.16	0.07	0.75	1.00	0.25	1.00	25.39	0.00	0.02	0.20	1156.00	0.05	3.32	1.00
Sult2a7	0.38	0.09	0.84	0.97	2.38	0.01	1.77	0.23	2.32	0.10	0.80	0.43	0.37	0.00
Sult5a1	0.87	0.77	1.74	0.00	1.27	0.54	1.22	1.00	1.23	0.68	0.61	0.01	0.85	0.10
Papss2	0.46	0.04	0.85	0.87	0.96	0.98	1.47	0.16	3.12	0.00	0.79	0.30	1.49	0.01
Gsta1	0.61	0.05	3.04	0.00	4.14	0.00	4.55	0.00	19.15	0.00	0.91	0.38	2.81	0.00
Gsta2	0.74	0.88	1.48	0.03	1.40	0.32	2.82	0.00	4.93	0.00	1.41	0.02	2.62	0.00
Gsta4	1.02	0.39	1.69	0.00	1.48	0.16	2.20	0.02	1.99	0.10	1.33	0.07	1.37	0.06
Gstk1	1.16	0.21	0.90	0.92	0.67	0.06	0.89	0.26	0.69	0.01	1.14	0.44	1.18	0.36
Gstm1	0.77	0.95	2.03	0.00	2.36	0.06	2.54	0.01	3.84	0.00	0.97	0.87	1.26	0.67
Gstm2	1.76	0.01	1.49	0.02	1.97	0.00	1.64	0.29	3.25	0.00	1.94	0.00	2.91	0.00
Gstm3	0.71	0.49	2.86	0.00	4.12	0.00	5.24	0.00	18.41	0.00	1.29	0.02	3.16	0.00
Gstm4	0.78	0.93	1.96	0.00	1.74	0.03	2.16	0.02	3.12	0.00	0.85	0.50	1.39	0.05
Gstm5	1.00	0.56	1.12	0.46	1.12	0.79	1.01	0.66	0.72	0.06	0.90	0.80	0.64	0.00
Gstm6	1.45	0.03	1.16	0.20	0.97	0.86	1.09	0.73	1.23	0.61	1.36	0.06	1.84	0.00
Gstm7	1.36	0.07	0.94	0.93	0.81	0.30	1.11	0.85	0.84	0.06	1.60	0.01	1.40	0.02
Gstp1	0.55	0.27	1.71	0.01	1.09	0.93	1.39	0.72	1.54	0.61	0.45	0.00	0.78	0.20
Gstp2	0.54	0.35	1.72	0.02	1.04	0.23	1.52	0.06	1.49	0.33	0.48	0.38	0.76	0.09
Gstt2	1.33	0.08	1.21	0.17	1.25	0.39	1.46	0.42	1.16	0.55	1.61	0.00	1.24	0.20
Gstt3	1.09	0.26	1.86	0.00	1.98	0.01	2.56	0.00	3.19	0.00	1.50	0.03	1.75	0.00
Gstz1	1.34	0.10	1.02	0.64	0.90	0.61	0.83	0.20	0.68	0.01	1.09	0.64	1.00	0.76
Gclc	0.62	0.22	0.77	0.44	0.86	0.57	1.42	0.21	2.70	0.00	1.15	0.30	1.96	0.00
Slco1a1	1.39	0.15	1.09	0.36	0.91	0.80	0.70	0.19	1.03	0.78	0.89	0.83	1.58	0.01
Slco1a4	0.90	0.93	1.01	0.60	1.26	0.25	1.74	0.04	3.11	0.00	1.56	0.00	2.22	0.00
Slco1b2	0.79	0.68	0.85	0.85	1.26	0.31	0.98	0.93	2.69	0.00	0.92	1.00	1.69	0.03
Slco2a1	0.87	0.79	1.06	0.47	0.88	0.47	1.13	0.93	0.79	0.03	0.93	0.78	0.79	0.02
Abcb1a	0.59	0.01	0.94	0.69	1.16	0.20	1.60	0.01	2.15	0.00	1.00	0.85	1.09	0.84
Abcb1b	0.96	1.00	1.32	0.03	1.26	0.09	1.30	1.00	1.66	1.00	0.94	1.00	1.26	0.29
Abcc2	0.64	0.28	0.93	0.87	1.24	0.35	1.43	0.21	2.97	0.00	0.99	0.91	1.54	0.04
Abcc3	0.82	0.98	1.42	0.04	1.36	0.30	1.52	0.26	1.89	0.10	0.88	0.55	1.14	0.69
Abcc4	0.58	0.25	1.82	0.00	2.43	0.00	1.75	0.12	3.91	0.00	0.56	0.00	0.93	0.36
Abcc10	0.42	0.04	0.47	0.01	0.55	0.02	0.95	0.73	2.21	0.04	0.86	0.54	1.70	0.00

CHAPTER 3: PBDEs Profoundly Alter Gut Microbiome and Increase Unconjugated Bile Acids in A Microbiota-dependent Manner

This chapter has been submitted to the Journal of Toxicological Sciences on 10/2017, and is under revision requested by the reviewers for 2nd submission as of 12/02/2017.

The authors of the manuscript are:

Cindy Yanfei Li[1], Joseph L. Dempsey[1], Dongfang Wang[2,3], Kris M. Weigel[1], Soowan Lee[1], Qiang Fei[2,4], Deepak K. Bhatt[5], Bhagwat Prasad[5], Daniel Raftery[2,6], Haiwei Gu[2,7*], and Julia Yue Cui[1*]

Email addresses:

Li: yanfeili@uw.edu; Dempsey: jld34@uw.edu; Wang: dwang@uw.edu; Weigel: kris11@uw.edu; Lee: slee499@uw.edu; Fei: feiqiang@jilin.edu.cn; Bhatt: bhatt81@uw.edu; Prasad: bhagwat@uw.edu; Raftery: draftery@uw.edu; Gu: haiweigu@asu.edu; Cui: juliacui@uw.edu

[1]Department of Environmental and Occupational Health Sciences, University of Washington, Seattle, WA 98105, USA; [2]Northwest Metabolomics Research Center, Department of Anesthesiology and Pain Medicine, University of Washington, 850 Republican St., Seattle, WA 98109, USA; [3]Department of Laboratorial Science and Technology, School of Public Health, Peking University, Beijing 100191, P. R. China; [4]Department of Chemistry, Jilin University, Changchun, Jilin Province 130061, P. R. China; [5]Department of Pharmaceutics, University of Washington, Seattle, WA 98105,

USA; [6]Division of Public Health Sciences, Fred Hutchinson Cancer Research Center, Seattle, WA 98109, USA; [7]Arizona Metabolomics Laboratory, Center for Metabolic and Vascular Biology, School of Nutrition and Health Promotion, College of Health Solutions, Arizona State University, Phoenix, AZ 85004, USA

Running title: Effect of PBDEs on gut microbiome and bile acid homeostasis

ABSTRACT

Polybrominated diphenyl ethers (PBDEs) are persistent environmental contaminants with well-characterized toxicities in host organs. However, little is known about interactions between PBDEs and gut microbiome, which is a newly discovered "organ" for xenobiotic biotransformation. Microbiomes metabolize primary bile acids (BAs) into more lipophilic secondary BAs that may be absorbed and interact with certain host receptors. The goal of this study is to test our hypothesis that PBDEs alter microbiome function, resulting in dysbiosis and aberrant regulation of BA homeostasis. Nine-week-old male C57BL/6J conventional (CV) or germ-free (GF) mice were administered corn oil (10mg/kg), BDE-47 (100μmol/kg) or BDE-99 (100μmol/kg) by gavage once daily for 4-days (n=3-5/group). Gut microbiomes were characterized using 16S rRNA sequencing in large intestinal content of CV mice. Both BDE-47 and BDE-99 profoundly decreased the alpha diversity of the gut microbiome. PBDEs differentially regulated 45 bacterial species. Most notably, both PBDE congeners profoundly increased *Akkermansia muciniphila* and *Erysipelotrichacea Allobaculum*, which have been previously reported to have anti-inflammatory and anti-obesity properties. Targeted

metabolomics of 56 BAs was conducted in serum, liver, small and large intestinal content (SIC and LIC) of CV and GF mice. BDE-99 markedly increased many unconjugated BAs in multiple bio-compartments in a gut microbiota-dependent manner, and this correlated with an increase in microbial 7α-dehydroxylation enzymes for secondary BA synthesis, and increased expression of host intestinal transporters for BA retrieval. Targeted proteomics showed that PBDEs down-regulated BA-synthesizing enzymes and transporters in livers of CV but not GF mice. In conclusion, there is a novel interaction between PBDEs and the endogenous BA-signaling through modifying the "gut-liver axis" at the doses of PBDEs used in this study.

INTRODUCTION

Polybrominated diphenyl ethers (PBDEs) are flame retardants that are added to a variety of consumer products, such as plastics, rubbers, textiles, furniture, and electronic devices. PBDEs are highly persistent and bioaccumulative in the environment and humans are exposed to PBDEs via food consumption and inhalation. Potentially toxicologically relevant concentrations of PBDEs have been detected in house dust, human blood, breast milk, and body fat (Frederiksen et al., 2009). Using animal models, numerous studies have shown that, at sufficient doses, PBDEs can affect thyroid hormone concentration, behavior, learning ability, memory, brain development, and cancer development (Gascon et al., 2011; Linares et al., 2015). Among the 209 PBDE congeners, 2, 2', 4, 4'-tetrabromodiphenyl ether (BDE-47) and 2, 2', 4, 4', 5-pentabromodiphenyl ether (BDE-99) are the most predominant ones detected in the environment and in human samples (Erratico et al., 2011). BDE-47 and BDE-99

activate the major xenobiotic-sensing nuclear receptors pregnane X receptor (PXR/Nr1i2) and constitutive androstane receptor (CAR/Nr1i3) in both rodents and human hepatocytes, leading to up-regulated expression of cytochrome P450s (Cyps) (Pacyniak et al., 2007; Sueyoshi et al., 2014). Using RNA-Seq, we recently demonstrated that BDE-47 and BDE-99 differentially regulated many other phase-I drug-metabolizing enzymes (i.e. enzymes involved in oxidation, reduction, and hydrolysis), phase-II enzymes (i.e. enzymes involved in conjugation) as well as transporters in mouse liver. In addition, we demonstrated that the lack of gut microbiota in germ free (GF) mice altered the oxidation of BDE-47 and BDE-99, and profoundly modified the PBDE-mediated transcriptomic response in liver (Li et al., 2017). This has provided the first evidence that there is a novel interaction between gut microbiota and environmental contaminants (PBDEs) that influence the host hepatic xenobiotic biotransformation. However, very little is known regarding the interactions between PBDEs and gut microbiota on intermediary metabolism.

Bile acids (BAs), which are jointly produced by liver and intestinal bacteria, are important signaling molecules for intermediary metabolism within the gut liver axis and in extrahepatic organs, such as brown adipose tissue and muscle. Primary BAs are synthesized in liver from cholesterol via classical and alternative pathways. The classical pathway accounts for at least 75% of the total BA pool. Enzymes involved in classic pathway of BA synthesis include the rate-limiting enzyme cholesterol 7α-hydroxylase (Cyp7a1) and 12α-hydroxylase (Cyp8b1), which determine the ratio of cholic acid (CA) over chenodeoxycholic acid (CDCA), as well as other enzymes

downstream. The alternative pathway is initiated by sterol-27 hydroxylase (Cyp27a1), followed by 7α-hydroxylase (encoded by Cyp7b1) and other downstream enzymes (Thomas et al., 2008). The major primary BAs in humans are CA and CDCA, whereas CDCA in mice is converted to the primary BAs α-muricholic acid (αMCA) and βMCA. BAs are conjugated with glycine or taurine in humans and primarily with taurine in mice. The primary BAs are secreted across the canalicular membrane of hepatocytes via the bile salt export pump (Bsep) into bile.

Gut microbiota contains a wide spectrum of microorganisms which reside in the gastrointestinal tract and play an important role in nutrient absorption, host intermediary metabolism, and xenobiotic biotransformation (Shreiner et al., 2015; Fu and Cui, 2017). Disruptions in the composition of gut microbial communities and altered interactions between microbiota-host have been linked to several diseases, such as cancer and metabolic disorders (Jumpertz et al., 2011). In the intestine, gut microbiota converts primary BAs to secondary BAs via dehydroxylation, deconjugation, and epimerization. The intestinal microbiota contains enzymes that metabolize BAs; for example, bile salt hydrolases (Bshs), which are widely present in intestinal bacteria, removes glycine or taurine from conjugated BAs. The bacteria *Clostridia* contain hydroxysteroid dehydrogenases and 7-dehydratases, which produce BA intermediates and secondary BAs (Ridlon et al., 2006).

Ninety-five percent of BAs undergo reabsorption from the intestinal lumen via active transport and recirculate to liver by the portal blood (Chiang, 2003). Specifically, BAs

are actively transported across the apical membrane of ileal enterocytes via the apical sodium bile acid transporter (Asbt/Slc10a2). They are then transported across the enterocytes via the heterodimer organic solute transporter α and β (Ostα/Ostβ) and enter portal circulation. In particular, the basolateral efflux transporter multidrug resistance related protein 4 (Mrp4/Abcc4) has been shown to have BA transport properties in liver (Dawson et al., 2009). We have recently shown that Mrp4 gene expression is higher in the intestine than that in the liver of mice (Fu et al., 2017). In human enterocyte-derived Caco-2 cells, MRP4 has been shown to be localized to the basolateral membrane (Ming and Thakker, 2010). These studies suggest that Mrp4 may also contribute in BA re-absorption in intestine. Upon reaching the liver BAs are taken up across the sinusoidal membrane of hepatocytes via sodium taurocholate cotransporting polypeptide (Ntcp/Slc10a1) and organic anion transporting polypeptide 1b2 (Oatp1b2/Slco1b2) transporters (Russell, 2003; Klaassen and Cui, 2015). Accumulation of BAs in hepatocytes or the biliary tract may lead to oxidative stress, inflammation, and cholestatic liver injury (Perez and Briz, 2009).

BAs functioning as signaling molecules not only regulate their own biosynthesis, but also communicate with distinct host receptors to regulate many physiological pathways in xenobiotic and intermediary metabolism (Chiang, 2003). The farnesoid-X-receptor (FXR) is a BA receptor that regulates BA synthesis in liver. In the intestine, BAs activate FXR in the ileum enterocytes, and induce the secretion of fibroblast growth factor (Fgf) 15 (FGF19 in humans). Fgf15 is then released into the portal blood and delivered to liver where it activates the FGF receptor 4 (Fgfr4) and negatively regulates

bile acid synthesis (Inagaki et al., 2005). Activation of hepatic FXR by BAs up-regulates the expression of small heterodimer partner (SHP) and subsequently represses hepatic BA synthesis (Goodwin et al., 2000). By using tissue-specific Fgf15-null mice, it has been demonstrated that the intestinal FXR/Fgf15 pathway is critical for suppressing both Cyp7a1 and Cyp8b1 gene expression, whereas the liver FXR/SHP pathway is important for suppressing Cyp8b1 gene expression and only has a minor role in suppressing Cyp7a1 gene expression (Kong et al., 2012). Activation of another BA receptor, namely TGR5 by BAs in brown adipose tissue, has been shown to promote thermogenesis and energy expenditure (Sajner and Krizek, 1984). Modulating the BA receptors FXR and TGR5 as well as gut microbiota has been shown to help reduce obesity, type-II diabetes, and inflammation (Klaassen and Cui, 2015).

Clinically, many therapeutic drugs have been shown to produce cholestatic liver injury by elevating hepatic BA levels (Padda et al., 2011). In laboratory animals, activation of xenobiotic sensor CAR by its activators, phenobarbital and TCPOBOP, led to decreased BAs in mouse liver, but increased fecal excretion of muricholic acids (Sberna et al., 2011; Lickteig et al., 2016). Lack of gut microbiota in GF mice resulted in higher BA concentrations in serum, liver, bile, and ileum than that in CV mice (Selwyn et al., 2015c). However, very little is known regarding to what extent environmental chemicals such as PBDEs may modulate the host BA homeostasis, and whether gut microbiota is involved in this process.

To investigate to what extent PBDEs modulate host BA homeostasis and the potential involvement of the "gut-liver axis" in this process, the present study utilized a multi-omics approach, including targeted proteomics (LC-MS/MS of BA-processing genes), targeted metabolomics (LC-MS/MS of 56 BAs), and bacterial metagenomics (16S rRNA sequencing in large intestinal content [LIC]), to test our working hypothesis that the gut microbiome, as a newly discovered "dispersed organ", serves as a critical interface in modulating the crosstalk between the environmental chemicals PBDEs and the endogenous BA-signaling pathways (Figure 1).

MATERIALS AND METHODS

Chemicals

BDE-47 was purchased from Chem Service, Inc. (West Chester, PA). BDE-99 was purchased from AccuStandard, Inc. (New Haven, CT). Phosphate-buffered saline (PBS, 10x, pH 7.4), LC-MS grade methanol, water, and acetonitrile were purchased from Thermo Fisher Scientific (Grand Island, NY). Bile acid standards and deuterated internal standards (IS) lithocholic acid-2,2,4,4-D4 (LCA-D4), deoxycholic acid-2,2,4,4-D4 (DCA-D4), cholic acid-2,2,4,4-D4 (CA-D4), glycochenodeoxycholic acid-2,2,4,4-D4 (GCDCA-D4), and glycocholic acid-2,2,4,4-d4 (GCA-d4) were purchased from Steraloids, Inc. (Newport, RI). All other chemicals and reagents, unless indicated otherwise, were purchased from Sigma-Aldrich (St. Louis, MO).

Animals and Procedures

Eight-week-old male C57BL/6J conventional (CV) mice were purchased from The Jackson Laboratory (Bar Harbor, ME) and were acclimated to the animal facility at University of Washington for one week prior to experiments. The initial breeding colony of germ-free (GF) mice in C57BL/6 background was established with mice purchased from the National Gnotobiotic Rodent Resource Center (University of North Carolina, Chapel Hill). All mice were housed according to the Association for Assessment and Accreditation of Laboratory Animal Care International guidelines, and the animal studies were approved by the Institutional Animal Care and Use Committee (IACUC) at the University of Washington. The CV mice were exposed to the same diet (laboratory autoclaved rodent diet #5010, LabDiet, St. Louis, MO), water (non-acidified autoclaved water), and bedding (autoclaved Enrich-N'Pure) as the GF mice. All chemical solutions were sterilized using the Steriflip Vacuum-driven Filtration System with a 0.22 μM Millipore Express Plus Membrane (EMD Millipore, Temecula, CA). All gavage needles and syringes were sterilized by autoclave. As described in Figure 1, at 9 weeks of age, CV and GF mice were randomly allocated for the treatment of vehicle (corn oil, 10 ml/kg), BDE-47 (100 μmol/kg), or BDE-99 (100 μmol/kg) via oral gavage once daily for 4 consecutive days (n = 3~5 per group). On the 5^{th} day (24 hours after the final dose), various tissues were collected. Blood was collected via cardiac puncture and centrifuged at 1500*g* for 10 min at 4°C to obtain serum. Livers were removed and immediately frozen in liquid nitrogen. Small and large intestinal contents (SIC and LIC) were flushed using PBS containing 10mM dithiothreitol (DTT) (Sigma Aldrich, St. Louis, MO), and centrifuged at 20,000*g* for 30 min at 4 °C. The intestinal tissues were

separated into various sections, namely duodenum, jejunum, ileum, and colon. All samples were stored at -80 °C until further analysis.

Quantification of Bacterial DNA and 16S rRNA Gene Sequencing

Total genomic bacterial DNA was extracted from the LIC of CV mice using OMEGA E.Z.N.A. DNA Stool Kit (Omega Bio-tek, Inc., Norcross, GA) according to the manufacturer's instructions. The concentration of total DNA was determined using a Qubit 2.0 Fluorometer (Life Technologies, Grand Island, NY). The integrity and quality of DNA samples were confirmed using an Agilent 2100 Bioanalyzer (Agilent Technologies Inc., Santa Clara, CA). The V4 region of 16S rRNA gene was amplified and sequenced using a HiSeq 2500 platform (250bp paired-end) (Beijing Genome Institute Americans Corporation, Cambridge, MA) (n=3 per group). The paired-end sequence reads were merged, de-multiplexed, and chimera-filtered using QIIME version 1.9.1 (Quantitative Insights Into Microbial Ecology) (Caporaso et al., 2010). Operational Taxonomy Unit (OTU) clustering and taxonomy classification were performed using open-reference operational taxonomic unit picking method (UCLUST version 1. 2. 22q) against the 99% representative databases for Greengenes (version 13.8). Functional profiles of microbial communities were predicted using PICRUSt (Phylogenetic Investigation of Communities by Reconstruction of Unobserved States) (Langille et al., 2013). Differentially enriched pathways were plotted as two-way hierarchical clustering dendrograms using JMP Genomics (SAS Institute, Inc., Cary, NC). Selected differentially regulated bacteria were validated by quantitative polymerase chain reaction (qPCR) using Bio-Rad CFX384 Real-Time PCR Detection System (Hercules,

CA). The 16S rRNA primers for the detection of *Akkermansia muciniphila*, *Erysipelotrichaceae Allobaculum*, and *Clostridium scindens* were designed based on the 16S rRNA sequences of these bacteria (Supplemental Table 1). The primers recognizing the universal bacterial 16S rRNA sequences were provided by the University of North Carolina Gnotobiotic core facilities (Supplemental Table 1). All primers were synthesized by Integrated DNA Technologies (Coralville, IA). The abundances of the genomic DNA were expressed as mean delta-delta cycle value of the quantitative PCR (ddCq) as compared to the universal bacteria.

Targeted Metabolomics of Bile Acids (BAs) using Liquid Chromatography-Tandem Mass Spectrometry (LC-MS/MS)

A standard stock solution of each individual BA and deuterated internal standards (IS) were prepared at a concentration of 2 mg/ml in methanol. IS (10 μM of LCA-D4, DCA-D4, CA-D4, GCDCA-D4, and GCA-D4) were added to the samples, and BAs were extracted from the serum, liver, SIC, and LIC using methods reported previously (Zhang and Klaassen, 2010). Fifty-six BAs were quantified as listed in Supplemental Table 2. Among them, T-αMCA and T-βMCA were summed together and expressed as T-α+βMCA. The concentrations of individual BAs were analyzed relative to their corresponding internal standards.

For serum BA extraction, 50 μl serum samples was spiked with 25 μl of the mixed internal standard solution. The samples were vortexed and put on ice for 5 min. Cold methanol (500 μl) was added for protein precipitation, and samples were vortexed 3 x

10s and maintained on ice for 10 min. After centrifugation at 12,000*g* for 10 min at 4 °C, supernatants were transferred to clean tubes. The residues were reconstituted in 500 µl methanol, vortexed for 10 min, and centrifuged at 12,000*g* for 10 min at 4 °C. The two extraction supernatants were pooled and dried under vacuum. The residue was then reconstituted by adding 100 µl methanol solution (methanol: water = 50:50, v/v), and centrifuged at 20,000*g* for 10 min at 4 °C. The supernatants were transferred to individual glass vials for MS analysis.

For liver BA extraction, approximately 60 mg frozen liver were accurately weighed and homogenized in 5 volumes of water (300 µl for 60 mg). For each 300 µl homogenate, 1.5 ml of acetonitrile (ACN) with 5% ammonia hydroxide (NH_4OH) and 25 µl of IS solution was added. Tubes were vortexed and shaken for 1 h at room temperature. The mixtures were centrifuged at 12,000*g* for 15 min at 4 °C, and supernatants were transferred to clean tubes. A second BA extraction was performed with 750 µl methanol, shaking for 20 min, sonicating for 5~10 min, and centrifuging at 15,000*g* for 20 min. Finally, the two extraction supernatants were pooled and dried under vacuum. The residue was then reconstituted by adding 100 µl 50% MeOH, vortexed, transferred onto the 0.22 µm Costar Spin-X centrifuge tube filter (Sigma-Aldrich, St. Louis, MO), and centrifuged at 20,000*g* for 10 min before injection.

For BA extraction from SIC and LIC, approximately 60 mg frozen pellets were accurately weighed and homogenized in 5 volumes of water (300 µl). For each 300 µl

homogenate, 1.5 ml ACN with 5% NH_4OH and 20 µl IS were added. The rest of the procedures were same as those for liver BA extraction.

For BAs measurements, 2 µL of each prepared sample was injected into a LC-MS/MS system (Waters Acquity I-Class UPLC TQS-micro MS, Waters, Milford, MA) for analysis using negative ionization mode. The LC-MS/MS system was equipped with an electrospray ionization source. Chromatographic separation was achieved on a Waters XSelect HSS T3 column (2.5 µm, 2.1 × 150 mm). The mobile phase A was 5 mM ammonium acetate in H_2O with 0.1% acetic acid, and the mobile phase B was acetonitrile with 0.1% acetic acid. After 1 min of isocratic elution of 75% of solvent A, the mobile phase composition changed to 5% A at t=15 min. It was then maintained at 5% A for 10 min, followed by a rapid increase at t=25 min to 75% A to prepare for the next injection. The total experimental time for each injection was 40 min. The flow rate was 0.3 mL/min, the auto-sampler temperature was 4℃, and column compartment temperature was 40℃. The targeted LC-MS/MS data was acquired using multiple-reaction-monitoring (MRM) mode. The experimental parameters for all the 56 BAs and five ISs, such as MRM transitions and retention times, were validated by spiking mixtures of standard compounds into a pooled study sample. TargetLynx software (Waters, Milford, MA) was used to integrate extracted MRM peaks. To determine absolute bile acid concentrations, calibration curves were first constructed for all the BAs standards in reference to their corresponding ISs. Concentrations of the bile acids in the study samples were then calculated from the peak areas and the slopes of the calibration curves.

Total RNA Isolation

Total RNA was isolated from liver and intestinal tissue sections using RNA-Bee reagent (Tel-Test Inc., Friendswood, TX). The concentration of total RNA was quantified using NanoDrop 1000 Spectrophotometer (Thermo Scientific, Waltham, MA) at 260 nm. The quality of RNA was evaluated by formaldehyde-agarose gel electrophoresis with visualization of 18S and 28S rRNA bands under ultraviolet light, and was confirmed using an Agilent 2100 Bioanalyzer (Agilent Technologies Inc. Santa Clara, CA). Liver samples with RNA integrity number (RIN) above 8.0 were used for RNA-sequencing.

Messenger RNA quantification

The mRNA of Cyp7a1 (Figure 12A) as well as the mRNAs of other BA-processing genes in liver were retrieved from our previously published RNA-Seq dataset (Li et al., 2017). The data have been deposited in the NCBI Gene Expression Omnibus and are accessible through the GEO Series accession number GSE101650. Intestinal mRNAs of various BA-processing genes were determined using RT-qPCR. Briefly, total RNA from intestinal tissue sections was transcribed to cDNA using a High Capacity cDNA Reverse Transcription Kit (Applied Biosystems, Foster City, CA). The cDNAs were amplified by PCR using SsoAdvanced Universal SYBR Green Supermix in a BioRad CFX384 Real-Time PCR Detection System (Bio-Rad, Hercules, CA). The PCR primers were synthesized by Integrated DNA Technologies (Coralville, IA) and the primer sequences are listed in Supplemental Table 1. The ddCq values were calculated for each target gene and were normalized to the expression of the housekeeping gene β-actin.

Targeted Proteomics by LC-MS/MS

The procedure is similar to a previous publication with a few modifications (Selwyn et al., 2015a; Li et al., 2017). Briefly, the membrane proteins of the mouse livers were isolated using a Mem-PER plus membrane protein extraction kit (Pierce Biotechnology, Rockford, IL). Eighty µl of the tissue extract (2 mg/ml total protein) was mixed with 10 µl DTT (250 mM), 20 µl of 0.2 mg/ml bovine serum albumin, 10 µl of 10 mg/ml human serum albumin, and 40 µl ammonium bicarbonate buffer (100 mM, pH 7.8), and incubated at 95 °C for 5 min (denaturation and reduction). Subsequently, 20 µl iodoacetamide (500 mM) was added and the sample was incubated for 30 min at ambient temperature in the dark (alkylation). Ice-cold methanol (0.5 ml), chloroform (0.1 ml) and water (0.4 ml) were added to each sample. After centrifugation at 16,000*g* for 5 min at 4 °C, the upper and lower layer were removed and the pellet was washed with ice-cold methanol (0.5 ml) and then centrifuged at 8,000*g* for 5 min at 4 °C. The pellet was resuspended with 60 µl 50 mM ammonium bicarbonate buffer. Trypsin (20 µl) was added at a 1:80 trypsin: protein ratio (w/w), and samples were incubated for 16 h at 37 °C. Trypsin digestion was stopped by adding 10 µl of chilled quenching solvent (80% acetonitrile with 0.5% formic acid) and 20 µl heavy peptide internal standard, samples were centrifuged for 5 min at 4,000*g* under 4 °C, and supernatant was collected into a LC-MS vial. The stable isotope-labeled heavy peptides were used as internal standards (Thermo Fisher Scientific, Rockford, IL). LC-MS/MS consisted of an Acquity LC (Waters Technologies, Milford, MA) coupled to an AB Sciex Triple Quadrupole 6500 MS system (Framingham, MA). One to three surrogate peptides per protein were designed

for the quantification of selected proteins (Supplemental Table 3) according to a previously published protocol (Prasad and Unadkat, 2014). The peptide separation was achieved on an Acquity UPLC column (HSS T3 1.8 µm, 2.1x100 mm, Waters, Hertfordshire, UK). Mobile phase A (water with 0.1% formic acid; v/v) and mobile phase B (acetonitrile with 0.1% formic acid; v/v) were used with a flow rate of 0.3 ml/min in a gradient manner. Peak integration and quantification were performed using Analyst (Version 1.6, Mass Spectrometry Toolkit v3.3, Framingham, MA, USA). A robust strategy was used to ensure optimal reproducibility when quantifying these proteins (Bhatt and Prasad, 2017). For example, ion suppression was addressed by using heavy peptide. Bovine serum albumin (BSA) was used as an exogenous internal standard, which was added to each sample to correct for protein loss during processing and digestion efficiency. In total, three-step data normalization was used; first average peak areas of light peptides were divided by corresponding average heavy peptide peak areas. This ratio was then divided by BSA light/heavy peak area ratio. Finally, the data were normalized to average quality control values (pooled representative sample). Specific peptides targeting these proteins are listed in Supplemental Table 3.

Statistical Analysis

Data are presented as mean ± standard error (SE). Statistically significant differences were determined by Analysis of variance (ANOVA) followed by Duncan's post-hoc test ($p<0.05$). Asterisks (*) represent statistically significant differences between corn oil- and PBDE-treated groups within CV or GF mouse colonies. Pounds (#) represent significant differences between CV and GF mice under the same treatment. A

hierarchical clustering dendrogram (Ward's minimum variance method, distance scale) of the differentially enriched pathways was generated by JMP Genomics software (SAS Institute, Inc., Cary, NC). Pearson's correlations between BAs and bacterial species were performed with R (ggplot2).

RESULTS

Effect of PBDEs on gut microbiome using 16S rRNA sequencing

To determine the effect of oral exposure to PBDEs on gut microbiome, 16S rRNA sequencing targeting V4 region was performed in the LIC of CV mice treated with corn oil, BDE-47 (100 μmol/kg), or BDE-99 (100 μmol/kg) (n=3 per group). The sequence analysis yielded a total of 104,282 ± 3,574 reads per sample (Supplemental Table 4). Rarefaction analysis (QIIME) was performed from 0 to 80,000 reads with an increment of 10,000 reads. The alpha diversity, which describes species richness, demonstrated that both BDE-47 and BDE-99 profoundly decreased microbial richness compared to corn oil-treated control group in the LIC of CV mice (Figure 2A). The beta diversity, which describes the species differences among different samples, was calculated using weighted UniFrac distance matrix and visualized by principle coordinates analysis (PCoA). As shown in Figure 2B, there was a clear separation between PBDE-treated samples and control samples. The BDE-47 treated samples were clustered separately from BDE-99 treated samples at PC2 direction in the PCoA plot (Figure 2B).

The majority of OTUs were assigned to the phyla *Firmicutes* (52.6 ± 1.6%), *Bacteroidetes* (35.1 ± 2.0%), and *Verrucomicrobia* (8.3 ± 1.8%); *Actinobacteria*,

Tenericutes, *Fusobacteria*, *Proteobacteria*, *Acidobacteria*, *Deferribacteres*, *Chlorobi*, *Planctomycetes*, *Crenarchaeota*, *Fibrobacteres*, *Nitrospirae*, and *Chloroflexi* were detected at levels <1%. In addition, 2.5 ± 0.4% of sequences were not assigned to any bacterial phylum (Supplemental Figure 1). To identify specific taxa affected by PBDE exposure, more in-depth comparisons at the class and species levels were conducted among corn oil, BDE-47, and BDE-99 treated conditions. At class level (Figure 2C), the abundance of *Actinobacteria* in *Actinobacteria* phylum decreased 69.2% by BDE-99. *Coriobacteriia* in *Actinobacteria* phylum and *Bacilli* in *Firmicutes* phylum were decreased by both BDE-47 (*Coriobacteriia*: 44.2%, *Bacilli*: 69.4%) and BDE-99 (*Coriobacteriia*: 54.7%, *Bacilli*: 68.0%). Conversely, *Erysipelotrichi* in *Firmicutes* phylum, *Gammaproteobacteria* in *Proteobacteria* phylum, and *Verrucomicrobiae* in *Verrucomicrobia* phylum were profoundly increased by both BDE-47 (7.5-, 6.1-, and 3.3-fold increase) and BDE-99 exposure (5.7-, 7.8-, and 5.2-fold increase) (Figure 2C). Analysis conducted at the species level identified 154 bacterial taxa, of which 41 were differentially regulated by PBDEs as compared to corn oil-treated control group. These bacterial species partitioned into three distinct patterns: Pattern I include 4 taxa that were increased by both BDE-47 and BDE-99, including *Allobaculum, Anaerotustis, Bacteroidales other,* and other unassigned bacterial species; Pattern II included 6 taxa that were decreased by BDE-47 but increased by BDE-99, including *Clostridiales, Peptostreptococcaceae, Clostridiaceae, Coprobacillus, SMB53,* and *muciniphila*; Pattern III was the largest cluster, which included 31 taxa that were consistently decreased by both BDE-47 and BDE-99. This third cluster included two species in the *Bifidobacterium* genus*, Bacteroidales, Bacillaceae,* two species in the *Clostridium* genus,

Bacillales other, *Staphylococcus*, *Bacillus other*, *Pseudobutyrivibrio*, *Planococcaceae*, *Staphylococcus other*, *Staphylococcaceae other*, *Adlercreutzia, Reuteri*, 2 species in the *Lactobacillus* genus, *Planococcaceae other*, *Cocleatum, Butyrivibrio*, *Salinicoccus*, *Lactobacillales*, *Granulicatella*, *Enterococcus*, *Facklamia*, *Dorea*, *Lachnospiraceae*, *Mogibacteriaceae*, *Erysipelotrichaceae*, *Dehalobacterium*, and *Ruminococcus* (Figure 3A). The relative abundance of these bacterial species was determined across all treatment groups. Figure 3B showed the top 10 most abundant bacterial species (note: all other taxa that were lower than the top 9 taxa were summed and labeled "other taxa" as the 10th category). On average, across all treatment groups, the predominant species were *S24-7* (32.8 ± 1.9%) in *Bacteroidetes* phylum and *Clostridiales* (16.3 ± 1.9%) in *Firmicutes* phylum. Most notably, *Akkermansia muciniphila* in *Verrucomicrobia* phylum and *Erysipelotrichaceae Allobaculum* in *Firmicutes* phylum were minimally present in corn oil treated control group, but were markedly increased after PBDE exposure, suggesting that they may be novel biomarkers for PBDE exposure (Figure 3B). The elevated levels of *Akkermansia muciniphila* and *Erysipelotrichaceae Allobaculum* by PBDEs were further confirmed by qPCR (Figure 3C).

To further examine the effect of PBDEs on BA-metabolizing bacteria and microbial enzymes, qPCR was performed on *Clostridium scindens*, which is a bacterium with known functions of 7α de-hydroxylation (Ridlon et al., 2006); the BA-inducible operons *baiCD* and *baiJ*, which are microbial enzymes involved in BA dehydroxylation (i.e. secondary BA synthesis); as well as bile salt hydrolase (*bsh*), which performs BA deconjugation. Interestingly, although PBDEs did not alter the abundance of

Clostridium scindens, baiCD was markedly increased by BDE-99 (1.8-fold increase), and *baiJ* was markedly increased by both BDE-47 (1.7-fold) and BDE-99 (1.9-fold). *Bsh* appeared to be increased by BDE-99 although a statistical significance was not achieved (Figure 3C). Together these data indicate that bacteria other than *Clostridium scindens*, which are likely from Pattern I and Pattern II may be responsible for the up-regulation of microbial BA-metabolizing enzymes.

Predicted functional composition of gut microbiome with PICRUSt

The functional profiles of gut microbiota were predicted by PICRUSt (Langille et al., 2013) across all three treatment groups. A total of 39 differentially enriched KEGG pathways by PBDEs were identified and plotted using the mean value for each treatment (Figure 4). These pathways can be grouped into 4 categories, namely bacteria-specific processes (Figure 4A), xenobiotic biodegradation and metabolism (Figure 4B), basal cellular processes (Figure 4C), and intermediary metabolism (Figure 4D). For bacteria-specific processes, BDE-99 increased the abundance of all 5 KEGG pathways, namely penicillin and cephalosporin biosynthesis, lipopolysaccharide biosynthesis, beta-lactam resistance, stilbenoid, diarylheptanoid and gingerol biosynthesis (which are reported to have anti-inflammatory or anti-cancer functions), and phosphotransferase system (PTS, a bacterial-specific pathway for carbohydrate metabolism). BDE-47 also increased stilbenoid, diarylheptanoid and gingerol biosynthesis and the PTS pathways (Figure 4A). These data indicate that there may be a compensatory mechanism to up-regulate these microbial processes to adapt to PBDE-induced dysbiosis.

For xenobiotic biodegradation and metabolism (Figure 4B), BDE-99 up-regulated 4 KEGG pathways, namely caffeine metabolism, fluorobenzoate degradation, geraniol degradation, as well as chlorocyclohexane and chlorobenzene degradation. Conversely, both BDE-47 and BDE99 decreased the KEGG pathways related to dioxin degradation, xylene degradation, drug metabolism, and ethylbenzene degradation (BDE-99 mediated decrease in ethylbenzene degradation was apparent, but not statistically significant). These data suggest that the microbial biotransformation of PBDEs may interact with the metabolism of other xenobiotics listed in this heatmap.

Regarding basal cellular functions (Figure 4C), BDE-47 increased the KEGG pathway of ion channels, but decreased the KEGG pathways involved in cell division, glycan biosynthesis and metabolism, glycosphingolipid biosynthesis, electron transfer carriers, basal transcription factors, and G protein-coupled receptors. BDE-99 markedly increased the KEGG pathways involved in cell motility and secretion, transcription related proteins, glycosaminoglycan degradation, ubiquitin system, non-homologous end-joining, and ion channels, but decreased the KEGG pathways involved in apoptosis, cell division, glycan biosynthesis and metabolism, electron transfer carriers, and basal transcription factors. These data further suggested that there is a compensatory mechanism of bacterial functions in order to adapt to PBDE-induced insults on the basal functions of the gut microbiota.

Within intermediary metabolism pathways (Figure 4D), BDE-47 decreased the KEGG pathways involved in ether lipid metabolism, mineral absorption, alpha-linolenic acid metabolism (which is anti-inflammatory), and cyanoamino acid metabolism, but increased arachidonic acid metabolism (which is involved in inflammation). BDE-99 also showed the same trend in regulating these pathways, and in addition, BDE-99 decreased the KEGG pathways involved in carbohydrate digestion and absorption, nicotinate and nicotinamide metabolism, but increased arachidonic acid metabolism, fatty acid elongation in mitochondria, steroid and steroid hormone biosynthesis, ubiquinone and other terpenoid-quinone biosynthesis, and carotenoid biosynthesis. These data suggest that PBDEs may lead to a pro-inflammatory stage in the GI tract, and perturb the absorption and biotransformation of essential micronutrients. The BDE-99-mediated increase in steroid/steroid hormone synthesis also coincides with increased microbial biotransformation of BAs (Figure 3C), which is part of the steroid hormone signaling.

BAs in serum, liver, SIC, and LIC of CV mice

BAs are a group of steroids that are synthesized jointly by hepatic and microbial enzymes. To determine how oral exposure to PBDEs affects BA homeostasis, targeted metabolomics analysis of BAs was performed in serum, liver, SIC, and LIC of CV mice treated with corn oil, BDE-47 (100 μmol/kg) or BDE-99 (100 μmol/kg) (n=3 per group).

In serum, 12 BAs were detectable in CV mice, including four unconjugated BAs (Figure 5A) and eight taurine (T)- or glycine (G)-conjugated BAs (Supplemental Figure 2A). In

general, PBDEs did not markedly alter the primary or secondary conjugated BAs in serum, except for a moderate decrease in G-CA (22.6%) by BDE-99, and an apparent decrease in T-α/βMCA by BDE-47 (although a statistical significance was not achieved) (Supplemental Figure 2A). Regarding the unconjugated BAs in serum, BDE-99 increased the primary BA β-MCA (3.4-fold) and also tended to increase the primary BA CA (1.7-fold) and the secondary BA ωMCA (1.9-fold); conversely, BDE-47 decreased the secondary BA 3DHCA (72%), and tended to decrease the primary BAs CA (51.7%), βMCA (62.8%), and the secondary BA ωMCA (58.4%), although a statistical significance was not achieved.

In the liver, 23 BAs were detected in CV mice, including 12 unconjugated BAs (Figure 5B) and 11 T- or G-conjugated BAs (Supplemental Figure 2B). In general, PBDEs had less effect on the conjugated BA profiles, except for an increase in the primary BA G-CA (3.3-fold) and the secondary BA T-DCA (3.2-fold) by BDE-99. In contrast, BDE-99 markedly increased most unconjugated primary BAs, including CA (6.3-fold), αMCA (3.6-fold), and βMCA (3.6-fold), as well as most unconjugated secondary BAs, including ωMCA (3.0-fold), Murocholic acid (3.2-fold), HDCA (3.5-fold), 12DHCA (3.1-fold), 5β-Cholanic Acid-3α, 6α-diol-7-one (3.3-fold), and 5 β-Cholanic Acid-3β, 12α-diol (2.1-fold) (Figure 5B).

In the SIC, 24 BAs were detected in CV mice, including 14 unconjugated BAs (Figure 6A) and 10 T- or G-conjugated BAs (Supplemental Figure 3A). For conjugated BAs, PBDEs in general decreased many primary and secondary BAs in SIC, namely T-α/βMCA by BDE-47 (66.1%), T-UDCA by BDE-47 and BDE-99 (58.9% and 52.2%), G-

CA by BDE-47 and BDE-99 (66.2% and 59.9%), T-LCA by BDE-47 and BDE-99 (72.7% and 56.5%), T-HCA by BDE-99 (47.4%), and T-HDCA by BDE-47 and BDE-99 (57.4% and 52.7%). Conversely, BDE-99 markedly increased conjugated BAs such as the primary BAs βMCA (2.1-fold) and UDCA (2.4-fold), and most unconjugated secondary BAs, including ωMCA (3.1-fold), DCA (2.4-fold), HCA (1.9-fold), 3 DHCA (3.5-fold), 3α-OH-12 Ketolithocholic Acid (2.1-fold), 8(14), (5β)-Cholenic Acid-3α, 12α-diol (2.1-fold), and 9(11), (5β)-Cholenic Acid-3α-ol-12-one (1.8-fold). BDE-47 also increased several unconjugated secondary BAs, including ωMCA (3.4-fold), HCA (2.7-fold), 3 DHCA (4.3-fold), and 9(11), (5β)-Cholenic Acid-3α-ol-12-one (1.6-fold) (Figure 6A).

In the LIC, 25 BAs were detected in CV mice, including 14 unconjugated BAs (Figure 6B) and 11 T- or G-conjugated BAs (Supplemental Figure 3B). For conjugated BAs, BDE-47 increased the primary BA T-α/βMCA (7.5-fold) and the secondary BA T-DCA (12.2-fold), whereas BDE-99 increased the primary BA G-CDCA (7.4-fold) and the secondary BA T-HDCA (5.1-fold) (Supplemental Figure 3B). Among unconjugated BAs, BDE-47 increased the primary BA αMCA (1.9-fold), as well as the secondary BAs LCA (2.2-fold), HCA (5.1-fold), HDCA (1.8-fold), 3 DHCA (20.1-fold), Allolithocholic acid (6.5-fold), Isolithochoilc acid (2.3-fold), and 3-Ketocholanic acid (1.8-fold). BDE-99 decreased the primary BA CDCA (65.6%), but increased UDCA (2.8-fold), as well as the secondary BAs DCA (2.8-fold) and Allolithocholic acid (4.7-fold) (Figure 6B).

Pearson's correlation between secondary BAs and bacterial species

Because secondary BAs were exclusively produced by gut microbiota, to determine which bacterial species may contribute to altered total secondary BA pool in CV mice, individual secondary BAs from all four compartments of CV mice were summed and then correlated with 41 bacterial species that were differentially regulated by PBDEs (Figure 7). Both unconjugated secondary BAs (which were exclusively produced by gut microbiota) and conjugated secondary BAs (which were produced by bacteria and then conjugated in liver) were considered. Pearson's correlation analysis revealed that 20 out of 41 bacterial species were positively correlated with taurine-conjugated secondary BAs (including T-ωMCA, T-HCA, T-HDCA, and T-LCA), but negatively correlated with many unconjugated secondary BAs.

A. muciniphila, which was markedly increased by both BDE-47 and BDE-99, was positively associated with DCA and its taurine-conjugate, suggesting that it may contribute to the conversion of CA to DCA. *A. muciniphila* also positively correlated with several other minor secondary BA species in the intestine. *E. Allobaculum*, which was also markedly increased by both BDE-47 and BDE-99, was positively correlated with the major secondary unconjugated BAs ωMCA and LCA, but was negatively correlated with their taurine-conjugates. This indicates that *E. Allobaculum* may be involved in the epimerization and dehydroxylation reactions in synthesizing these secondary BAs, but may inhibit the bacteria that perform deconjugation reactions.

In addition, for other bacteria that were differentially regulated by PBDEs, T-ωMCA, the predominant secondary BA in LIC of CV mice, was positively correlated with *Dorea,*

Bifidobacterium, Ruminococcus, Enterococcus, Clostridium, Dehalobacterium, Lactobacillus, and *Mogibacteriaceae* (with correlation r>0.7), whereas most of these bacteria showed negative correlation with its unconjugated BA ωMCA. These findings suggested that these bacteria may also contribute to ωMCA synthesis through epimerization reactions, while inhibiting other bacteria that can perform deconjugation of T-ωMCA in the intestine. *Anaerofustis,* which showed negative correlation with T-ωMCA, was highly positively correlated with ωMCA, suggesting that this bacterium is responsible for the deconjugation of T-ωMCA. Similarly, the major secondary BA T-LCA was found negatively correlated with *Bacteroidales* and *Anaerofustis*, whereas its unconjugated metabolite LCA was positively correlated with *Bacteroidales.* Therefore, *Bacteroidales* was likely responsible for the deconjugation of T-LCA.

Comparison of PBDE-mediated changes in BA compositions in serum, liver, SIC, and LIC between CV and GF mice

To determine the BA compositional changes caused by PBDEs and the necessity of gut microbiota in modulating the basal and PBDE-regulated BA profiles, the proportions of individual BAs in serum, liver, SIC, and LIC of CV and GF mice were analyzed across all three treatment groups. The BAs with a percentage value above 1% were labeled (Figure 8-11).

In serum (Figure 8), compared to corn oil-treated CV mice with more diversified BA profiles, the BA profiles in corn oil-treated GF mice were predominated by the primary BAs T-α/βMCA (58%) and T-CA (35%), whereas other BAs were minimally detected.

Following PBDE exposure, BDE-99 had a more prominent effect on BA compositional changes than BDE-47 in CV mice, namely an apparent decrease in the major primary conjugated BAs T-CA (from 18% in controls to 10%) and T-α/βMCA (from 30% in controls to 26%). Conversely, the major secondary BA ωMCA increased from 9% control levels to 15% following BDE-99 exposure. In PBDE-exposed GF mice, serum BA profiles were still predominated by T- /βMCA and T-CA. In particular, BDE-47 treatment led to an apparent increase in T-α/βMCA (from 58% in controls to 69%), whereas BDE-99 treatment led to an apparent increase in βMCA (from below 1% in controls to 3%).

In the liver (Figure 9), under control conditions, Tα/βMCA and T-CA were the predominant BAs detected, whereas lack of gut microbiota increased the percentage of T-α/βMCA (from 64% CV levels to 74%), but decreased the percentage of T-CA (from 22% CV levels to 14%); in addition, there was a marked increase in hepatic βMCA in control GF mice (from 2% CV levels to 8%). Following PBDE treatment in CV mice, both BDE-47 and BDE-99 increased the proportions of T-CA and also doubled the percentage of the major secondary BAs T-DCA and ωMCA (from 1% in controls to 2% by either PBDE). In addition, the percentage of the primary unconjugated BA βMCA was doubled by BDE-99 (from 2% in controls to 4%) in livers of CV mice. In livers of GF mice, PBDEs had much smaller effect, except for an apparent decrease in the proportions of Tα+βMCA by BDE-99 (from 74% in controls to 67%).

In SIC (Figure 10), under control conditions, in CV mice, the predominant BA species were T-α/βMCA (54%), CA (25%), and T-CA (9%), suggesting extensive deconjugation

reactions from T-CA to CA that occur in this bio-compartment. In control GF mice, however, the predominant BA species were T-α/βMCA (82%) and T-CA (13%), whereas other BAs were minimal. Following PBDE exposure, the proportions of BA species remained relatively constant in GF mice; however, in CV mice, there was a marked increase in the percentage of CA (from 25% in controls to 42% by BDE-47 and to 35% by BDE-99), and correspondingly, the percentage of the primary BA T-CA was also reduced by BDE-99 in CV mice (from 9% to 4%). The percentage of T-α/βMCA was also reduced (from 54% in controls to 31% by BDE-47 and to 43% by BDE-99) (Figure 10). These data suggested that PBDEs further enhanced the BA deconjugation reactions in a microbiota-dependent manner.

In LIC (Figure 11), under control conditions, the BA profiles in CV mice were more diverse than those in GF mice, and the most predominant BAs were T-α/βMCA (36%) and ωMCA (17%). In GF mice, the LIC BAs were predominated by T-α/βMCA (89%), followed by T-CA that increased from 3% in CV mice to 7%, whereas other BA levels were minimal. Following PBDE exposure, the BAs in GF mice remained relatively constant; in contrast, in CV mice, both PBDEs increased the percentage of T-α/βMCA (from 36% in controls to 72% by BDE-47 and to 52% by BDE-99), but decreased the percentages of ωMCA (from 17% in controls to 7% by BDE-47 and to 4% by BDE-99) and β-MCA (from 6% in controls to 1% by both PBDEs). BDE-99 exposure also led to an apparent increase in the percentages of the secondary BAs DCA (from 6% in controls to 10%) and T-HDCA (from 2% in controls to 5%), as well as the primary BA UDCA (from 5% in controls to 9%) (Figure 11).

Host BA-processing gene expression in livers of CV and GF mice

To determine to what extent BA-metabolizing enzymes and transporters are affected by PBDEs and gut microbiota interactions, the expression of major BA-processing genes involved in BA biosynthesis (Cyp7a1, Cyp8b1, Cyp27a1, Cyp7b1, Hsd3b7, Akr1c14), conjugation (Slc27a5), and transport (Ntcp, Oatp1b2, Bsep) were quantified using targeted proteomics (except for Cyp7a1 which was below the LC-MS detection limit, thus the mRNA level was shown instead) (Figure 12A-B).

Cyp7a1 and Cyp8b1 are involved in the classical pathway of BA synthesis. Under control conditions, the mRNA of the rate-limiting enzyme Cyp7a1 was higher in CV mice than that in GF mice. Following PBDE exposure, Cyp7a1 mRNA was increased 1.6-fold by BDE-47 and 2.0-fold by BDE-99 in CV mice. However, in GF mice, Cyp7a1 mRNA was not altered by BDE-47, but increased 4.2-fold by BDE-99, suggesting that the BDE-47 mediated increase in Cyp7a1 mRNA was dependent on gut microbiota, whereas the lack of gut microbiome augmented BDE-99 mediated up-regulation of Cyp7a1 in liver. Cyp8b1 protein was lower in GF mice than CV mice under control conditions (62.4%), whereas BDE-99 decreased Cyp8b1 protein expression (41.3%) in CV mice (BDE-47 also tended to lower Cyp8b1 protein in CV mice, although a statistical significance was not achieved). The PBDE-mediated decrease in Cyp8b1 was completely abolished in livers of GF mice. Cyp27a1 and Cyp7b1 are key enzymes in the alternative pathway of BA synthesis. The level of Cyp27a1 protein was lower in control GF mice (31.4%) as compared to control CV mice, whereas both BDE-47 and BDE-99 decreased Cyp27a1

protein in livers of CV mice (39.3% and 30.6%, respectively) but not in GF mice, suggesting that the down-regulation of Cyp27a1 protein by PBDEs is gut microbiome dependent. The Cyp7b1 protein was not altered by either PBDEs or gut microbiota. The proteins of the downstream BA-synthetic enzymes, namely Hsd3b7 (which catalyzes the inversion of 3β-hydroxyl group of cholesterol to the 3α-hydroxyl group of bile acids) and Akr1c14 (aldo-keto reductase), were also determined. Both enzymes were lower in control GF mice as compared to control CV mice, whereas both BDE-47 and BDE-99 decreased their protein levels (39.0% by BDE-47 and 40.0% by BDE-99 for Hsd3b7; 30.0% by BDE-47 and 32.3% by BDE-99 for Akr1c14). This down-regulation in their protein expression was absent in livers of GF mice. Regarding BA conjugation, Slc27a5 is a bile acid-CoA ligase (Bal) that mediates the conjugation of primary BAs with glycine or taurine before excretion into bile canaliculi. The Slc27a5 protein was decreased 35.2% by BDE-47 in CV mice but not in GF mice (Figure 12A).

Regarding BA transporters, the proteins of the major basolateral uptake transporter for conjugated BAs, sodium taurocholate cotransporting polypeptide (Ntcp/Slc10a1), as well as the major basolateral uptake transporter for unconjugated BAs, organic anion transporting polypeptide (Oatp/Slco) 1b2, were both lower in control GF mice than those in control CV mice. Both BDE-47 and BDE-99 decreased the proteins of Ntcp (41.0% and 38.6%) and Oatp1b2 (32.9% and 28.7%) in a gut microbiota-dependent manner. The protein of the rate-limiting canalicular BA efflux transporter Bsep was similar between livers of CV and GF mice under control conditions, whereas both BDE-47 and BDE-99 decreased its expression (33.7% and 32.4%) in livers of CV mice. This down-

regulation was dampened by the lack of gut microbiota, since there was no change in Bsep protein expression by BDE-47 and a 20.5% decrease by BDE-99 in livers of GF mice (Figure 12B).

The mRNA expression of many other genes involved in BA homeostasis were also quantified in livers of CV and GF mice, including the BA-synthetic enzymes Cyp39a1 and Akr1d1, the BA-conjugation enzyme Baat (bile acid CoA:animo acid N-acyltransferase), the basolateral BA-efflux transporters Ostα (Slc51a) and Ostβ (Slc51b), the cholesterol efflux transporter Abca1, the lipid uptake transporter Atp8b1, the BA-efflux transporter Asbt (Slc10a2), as well as various transcription factors, including Nr1h4 (or FXR), Nr0b2 (or Shp), Mafg (Musculoaponeurotic fibrosarcoma oncogene homolog G), Crip2 (cysteine-rich intestinal protein 2), Zfp385a (Zinc-finger protein 385a), Nr1h2 (or LXRβ), and Nr1h3 (or LXRα) (Supplemental Figure 4). The mRNAs of Abcb4, Abcg5, and Abcg8 were not altered by lack of gut microbiota or PBDEs (data not shown). Under control conditions, lack of gut microbiome moderately decreased Cyp39a1 mRNA (54.1%). Following PBDE exposure, many of the mRNAs in CV mice were not affected. However, in GF mice BDE-47 increased the mRNAs of Cyp39a1 (2.0-fold) and Slc51b (5.7-fold), and BDE-99 increased Akr1d1 (2.4-fold), Slc51b (5.1-fold), Abca1 (2.0-fold), Atp8b1 (2.0-fold), Slc10a2 (3.9-fold), and Mafg (2.3-fold). Conversely, the mRNAs of the majority of transcription factors were decreased by BDE-99 in GF mice, including Nr0b2 (22.4%), Crip2 (28.0%), Zfp385a (43.1%), Nr1h2 (24.1%), and Nr1h3 (37.8%) (Supplemental Figure 4).

In summary, in regards to gut microbiota- and PBDE exposure-mediated changes in BA homeostasis, host hepatic BA-processing genes were differentially regulated. At the protein level, most of the BA-synthetic enzymes and transporters were down-regulated by PBDEs in a gut microbiota-dependent manner. The BDE-99-mediated increase in most hepatic unconjugated BAs as well as two conjugated BAs (G-CA and T-DCA) (Fig. 5B and Supplemental Figure 2B) correlated with the compensatory decrease in BA-synthesizing enzymes as well as BA-transporters. BDE-47 decreased the proteins of many BA-processing genes without altering hepatic BA levels, suggesting the involvement of other unknown mechanisms.

BA-transporters and Fgf15 gene expression in various parts of the intestine

The mRNA expression of major intestinal transporters involved in enterohepatic circulation of BAs was determined in four intestinal sections of CV and GF mice, including uptake transporter Asbt and efflux transporters Ostα, Ostβ, and Mrp4. The intestinal hormone Fgf15, which regulates hepatic BA-synthesis, was also determined (Figure 12C).

The apical sodium dependent bile acid transporter (Asbt) brings BAs from the intestinal lumen into enterocytes. In ileum, where the peak basal expression of Asbt was observed, both BDE-47 and BDE-99 markedly increased Asbt mRNA in CV mice (5.0-fold and 3.8-fold); however, in GF mice, only BDE-47 increased Asbt mRNA (13.9-fold), whereas BDE-99 did not alter Asbt mRNA. Asbt mRNA was not affected by either lack of gut microbiota or PBDE exposure in other sections of intestine. The basolateral BA

efflux transporters Ostα and Ostβ transport the reabsorbed BAs from enterocyte to portal blood. The mRNA expression of Ostα was not affected by lack of gut microbiota under control conditions, and PBDEs exposure did not affect Ostα in CV mice. In GF mice, BDE-47 increased Ostα mRNA (10.1-fold) in jejunum, and BDE-99 increased Ostα mRNA (3.3-fold) in colon. The basal mRNA expression of Ostβ was lower in jejunum and ileum of GF mice (37.5% and 67.3%, respectively). In CV mice, BDE-99 moderately increased Ostβ in duodenum (30%). For the basolateral efflux transporter Mrp4, its basal expression in duodenum was higher in GF mice (1.78-fold), and interestingly, Mrp4 mRNA was consistently up-regulated by BDE-99 in all four sections of intestine of CV mice (duodenum: 1.7-fold, jejunum: 2.0-fold, ileum: 2.6-fold, and colon: 2.1-fold) in a gut microbiota-dependent manner.

The mRNA of the intestinal hormone Fgf15 was not altered by lack of gut microbiota under control conditions, and remained unchanged following PBDE exposure in CV mice. However, in GF mice, BDE-47 increased Fgf15 mRNA in duodenum (8.0-fold) and BDE-99 increased Fgf15 mRNA in colon (9.1-fold).

In summary, the PBDE (and especially BDE-99) mediated up-regulation in transporters for intestinal BA-retrieval correlated well with the rise of hepatic BA levels in CV mice (Fig. 5B and Supplemental Figure 2B). The lack of up-regulation of the intestinal hormone Fgf15 in CV mice may provide an additional explanation for a permissive environment of higher BA levels in livers of CV mice.

DISCUSSION

Taken together, the present study provides the first evidence of the effect of PBDEs on gut microbiota and BA homeostasis *in vivo*. Specifically, 100 umol/kg PBDEs, administered once daily for four days by gavage, decreased the bacterial richness and differentially regulated various bacterial species in the large intestine of mice. We identified for the first time two bacteria that were overwhelmingly up-regulated by PBDEs, namely *Akkermansia muciniphila*, which has been shown to be important for anti-inflammation, anti-obesity, and positively correlated with circulating primary BAs (Png et al., 2010; Pierre et al., 2016; Derrien et al., 2017), as well as *Erysipelotrichaceae Allobaculum*, which has been shown to have anti-obesity properties (Ravussin et al., 2012). These data suggest that, at least at the doses used in this study, there is a novel interaction between PBDEs and the gut microbiome, which in turn modified BA composition, which may have significant impacts on nutrition. Regarding BA profiles, PBDEs (and especially BDE-99) increased the unconjugated BAs in serum, liver, as well as SIC and LIC of CV mice. The lack of gut microbiome resulted in a shift in BA composition toward an increase in conjugated muricholic acids in all four compartments of GF mice.

To date, studies of PBDEs have focused mainly on detection of PBDEs in the environment and their potential adverse health effects. Very little is known about the effect of PBDEs on bacterial community structure in the GI tract. In the environment, it has been reported that PBDEs can be debrominated by anaerobic microbes in the sediment using single strain or mixed bacteria (Robrock et al., 2008; Yang et al., 2017a).

The bacteria that are positively correlated with anaerobic degradation of BDE-209 and BDE-28 are from five bacterial classes, namely *Clostridia*, *Bacilli*, *Betaproteobacteria*, *Alphaproteobacteria*, and *Gammaproteobacteria* (Yang et al., 2017a). *Actinobacteria* and *Erysipelotrichi* were also positively related with the biodegradation of lesser-brominated PBDE congeners, tri-BDE, and tetra-BDE (Xu et al., 2012). Additionally, reductive debromination of deca-BDE, octa-BDE mixture, and penta-BDEs, such as BDE-47 and BDE-99, has been demonstrated with anaerobic bacteria *Dehalococcoides* species in sediment and sewage sludge (Wehrbein and Diedrich, 1992; Gerecke et al., 2006; He et al., 2006; Robrock et al., 2008). As the human intestinal microbiota is dominated by strict anaerobic bacteria, there has been limited information regarding how GI bacteria respond to PBDE exposure. The present study has provided the first evidence that at class level oral exposure to BDE-47 and BDE-99 decreased *Actinobacteria*, *Coriobacteriia*, and *Bacilli*, but increased *Erysipelotrichi*, *Gammaproteobacteria*, and *Verrucomicrobiae* in LIC of CV mice. The elevated abundance of *Gammaproteobacteria* and *Erysipelotrichi* in the present study was consistent with previous results from sediment at the class level. It is possible that the exact taxa at the order, family, genus, and species levels may be different between sediment microbes and the GI tract; nevertheless, if the intestinal *Gammaproteobacteria* and *Erysipelotrichi* share similar microbial genes as compared to the bacteria detected in sediment, our study suggests that they may contribute to the debromination of PBDEs in the GI tract as well. Although *Bacilli* and *Actinobacteria* were positively correlated with degradation of PBDEs (BDE-209 and BDE-28) in the sediment, the abundances of *Bacilli*, *Actinobacteria* and *Coriobacteriia* (which is also from

Actinobacteria phylum) in the present study were decreased in response to BDE-47 and BDE-99 exposure. It is possible that these bacterial species are more sensitive and susceptible to BDE-47 and BDE-99-mediated effects.

At the bacterial class level, *Verrucomicrobiae* and *Erysipelotrichi* were also increased by PBDE treatment. The increased abundances of *Akkermansia muciniphila* from Verrucomicrobiae class and *Erysipelotrichaceae Allobaculum* from Erysipelotrichi class were further confirmed by qPCR. *Akkermansia muciniphila* is a mucin degrader residing in the mucus layer of the human intestinal tract and maintains the gut barrier. It is abundant in human gut microbiota, accounting for 1-4% of the bacterial population in the colon of healthy subjects (van Passel et al., 2011; Zhao et al., 2017). *A. muciniphila* is thought to have anti-inflammatory effects in humans, and studies have shown inverse relationships between *A. muciniphila* colonization and inflammatory conditions, such as irritable bowel syndrome (Png et al., 2010). Reduced levels of *A. muciniphila* have also been found in patients with metabolic disorders such as diabetes and obesity, which suggests that it may also have anti-obesogenic properties (Derrien et al., 2017). Similarly, lower abundances of *E. Allobaculum* was found in mice fed with high-fat diet compared to mice fed with control diet, and *E. Allobaculum* was enriched in the weight reduced mice. These findings suggest that *E. Allobaculum* also has anti-obesogenic effects (Ravussin et al., 2012). Moreover, *A. muciniphila* and *E. Allobaculum* abundances were found negatively correlated with circulating leptin concentrations in obese mice (Ravussin et al., 2012). The mechanisms underlying the effects of *A. muciniphila* and *E. Allobaculum* in inflammation and metabolic disorders are not

completely understood, and no studies have linked these two bacterial species with environmental chemical exposure in the literature. The involvement of PBDEs in modulating the nutrition response by altering these two bacteria is worth investigating in future studies.

Another interesting finding is that we have identified certain taxa as novel biomarkers to differentiate BDE-47 from BDE-99 exposures. The present study showed that certain bacteria were decreased by BDE-47 but increased by BDE-99 exposure, including *Clostridiales, Peptostreptococcaceae, Clostridiaceae, Coprobacillus*, and *SMB53*. Clinically, *Peptostreptococcaceae* from *Clostridia* class was found higher in the guts of colorectal cancer patients (Ahn et al., 2013). *SMB53*, a bacteria from the *Clostridiaceae* family, is highly enriched in the jejunum and ileum of small intestine, and it has been linked with barrier defense that help fight infections with ulcerative colitis (Goodrich et al., 2016; Yang et al., 2016a). Given that most studies in the literature have shown similar features of BDE-47 and BDE-99 regarding metabolism and host response, our study may add values to the research field on PBDEs by providing congener-specific biomarkers from the stool sample to pinpoint the specific chemical exposure.

In the present study, we dosed conventional (CV) and germ-free(GF) mice with 100 μmol/kg of PBDEs (which is equivalent to 50 mg/kg body weight) for four consecutive days. This dose is relatively higher than those of environmental exposure to humans. However, this dose is still relevant to assess the exposure risk to humans because the bio-accumulative potential of PBDEs in infants and children. This dose and dosing

regimen are similar to what have been used in adult mice to induce Cyps (Pacyniak et al., 2007). According to the literature, the concentrations of BDE-47 in human plasma from the United States range from 10 to 511 ng/g of lipid weight (lwt), with an average of 50 ng/g lipid (Petreas et al., 2003). The blood concentration of BDE-99 in the general U.S. populations ranges from 2.46 to 241 ng/g lwt, with an average of 11.6 ng/g lipid (Fitzgerald et al., 2012). In human breast milk, the mean BDE-47 and BDE-99 are approximately 27.8 ng/g lwt and 5.7ng/g lwt (Frederiksen et al., 2009). Because of the limited information on the level of BDE-47 and BDE-99 that are adverse for humans, the findings from the present study may provide some clues for the potential targets of PBDE considering the potential uncertainty factors including the interspecies differences (mouse to human), intraspecies differenes (infants and children are more vulnerable and have higher exposure level than adults), and exposure duration (acute to lifetime exposure), as well as the data deficiency for human daily exposure.

In addition to xenobiotic metabolism, our present study showed that PBDEs also differentially regulated many pathways involved in intermediary metabolism, such as steroid and steroid hormone biosynthesis. From BA metabolomics, we found that the majority of unconjugated secondary BAs were increased by PBDEs in serum, liver, SIC, and LIC of CV mice. These findings were consistent with the increased abundance of bacteria (*Clostridiales* and *Clostridiaceae*) and the increased expression of microbial enzymes (*baiCD* and *baiJ*) that are involved in BA metabolism (Figure 3A and 3C). The microbial enzymes *baiCD* and *baiJ* are involved in BA dehydroxylation to convert primary BAs to secondary BAs, and *Bsh* is involved in bile acid deconjugation to remove

glycine or taurine conjugates. Our result showed that *Bsh* was increased by BDE-99, but was not significant. *Bsh* activity is widely present in the microbes in the large and small intestines, including *Clostridium, Enterococcus, Bifidobacterium, Lactobacillus, and Bacteroides (Ridlon et al., 2006)*. In addition, BA metabolism is carried out by a variety of other bacterial species, including genera *Bacteroides, Clostridium, Lactobacillus, Bifidobacterium, Enbacterium*, and *Escherichia (Ridlon et al., 2006)*. Discovering novel bacteria and microbial enzymes involved in BA deconjugation and dehydroxylation will help us further understand the connection between the gut microbiome and BA homeostasis.

The BA profiles of GF mice differ markedly from those of CV mice under both control and PBDE treated conditions. As expected, in the absence of gut microbiome, GF mice have increased conjugated BAs and decreased secondary BAs. T-α/βMCA becomes the major BAs in GF mice. Under control condition, the percentage of T-α/βMCA is much higher in GF mice than that in CV mice, with a 1.9-fold increase in serum, 1.2-fold increase in liver, 1.5-fold increase in SIC, and 2.5-fold increase in LIC (Figure 8 to Figure 11). These findings are consistent with previous studies (Sayin et al., 2013; Hu et al., 2014; Miyata et al., 2015; Selwyn et al., 2015c). T-CA was increased in all compartments, except in the liver. In contrast, the unconjugated BAs were decreased in all four compartments of GF mice compared with those of CV mice.

Many enzymes and transporters that are involved in BA synthesis, conjugation and transport were decreased by PBDEs in a gut microbiome dependent manner. Under

normal conditions, the nuclear receptor FXR regulates hepatic BA synthesis. Increased BAs in the liver activate FXR, which activates Shp and decreases the expression of Cyp7a1 for bile synthesis. Increased BAs in the ileum can also activate FXR, which induces the secretion of Fgf15 into the portal circulation and decreases the transcription of Cyp7a1 (Chiang, 2004). With the increase in total BAs in serum, liver, and LIC following BDE-99 exposure (Supplemental Table 5), we observed decreased protein expression of Cyp8b1, Cyp27a1, Hsd3b7, Akr1c14, Slc27a5, and transporters Ntcp, Oatp1b2, and Bsep in the liver of CV mice. T-βMCA is an FXR antagonist that decreases the feedback secretion of intestinal Fgf15 and thus increases hepatic mRNA expression of BA-processing genes (Sayin et al., 2013). In the present study, we observed a marked decrease of T-α/βMCA in the SIC of CV mice after PBDE treatment, and we would expect to see increased Fgf15 in the ileum which would ultimately down-regulate the BA related enzymes. However, there was neither an increase in the mRNA of Nr0b2 (Shp) in liver nor increased Fgf15 in ileum of CV mice. Therefore, in addition to FXR, it is possible that there are other alternative pathways can modulate the down-regulation of BAs synthesis in liver. Activation of human PXR by its prototypical ligand Rifampicin can reduce hepatic BA levels in patients with cholestasis (Geenes et al., 2015). PXR has been linked with hepatocyte nuclear factor 4 alpha (HNF-4α), a key hepatic regulator of genes involved in bile acid synthesis including Cyp7a1 and Cyp8b1 genes. BA activation of PXR leads to repression of the CYP7A1 gene (Staudinger et al., 2001). Because BDE-47 and BDE-99 are known activators of human and mouse PXR, the activated PXR may mediate the down-regulation of BAs-processing enzymes and transporters in liver. However, the increased mRNA of Cyp7a1 by BDE-47 and BDE-

99 may be due to the down-regulated mRNA of Nr0b2 (Shp) in livers of CV mice. These findings suggest that, at the dose used in this study, PBDE exposure mainly affects PXR signaling to modulate the BAs pathway in CV mice with a minor effect from FXR activation.

In the present study, we found that the mRNA of Asbt was up-regulated by both BDE-47 and BDE-99 in the ileum. The ileal BA uptake transporter Asbt is thought to be responsible for the reabsorption of most of the BAs from the intestine. Combined with the decreased total BAs in SIC and increased total BAs in serum and liver following BDE-99 exposure (Supplemental Table 5), these changes suggested that there was an increase in the reabsorption of BAs. Mrp4 is a basolateral efflux transporter that actively transports BAs from enterocyte to portal circulation. Our result showed that the mRNA of Mrp4 was increased by BDE-99 in all four sections of intestine in CV mice (Figure 12C), which was also consistent with the increased total BAs in serum and liver. Considering Mrp4 is a well-known CAR-target gene (Aleksunes and Klaassen, 2012), our results suggest, in addition to PXR and FXR mentioned above, there may be crosstalk between PXR, FXR, and CAR in BDE-99 mediated alterations in BAs homeostasis.

In conclusion, our study is the first report of novel interactions between the gut microbiome and PBDE exposure on BA homeostasis using multi-omics approach. The most notable findings in PBDE-treated CV and GF mice are: 1) PBDEs decreased bacterial diversity, but increased bacterial species *Akkermansia muciniphila* and

Erysipelotrichaceae Allobaculum; 2) PBDEs, especially BDE-99, increase unconjugated BAs in the serum, liver, SIC, and LIC of CV mice; 3) the lack of gut microbiome mediates a shift in BA composition toward an increase in T-α/βMCA in GF mice; 4) PBDEs down-regulated enzymes and transporters involved in BA metabolism, in a gut microbiome dependent manner. Our study focused on the associative rather than causal relationship between PBDE exposure and gut microbiome. It remains to be determined which specific bacteria are responsible for intestinal degradation of PBDEs, which can be applied into the natural environment to reduce the health threat of PBDEs. In addition, further research should be carried out to investigate the mechanism of *Akkermansia muciniphila* and *Erysipelotrichaceae Allobaculum* in host metabolism.

Figure 1

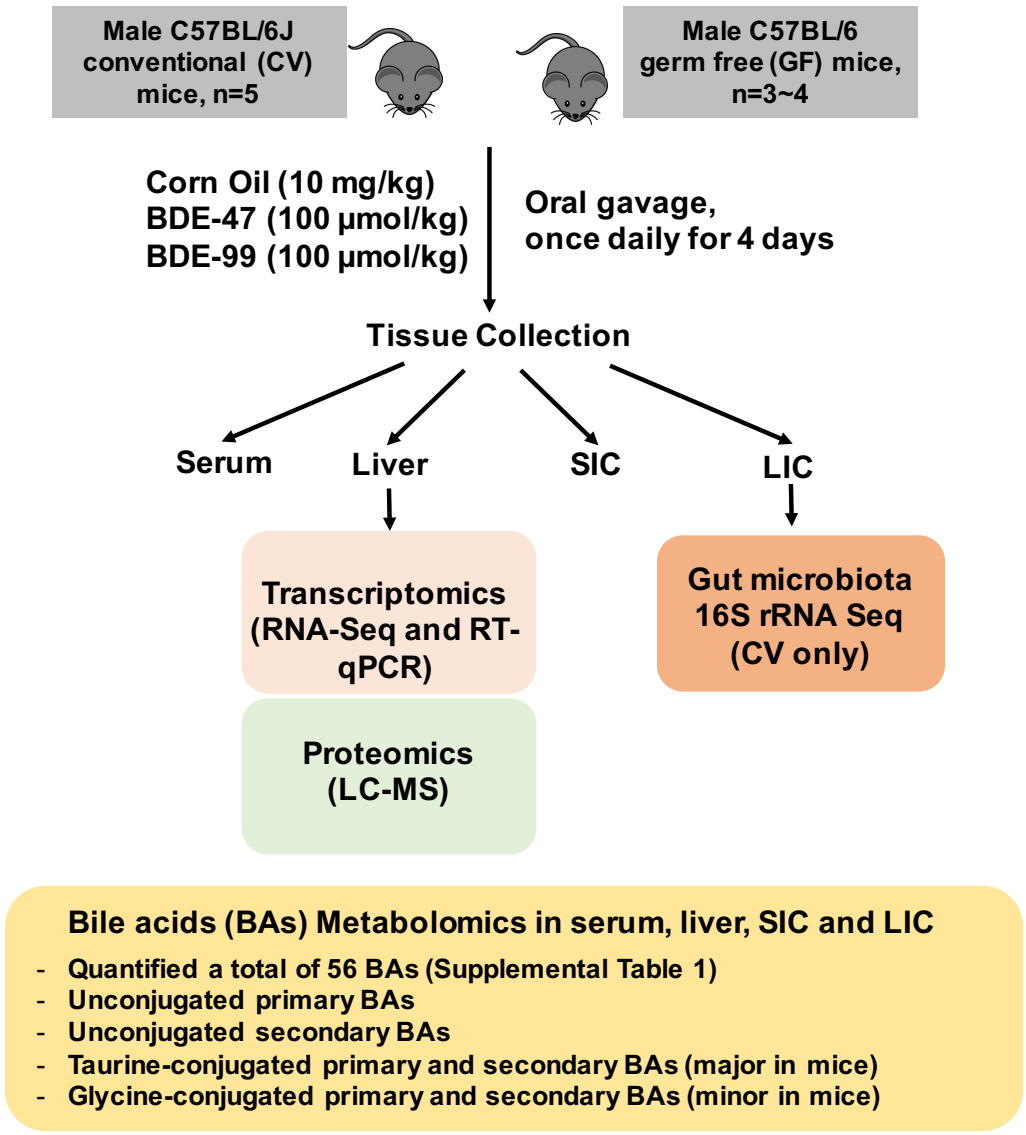

Figure 1. A diagram illustrating the experimental design and dosing regimen of mice. Briefly, 9-week-old C57BL/6J CV and GF mice were treated with vehicle (corn oil, 10ml/kg, oral gavage), BDE-47 (100 µmol/kg, oral gavage) or BDE-99 (100 µmol/kg, oral gavage) once daily for 4 consecutive days. Tissues were collected 24h after the final dose (n = 3-5 per group). The expression of genes involved in BA synthesis, conjugation, and transport was determined by RNA-Seq and targeted proteomics using LC-MS/MS. The gut microbiota from LIC of CV mice was determined by 16S rRNA sequencing. BAs in serum, liver, SIC and LIC were determined by targeted metabolomics. A total of 56 BAs was quantified (as listed in Supplemental Table 1), including primary and secondary BAs in either conjugated or unconjugated form.

Figure 2

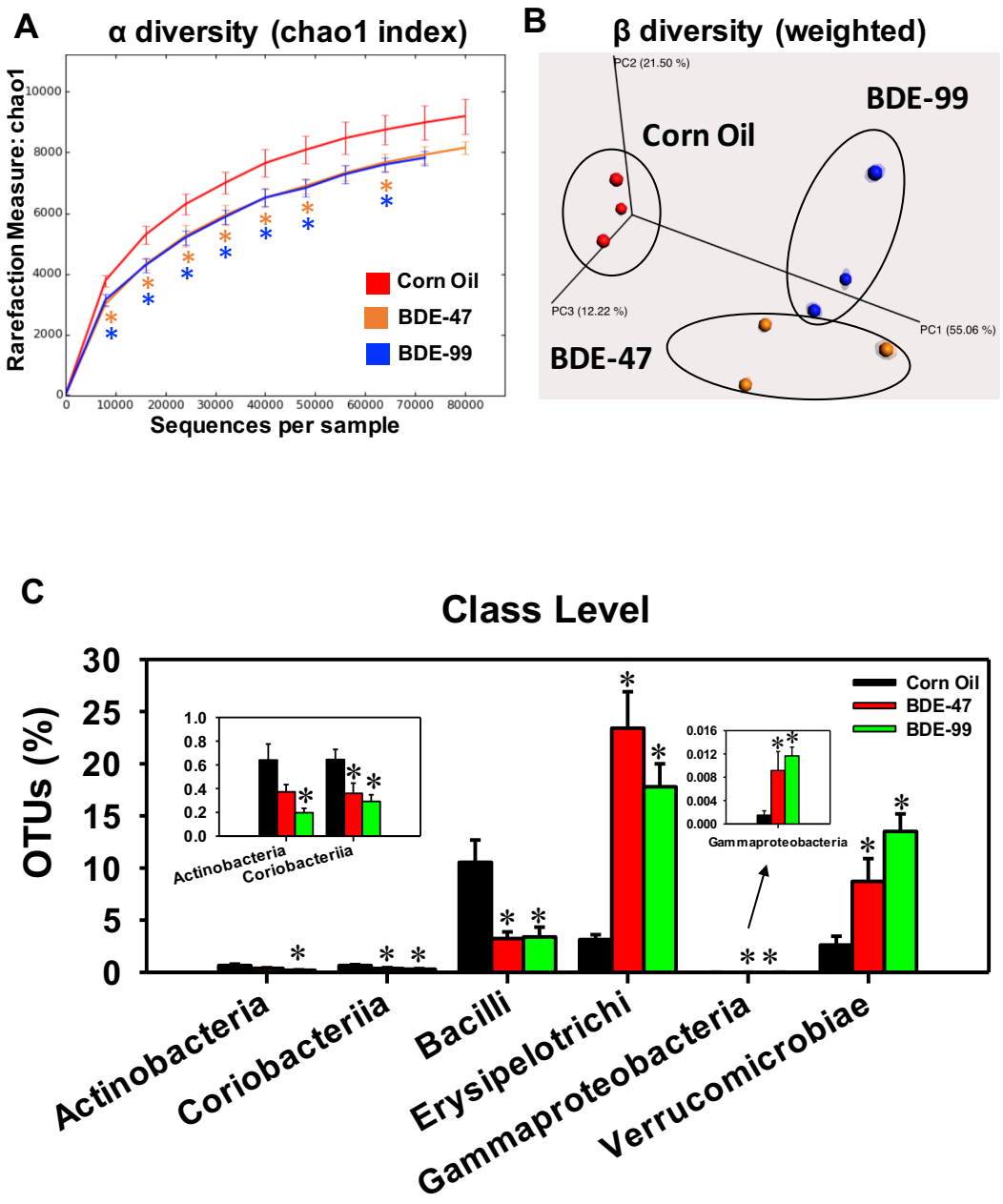

Figure 2. Alpha diversity (**A**) and beta diversity (**B**) of gut microbiota in LIC of CV mice treated with corn oil, BDE-47 (100 μmol/kg, oral gavage), or BDE-99 (100 μmol/kg, oral gavage) (n=3 per group). Data were analyzed using QIIME as described in Materials and Methods. Asterisks represent statistically significant differences as compared to corn oil-treated group (t-test, $p<0.05$). (**C**) The differentially regulated taxa at class level by BDE-47 and BDE-99 compared with corn oil-treated group. Data were presented as mean percentage of operational taxonomical units (OTUs) ± SE. Asterisks represent statistically significant differences as compared to corn oil-treated group (ANOVA, Duncan's post hoc test, $p<0.05$).

Figure 3

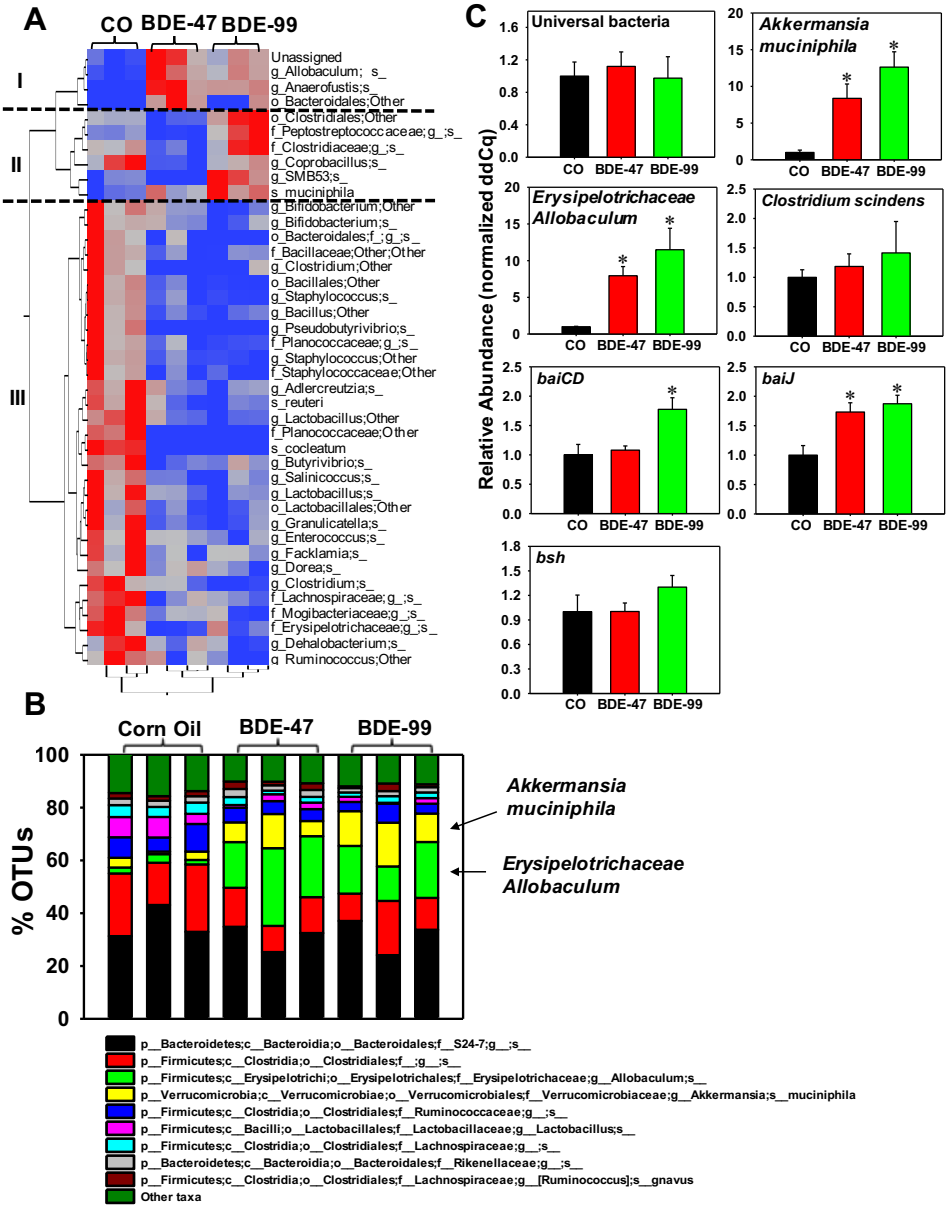

Figure 3. Differentially regulated taxa at the species level by PBDEs in LIC of CV mice. (**A**) A two-way hierarchical clustering dendrogram of the differentially regulated taxa at the species level (41 in total). Data were analyzed using JMP Genomics as described in Materials and Methods. Red represents relatively high abundance and blue represents relatively low abundance. (**B**) The top 10 most abundant bacterial species that were differentially regulated by PBDEs in LIC of CV mice. The taxa that were lower than the top 9 were summed and presented as "other taxa" as the 10th category. (**C**) QPCR quanification of *Akkermansia muciniphila*, *Erysipelotrichaceae Allobaculum* and *Clostridium scindens*, as well as microbial enzymes involved in secondary BA synthesis (*baiJ*, *baiCD*, and *bsh*) in LIC of CV mice (n=3 per group). Asterisks represent statistically significant differences as compared to corn oil-treated group (ANOVA, Duncan's post hoc test, $p<0.05$).

Figure 4

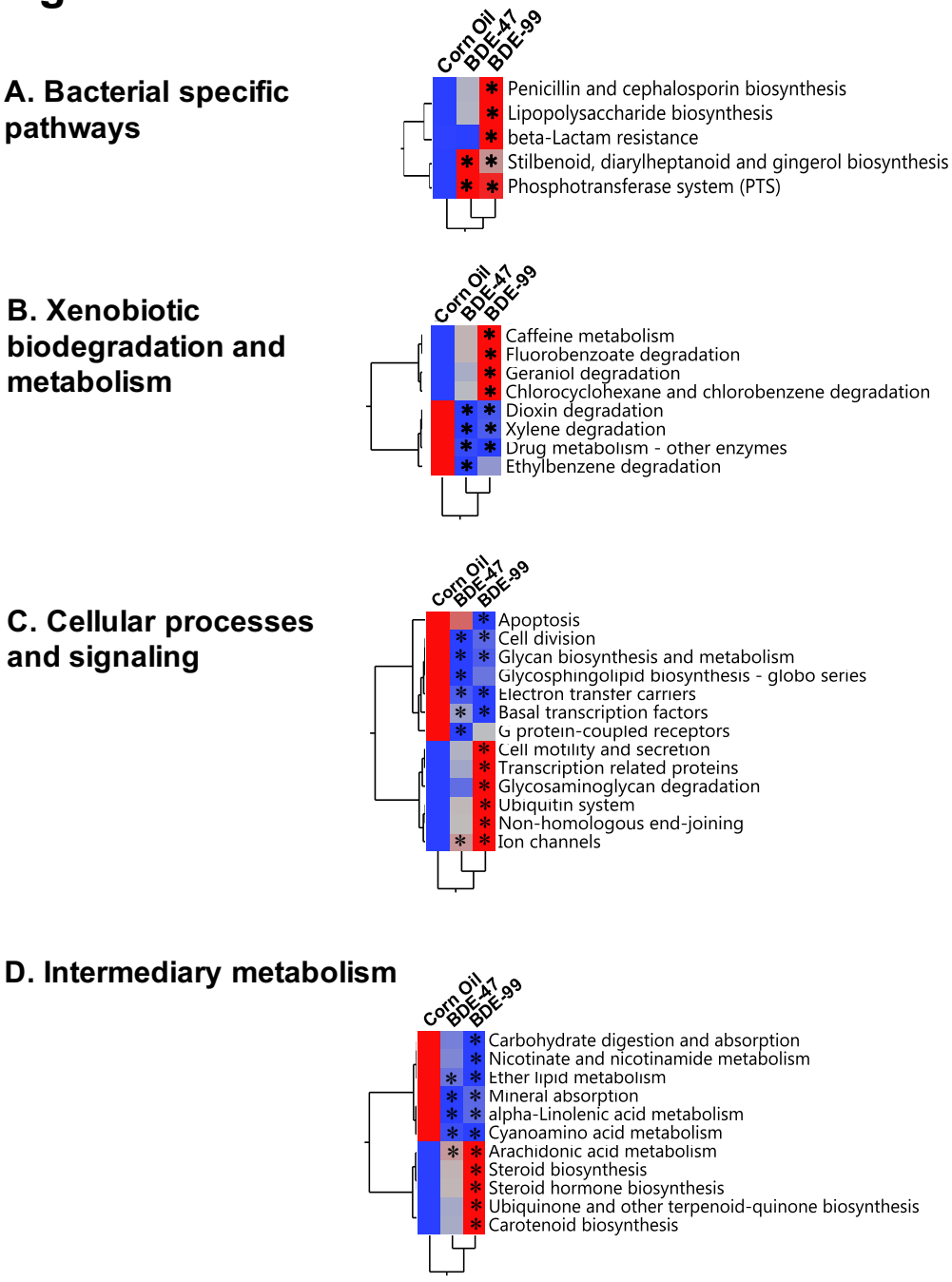

Figure 4. Hierarchical clustering dendrograms of differentially regulated KEGG pathways predicted by PICRUSt, as described in Materials and Methods. (**A**) Bacteria-specific processes. (**B**) Xenobiotic biodegradation and metabolism. (**C**) Basal cellular processes. (**D**) Intermediary metabolism. Data were analyzed using JMP Genomics as described in Materials and Methods. Red represents relatively high expression, and blue represents relatively low expression. Asterisks (*) represent statistically significant differences as compared to corn oil-treated group (ANOVA, Duncan's post hoc test, $p<0.05$).

Figure 5

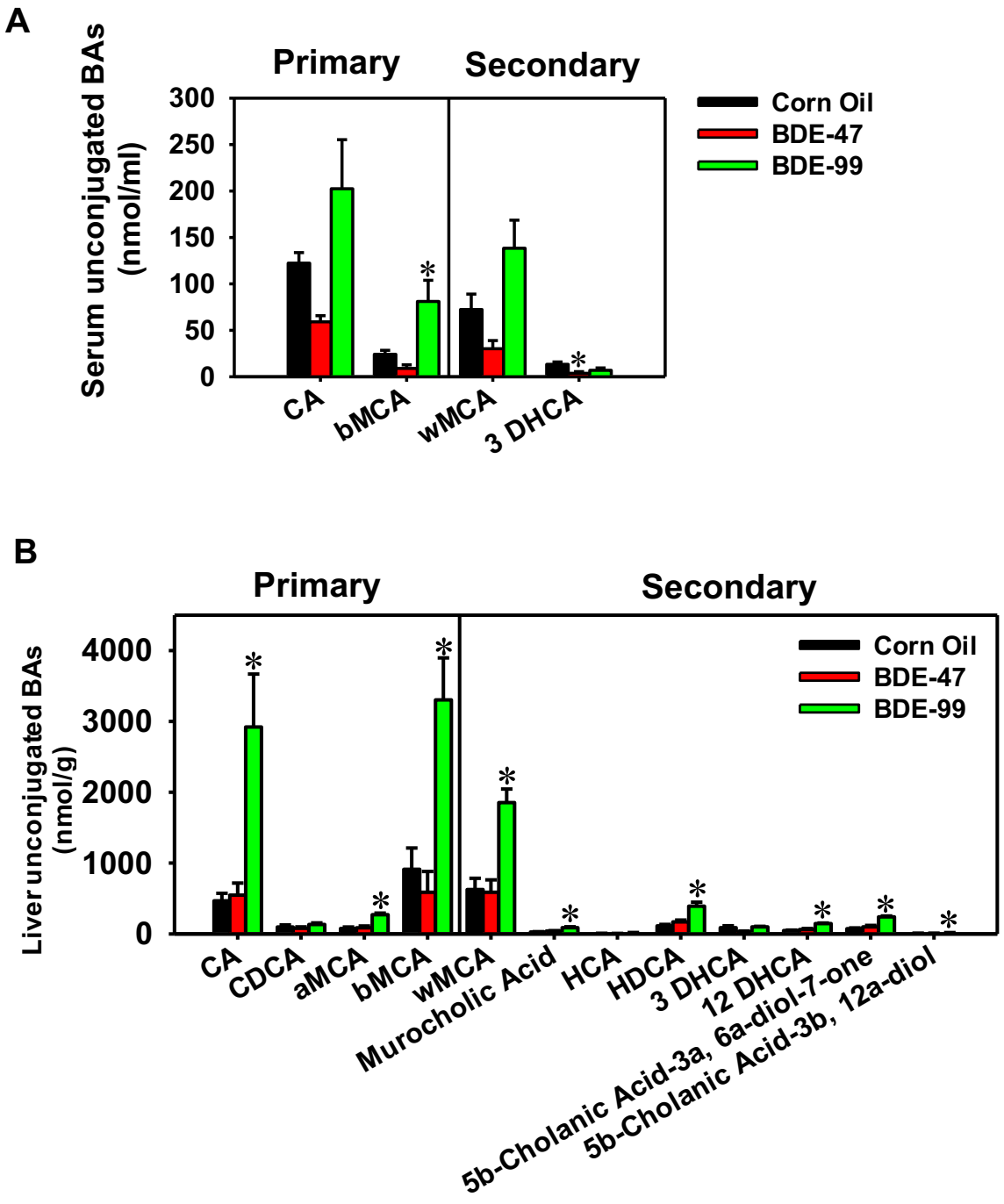

Figure 5. Concentrations of unconjugated primary and secondary BAs in serum (**A**) and liver (**B**) of CV mice treated with corn oil, BDE-47 (100 µmol/kg), or BDE-99 (100 µmol/kg). BAs were quantified using LC-MS/MS as described in Materials and Methods. Data were presented as mean ± SE (n=3 per group). Asterisks (*) represent statistically significant differences as compared to corn oil-treated group by ANOVA (Duncan's post hoc test, $p<0.05$).

Figure 6

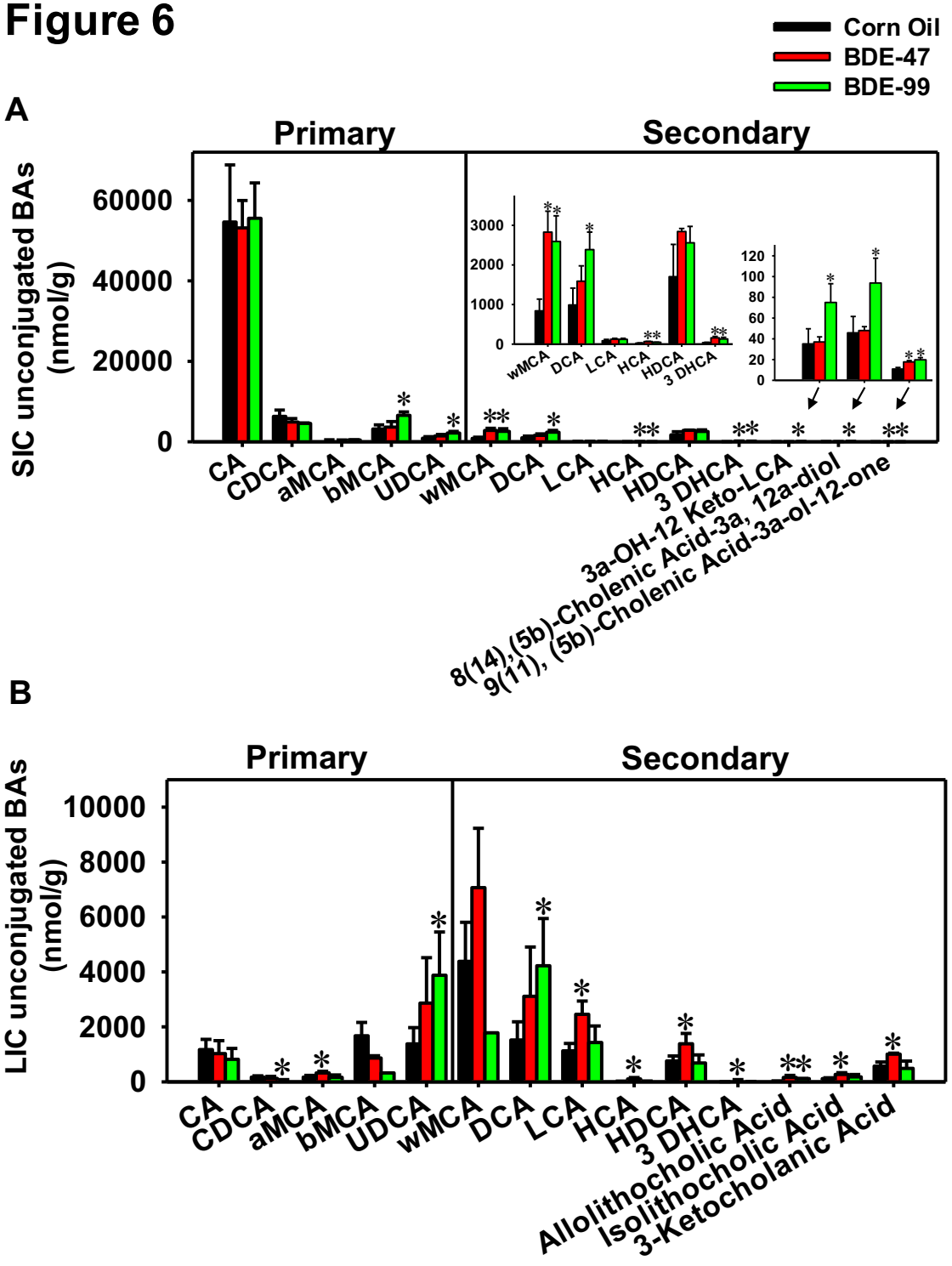

Figure 6. Concentrations of unconjugated primary and secondary BAs in SIC (**A**) and LIC (**B**) of CV mice treated with corn oil, BDE-47(100 µmol/kg), or BDE-99 (100 µmol/kg). BAs were quantified using LC-MS/MS as described in Materials and Methods. Data were presented as mean ± SE (n= 3 per group). Asterisks (*) represent statistically significant differences as compared to corn oil-treated group by ANOVA (Duncan's post hoc test, $p<0.05$).

Figure 7

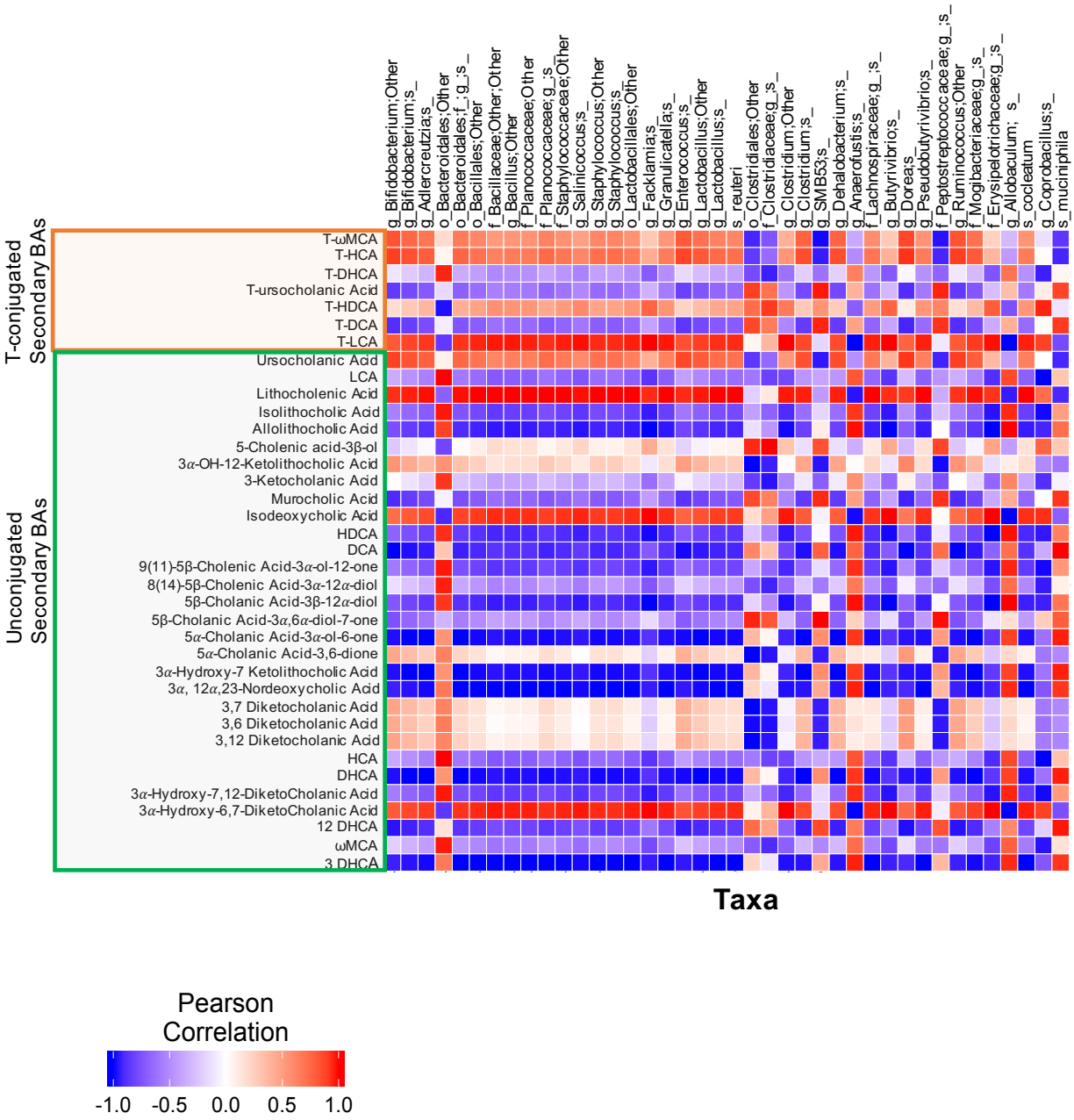

Figure 7. Pearson's correlation between secondary BAs (including both taurine-conjugated and unconjugated BAs) and bacterial species that were differentially regulated by PBDE exposure. Red represents positively correlated, and blue represents negatively correlated.

Figure 8

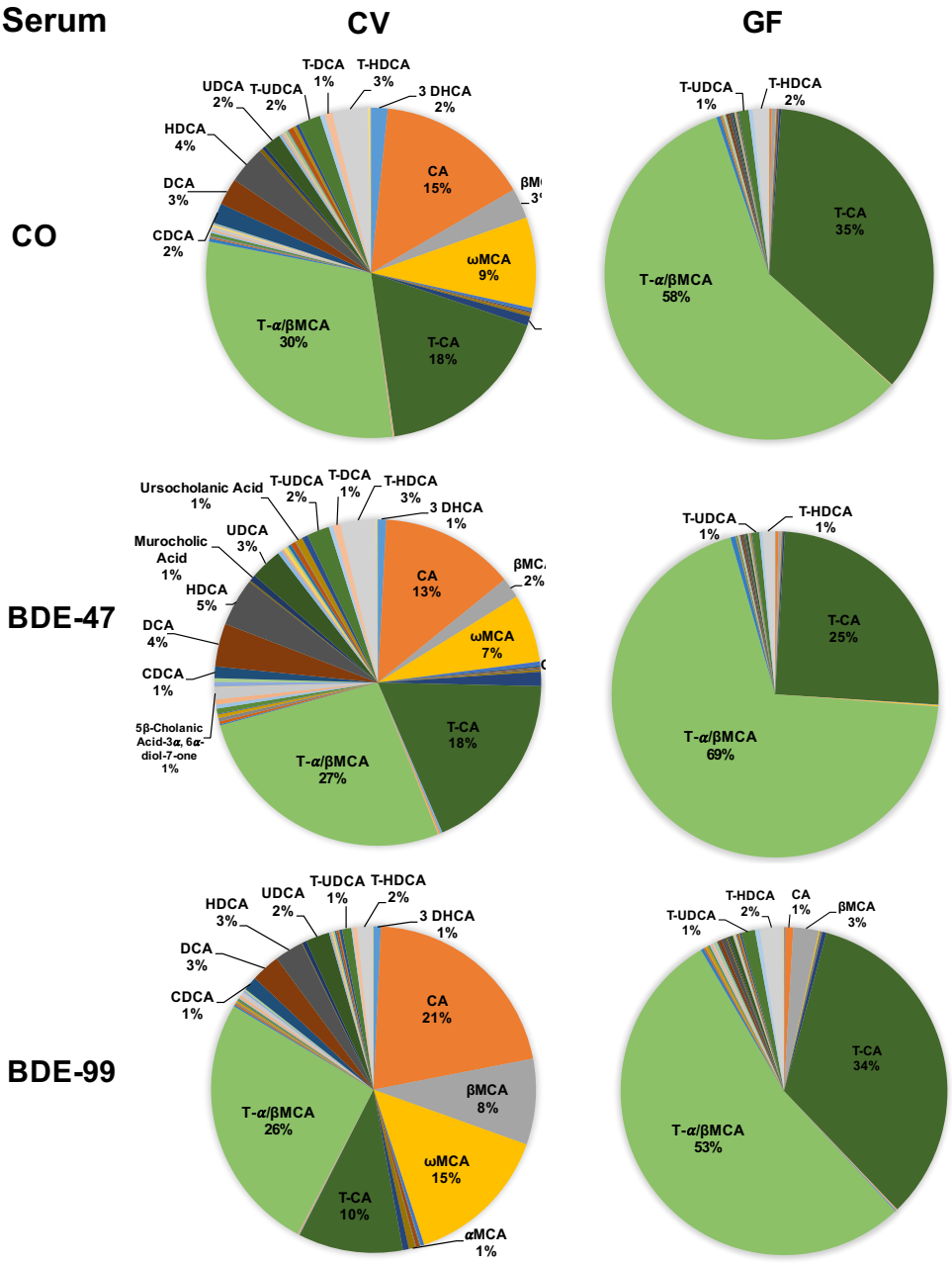

Figure 8. Pie charts illustrating the proportion of individual BAs in serum of CV and GF mice treated with corn oil, BDE-47 (100 μmol/kg), or BDE-99 (100 μmol/kg). BAs with an average percentage higher than 1% were plotted.

Figure 9

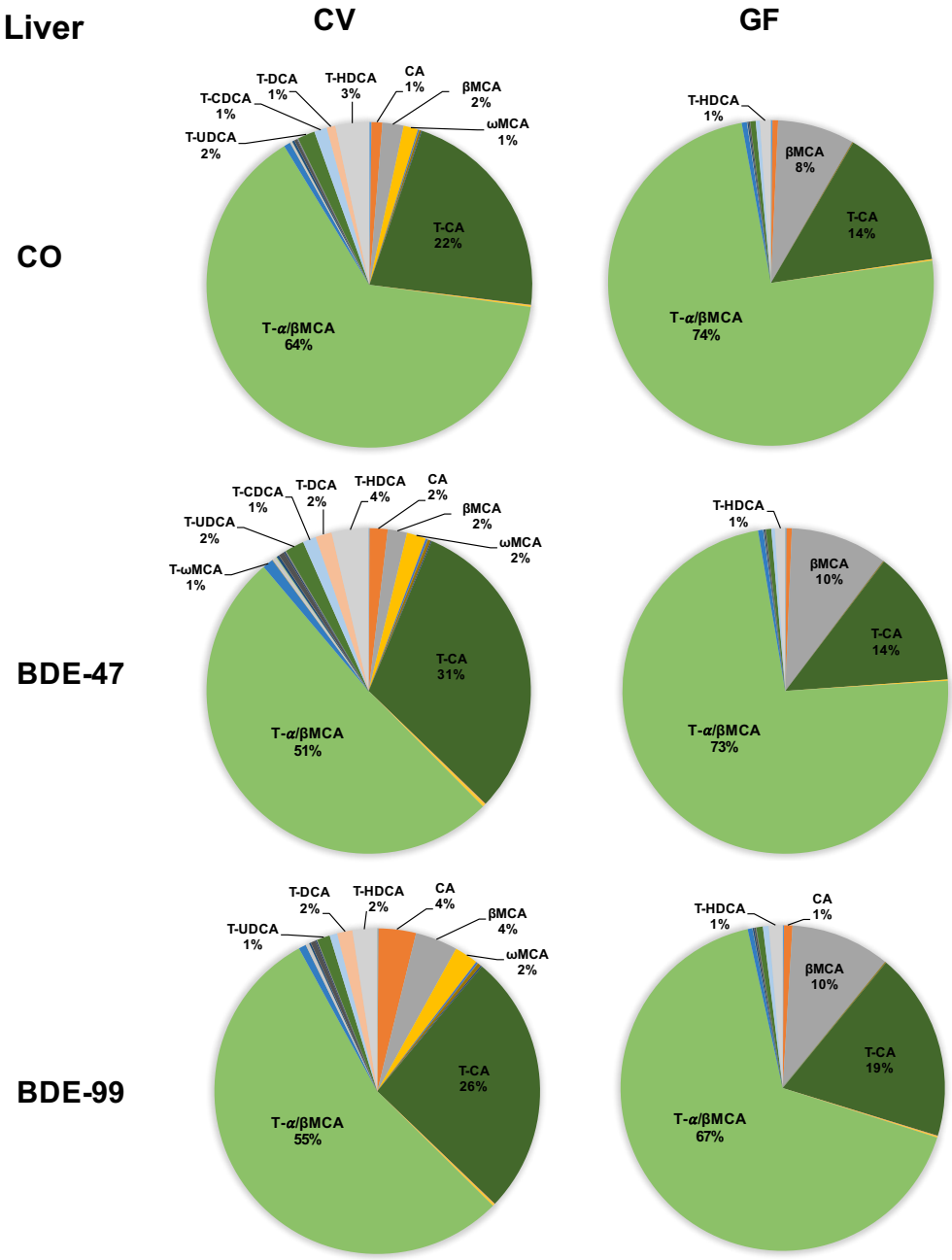

Figure 9. Pie charts illustrating the proportion of individual BAs in liver of CV and GF mice treated with corn oil, BDE-47 (100 μmol/kg), or BDE-99 (100 μmol/kg). BAs with an average percentage higher than 1% were plotted.

Figure 10

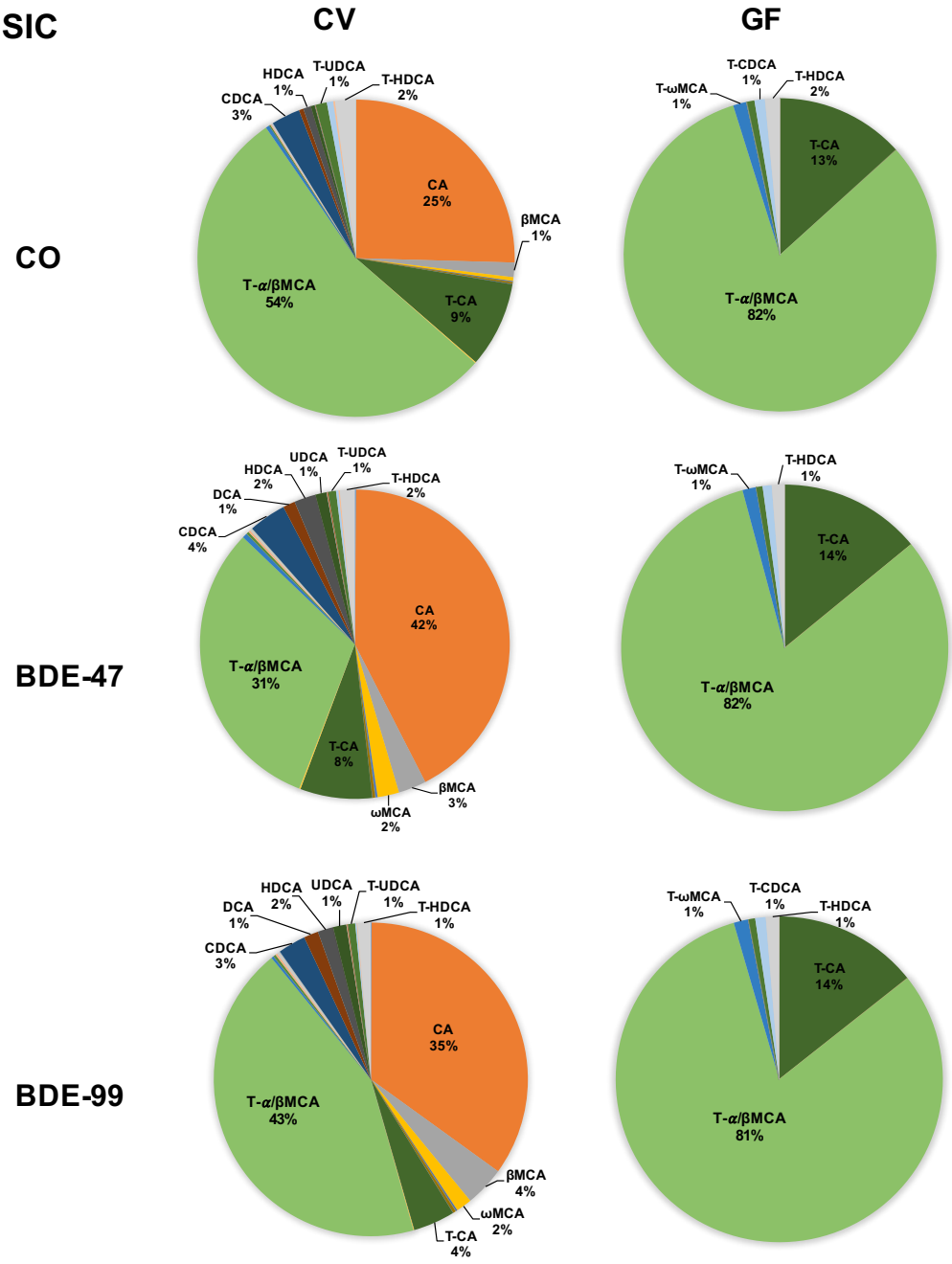

Figure 10. Pie charts illustrating the proportion of individual BAs in SIC of CV and GF mice treated with corn oil, BDE-47 (100 μmol/kg), or BDE-99 (100 μmol/kg). BAs with an average percentage higher than 1% were plotted.

Figure 11

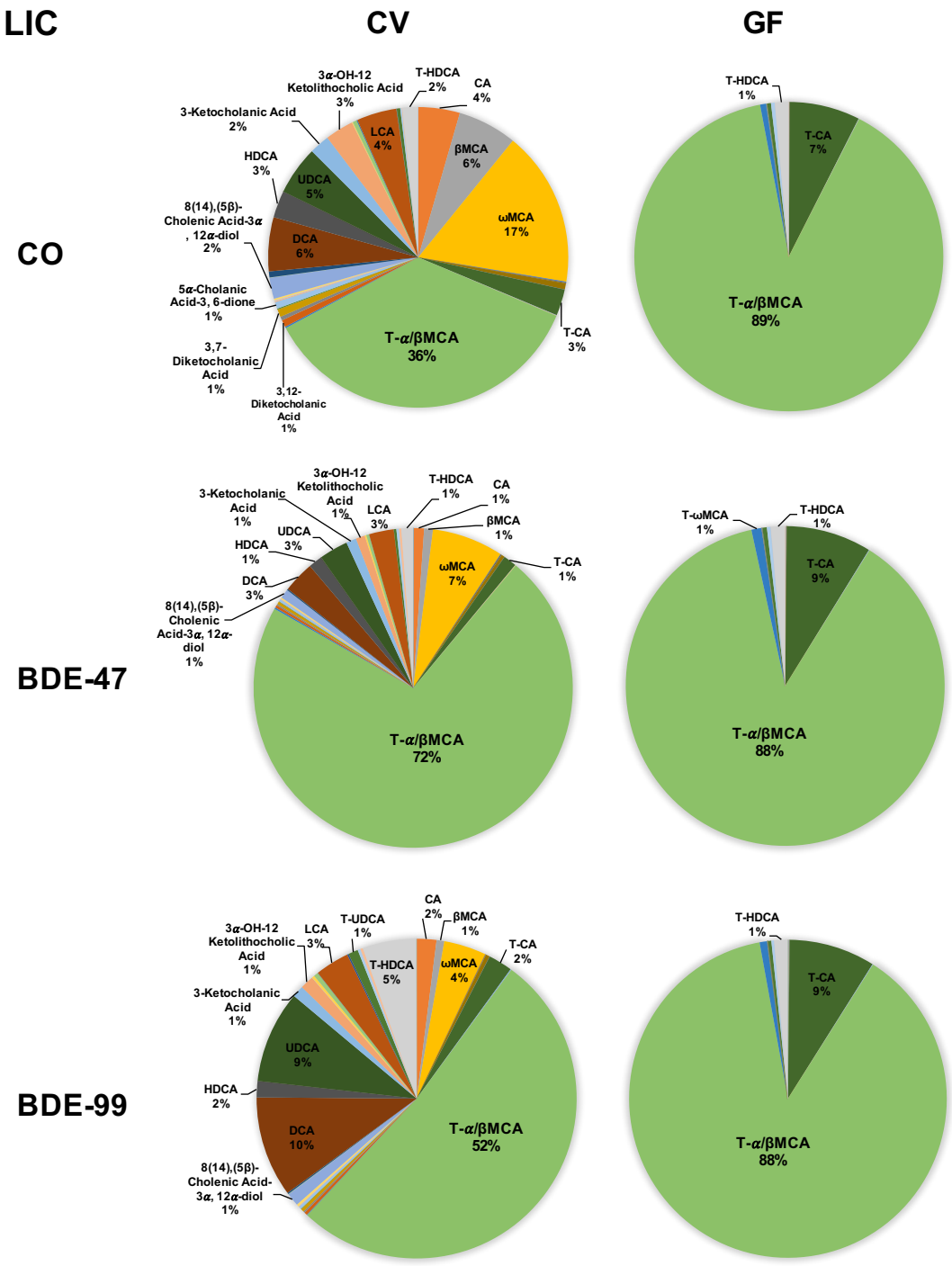

Figure 11. Pie charts illustrating the proportion of individual BAs in LIC of CV and GF mice treated with corn oil, BDE-47 (100 μmol/kg), or BDE-99 (100 μmol/kg). BAs with an average percentage higher than 1% were plotted.

Figure 12

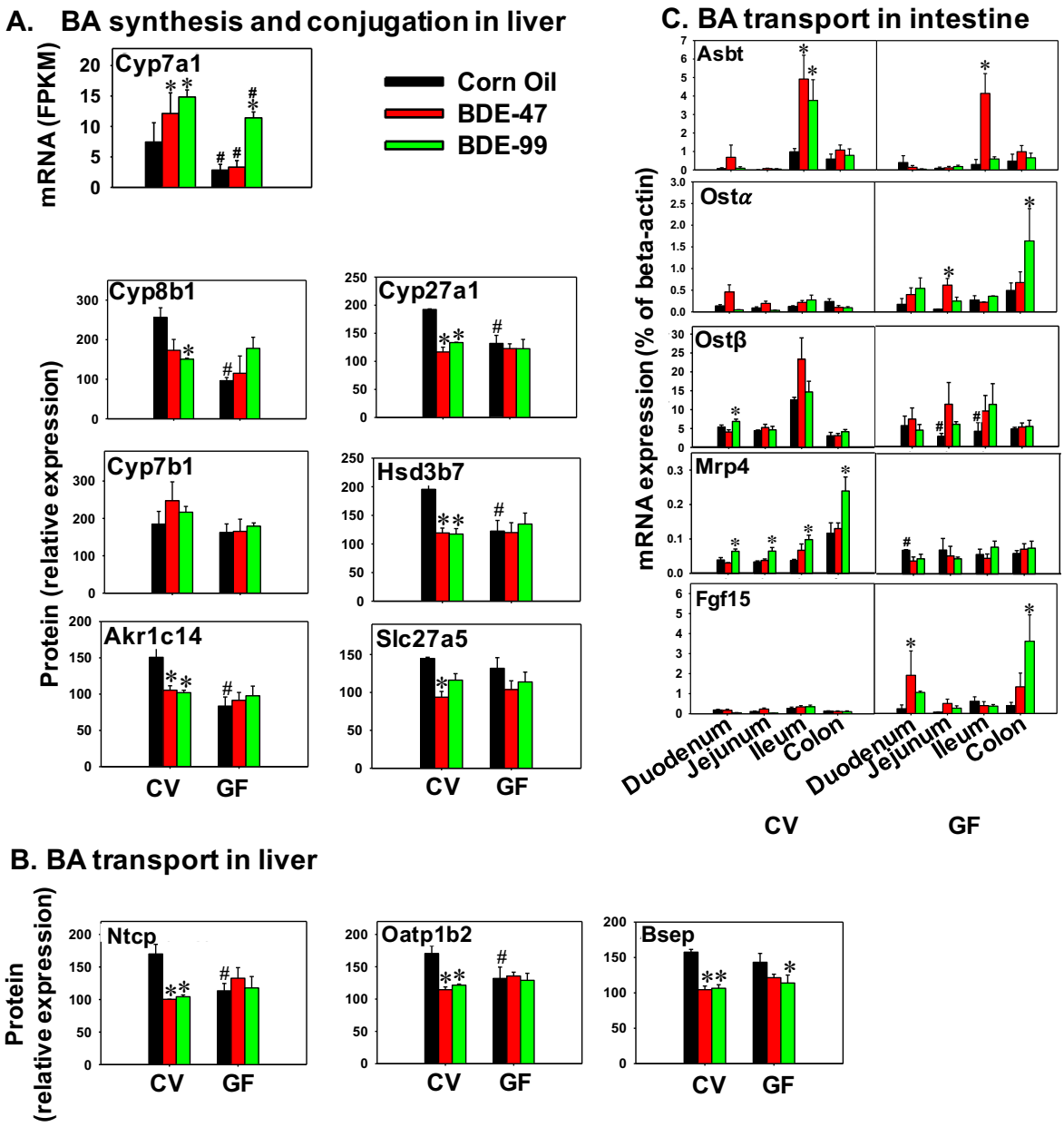

Figure 12. Messenger RNA and protein expression of various BA-processing genes in liver and intestine of CV and GF mice treated with corn oil, BDE-47 (100 μmol/kg), or BDE-99 (100 μmol/kg). (**A**) Hepatic mRNA of Cyp7a1 and protein expression of other genes involved in BA synthesis (Cyp8b1, Cyp27a1, Cyp7b1, Hsd3b7, and Akr1c14) and conjugation (Slc27a5). (**B**) Hepatic protein expression of uptake transporters Ntcp and Oatp1b2, as well as the efflux transporter Bsep. (**C**) Messenger RNA expression of Asbt, Ostα, Ostβ, Mrp4, and Fgf15 in intestine of CV and GF mice. Asterisks (*) represent statistically significant differences between corn oil- and PBDE-treated groups within CV or GF mouse colonies. Pounds (#) represent statistically significant differences between CV and GF mice under the same treatment ($p<0.05$).

Supplemental Figure 1- Bacterial composition at Phylum level

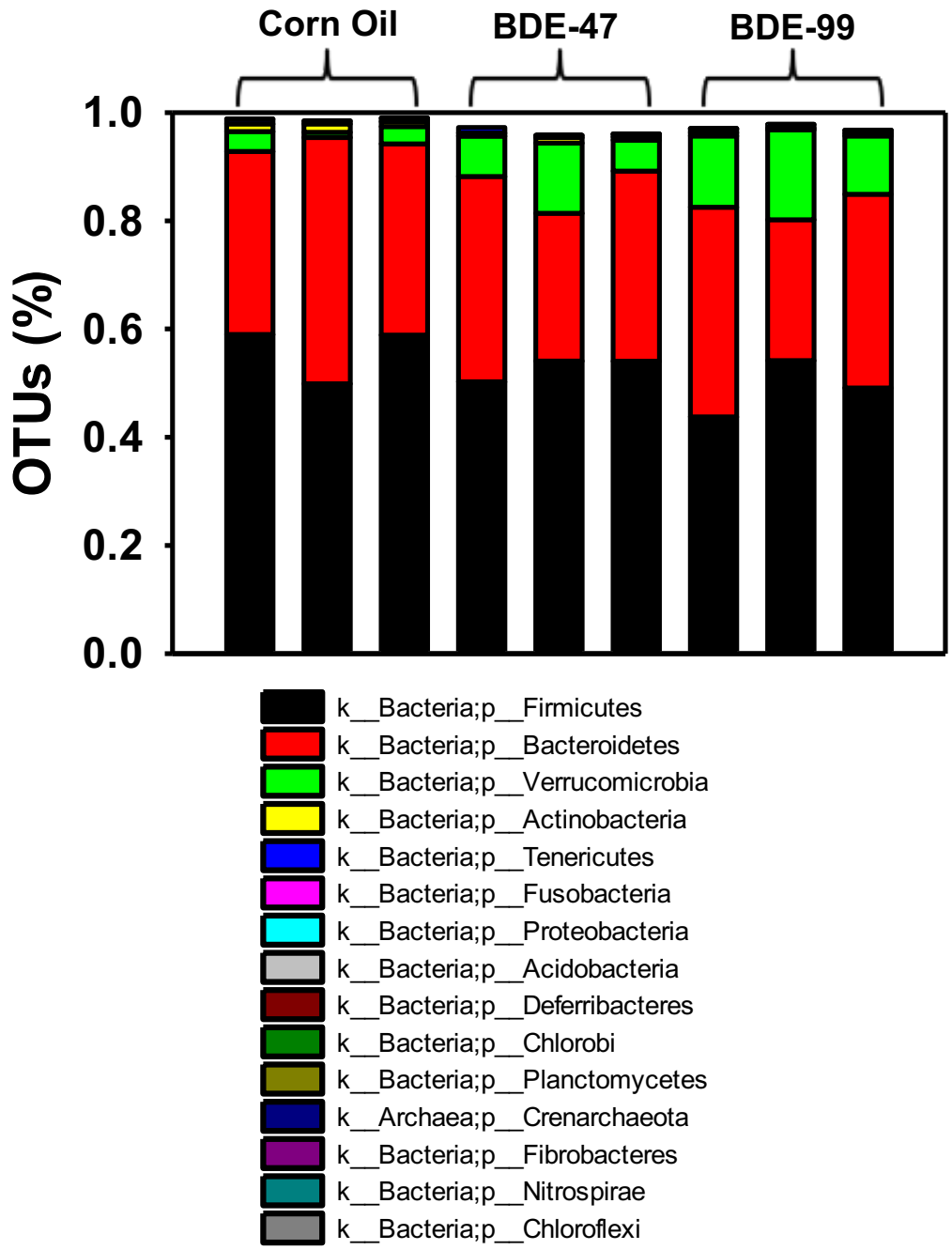

Supplemental Figure 1. Differentially regulated taxa at phylum level by BDE-47 and BDE-99 compared with corn oil-treated group. Bacterial 16S rRNA sequencing was performed in large intestinal content of CV mice as described in MATERIALS AND METHODS.

Supplemental Figure 2. Serum and liver conjugated BAs in CV mice

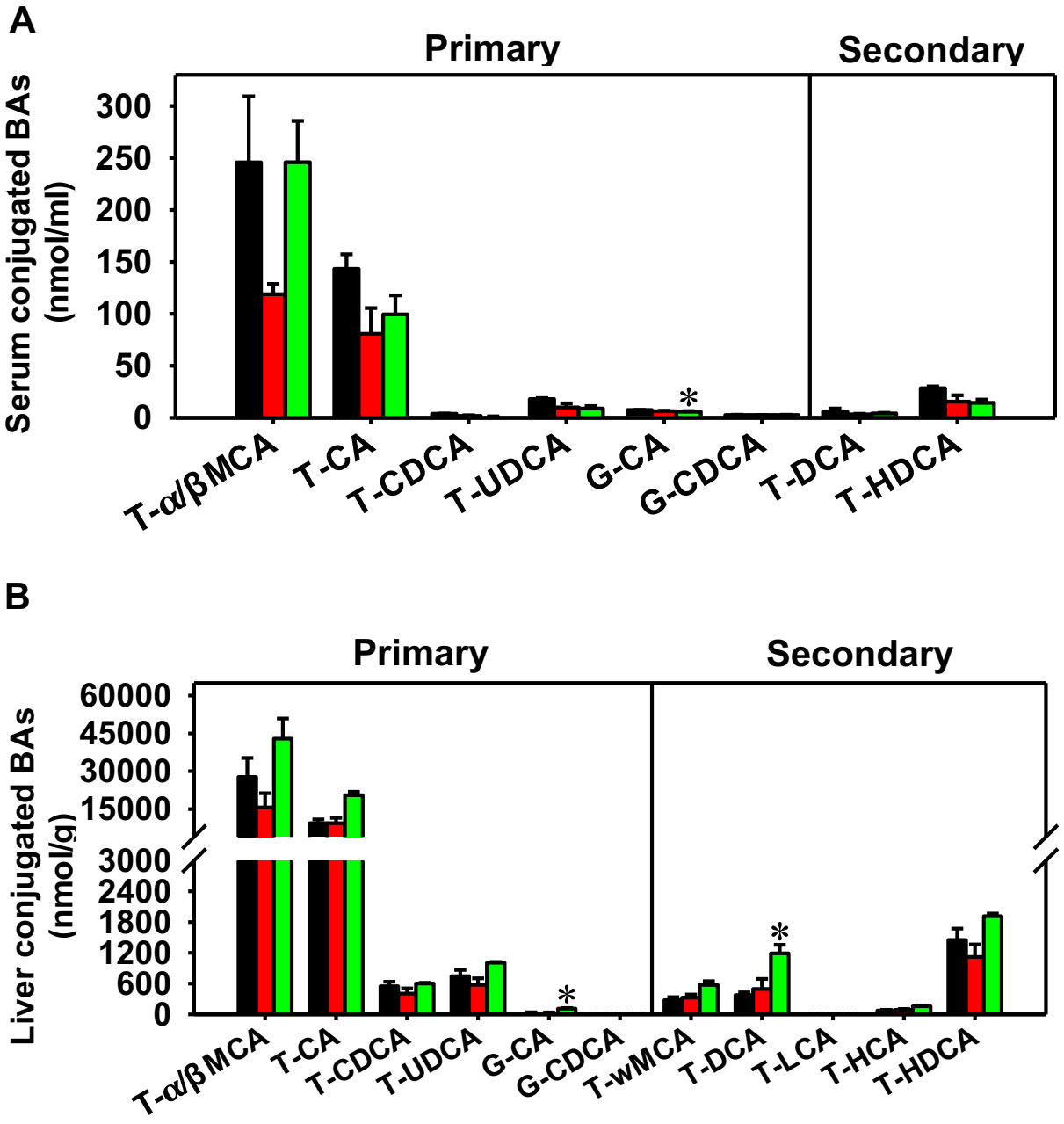

Supplemental Figure 2. Concentrations of conjugated primary and secondary BAs in serum (**A**) and liver (**B**) of CV mice treated with corn oil, BDE-47 (100 μmol/kg) or BDE-99 (100 μmol/kg). BAs were quantified by LC-MS/MS as described in MATERIALS AND METHODS. Data are presented as mean ± S.E. n= 3 per group. Asterisks (*) represent statistically significant differences as compared to corn oil-treated group by ANOVA (Duncan's post hoc test, $p<0.05$).

Supplemental Figure 3. SIC and LIC conjugated BAs in CV mice

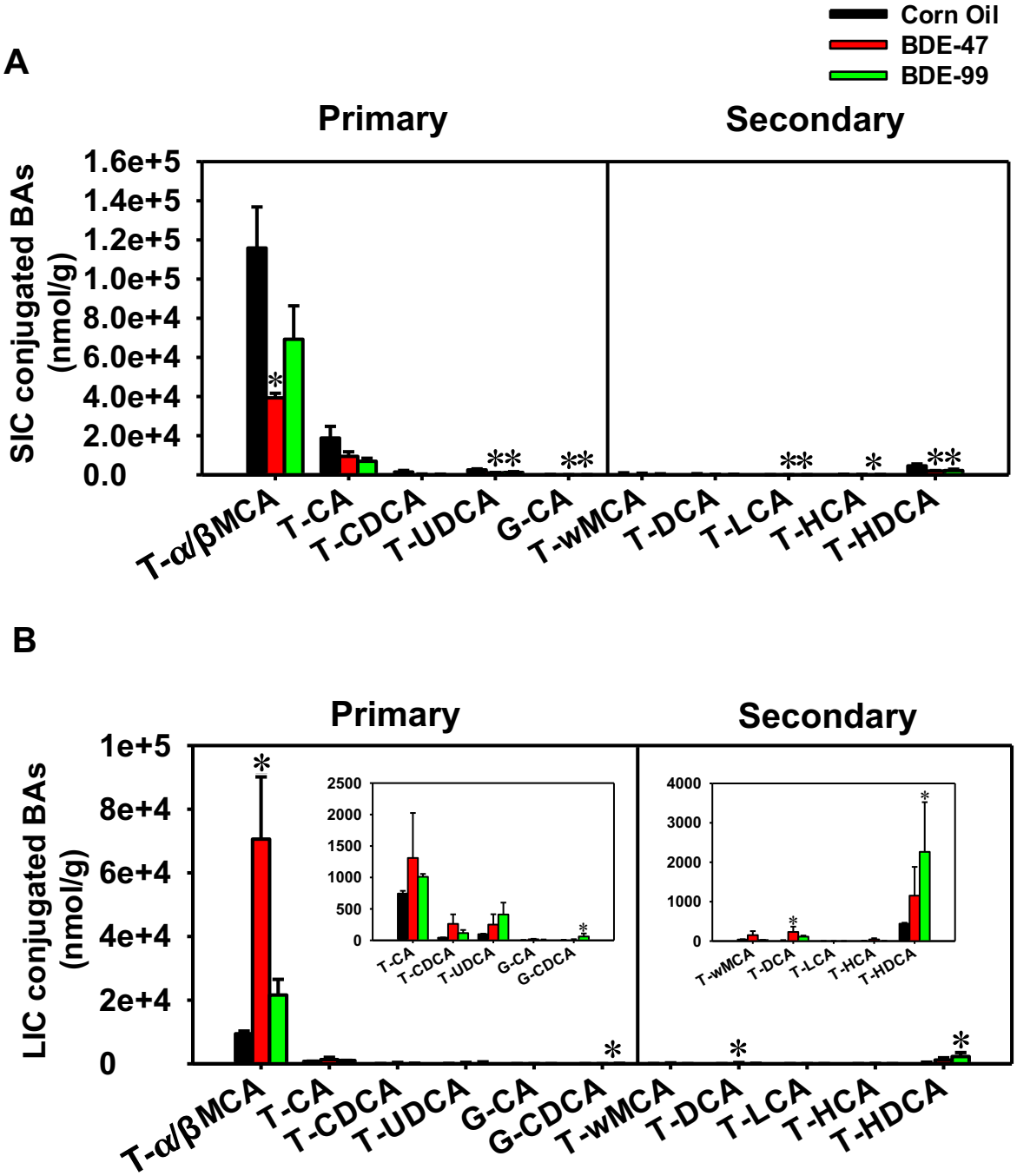

Supplemental Figure 3. Concentrations of conjugated primary and secondary BAs in small intestinal content (SIC) (**A**) and large intestinal content (LIC) (**B**) of CV mice treated with corn oil, BDE-47 (100 μmol/kg) or BDE-99 (100 μmol/kg). BAs were quantified by LC-MS/MS as described in MATERIALS AND METHODS. Data are presented as mean ± S.E. n= 3 per group. Asterisks (*) represent statistically significant differences as compared to corn oil-treated group by ANOVA (Duncan's post hoc test, $p<0.05$).

Supplemental Figure 4

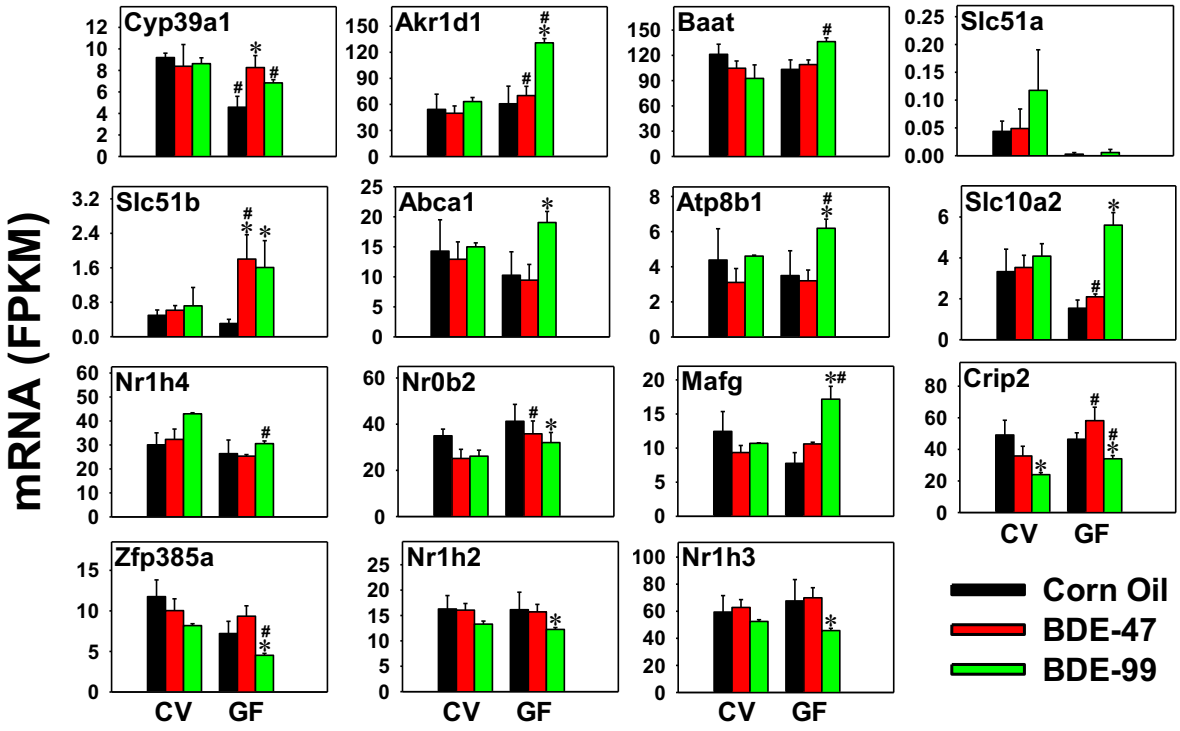

Supplemental Figure 4. Hepatic expression of other genes involved in BA homeostasis. Asterisks (*) represent statistically significant differences between corn oil- and PBDE-treated groups within CV or GF mouse colonies. Pounds (#) represent statistically significant differences between CV and GF mice under the same treatment (p<0.05). Data were analyzed from our RNA-Seq dataset (Li et al., 2017), which can be accessed from GSE101650.

Supplemental Table 1. Primer sequences specific for bacterial cDNA and intestinal mRNA.

Target	Genes	Forward Primer (5'-3')	Reverse Primer (5'-3')
Bacterial DNA	*Universal bacteria*	GTGSTGCAYGGYTGTCGTCA	ACGTCRTCCMCACCTTCCTC
	Akkermansia muciniphila	TCCATTTGGTCCAGCAATTT	CGTGCGCCACTAGAGAATTA
	Clostridium scindens	TGACCGCGATCACAACTTT	GGCGCTTCGTTCGACTT
	Erysipelotrichaceae allobaculum	AGCGTTATCCGGAATGATTG	CCGCTACACATGGAGTTC
		CACGTAGTTAGCCGTGAC	GTAACACGTAGGGAACCTG
		CAGGAGAGGGCGGTGGAA	TTCGTGCCTCAGCGTCAG
		TCCTCGCCGGGTACCATC	TGAGCAAAGAGGAGGCATC
	baiCD	CAGCCCRCAGATGTTCTTTG	GCATGGAATTCWACTGCYTC
	baiJ	TCAGGACGTGGAGGCGATCCA	TACRTGATACTGGTAGCTCCA
	bsh	ATGGGCGGACTAGGATTACC	TGCCACTCTCTGTCTGCATC
Host mRNA	β-actin	GGCCAACCGTGAAAAGATGA	CAGCCTGGATGGCTACGTACA
	Asbt	ACAGCCTGGGTTTCTTCCTG	GGGGGAGAAGGAGAGCTGTA
	Ostα	TTGTGATCAACCGCATTTGT	CTCCTCAAGCCTCCAGTGTC
	Ostβ	ATCCTGGCAAACAGAAATCG	GGCCAAGTCTGGTTTCTCTG
	Mrp4	GCAAAGCCCATGTACCATCT	ACCACGGCTAACAACTCACC
	Fgf15	AGAACAGCTCCAGGACCAGA	TCCATGCTGTCACTCTCCAG

Supplemental Table 2. BAs quantified and normalized to corresponding internal standards.

BA names	IS used for normalization
12 Dehydrocholic Acid (12-dehydroCA)	CA-d4
3 Dehydrocholic Acid (3-dehydroCA)	CA-d4
5belta-Cholanic Acid-3alpha, 6alpha-diol-7-one (5b-Cholanic Acid-3a,6a-diol-7-one)	DCA-D4
alpha-Muricholic Acid (aMCA)	CA-D4
belta-Muricholic Acid (bMCA)	CA-D4
Chenodeoxycholic Acid (CDCA)	GCDCA-D4
Cholic Acid (CA)	CA-D4
Deoxycholic Acid (DCA)	DCA-D4
Glycochenodeoxycholic Acid (G-CDCA)	GCDCA-D4
Glycocholic Acid (G-CA)	GCA-D4
Hyodeoxycholic Acid (HDCA)	DCA-D4
Murocholic Acid (MCA)	DCA-D4
omega-Muricholic Acid (wMCA)	CA-D4
Tauro-alpha+Tauro-belta Muricholic Acid (T-a/bMCA)	GCA-D4
Tauro-ursodeoxycholic Acid (T-UDCA)	GCDCA-D4
Taurochenodeoxycholic Acid (T-CDCA)	GCDCA-D4
Taurocholic Acid (T-CA)	GCA-D4
Taurodeoxycholic Acid (T-DCA)	GCDCA-D4
Taurohyodeoxycholic Acid (T-HDCA)	GCDCA-D4
Taurolithocholic Acid (T-LCA)	LCA-D4
Ursodeoxycholic Acid (UDCA)	DCA-D4
3,12-Diketocholanic Acid	N/A (not enriched in samples)
3,6-Diketocholanic Acid	N/A (not enriched in samples)
3,7-Diketocholanic Acid	N/A (not enriched in samples)
3-Ketocholanic Acid	N/A (not enriched in samples)
3alpha,12alpha,23-Nordeoxycholic Acid	N/A (not enriched in samples)
3alpha-Hydroxy-12 Ketolithocholic Acid	N/A (not enriched in samples)
3alpha-Hydroxy-6,7-DiketoCholanic Acid	N/A (not enriched in samples)
3alpha-Hydroxy-7 Ketolithocholic Acid	N/A (not enriched in samples)
3alpha-Hydroxy-7,12-DiketoCholanic Acid	N/A (not enriched in samples)
5-Cholenic acid-3belta-ol	N/A (not enriched in samples)
5alpha-Cholanic Acid-3, 6-dione	N/A (not enriched in samples)
5alpha-Cholanic Acid-3alpha-ol-6-one	N/A (not enriched in samples)
5belta-Cholanic Acid-3belta, 12alpha-diol	N/A (not enriched in samples)
8(14),(5belta)-Cholenic Acid-3alpha, 12alpha-diol	N/A (not enriched in samples)
9(11), (5belta)-Cholenic Acid-3alpha-ol-12-one	N/A (not enriched in samples)
Allolithocholic Acid	N/A (not enriched in samples)
Dehydrocholic acid	N/A (not enriched in samples)
Glyco-ursocholanic Acid	N/A (not enriched in samples)
Glycodehydrocholic Acid	N/A (not enriched in samples)
Glycodeoxycholic Acid	N/A (not enriched in samples)
Glycohyodeoxycholic Acid	N/A (not enriched in samples)
Glycolithocholic Acid	N/A (not enriched in samples)
Glycoursodeoxycholic Acid	N/A (not enriched in samples)
Hyocholic Acid	N/A (not enriched in samples)
Isodeoxycholic Acid	N/A (not enriched in samples)
Isolithocholic Acid	N/A (not enriched in samples)
Lithocholenic Acid	N/A (not enriched in samples)
Lithocholic Acid (LCA)	N/A (not enriched in samples)
Tauro-omega Muricholic Acid (T-ωMCA)	N/A (not enriched in samples)
Tauro-ursocholanic Acid	N/A (not enriched in samples)
Taurodehydrocholic Acid	N/A (not enriched in samples)
Taurohyocholic Acid	N/A (not enriched in samples)
Ursocholanic Acid	N/A (not enriched in samples)
glycohyocholic Acid	N/A (not enriched in samples)

Supplemental Table 3 – Optimized LC-MS/MS parameters for analysis of surrogate peptides of mouse enzymes and transporter proteins that are involved in BA homeostasis.

(DP- declustering potential, CE- Collision energy and RT-retention time)

Protein	Peptide sequence	Light/Heavy	Parent ion (m/z)	Daughter ion (m/z)	DP (V)	CE (eV)	RT (min)
Cyp8b1	FVYSLLGPR	Light	526.3	805.5	60	21	16
			526.3	642.4	60	21	16
			526.3	442.3	60	21	16
		Heavy	531.3	815.5	60	21	16
			531.3	652.4	60	21	16
			531.3	452.3	60	21	16
			531.3	723.4	60	21	16
Cyp27a1	AQLQETGPDGVR	Light	635.8	958.5	68	25	9
			635.8	830.4	68	25	9
			635.8	600.3	68	25	9
		Heavy	640.8	968.5	68	25	9
			640.8	840.4	68	25	9
			640.8	610.3	68	25	9
	EADNPGILHPFGSVPFGYGVR	Light	743.7	900.5	75	31	17
			743.7	852.0	75	31	17
			743.7	766.9	75	31	17
		Heavy	747.0	905.5	75	31	17
			747.0	857.0	75	31	17
			747.0	771.9	75	31	17
Cyp7b1	MFLGIQHPDSAVSFR	Light	569.0	787.4	63	22	15
			569.0	713.9	63	22	15
			569.0	657.3	63	22	15
		Heavy	572.3	792.4	63	22	15
			572.3	718.9	63	22	15
			572.3	662.3	63	22	15
Akr1c14	HFDSAYLYQIEEEVGQAIR	Light	756.7	834.4	76	32	20
			756.7	997.4	76	32	20
		Heavy	760.0	834.4	76	32	20
			760.0	997.4	76	32	20
Hsd3b7	TIQWVQAMEGSAR	Light	738.9	948.5	75	29	15
			738.9	849.4	75	29	15
		Heavy	743.9	958.5	75	29	15
			743.9	859.4	75	29	15
Slc27a5	SWLPAYATPHFIR	Light	520.3	643.4	59	19	16
			520.3	586.8	59	19	16
		Heavy	523.6	648.4	59	19	16
			523.6	591.8	59	19	16
	QGFCIPVEPGKPGLLLTK	Light	652.0	811.5	69	26	16
			652.0	674.9	69	26	16
			652.0	512.3	69	26	16
		Heavy	654.0	814.5	69	26	16
			654.0	677.9	69	26	16
			654.0	515.3	69	26	16

Supplemental Table 4. 16S rRNA sequencing reads for bacterial samples from LIC of CV mice treated with corn oil, BDE-47 (100 μmol/kg), or BDE-99 (100 μmol/kg), n=3 per group.

Samples	Total Number of Sequence Reads
Corn Oil_1	117299
Corn Oil_2	104804
Corn Oil_3	124805
BDE-47_1	104760
BDE-47_2	100873
BDE-47_3	99396
BDE-99_1	89378
BDE-99_2	100445
BDE-99_3	96781
Total	938541
Average	104282.3333
SE	3574.111871

Supplemental Table 5. The average value of total, conjugated or unconjugated bile acids in serum, liver, SIC and LIC of CV and GF mice treated with corn oil, BDE-47 or BDE-99.

		CV			GF		
		Corn Oil	**BDE-47**	**BDE-99**	**Corn Oil**	**BDE-47**	**BDE-99**
Serum (nmol/ml)	Total	816.85	444.25	953.95	3129.25	3778.66	1161.59
	Conjugated	463.33	243.10	387.91	3047.16	3689.70	1035.64
	Unconjugated	353.52	201.15	566.04	82.09	88.97	125.95
Liver (nmol/g)	Total	43301.64	30528.04	78604.67	201752.25	162959.31	78134.88
	Conjugated	40694.03	28131.94	69026.64	184093.96	145626.89	69251.89
	Unconjugated	2607.60	2396.10	9578.03	17658.29	17332.42	8882.98
SIC (nmol/g)	Total	214886.92	125478.18	159234.59	690838.25	738743.74	787466.81
	Conjugated	144588.21	53031.56	80425.68	690649.24	738533.36	787074.19
	Unconjugated	70298.71	72446.62	78808.91	189.02	210.38	392.62
LIC (nmol/g)	Total	26229.23	89158.92	40516.16	88653.29	66322.45	87939.26
	Conjugated	10820.37	73151.82	25630.97	88510.77	66167.49	87732.08
	Unconjugated	15408.86	16007.10	14885.19	142.52	154.96	207.18

CHAPTER 4: Gut microbiome modifies the PBDE-mediated coordinate regulation of protein-coding genes and long non-coding RNAs in livers of conventional and germ-free mice

This chapter is in preparation for submission. The authors of the manuscript are:

Cindy Yanfei Li and Julia Yue Cui*

Department of Environmental and Occupational Health Sciences, University of Washington, Seattle, WA 98105

Running title: Regulation of hepatic transcriptome by gut microbiome and PBDEs

Abstract

Gut microbiome communicates with the host liver to modify the hepatic xenobiotic biotransformation and nutrient homeostasis. Polybrominated diphenyl ethers (PBDEs) are persistent environmental contaminants that are detected in fatty food, household dust, and human breast milk that may have significant implications for human health. Recently, it has been increasingly recognized that long noncoding RNAs (lncRNAs) are novel biomarkers for toxicological response and may regulate the transcriptional/translational output of protein-coding genes (PCGs). However, very little is known regarding to what extent the interactions between PBDEs and gut microbiome modulate the hepatic lncRNAs and PCGs, and what critical signaling pathways are impacted on a transcriptomic scale. In the present study, we performed RNA-Seq in

livers of nine-week-old male conventional (CV) and germ-free (GF) mice orally exposed to the most prevalent PBDE congeners BDE-47 and BDE-99 (100 μmol/kg once daily for 4-days; vehicle: corn oil, 10ml/kg), and unveiled the molecular pathways regulated by PCGs that were co-regulated with neighboring lncRNAs. Lack of a gut microbiome profoundly altered the PBDE-mediated transcriptomic response in liver, and the most prominent effect was observed in livers of BDE-99-treated GF mice. The top pathways of PCGs that were consistently up-regulated by PBDEs in both enterotypes were xenobiotic metabolism, whereas PBDEs down-regulated genes were involved in lipid metabolism and protein synthesis. Genomic annotation of the differentially regulated lncRNAs revealed that majority of these lncRNAs overlapped with introns and 3'-UTRs of PCGs, and lack of gut microbiome profoundly increased the percentage of PBDE-regulated lncRNAs mapped to the 3'-UTRs of PCGs, suggesting the potential involvement of lncRNAs in increasing the translational efficiency of PCGs by preventing miRNA-3'-UTR as a compensatory mechanism following PBDE toxic insult. Pathway analysis of PCGs paired with lncRNAs revealed that in CV mice, BDE-47-regulated pathways were nucleic acid and retinol metabolism as well as circadian rhythm; whereas BDE-99-regulated metabolic pathways such as PPARα-target genes mediated fatty acid metabolism. In GF mice, 19 lncRNA-PCG pairs were differentially regulated by BDE-47 and they were associated with glutathione conjugation and transcriptional regulation. In contrast, BDE-99 up-regulated Cyp3a genes that are involved in metabolic pathway, but down-regulated Cyp4 genes that are involved in lipid metabolism, and the neighboring lncRNAs followed a similar expression pattern. Taken together, the present study has revealed common and unique lncRNA and PCG targets

of PBDEs in mouse liver, and showed for the first time that lack of gut microbiome in mice sensitizes the liver to the toxic effects of BDE-99 but not BDE-47. LncRNAs may serve as specific biomarkers to reflect the exposure to specific PBDE congeners and changes in gut microbiome, and these lncRNAs may act in concert with PCGs to modulate PBDE-mediated toxicities.

Introduction

Polybrominated diphenyl ethers (PBDEs) are flame retardants with widespread application in plastics, rubbers, furniture, and electronic devices. Although the industrial use of PBDEs have been recently banned, due to their lipophilic feature, PBDEs are persistent and bio-accumulative in the environment. PBDEs have been detected in human blood and breast milk (Frederiksen et al., 2009), raising potentially significant concerns for human health. Animal studies have shown that PBDEs cause a variety of adverse effects, including neurodevelopmental disorders (Madia et al., 2004), thyroid toxicity (Chevrier et al., 2010), hepatic oxidative stress (Fernie et al., 2005), and carcinogenesis (National Toxicology, 1986). BDE-47 and BDE-99, which are the predominant PBDE congeners detected in humans (Lorber, 2008), have been shown to activate the xenobiotic-sensing nuclear receptors pregnane X receptor (PXR) and constitutive androstane receptor (CAR) in rodent livers and human hepatocytes, leading to up-regulated expression of cytochrome P450s (Cyps) (Pacyniak et al., 2007; Erratico et al., 2011; Sueyoshi et al., 2014).

Liver is a major organ for xenobiotic biotransformation. Within the gut-liver axis, liver is connected with gut via portal vein circulation, from which the absorbed nutrients and gut microbial metabolites may interact with distinct receptors in liver to modify various metabolic pathways through remote-sensing mechanisms (Fu and Cui, 2017). We have recently shown that lack of gut microbiome altered the basal expression of many Cyps and other drug-processing genes (DPGs) in liver (Selwyn et al., 2015a; Selwyn et al., 2015b), and we also showed that there is a novel interaction between PBDEs and gut microbiome in modulating the expression of many DPGs by PBDEs in mouse liver. Specifically, the presence of gut microbiome is necessary in PBDE-mediated transcriptional regulation of many hepatic DPGs, and GF mice had altered hepatic oxidation of major PBDE metabolites (Li et al., 2017). Therefore, the gut microbiome is a novel regulator that modifies hepatic xenobiotic biotransformation. However, besides drug metabolism, very little is known regarding to what extent gut microbiome and PBDEs modulate intermediary metabolism, which is another important pathway in liver. Specifically, the liver serves as a central hub for lipogenesis, gluconeogenesis, cholesterol metabolism, bile acid metabolism and protein synthesis (Rui, 2014). Disrupted intermediary metabolism in liver is closely associated with inflammatory, proliferative and apoptotic signaling (Bechmann et al., 2012). Therefore, as a first step to understand the regulation of various metabolic pathways by PBDE-gut microbiome interactions, we used RNA-Seq as a transcriptomic approach to unveil the targeted PCGs in a high throughput manner.

In addition to PCGs, lncRNAs are increasing recognized as novel biomarkers and key regulators of toxicological response (Dempsey and Cui, 2016). LncRNAs are transcribed from the mammalian genome and are usually >200 nucleotides in length but generally appear to lack protein coding capacity, while certain lncRNAs do code for nonclassical small bioactive peptides called micropeptides (Rion and Ruegg, 2017). Various modes of action for lncRNAs have been proposed. lncRNAs may serve as scaffold to transport transcription factors to their promoter region, resulting in transcription activation or repression. lncRNAs can also function as a 'decoy' or 'molecular sink' to bind with chromatin regulatory proteins thereby inhibiting their function (Wang and Chang, 2011; Dempsey and Cui, 2016). Some lncRNAs act in *cis* to activate the transcription of the neighboring genes, whereas others act in *trans* may exhibit suppressive function (Zhou et al., 2015). Increasing evidence suggests that lncRNAs play a critical role in the regulation of numerous cellular processes, including stem cell pluripotency, development, cell differentiation and apoptosis (Guttman et al., 2009; Loewer et al., 2010; Guttman et al., 2011; Hung et al., 2011; Parasramka et al., 2016). Aberrant lncRNAs expression has been reported in various human diseases such as cancer (Gupta et al., 2010; Chen et al., 2015; Parasramka et al., 2016). LncRNAs have been linked to cellular cholesterol metabolism (Lan et al., 2016), lipid metabolism and bile acid homeostasis (Li et al., 2015). In addition, lncRNAs have been shown to be novel biomarkers for toxic exposure to classic toxicants such as polycyclic aromatic hydrocarbons (Gao et al., 2016), benzene (Bai et al., 2014), cadmium (Zhou et al., 2015), and bisphenol A (Kumamoto and Oshio, 2013). However, very little is known regarding to what extent PBDEs and gut microbiomes modulate lncRNA gene

expression in liver, and what the potential PCG targets are that may be influenced by differentially regulated lncRNAs.

Therefore, the goal of the present study is 1) to characterize the functional interactions between gut microbiome and PBDEs and the subsequent changes on hepatic transcriptome including PCGs and lncRNAs; and more importantly, 2) unveil critical signaling pathways that are targeted by lncRNA-PCG gene pairs. This study is among the first to characterize the regulation of lncRNAs and PCGs simultaneously in response to gut microbiome-PBDE interactions, paving the path for future investigations to identify the mechanistic roles of lncRNAs and gut microbiome in PBDE-mediated toxicities.

Materials and methods

Animals and procedures

As we described previously (Li et al., 2017), eight-week-old C57BL/6J wild type conventional (CV) mice were purchased from the Jackson Laboratory (Bar Harbor, ME). The initial breeding colony of GF mice in C57BL/6 background was established with mice purchased from the National Gnotobiotic Rodent Resource Center (University of North Carolina, Chapel Hill). All mice in this study were exposed to the same diet (LabDiet # 5010), bedding (autoclaved Enrich-N'Pure), and water. Mice were housed according to the American Animal Association Laboratory animal care guidelines. As described in Fig. 1, at 9-week of age, CV and GF mice (n=3-5 per group) were orally dosed with sterile vehicle (corn oil, 10 ml/kg), BDE-47 (100 μmol/kg) or BDE-99 (100 μmol/kg) once daily for four consecutive days. Livers were collected 24 hours after the

final dose, immediately frozen in liquid nitrogen, and stored in a -80°C freezer. All studies were approved by the Institutional Animal Care and Use Committee (IACUC) at the University of Washington.

Total RNA extraction, DNA library construction and RNA-sequencing

RNA extraction, cDNA library construction and RNA-Sequencing were performed as previously described (Li et al., 2017). Briefly, total RNA was extracted from livers of CV and GF mice using RNA-Bee reagent following the manufacturer's instructions (Tel-Test Inc., Friendswood, TX). RNA concentrations were quantified using a NanoDrop 1000 Spectrophotometer (Thermo Scientific, Waltham, MA). Integrity of total RNA samples was evaluated by Agilent 2100 Bioanalyzer (Agilent Technologies Inc. Santa Clara, CA). Samples with RNA integrity values above 8.0 were sent for RNA-sequencing. The complementary DNA (cDNA) libraries were constructed from total RNA samples using an Illumina TruSeq Stranded RNA kit with Poly-A tail selection (Illumina, San Diego, CA). Sequencing was performed on an Illumina HiSeq2000 sequencer using a 50bp pair-end multiplexing strategy at the University of Washington Genome Sciences Sequencing Facilities.

RNA sequencing data analysis

The raw and analyzed RNA-Seq data were deposited in Gene Expression Onmibus (GEO) database (accession number: GSE101650), and the FASTQ files were analyzed in the present study for lncRNA and PCG expression. As described in Fig. 1, the FASTQ files containing pair-end sequence reads were mapped to the mouse reference

genome (GRCm38/mm10) using HISAT (Hierarchical Indexing for Spliced Alignment of Transcripts) (version 0.1.6 beta) (Kim et al., 2015). The output SAM (sequencing alignment/map) files were converted to BAM (binary alignment/map) files and sorted using SAMtools (version 1.2) (Li et al., 2009a). For the analysis of PCGs and lncRNAs, the transcript abundance was estimated by Cufflinks (version 2.2.1) using the UCSC mm10 PCG and NONCODE 2016 lncRNA reference databases in gene transfer format (gtf), respectively. The mRNA abundance was expressed as fragments per kilobase of transcript per million mapped reads (FPKM). PCGs with average FPKM value above 1 in at least one group were defined as significantly expressed in liver. Differential expression analysis was performed using Cuffdiff with p-value <0.05 between chemical-exposed groups and vehicle-exposed group of the same enterotypes of mice. Data were expressed as mean FPKM ± S.E. Asterisks (*) represent significant differences between corn oil- and PBDE-treated groups of the same enterotype of mice. The Venn diagrams of the differentially expressed PCGs and lncRNAs were generated based on their standardized mean FPKM values, using the JMP Genome Software (SAS Institute, Cary, NC).

Genomic annotation of lncRNAs and lncRNA-PCG pair identification

The web-based tool peak annotation and visualization (PAVIS, https://manticore.niehs.nih.gov/pavis2/) (Huang et al., 2013) was used to annotate and visualize the genomic location of lncRNAs relative to the closest PCGs, including up to 5 kb upstream of transcription start site (TSS), intronic, exonic, 5'-untranslated region (UTR), 3'-UTR, or up to 1 kb downstream of transcriptional termination site (TTS). A

lncRNA-PCG pair is defined as: 1) the lncRNA overlapped with or was within 5 kb upstream of TSS or 1 kb downstream of TTS of the closest PCG, and 2) both the PCG and the neighboring lncRNA were differentially regulated by PBDE exposure compared to vehicle-treated group of the same enterotype of mice ($p < 0.05$). The gene structure and relative genomic location of the lncRNA-PCG pairs were visualized using Integrated Genome Viewer (Broad Institute, Cambridge, MA).

Pathway analysis of differentially regulated PCGs and lncRNAs

The differentially regulated PCGs by 1) BDE-47 in CV mice, 2) BDE-99 in CV mice, 3) BDE-47 in GF mice or 4) BDE-99 in GF mice were each analyzed using Ingenuity Pathway Analysis (IPA, QIAGEN, Vallencia, CA) to determine significantly altered gene networks. The PCGs that were uniquely regulated by each of the above four criteria were further analyzed by IPA to determine the specific effect of BDE-47 and BDE-99 in CV and GF conditions. The differentially regulated lncRNAs that match each of the above four criteria were separated into four datasets, and their paired PCGs in each dataset were submit for STRING (Search Tool for the Retrieval of Interacting Genes/Proteins) analysis (https://string-db.org/).

Results

The present study utilized RNA-Seq and in vivo CV and GF mouse models to determine the effect of functional interactions between the gut microbiome and PBDEs on the hepatic transcriptome of PCGs and lncRNAs. RNA-Seq generated approximately 39 to 127 million reads per sample, among which 63% to 94% of the reads were uniquely

mapped to the mouse reference genome (NCBI GRCm38/mm10), which were equivalent to 35 million to 115 million uniquely mapped reads (Supplemental Table 1).

Regulation of PCGs by PBDEs and gut microbiome

Among the 24,487 annotated PCGs in the mouse reference genome (Fig. 2A), 14,026 genes were not expressed in livers of any groups (threshold: average FPKM < 1 in all treatment groups). Among the expressed genes (FPKM> 1 in at least one treatment group), 6,799 genes were stably expressed across all treatment groups, whereas a total of 3,662 genes were differentially expressed by PBDEs in CV and GF mice (criteria: p < 0.05 in at least one of the 4 comparisons between corn oil (CO) and PBDE-exposed groups of the same enterotype, namely 1) corn oil exposed CV mice (CV_CO) vs. CV_BDE-47, 2) CV_CO vs. CV_BDE-99, 3) corn oil exposed GF mice (GF_CO) vs. GF_BDE-47, and 4) GF_CO vs. GF_BDE-99).

To unveil the common and unique PCG targets by PBDEs and gut microbiome interactions, a venn diagram of the 3,662 differentially expressed PCGs was generated which revealed a clear separation by differences in both PBDE congeners (BDE-47 or BDE-99) and in enterotypes (presence or absence of gut microbiome) (Fig. 2B). There were 49 DPGs that were consistently differentially regulated in all 4 comparisons, whereas uniquely regulated DPGs in each comparison were also observed, and especially, the number of PCGs uniquely regulated by BDE-99 in GF conditions (2442) was much higher than that in CV conditions (223), suggesting that lack of gut microbiome sensitized the hepatic protein-coding transcriptome to BDE-99 mediated

insult. Conversely, the numbers of PCGs uniquely regulated by BDE-47 were 140 in CV conditions and 22 in GF conditions. Therefore, the two PBDE congeners lead to different transcriptomic outcomes during PBDE-gut microbiome interactions.

To determine the top differentially regulated molecules and the associated signaling networks, Ingenuity Pathway Analysis (IPA) was performed for the differentiated regulated PCGs ($p < 0.05$) among the 4 comparisons (CV_CO vs. CV_BDE-47, CV_CO vs. CV_BDE-99, GF_CO vs. GF_BDE-47, and GF_CO vs. GF_BDE-99). Regarding the top molecules (Table 1), in livers of CV mice, the top 10 most up-regulated PCGs following BDE-47 exposure include the phase-I drug-metabolizing enzymes cytochrome P450 (Cyp) family, namely Cyp2b10, Cyp2b13, and Cyp2c55; metallothionein (Mt) 1 and Mt2, which are involved in zinc homeostasis and heavy metal detoxification (Ruttkay-Nedecky et al., 2013); D site albumin promoter binding protein (Dbp) and circadian associated repressor of transcription (Ciart, also known as Gm129), which modulate important clock genes involved in circadian rhythm (Yamaguchi et al., 2000; Annayev et al., 2014); regulator of G-protein signaling 16 (Rgs16), which inhibits signaling cascades related to fatty acid oxidation in hepatocytes (Pashkov et al., 2011); serum amyloid A2 (Saa2), which is an apolipoprotein and is highly expressed in liver in response to inflammation (Zhang et al., 2005); and lipocalin 2 (Lcn2), which is an iron-trafficking protein that maintains iron homeostasis (Srinivasan et al., 2012). Hepatocyte-derived Lcn2 has also been reported to protect against bacterial infection and promote liver regeneration (Xu et al., 2015a). In livers of CV mice, the top 10 most down-regulated PCGs following BDE-47 exposure include growth arrest and DNA

damage 45g (Gadd45g) and proline-rich acidic protein 1 (Prap1), which are involved in regulation of development, cell differentiation and survival (Zhang et al., 2003; Zhang et al., 2014); trefoil factor 2 (Tff2), which mediates gastric cytoprotection and repair (Farrell et al., 2002); regenerating islet-derived 3 beta (Reg3b) and deleted in malignant brain tumors 1 (Dmbt1), which maintain intestinal homeostasis and prevent bacterial infection (van Ampting et al., 2012; Reichold et al., 2013), as well as neuronal PAS domain protein 2 (Npas2), which functions as a transcription activator involved in circadian rhythms (DeBruyne et al., 2007) (Table 1).

In livers of CV mice, the top 15 networks of PCGs that were differentially regulated by BDE-47 exposure are shown in Supplemental Table 2, which include pathways related to RNA post-transcriptional modification, cellular development, cellular growth and proliferation, cell cycle, gene expression, lipid metabolism, small molecule biochemistry, carbohydrate metabolism, and drug metabolism. An example network (lipid and drug metabolism, Network #14 as shown in red in Supplemental Table 2) is visualized in Supplemental Fig. 1. BDE-47 markedly up-regulated Cyp2b family members that are involved in xenobiotic metabolism. BDE-47 also up-regulated Cyp7a1 and Cyp7b1, which are responsible for bile acid synthesis (Chiang, 2002); conversely, BDE-47 down-regulated Cyp4a14, which is the prototypical target gene of lipid sensor peroxisome proliferator-activated receptor alpha (PPARα) and is involved in fatty acid oxidation (Zhang et al., 2017a), suggesting that BDE-47 may activate the xenobiotic oxidation and bile acid synthesis but suppress the hydroxylation of fatty acids and lipid metabolism signaling.

In livers of CV mice, the top 10 most up-regulated genes following BDE-99 exposure include carboxyl ester lipase (Cel) and pancreatic lipase (Pnlip), which catalyze fat digestion/absorption and glycerolipid metabolism (Hui and Howles, 2002; Zechner et al., 2012); BDE-99 also up-regulated certain genes, such as chymotrypsinogen B1 (Ctrb1), carboxypeptidase B1 (Cpb1), protease serine 2 (Prss2), Prss3, and trypsin 5 (Try5), which involved in protein digestion and absorption (Kido et al., 1985); ribonuclease (Rnase1), which catalyzes the cleavage of RNA (Verbeure et al., 2001); and Saa2 and Lcn2, which suppress bacterial infection (Zhang et al., 2005; Xu et al., 2015a) (Table 1). Interestingly, the fold increases of the top 10 PCG transcripts by BDE-99 exposure were in general much greater than those of the top 10 PCG transcripts by BDE-47 exposure, suggesting that at equal molar doses, BDE-99 is more potent than BDE-47 in up-regulating the expression of hepatic PCGs (Table 1). In livers of CV mice, the top 10 most down-regulated PCGs following BDE-99 exposure include cyclin-dependent kinase inhibitor 1A (Cdkn1a) and Gadd45g, which are involved in p53 signaling in response to DNA damage (Tanikawa et al., 2017); lysyl oxidase-like 4 (Loxl4), which modulates the formation of extracellular matrix (Kim et al., 2003); hyperpolarization-activated cyclic nucleotide-gated channel (Hcn3), which is a potassium channel and controls cellular excitability (Cao-Ehlker et al., 2013). BDE-99 also down-regulated certain PCGs involved in circadian rhythm, such as the transcriptional activator Arntl (Aryl hydrocarbon receptor nuclear translocator-like), the transcriptional repressor Npas2, as well as Chka (choline kinase alpha), which is regulated by the clock transcription factor REV-ERB (Grechez-Cassiau et al., 2015). In addition, elongation of

very long chain fatty acids (Elovl3), as well as chloride intracellular channel 3 (Clic3) which forms chloride ion channel and controls cellular growth, were down-regulated by BDE-99 exposure in livers of CV mice (Table 1).

In livers of CV mice, the top 15 networks of genes that were differentially regulate by BDE-99 exposure are shown in Supplemental Table 2, which include lipid metabolism, small molecule biochemistry, molecular transport, gene expression, drug metabolism, protein synthesis, RNA post-transcriptional modification, cell cycle, and carbohydrate metabolism. An example network (#13) is shown in Supplemental Fig. 2, which is lipid metabolism, small molecule biochemistry, vitamin and mineral metabolism. In this network, a variety of P450s including Cyp2a, Cyp2b, Cyp2c, Cyp2g1, Cyp3a and the cytochrome P450 oxidoreductase (Por), were all moderately up-regulated by BDE-99. BDE-99 also up-regulated Cyp7b1, which is involved in the alternative bile acid synthesis pathway, but down-regulated Cyp8b1, which is involved in the classic bile acid synthesis pathway. BDE-99 also down-regulated many genes involve in lipid metabolism and fatty acid degradation, including a consistent down-regulation of the PPARα-targeted Cyp4 family members (Cyp4a11, Cyp4a14, Cyp4f14 [mouse homolog of human CYP4F12]); Cyp46a1, which is the rate-limiting enzyme for cholesterol degradation (Boussicault et al., 2016); 3-hydroxymethylglutaryl-CoA synthase (Hmgcs1), which forms the intermediate HMG-CoA for cholesterol synthesis and ketogenesis (Harris et al., 2000); and acyl-CoA synthetase (Acsl), which activates long-chain fatty acids for both synthesis of cellular lipids and degradation via beta-oxidation (Li et al.,

2009b). In addition, BDE-99 down-regulated Cyp26a1, which is involved in the metabolism of retinoic acid (Ross and Zolfaghari, 2011).

In livers of GF mice, the top 10 most up-regulated genes following BDE-47 exposure include many phase I and phase II drug metabolizing enzymes, such as Sult2a2, Sult2a1, Cyp2b10, Cyp2c55, Cyp2b13, Akr1b7, Fmo3, and Cyp3a16; BDE-47 also up-regulated alpha-1-B glycoprotein (A1bg), and pancreatic lipase protein 1 (Pnliprp1), which has been associated with dietary lipid absorption and fatty liver development (Hoekstra et al., 2010). In livers of GF mice, the top 10 most down-regulated PCGs following BDE-47 exposure include serine peptidase inhibitor member 9 (Serpina9); alpha thalassemia/mental retardation syndrome X-linked homolog (Atrx), which is involved in transcriptional regulation and chromatin remodeling (Lee et al., 2015); pleckstrin homology domain interacting protein (Phip), which modulates insulin signaling (Farhang-Fallah et al., 2000); IgA inducing protein (Igip), which induces the production of IgA in maintaining gut homeostasis (Endsley et al., 2009); Rho-associated protein kinase 1 (Rock1), which regulates actin cytoskeleton organization, cell motility, proliferation and apoptosis (Hartmann et al., 2015); B cell leukemia/lymphoma 6 (Bcl6), which functions as a transcriptional repressor in modulating interleukin-4 signaling (Lossos et al., 2003); and small nucleolar RNA 7A (Snora7a), which is involved in cell proliferation especially in tumor cells (Lindahl et al., 1989).

In livers of GF mice, the top 12 networks of PCGs that were differentially regulated by BDE-47 exposure are shown in Supplemental Table 2, which include pathways related

to drug metabolism, glutathione depletion, lipid metabolism, carbohydrate metabolism, and cell-cell signaling and interaction. An example network (drug metabolism, glutathione depletion in liver, lipid metabolism, network #1 as shown in red in Supplemental Table 2) is visualized in Supplemental Fig. 3. BDE-47 markedly up-regulated Cyp2b10 (mouse homolog of human CYP2B6) and Cyp3a11 (mouse homolog of human CYP3A5) that are involved in xenobiotic metabolism. BDE-47 also up-regulated Cyp2a, Cyp2c54, Cyp2c55 (mouse homolog of human CYP2C18), and many other Cyp2c family members. The glutathione *S*-transferases (Gst), including Gsta4, Gsta5, Gstm3-5, and Gstt3 that are important for the detoxification and reduction of reactive oxygen species, were also up-regulated by BDE-47 in GF mice.

In GF mice, the top 10 most up-regulated PCGs following BDE-99 exposure included drug metabolizing enzymes Cyp2b10, Cyp2c55, Gsta1, Gstm3, Sult1e1, and Akr1b7. BDE-99 also up-regulated meiosis expressed gene 1 (Meig1), V-set domain containing T cell activation inhibitor 1 (Vtcn1, also known as B7-H4), which suppresses T cell function via inhibiting cell proliferation and cytokine secretion (Diao et al., 2017), Pnliprp1, and small nucleolar RNA host gene 11 (Snhg11). Interestingly, the fold increases of the top 10 PCG transcripts by BDE-99 exposure were in general much greater than those of the top 10 PCG transcripts by BDE-47 exposure, again suggesting that at equal molar doses, BDE-99 is more potent than BDE-47 in up-regulating the hepatic PCGs expression (Table 1). In livers of GF mice, the top 10 most down-regulated genes following BDE-99 exposure included trefoil factor 3 (Tff3), which maintains the intestinal mucosa (Ge et al., 2015); histocompatibility 2, class II antigen A,

beta 1 (H2-Ab1); FLYWCH family member 2 (Flywch2); hemoglobin, beta adult t chain (Hbb-bt), which transports oxygen to peripheral tissues; serine peptidase inhibitor member 3C (Serpina3c); Serpina12; Cyp46a1, which is the rate-limiting enzyme for cholesterol degradation (Boussicault et al., 2016); RAD51 homolog b (Rad51b), which is involved in DNA repair (Lio et al., 2003); and acyl-CoA thioesterase 1 (Acot1), which catalyzes the hydrolysis of acyl-CoAs to free fatty acid and Coenzyme A. Knockdown of Acot1 in mice resulted in enhanced hepatic oxidative stress and inflammation (Franklin et al., 2017). Additionally, Sult2a1, which catalyzes sulfonation of hydroxysteroids and xenobiotics, was completely abolished in livers of GF mice following BDE-99 exposure.

In livers of GF mice, the top 15 networks of PCGs that were differentially regulated by BDE-99 exposure are shown in Supplemental Table 2, which include pathways related to cancer, developmental disorder, RNA post-transcriptional modification, metabolic disease, carbohydrate metabolism, gene expression, protein synthesis, and various cellular signaling pathways. An example network (gene expression, protein synthesis, lipid metabolism, network #8 as shown in red in Supplemental Table 2) is visualized in Supplemental Fig. 4. BDE-99 markedly down-regulated a series of mitochondrial ribosomal proteins (Mrpl), which are essential for oxidative phosphorylation to produce ATP (Sylvester et al., 2004). This massive down-regulation of Mrpl by BDE-99 may lead to disordered oxidative phosphorylation and various mitochondrial diseases (O'Brien et al., 2000).

In summary, both PBDE exposure and gut microbiome regulated the hepatic transcriptome in mice, and lack of gut microbiome appeared to sensitize mouse liver to BDE-99 mediated effects on the transcriptome of PCGs.

PCGs that were commonly or uniquely regulated by PBDEs in CV and GF mice

Regarding the 49 consistently differentially regulated genes (Figure 2B), 32 of them were shown in Fig. 3; whereas the rest 17 genes (including Cyp2a, Cyp2b, Cyp2c, Ugt2b, Sults and Gsts) have been described previously in our recent publication (Li et al., 2017), and all of them were up-regulated by BDE-47 and BDE-99 in livers of CV and GF mice. KEGG pathway analysis (performed using STRING Analysis) of these 32 commonly regulated genes indicated they were enriched in metabolic pathway, chemical carcinogenesis, retinol metabolism, steroid hormone biosynthesis, and arachidonic acid metabolism (Supplemental Fig. 5). As shown in Fig. 3, these genes were categorized into four distinct patterns. Pattern 1 included 16 genes (Fig. 3A), which were up-regulated by both PBDEs in CV and GF mice, including RIKEN-derived genes (1700067K01Rik and 4931406C07Rik); Aldo-keto reductase (Akr1b7) which is a phase-I drug metabolizing enzyme (Liu et al., 2009); aminolevulinic acid synthase 1 (Alas1), which is the rate-limiting enzyme for heme synthesis in liver (Kubota et al., 2016), and human hepatic ALAS1 is the target gene of the bile acid-activated nuclear receptor farnesoid X receptor (FXR) (Peyer et al., 2007); Cyp2c53-ps (Cyp pseudogene); Gadd45b; Gm10872; Gm3776; interferon alpha-inducible protein 27 like 2B (Ifi27l2b); interferon-stimulated gene 15 (Isg15); leukocyte cell derived chemotaxin 1 (Lect1); Meig1; orosomucoid 3 (Orm3), which is expressed in hepatocytes under stress

condition and is a direct FXR target gene (Porez et al., 2013); sphingomyelin phosphodiesterase 3 (Smpd3) , which produces ceramide for cell growth, differentiation, and apoptosis (Stoffel et al., 2005); suppressor of cytokine signaling 2 (Socs2), which regulates hepatic homeostasis under high-fat dietary conditions (Zadjali et al., 2012); and starch-binding domain 1 (Stbd1), which participates the metabolism and cellular trafficking of glycogen (Jiang et al., 2010).

Pattern 2 included 5 genes (Fig. 3B), which were down-regulated by both PBDEs in CV and GF mice, including family with sequence similarity genes (Fam222a); Fam89a; nuclear factor interleukin 3 (Nfil3), which plays a critical role in the regulation of apoptosis in lymphocytes (Kamizono et al., 2009); Ppard, which suppresses hepatic lipogenesis in obese mice (Qin et al., 2008); and transforming growth factor beta-stimulated clone 22 homolog (Tsc22d1), which controls systemic cholesterol metabolism. Overexpression of Tsc22d1 promotes high levels of high-density lipoprotein (HDL) cholesterol in mice (Jager et al., 2014). Pattern 3 included 9 genes (Fig. 3C), which were consistently down-regulated by BDE-47 in CV and GF mice, but were down-regulated by BDE-99 in CV mice and up-regulated by BDE-99 in GF mice. These genes included RIKEN-derived genes (1500017E21Rik, D930016D06Rik, F830016B08Rik), coiled-coil domain containing 141 (Ccdc141), leukocyte receptor cluster member 8 (Leng8), olfactory receptor 1033 (Olfr1033), peptidylprolyl isomerase G (Ppig), Rock1, and up-frameshift suppressor 3 homolog B (Upf3b). Pattern 4 consisted of 2 genes (Fig. 3D), which were up-regulated by both BDE-47 and BDE-99 in CV mice, but were down-regulated in GF mice. These two genes are Mt1, which is

involved in zinc homeostasis and heavy metal detoxification (Ruttkay-Nedecky et al., 2013), and nicotinamide N-methyltransferase (Nnmt), which regulates hepatic nutrient metabolism (Hong et al., 2015). The PBDE-mediated up-regulation of Mt1 and Nnmt only occur with the presence of gut microbiome suggests a gut microbiome dependent manner.

Regarding the unique effect of BDE-47 in CV mice, the top 10 most up-regulated PCGs by BDE-47 are shown in Table 2, including Gm7694; major urinary protein family members (Mup12 and Mup8), which regulate glucose and energy metabolism (Zhou et al., 2009), oligoadenylate synthases (Oas1a and Oas1g), which regulate the early phase of viral infection and inhibit viral replication (Choi et al., 2015); 2010003K11Rik; calcium and integrin binding protein 3 (Cib3), which is involved in integrin signaling pathway (Huang et al., 2012); phospholipid scramblase 1 (Plscr1), which is required for maturation and differentiation of hematopoietic cells from progenitor cells (Dong et al., 2004); membrane-spanning 4-domains subfamily A member 6D (Ms4a6d), which regulates signal transduction (Ding et al., 2008); and Cyp4a12b, which is important for fatty acid oxidation (Muller et al., 2007). The top 10 most down-regulated genes by BDE-47 exclusively in livers of CV mice included zinc finger protein (Zfp935); small nucleolar RNA host gene 5 (Snhg5), which is up-regulated in colorectal cancer and causes tumor outgrowth *in vivo* (Damas et al., 2016); mitogen-activated protein kinase 8 interacting protein 3 (Mapk8ip3, also known as Jip3), which is involved in JNK signaling pathway and down-regulates oxidative stress and inflammatory response in high fat diet-treated mice (Rao et al., 2017); Ras related oncogene family member (Rab26os),

which modulates intracellular membrane trafficking (Li et al., 2012); AT-rich interaction domain 4B (Arid4b), which is a subunit of transcriptional repressor complex and involves in cell proliferation, differentiation, apoptosis and cell fate determination (Tsai et al., 2017); Ly6/PLAUR domain containing 8 (Lypd8), which prevents microbiota invading the colonic epithelia in mice (Okumura et al., 2016); pre-mRNA processing factor (Prpf39), which correlates with cisplatin cytotoxicity and knockdown of Prpf39 results in a significant increase in cisplatin resistance (Stark et al., 2012); and proline rich acidic protein 1 (Prap1), which maintains normal growth homeostasis in epithelial cells (Zhang et al., 2003). Ingenuity Pathway Analysis (IPA) was performed for PCGs that were uniquely regulated following BDE-47 exposure in CV mice, and is shown in Supplemental Fig. 6, which include pathways related to cellular development, cancer, cell death and survival, carbohydrate metabolism, lipid metabolism, and inflammatory response. An example network (cellular development, cancer, cell death and survival, network #1) is visualized in Supplemental Fig. 6. BDE-47 up-regulated Iron-binding nuclear protein (Pir), Gstp1, and heme oxygenase 1 (Hmox1), which protect cells from oxidative stress (Brzoska et al., 2011; Dunn et al., 2014). BDE-47 also up-regulated mothers against decapentaplegic homolog 9 (Smad9; also known as Smad8), which modulates transforming growth factor beta (TGF-β) cellular signaling during proliferation, differentiation and development (Watanabe et al., 1997); guanylate binding protein 2 (Gbp2), which alters cell proliferation and inhibits cell spreading (Balasubramanian et al., 2011); and hairy and enhancer of split-1 (Hes1), which encodes a transcription repressor that influences cell proliferation and differentiation during embryogenesis (Kageyama et al., 2007). Conversely, BDE-47 down-regulated lectin, galactoside-

binding soluble 4 (Lgals4), which inhibits cell proliferation as a tumor suppressor (Satelli et al., 2011); polycystin 2 (Pkd2), which transports calcium ions into the cell and regulates cell growth and division, cell movement, and cell-cell interaction (Arnould et al., 1999); and retinol binding protein 2 (Rbp2), which participates in the uptake and intracellular metabolism of vitamin A for cell differentiation, proliferation, and apoptosis (Doldo et al., 2015).

Regarding the unique effect of BDE-99 in CV mice, the top 10 most up-regulated genes by BDE-99 are shown in Table 2, including carboxyl ester lipase (Cel), which is important for cholesterol and lipid-soluble vitamin ester hydrolysis and absorption (Hui and Howles, 2002); Ctrb1, Rnase1, Cpb1, Prss2, Try5, and Prss3. BDE-99 also up-regulated pancreatic lipase (pnlip), which hydrolyzes triglycerides in the small intestine and digests dietary fats (Szabo et al., 2015), 2210010C04Rik, and carboxypeptidase A1 (Cpa1). Conversely, the top 10 most down-regulated genes by BDE-99 in CV mice included folylpolyglutamyl synthetase (Fpgs), which maintains folate homeostasis for cell proliferation (Shane, 1989); N-myc downstream regulated gene 1 (Ndrg1), which responds to cellular stress signals (Ellen et al., 2008); seizure threshold 2 (Szt2), which controls cell growth (Peng et al., 2017); inhibitor of DNA biding 3 (Id3), which inhibits transcription (Lasorella et al., 2014); ELOVL fatty acid elongase 5 (Elovl5); phosphoethanolamine/phosphocholine phosphatase (Phospho1), which is important for skeletal development; Myb related transcription factor (Mypop), which regulates hematopoiesis and tumorigenesis (Vargova et al., 2011); nerve growth factor receptor (Ngfr); and tubulin beta 2B class IIb (Tubb2b), which encodes tubulin that is major

component of microtubules (Jaglin et al., 2009). Ingenuity pathway analysis (IPA) was performed for the genes that were uniquely regulated following BDE-99 exposure in CV mice, and is shown in Supplemental Fig. 7, which included carbohydrate metabolism, lipid metabolism, small molecule biochemistry, post-translational modification, protein degradation, protein synthesis, cancer, and cellular assembly and organization. Examples of the top two networks are visualized in Supplemental Fig. 7. For example, within the network of carbohydrate metabolism and lipid metabolism, BDE-99 down-regulated regulatory factor X4 (Rfx4); MYCL proto-oncogene (Mycl); persulfide dioxygenase (Ethe1), which modulates sulfide detoxification and regulates mitochondrial catabolism of fatty acids (Hildebrandt et al., 2013); Forkhead Box protein A2 (Foxa2), which regulates lipid metabolism and ketogenesis in the liver during fasting and in diabetes (Wolfrum et al., 2004); mediator complex subunit 24 (Med24), which is involved in adipogenesis (Chu et al., 2014); and Neural precursor cell expressed, developmentally down-regulated gene 4-like (Nedd4l), which is associated with diabetes and obesity (Wang et al., 2013b). Conversely, BDE-99 markedly up-regulated the digestive enzyme Rnase1 and pnlip, which hydrolyze triglycerides in the small intestine and digests dietary fats (Szabo et al., 2015). Within the network of post-translational modification, BDE-99 also up-regulated a series of genes involved in protein degradation such as serine protease, trypsinogen, and chymotrypsin, but down-regulated many collagen-related protein synthesis, such as collagen type V alpha 1 chain (Col5a1), Col3a1, ERBB receptor feedback inhibitor 1 (Errfl1), serpin family H member 1 (Serpinh1), and phospholipase C beta 3 (Plcb3).

Regarding the unique effect of BDE-47 in GF mice, the top 10 most up-regulated genes by BDE-47 are shown in Table 2, including Sult2a2, which is a bile salt sulfotransferase that catalyzes sulfonation of hydroxysteroids (Runge-Morris et al., 2013); alpha-1B glycoprotein (A1bg); prostaglandin D2 synthase (Ptgds); GDP-mannose 4,6-dehydratase (Gmds); Mup4; Acyl-CoA thioesterase 3 (Acot3), which catalyzes the hydrolysis of acyl-CoAs to free fatty acid (Hunt et al., 2012); Fam213b; Eukaryotic translation initiation factor 4E binding protein 3 (Eif4ebp3); Cyp39a1, which catalyzes the hydroxylation of cholesterol in the alternative bile acid synthesis pathway (Ikeda et al., 2003); and Mup19. Conversely, the top most down-regulated genes by BDE-47 included glutamic-oxaloacetic transaminase 1 (Got1), which is important for amino acid metabolism and the urea and tricarboxylic acid cycles (Abrego et al., 2017); Sestrin 2 (Sesn2) and dopachrome tautomerase (Dct), both of which protect cells from oxidative stress (Lee et al., 2010; Ainger et al., 2014); ephrin type-A receptor A2 (Epha2), which mediates neural development (Park et al., 2013); and small nucleolar RNA 7A (Snora7a). Snora7a has been reported to promote cell proliferation and suppress differentiation in mesenchymal stem cell (Zhang et al., 2017b). These results suggested that without the presence of gut microbiome, not only steroid and bile acid signaling pathways but the cellular signaling were distinctly regulated by BDE-47 in GF mice.

Regarding the unique effect of BDE-99 in GF mice, the top 10 most up-regulated genes by BDE-99 included Sult1e1, Gm11974, monocyte to macrophage differentiation associated 2 (Mmd2), Gm14403, and heat shock protein 90 alpha family class A

member 1 (Hsp90aa1), which encodes protein Hsp90A that interacts with a number of tumor promoting proteins (Zuehlke et al., 2015). BDE-99 also up-regulated zinc finger protein 445 (Zfp445); sterile alpha motif domain containing 9 like (Samd9l), which acts as a tumor suppressor (Tesi et al., 2017); aldehyde oxidase 1 (Aox1); roundabout guidance receptor 1 (Robo1); and solute carrier family 10 member 2 (Slc10a2, also known as apical sodium-bile acid transporters (Asbt)), which is responsible for the uptake of bile acids from the intestine to enterohepatic circulation. Conversely, the top 10 most down-regulated genes by BDE-99 in GF mice included C-C motif chemokine ligand 5 (Ccl5), which recruits leukocytes into inflammatory sites (Maghazachi et al., 1996); calcium/calmodulin dependent protein kinase II beta (Camk2b), which promotes synapse formation and maintains synaptic plasticity in brain (Kool et al., 2016); microtubule associated protein 1 light chain 3 alpha (Map1lc3a), which mediates the interactions between microtubules and cytoskeleton (Mann and Hammarback, 1996); calneuron 1 or calcium-binding protein (Caln1); carboxylesterase 4A (Ces4a), which is responsible for the hydrolysis of xenobiotics and also involved in fatty acid metabolism (Holmes et al., 2010); WAP four-disulfide core domain 2 (Wfdc2), which constitutes the core of the protein and functions as protease inhibitor (Hellstrom et al., 2003); guanylate cyclase activator 1A (Guca1a), which is involved in the calcium-dependent regulation of guanylate cyclases in the retina (Kitiratschky et al., 2009); H2-Eb1, Flywch2, and Serpina3c. Ingenuity pathway analysis (IPA) was performed for the genes that were uniquely regulated following BDE-99 exposure in GF mice, and is shown in Supplemental Fig. 8, which includes pathways related to developmental disorder; gene expression, protein synthesis, cellular assembly and organization; cellular development;

and DNA replication, recombination and repair. An example network (gene expression, protein synthesis, cellular assembly and organization, network #2) is visualized in Supplemental Fig. 8. BDE-99 down-regulated a large number of mitochondrial ribosomal proteins (Mrpl) in GF mice. Mitochondrial ribosomal proteins are responsible for oxidative phosphorylation to produce energy for cell growth, differentiation and development (Sylvester et al., 2004). The down-regulated Mrpl by BDE-99 treatment may lower ATP production and disturb normal cellular functions, which may ultimately lead to cell death. The same finding was also observed in BDE-99 treated CV mice, indicating BDE-99 mediated reduction of Mrpl are independent of gut microbiome.

Hepatic transcriptome of lncRNAs that were differentially regulated by PBDEs

As shown in Fig. 4A, among the 125,692 annotated lncRNAs, 119,820 lncRNAs were not detected at significant levels in liver of any groups (threshold: average FPKM < 1 in all treatment groups). Among the detected lncRNAs (average FPKM >1 in at least one of the groups), 4,546 lncRNAs were stably expressed across all treatment groups, whereas a total of 1,326 lncRNAs were differentially expressed by PBDEs in livers of CV and GF mice (criteria: $p < 0.05$ in at least one of the 4 comparisons between corn oil (CO) and PBDE-exposed groups of the same enterotype, namely 1) corn oil exposed CV mice (CV_CO) vs. CV_BDE-47, 2) CV_CO vs. CV_BDE-99, 3) corn oil exposed GF mice (GF_CO) vs. GF_BDE-47, and 4) GF_CO vs. GF_BDE-99).

A Venn diagram of these 1,326 lncRNAs revealed a clear separation by PBDE exposure and enterotypes (Fig. 4B). Regarding the effects of PBDEs, between CV

BDE-47 (pink color) and CV BDE-99 (green color), there were 143 lncRNAs commonly regulated by both PBDEs, whereas 202 lncRNAs were uniquely regulated by CV BDE-47, and 172 lncRNAs were uniquely regulated by CV BDE-99. Similarly, between GF BDE-47 (purple color) and GF BDE-99 (orange color), there were 42 lncRNAs commonly regulated by both PBDEs, whereas 38 lncRNAs were uniquely regulated by GF BDE-47, and 926 lncRNAs were uniquely regulated by BDE-99 in livers of GF mice. Regarding the necessity of gut microbiome in modulating PBDE-mediated lncRNAs expression, between CV BDE-47 and GF BDE-47, there were 38 lncRNAs commonly regulated by BDE-47 in both CV and GF mice, whereas 307 lncRNAs were uniquely regulated by BDE-47 in CV mice, and only 42 lncRNAs were uniquely regulated by BDE-47 in GF mice. Between CV BDE-99 and GF BDE-99, there were 103 lncRNAs commonly regulated by BDE-99 in both CV and GF mice. To note, there were many more lncRNAs that were uniquely regulated by BDE-99 in GF mice (865 lncRNAs in total) compared to that in CV mice (212 lncRNAs in total). In summary, both PBDEs and the presence of a gut microbiome regulated the hepatic transcriptome of lncRNAs in mice, and the lack of gut microbiome appeared to sensitize mouse liver to BDE-99-mediated transcriptional regulation of lncRNAs. This trend (Fig. 4B) shared a high similarity as compared to the regulation of PCGs (Fig. 2B).

Among the 4 comparison groups (CV_CO vs. CV_BDE-47, CV_CO vs. CV_BDE-99, GF_CO vs. GF_BDE-47, and GF_CO vs. GF_BDE-99), there were 12 lncRNAs that were commonly regulated by both BDE-47 and BDE-99 in livers of both CV and GF mice. Further analysis of these 12 lnRNAs revealed 2 distinct patterns (Fig. 5): pattern

1 included 7 lncRNAs that were consistently up-regulated or consistently down-regulated by both PBDEs in CV and GF mice, including NONMMUG002974.2, NONMMUG004627.2, NONMMUG014825.2, NONMMUG017205.2, NONMMUG021324.2, NONMMUG029461.1, and NONMMUG013481.2 (Fig. 5A). Pattern 2 included 5 lncRNAs that were consistently down-regulated by BDE-47 in livers of both CV and GF mice, but were regulated by BDE-99 in a completely opposite manner (Fig. 5B), in that the lack of a gut microbiome abolished BDE-99-mediated down-regulation of these 5 lncRNAs in CV mice, resulting in a marked up-regulation of these lncRNAs in livers of GF mice.

Genomic annotation of lncRNAs that were differentially regulated by PBDEs

To test our hypothesis that the differentially regulated lncRNAs by PBDEs and gut microbiome are produced from distinct genomic regions proximal to key regulatory DNA elements for the expression of PCGs, we used PAVIS to annotate the genomic locations of differentially regulated lncRNAs relative to their neighboring PCGs (within 5 kb upstream and 1 kb downstream of the neighboring PCGs).

Under control conditions, lack of a gut microbiome altered the basal expression of 211 lncRNAs in liver, among which 90 lncRNAs were located within the genomic distance of neighboring PCGs. As shown in Supplemental Fig. 9, the majority of these lncRNAs were mapped to the intron region (35%) of neighboring PCGs, followed by 3'-untranslated region (UTR) (27%), intergenic region (18%), upstream of transcriptional

start site (TSS) (7%), downstream of transcriptional termination site (TTS) (6%), exonic region (6%), and 5'-UTR region (1%).

Regarding the BDE-47 effect, in livers of CV mice, BDE-47 regulated 345 lncRNAs, among which 255 lncRNAs were located within the genomic distance to their neighboring PCGs. As shown in Fig. 6A, the majority of these lncRNAs were mapped to the intron region (44%) of neighboring PCGs, followed by intergenic region (26%), 3'-UTR (16%), downstream of TTS (5%), upstream of TSS (4%), exonic region (4%), and 5'-UTR region (1%). In livers of GF mice, BDE-47 differentially regulated 80 lncRNAs compared to the control GF group, among which 68 lncRNAs were located within the genomic distance of neighboring PCGs. As shown in Fig. 6A, similar to data in CV mice, the majority of them were likewise mapped to the intron region of neighboring PCGs (47%), followed by 3'-UTR region (24%), intergenic region (14%), upstream of TSS (6%), exonic region (6%), and downstream of TTS (3%). Comparing to CV BDE-47 group, there were more differentially regulated lncRNAs mapped to the 3'-UTR (from 16% CV conditions to 24% GF conditions) in the GF BDE-47 group, but less lncRNAs mapped to the intergenic region (from 26% CV conditions to 14% GF conditions). Additionally, 1% of differentially regulated lncRNAs by BDE-47 exposure were mapped to the 5'-UTR region in CV conditions, but there were no differentially regulated lncRNAs by BDE-47 mapped to this region in GF conditions.

Regarding the BDE-99 effect, in liver of CV mice, BDE-99 differentially regulated 315 lncRNAs, among which 214 lncRNAs were located within the genomic distance to their

neighboring PCGs. As shown in Fig. 6B, the majority of these lncRNAs were mapped to the intron region (35%) of neighboring PCGs, followed by intergenic region (32%), 3'-UTR (14%), upstream of TSS (7%), exonic region (6%), downstream of TTS (4%), and 5'-UTR region (2%). In livers of GF mice, BDE-99 differentially regulated 968 lncRNAs compared to the control GF group, among which 794 lncRNAs were located within the genomic distance of neighboring PCGs. As shown in Fig. 6B, similar to CV conditions, the majority of them were likewise mapped to the intron region of neighboring PCGs (35%), followed by 3'-UTR region (27%), intergenic region (18%), upstream of TSS (7%), exonic region (6%), downstream of TTS (6%), and 5'-UTR region (1%). Comparing to BDE-99-treated CV mice, there were more lncRNAs mapped to the 3'-UTR region (from 14% CV conditions to 27% GF conditions), but less lncRNAs mapped to the intergenic region (from 32% CV conditions to 18% GF conditions) in BDE-99-treated GF mice. LncRNAs have been reported to function as miRNA decoys in regulating the expression of PCGs via competing with miRNAs for the 3'-UTR binding sites (Wang et al., 2013a; Yoon et al., 2014). The increased lncRNAs mapped to 3'-UTR regions in the GF conditions suggested that they may contribute to increased translation efficiency of the neighboring PCGs by preventing miRNA functions.

lncRNA-PCG pairs that were differentially regulated by PBDEs

To predict the potential functions of the differentially regulated lncRNAs by PBDEs, we paired the differentially regulated lncRNAs with their neighboring PCGs as defined by two criteria: 1) the lncRNA overlaps within 5 kb upstream of TTS and 1 kb downstream of TTS of its closest PCG; 2) both lncRNA and its neighboring PCG are significantly

differentially regulated by PBDEs (p <0.05). As shown in Table 3, in livers of CV mice, there were 132 lncRNA-PCG pairs differentially regulated by BDE-47 and 130 pairs differentially regulated by BDE-99; whereas in livers of GF mice, there were 19 lncRNA-PCG pairs differentially regulated by BDE-47, and 544 pairs differentially regulated by BDE-99. The gene symbols of the identified lncRNA-PCG pairs from each comparison are present in Supplemental Table 3. Pathway analysis was performed using the paired neighboring PCGs to predict the signaling pathways potentially regulated by the neighboring co-regulated lncRNAs.

As shown in Fig. 7, in livers of CV mice exposed to BDE-47, the major pathways for the differentially regulated PCGs that were paired with lncRNAs include nucleic acid metabolic process, cellular metabolic process, retinol metabolism, and circadian rhythm. Examples of the lncRNA-PCG pairs involved in retinol metabolism and circadian rhythm are shown in Fig. 8 and Fig. 9, which describe not only their genomic structures but also the expression of the PCG and the paired lncRNA. For example, the lncRNA NONMMUG030290.1 is located at chromosome 4 and its size is 2508 base pairs (bp). NONMMUG030290.1 is transcribed from the intron region of its neighboring PCG Cyp4a12a (a fatty acid oxidation enzyme) and ends up at its 3'-UTR region (Fig. 8A). Both NONMMUG030290.1 and Cyp4a12a were up-regulated by BDE-47 in livers of CV mice (Fig. 8B). NONMMUG020961.1 is another intronic lncRNA, which is located at chromosome 19 and its size is 74,299 bp. NONMMUG020961.1 and its neighboring PCG Aldh1a1 were both up-regulated by BDE-47 in livers of CV mice (Fig. 8A and 8B). The lncRNA NONMMUG032898.1 is located at chromosome 5 with 8.4 kb in length. It

is an intronic lnRNA and is transcribed from the intron region of its neighboring PCG Ugt2b1 (a phase II drug metabolizing enzyme involved in glucuronidation) (Fig. 8A). NONMMUG032898.1 and Ugt2b1 were both up-regulated by BDE-47 in livers of CV mice (Fig. 8B). Cyp4a12a, Aldh1a1 and Ugt2b1 are known involved in the oxidative metabolism and glucuronidation of retinoid substrates (Radominska et al., 1997; Molotkov and Duester, 2003). Other co-upregulated lncRNA-PCG pairs include: the lncRNA NONMMUG034010.1, which is transcribed from the intron region of Por and also overlaps with several exon regions of Por; the lncRNA NONMMUG007536.2, which is antisense to Nr1d1 (also known as Rev-Erbα) that is involved in circadian rhythm (Bugge et al., 2012); and NONMMUG005353.2 and NONMMUG005354.2, which are transcribed from the upstream and the first intron of epidermal growth factor receptor (Egfr). Egfr signaling regulates growth, differentiation, proliferation and migration in multiple organ systems, as well as macrophage function against bacterial infection (Fraguas et al., 2011; Hardbower et al., 2016) (Fig. 9).

In livers of CV mice, the top pathways for the lnRNA-PCG pairs that were differentially regulated by BDE-99 include metabolic pathway and cellular biosynthetic process (Fig. 10). Examples of the lncRNA-PCG pairs that were differentially regulated by CV BDE-99 are shown in Fig. 11, Fig. 12, and Supplemental Fig. 10. For example, the lncRNA NONMMUG030301.1, which is transcribed from the upstream of Cyp4a10, NONMMUG030286.2, which is transcribed from the downstream of Cyp4a14, and NONMMUG018018.1, which is transcribed from the intron region of Cyp4f1, were consistently down-regulated by BDE-99 in livers of CV mice (Fig. 11A and Fig. 11B).

Their neighboring PCGs Cyp4a10, Cyp4a14, and Cyp4f17 were also down-regulated by BDE-99 in livers of CV mice (Fig. 11B). Cyp4 family are well known target genes of lipid sensor PPARα and are involved in hydroxylation of fatty acids in liver (Bumpus and Johnson, 2011). The lncRNA NONMMUG041315.2, which is transcribed from chromosome 8 with 7160 bp in length, is located in the upstream region of its neighboring PCG Mt2 that protects cell from oxidative stress (Ruttkay-Nedecky et al., 2013) (Fig. 11A). Both NONMMUG041315.2 and Mt2 were up-regulated by BDE-99 in livers of CV mice (Fig. 11B). As shown in Fig. 12, NONMMUG032904.1, which is transcribed from the first intron of Ugt2b37, was up-regulated by BDE-99 in livers of CV mice. Conversely, NONMMUG007594.1, which is located at chromosome 11 and antisense to ATP citrate lyase (Acly). Both of NONMMUG007594.1 and Acly were down-regulated by BDE-99 in CV mice. Acly is important for the pyruvate citrate shuttle and lipid synthesis. Hepatic Acly may also serve as a potential target to treat NAFLD and type 2 diabetes (Wang et al., 2009). NONMMUG025007.2, which is transcribed from the 3'-UTR region of Forkhead box A2 (Foxa2) in the opposite direction, was down-regulated by BDE-99 in livers of CV mice (Fig. 12A and 12B). Foxa2 (also known as HNF3β) is a critical transcription factor in regulating the earliest stages of liver development and function (Wederell et al., 2008). Other co-regulated lncRNA-PCG pairs are shown in Supplemental Fig. 10, including NONMMUG052556.1, which is located at chromosome 11 and overlaps with the PCG histone deacetylase 5 (Hdac5), an epigenetic mark for transcription repression that regulates cell differentiation and liver gluconeogenesis (Fogg et al., 2014); and NONMMUG034010.1, which is transcribed from the intron region of P450 oxidoreductase Por (Supplemental Fig 10A).

Both NONMMUG052556.1 and Hdac5 were down-regulated by BDE-99 in livers of CV mice, whereas NONMMUG034010.1 and Por were up-regulated by BDE-99 in livers of CV mice (Supplemental Fig 10B).

In livers of GF mice, there were only 19 lnRNA-PCG pairs differentially regulated by BDE-47 and do not readily form gene networks. Examples of them are shown in Fig. 13, as well as Supplemental Fig. 11 and 12. For example, NONMMUG021324.2, which is located at chromosome 4, is completely overlapped with the pseudogene Cyp2c53-ps (Fig. 13A). Both NONMMUG021324.2 and Cyp2c53-ps were up-regulated by BDE-47 in livers of GF mice (Fig. 13B). NONMMUG004004.2, which is located at chromosome 10 and is antisense to Gstt3. NONMMUG004004.2 and Gstt3 were also up-regulated by BDE-47 in livers of GF mice. Another two lncRNAs, namely NONMMUG029461.1 and NONMMUG029462.1, which are both located at chromosome 4, are transcribed from intronic and 3'-UTR region of Mup20. The expression of these two lnRNAs and Mup20 was up-regulated by BDE-47 in livers of GF mice. Supplemental Fig 11 and 12 showed more lncRNA-PCG pairs that were differentially regulated by BDE-47 in livers of GF mice, including NONMMUG041080.2, which is transcribed from the intronic region of 170067K01Rik; NONMMUG031557.2, which is transcribed downstream from Fam213b which is related to fat metabolism (Wang et al., 2017); NONMMUG065104.1, which is transcribed from the intronic region of tetratricopeptide repeat-containing protein (Ttc39c) which is involved in protein complex formation (Xu et al., 2015b); NONMMUG029453.1, which is transcribed from the downstream region of Gm2083; NONMMUG013481.2, which is transcribed from the intronic region of Tsc22d1 which is

related to cholesterol metabolism (Jager et al., 2014); as well as NONMMUG020688.1, which is transcribed from the intronic region of transmembrane 7 superfamily member 2 (Tm7sf2, also known as delta(14)-sterol reductase) which is responsible for sterol biosynthesis (Bellezza et al., 2013). All these lncRNAs were co-regulated along with their neighboring PCGs by BDE-47 in livers of GF mice.

In livers of GF mice, the lncRNA-PCG pairs that were differentially regulated by BDE-99 were highly associated with the PPAR signaling pathway, metabolic pathways that contain a number of PCGs (e.g., 7 Cyps, Aldh2, Ugt2b 36, Gclc), RIG-I-like receptor signaling pathway, hepatitis C and pancreatic cancer (Figure 14; Supplemental Fig. 13). The top two pathways, namely PPAR signaling pathway and metabolic signaling, are visualized in Figure 14. Examples of lncRNA-PCG pairs involved in these two pathways are shown in Figure 15, 16 and Supplemental 14 to 16. For example, the lncRNA NONMMUG001037.1, which is located at chromosome 1 with 1256 bp in length, is transcribed from the exon and intron region of Cyp27a1 (Fig. 15A). Cyp27a1 is the rate-limiting enzyme for the alternative pathway for bile acid synthesis (Li and Chiang, 2009). Both NONMMUG001037.1 and Cyp27a1 were down-regulated by BDE-99 in livers of GF mice (Fig. 15B). NONMMUG078162.1, which is located at chromosome 7, is transcribed from the intron region of Slc27a5 (fatty acid transporters) and into its 5'-UTR region (Steinberg et al., 2000). Although NONMMUG078162.1 and Slc27a5 are transcribed at the opposite direction, both of them are down-regulated by BDE-99 in livers of GF mice. Similarly, NONMMUG030301.1 and its neighboring PCG Cyp4a10, and NONMMUG030286.2 and its neighboring PCG Cyp4a14 were consistently down-

regulated by BDE-99 in GF mice (Fig. 15). NONMMUG034289.1, which is located at chromosome 5, is transcribed from the intronic region of Cyp3a11 at the opposite direction (Fig. 16). Both NONMMUG034289.1 and Cyp3a11 were markedly up-regulated by BDE-99 in GF mice. Consistently, NONMMUG034299.1, which is located at chromosome 5 and transcribed from the intronic region of Cyp3a25, was also up-regulated by BDE-99 in GF mice, as was its neighboring PCG Cyp3a25. Conversely, NONMMUG018026.1 and NONMMUG018025.1, which are both transcribed from the intronic region of Cyp4f genes, were down-regulated by BDE-99 in GF mice. More lncRNA-PCG pairs that were differentially regulated by BDE-99 in GF conditions are shown in Supplemental Fig. 14, 15 and 16. Most notably, NONMMUG032900.1, which is transcribed from the intronic region of phase II drug metabolizing enzyme Ugt2b36, was markedly up-regulated by BDE-99 in livers of GF mice. NONMMUG043407.1 is transcribed from the intronic region of glutamate-cysteine ligase (Gclc), which is the rate-limiting enzyme of glutathione synthesis against oxidative stress (Lu, 2009). Both NONMMUG043407.1 and Gclc were up-regulated by BDE-99 in livers of GF mice (Supplemental Figure 16).

Discussion

Taken together, the present study has systematically characterized the effect of the interactions between orally exposed PBDEs and the mouse gut microbiome on mouse liver transcriptome including both protein-coding genes and long noncoding RNAs. This study demonstrated for the first time that the presence of gut microbiota is necessary in remotely modulating the PBDE-mediated differential expression of PCGs and lncRNAs

in liver; whereas lack of a functional gut microbiota sensitized the liver to greater transcriptomic response to the BDE-99 congener but not to the BDE-47 congener. Regarding the signaling pathways, not only xenobiotic metabolism, but also intermediary metabolism (such as PPARα-mediated lipid metabolism, as well as bile acid synthesis), were also impacted by the interactions between PBDEs and gut microbiota. Unique lncRNA-PCG pairs were identified that were co-differentially regulated by PBDEs and the absence of a gut microbiome. These co-regulated lncRNAs may act in concert with transcription factors to promote the formation of the PCG transcripts in the same genomic neighborhood to increase the transcription efficiency. Furthermore, these results suggest that increased percentages of differentially regulated lncRNAs mapping to the 3'-UTR region in livers of PBDE-exposed GF mice may increase the translation efficiency of PCGs by antagonizing miRNA functions, in response to increased xenobiotic insult as a result of lacking microbial transformation pathways (such as reduction and hydrolysis) in the intestine of GF mice.

Regarding the regulation of PCGs, after oral exposure, BDE-47 and BDE-99 produce overlapping and unique effects in regulating hepatic gene expression in mice. It has been shown that BDE-47 and BDE-99 are activators of xenobiotic sensors CAR and PXR in rodent livers and human hepatocytes, leading to induced expression of cytochrome P450s (Pacyniak et al., 2007; Sueyoshi et al., 2014). Data from the present study are consistent with previous findings regarding the up-regulation of Cyp2b10, which is the prototypical target gene of CAR, by both PBDEs in livers of CV and GF

mice. Moreover, BDE-47 and BDE-99 also up-regulate many genes that are known CAR and PXR targets in mice, such as Cyp2b13, Cyp2c55, Alas1, Akr1b7, and Gstm3 (Table 1 and Figure 3) (Podvinec et al., 2004; Liu et al., 2009; Li et al., 2016a). Among them, Alas1 encodes 5-aminolevulinate synthase, which is the rate-limiting enzyme in heme biosynthesis (Fraser et al., 2003; Podvinec et al., 2004). Up-regulation of Alas1 by PBDEs may increase the rate of heme biosynthesis. Akr1b7 is important for the detoxification of lipid peroxides (Liu et al., 2009). Interestingly, both Alas1 and Akr1b7 have also been shown to be target genes of bile acid-activated nuclear receptor farnesoid X receptor (FXR), which regulates lipid and glucose homeostasis (Peyer et al., 2007; Ge et al., 2011). Besides xenobiotic metabolism, the activation of CAR and PXR have been linked to diverse physiological pathways, including lipid metabolism, glucose homeostasis, inflammation, and hepatogenesis (Moreau et al., 2008; Yan et al., 2015). All of these pathways ranked at the top of PBDE-mediated effects in the present study (Supplemental Fig. 5). PBDEs may also impact bile acid synthesis and fatty acid oxidation, because in CV mice, PBDEs up-regulate Cyp7a1 and Cyp7b1 involved in bile acid synthesis, but down-regulate Cyp4a family members involved in lipid metabolism (Supplemental Fig 1 and 2). Another interesting finding is that the absence of gut microbiota potentiated BDE-47 mediated up-regulation of many Gsts, which protect cells from oxidative stress, whereas potentiated BDE-99 mediated down-regulation of a large number of mitochondrial ribosomal proteins that are essential for energy production; these data suggest that livers of GF mice are more vulnerable to oxidative stress and mitochondrial damage following additional insult, likely because gut

microbiota are responsible for the majority of reduction reactions of the whole organism (Swanson, 2015; Wilson and Nicholson, 2017).

Regarding the regulation of lncRNAs, lncRNAs have been increasingly recognized as key regulators of human diseases, and may serve as novel biomarkers of environmental exposure (Karlsson and Baccarelli, 2016). However, prior to this study, there was no information regarding the regulation of hepatic lncRNAs by PBDEs and the gut microbiome, both of which are known to modulate xenobiotic biotransformation in the liver (Pacyniak et al., 2007; Sueyoshi et al., 2014; Selwyn et al., 2015a; Selwyn et al., 2015b). The present study has filled this critical knowledge gap and demonstrated that both PBDEs and the lack of a gut microbiome profoundly altered lncRNAs in mouse livers, suggesting that the differentially regulated lncRNAs may also play important roles in PBDE-mediated toxicity.

Importantly, the present study has unveiled the potential interactions between lncRNAs and PCGs by identifying lncRNA-PCG pairs that were uniquely regulated by different PBDE congeners and by the absence of gut microbiome. The lncRNAs that were paired with PCGs in the same genomic region may have a greater opportunity to interact with transcription factors that regulate transcription, alternative splicing, and inhibition of miRNA binding to the 3'-UTR of these PCGs, simply because of the "geographical advantage". It has been demonstrated that when lncRNAs reside on the opposite strand of a protein-coding gene, they can regulate the transcription of the protein-coding genes (Wright and Bruford, 2011; Engreitz et al., 2016). The molecular

mechanisms for lncRNAs to regulate gene expression are mainly dependent on their ability to tether with proteins like transcription factors or chromatin modifiers, to either activate or repress their activity in transcription (Peng et al., 2014). For example, in CV mice, NONMMUG034010.1, which overlaps with Por, is up-regulated by both BDE-47 and BDE-99 in the same pattern as Por (Fig. 9 and Supplemental Fig. 10). NONMMUG030301.1, which is transcribed from the upstream of Cyp4a10 in the same direction, is down-regulated by BDE-99 as Cyp4a10. Whereas NONMMUG030286.2, which is antisense and overlaps with Cyp4a14, was also down-regulated by BDE-99 as was Cyp4a14 (Fig. 11). The down-regulation of Cyp4a10 and Cyp4a14 along with their paired lncRNAs were also observed in BDE-99 treated GF mice (Fig. 15). In addition, NONMMUG034289.1, which is antisense and overlapping with Cyp3a11, is markedly up-regulated by BDE-99 as Cyp3a11 in GF mice (Fig. 16). Further studies, such as RNA-immunoprecipitation assays, are required to elucidate the functions of differentially regulated lncRNAs by PBDEs and their impact on related signaling pathways such as metabolic processes.

Although PBDEs as an entire class of persistent environmental chemicals are generally thought to display many similar features such as receptor interaction and toxicities, our study showed that the regulation of PCGs and lncRNAs is PBDE congener-specific, and such regulation is further modified by the absence of a gut microbiome. GF mice are more responsive to BDE-99-, but not BDE-47-, induced changes in gene expression, as indicated by the approximately 3 to 4-fold greater number of responsive lncRNAs and PCGs in GF mice than in CV mice, and by the larger magnitude of gene responses in

GF mice after BDE-99 exposure (Fig. 2 and 4). In contrast, for BDE-47, there are many more lncRNAs and PCGs differentially regulated in CV mice than in GF mice, indicating the BDE-47 mediated effects on hepatic gene expression are more gut microbiome-dependent. Pathway analysis of the neighboring PCGs indicated that BDE-47 in CV mice mainly affect genes involved in nucleic acid metabolic process, cellular metabolic processes, retinol metabolism, and circadian rhythm; whereas BDE-99 in CV mice produced more effect on metabolic pathway and cellular biosynthetic process. Livers of GF mice were more resistant to BDE-47-mediated effects with less than 100 lncRNAs differentially expressed. Conversely, there were 968 lncRNAs differentially regulated by BDE-99 in GF mice, among which 544 lncRNAs are located closely with nearby PCGs. Pathway analysis indicated that in livers of GF mice, BDE-99 affects diverse biological processes, from which PPARα-signaling and metabolic processes are the top two most affected pathways.

However, the mechanisms of gut microbiome-mediated regulation of PBDE metabolism and the subsequent regulation of hepatic gene expression is not completely understood. Studies have found that the enterohepatic circulation of PBDEs is affected by variation in gut microbial populations, leading to increased residence time in the body and toxicity (Stapleton et al., 2009). Higher levels of hydroxylated BDE-99 metabolites have been detected in liver relative to hydroxylated metabolites of BDE-47 (Li et al., 2017). Therefore, in addition to hepatic transcriptional factors, gut microbiota and gut-derived PBDE metabolites may function together to further modify the expression of the hepatic transcriptome. Because the sequencing libraries in the present study were constructed

from poly-A tail selected RNAs, the detected lncRNAs are mainly polyadenylated, which may miss 40% of lncRNA transcripts that are nonpolyadenylated (Cheng et al., 2005). Future studies using whole transcriptome sequencing, which only removes ribosomal RNA, will capture all forms of lncRNAs.

In conclusion, the present study identified the distinct role of the gut microbiome in modulating PBDE-mediated gene expression in liver at a transcriptome scale, and for the first time demonstrated that a large number of lncRNAs are dysregulated by PBDEs. Many of the lncRNAs are novel and co-regulated with neighboring PCGs. Studies of the regulation and interaction of differentially regulated lncRNAs and PCGs will provide more clues to the mechanisms of PBDEs-mediated effects in diverse biological processes. Moreover, the present study has laid the foundation for future investigations regarding the mechanisms of PBDE-mediated toxicity and molecular biomarkers for PBDE exposure. Further studies will be required to validate the direct binding of lncRNAs to the targeted PCGs that share a similar or opposite expression pattern, and determine the translation efficiency of the targeted PCGs using proteomics to unveil the functional impact of lncRNAs on PCG protein expression.

Figure 1

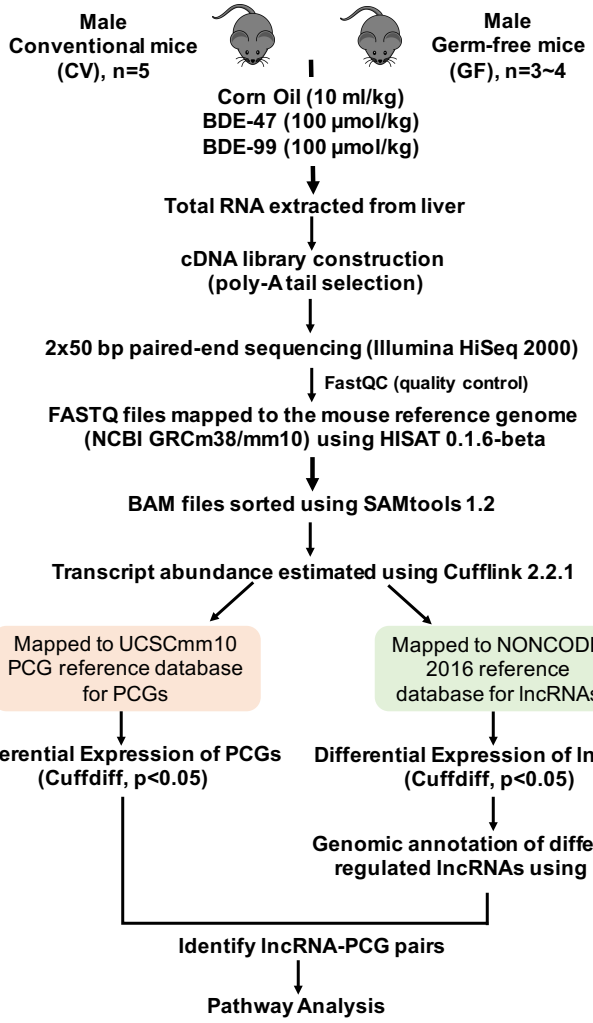

Figure 1. Experimental design and workflow for RNA-Seq data analysis. Briefly, 9-week-old male C57BL/6J conventional (CV) and germ-free (GF) mice in C57BL/6 background were exposed to vehicle (corn oil, 10 ml/kg), BDE-47 (100 µmol/kg) or BDE-99 (100 µmol/kg) via oral gavage once daily for 4 consecutive days. Livers were collected 24 hours after the final dose (n=3~5 per group). Total RNAs were extracted from liver and sent for 50 bp paired-end RNA-Sequencing. RNA-Seq data were quality-checked with FastQC and further analyzed by HISAT, SAMtools, and Cufflinks as described in Materials and Methods. The transcript abundance of protein-coding genes (PCGs) and long non-coding RNAs (lncRNAs) was estimated using the mouse UCSC mm10 PCG and NONCODE 2016 as reference databases, respectively. The differentially expressed PCGs and lncRNAs were analyzed by Cuffdiff between chemical-treated groups and vehicle-treated groups of the same enterotypes of mice ($p < 0.05$). The genomic annotation of differentially regulated lncRNAs in at least one comparison and their closest PCGs were annotated using PAVIS. A lncRNA is considered paired with the neighboring PCG if: 1) lncRNA was transcribed within 5 kb upstream and 1 kb downstream of the neighboring PCG, and 2) both lncRNA and the neighboring PCG were differentially expressed by PBDEs in livers of CV and GF mice ($p < 0.05$).

Figure 2

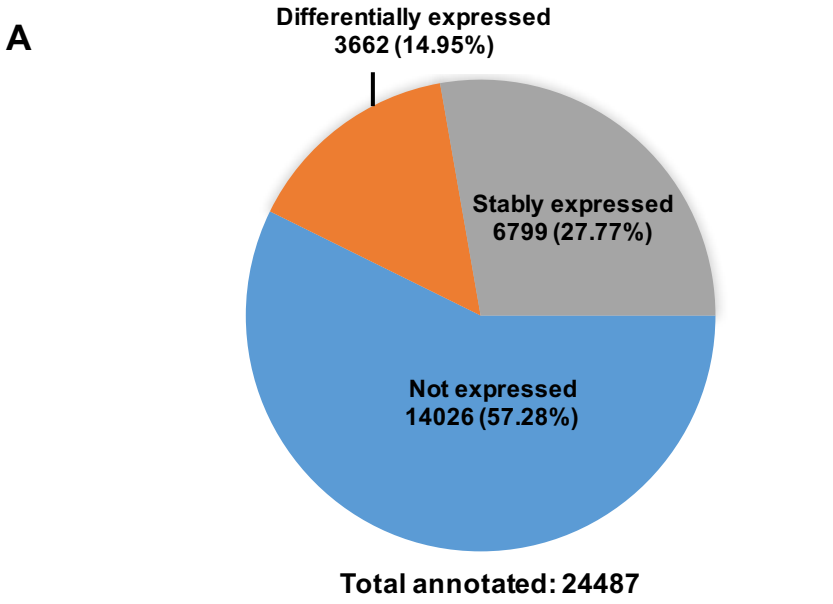

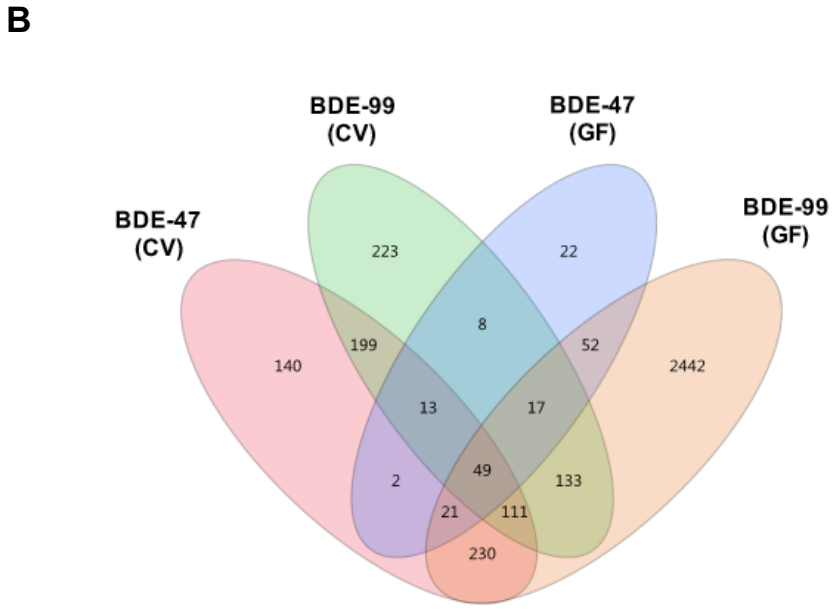

Figure 2. Regulation of protein-coding genes (PCGs) in livers of CV and GF mice exposed to corn oil, BDE-47 (100 µmol/kg), or BDE-99 (100 µmol/kg). (A) A pie chart showing PCGs that were not expressed in any treatment groups (blue), stably expressed in all groups (grey), and differentially expressed by PBDE exposure in at least one of the four comparisons (orange). These four comparisons are: CV_CO (corn oil) vs CV_BDE-47; CV_CO vs CV_BDE-99; GF_CO vs GF_BDE-47; and GF_CO vs GF_BDE-99, FDR adjusted p-value <0.05). **(B)** A Venn diagram showing the differentially expressed PCGs that were commonly or uniquely regulated by PBDEs among the four comparisons as described in Fig. 2A. Venn diagram was generated using JMP Genomics.

Figure 3

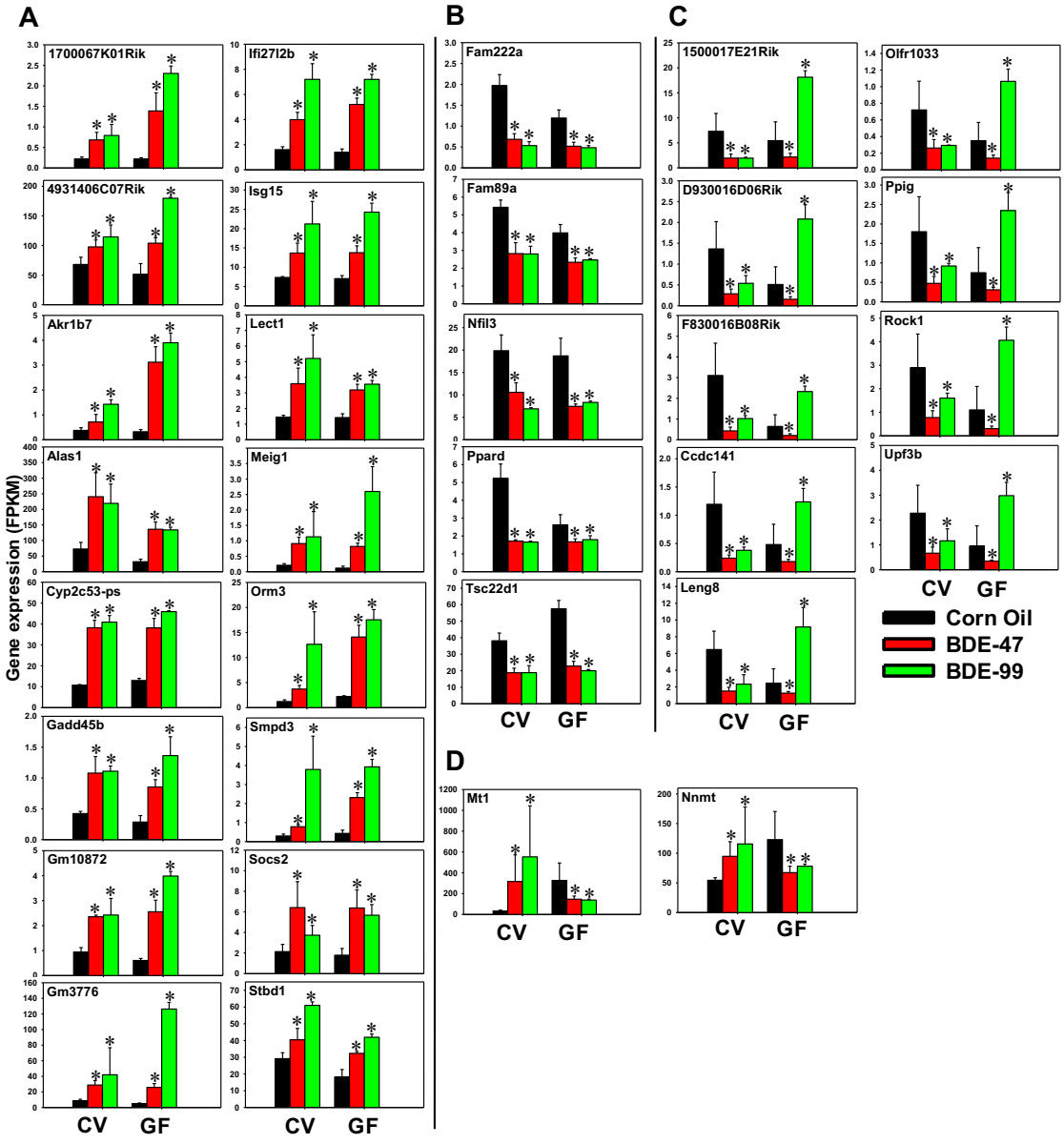

Figure 3. PCGs that were differentially regulated by both PBDEs in livers of CV and GF mice. **(A)** PCGs that were commonly up-regulated by BDE-47 and BDE-99 in livers of both CV and GF mice. **(B)** PCGs that were commonly down-regulated by BDE-47 and BDE-99 in livers of both CV and GF mice. **(C)** PCGs that were consistently down-regulated by BDE-47 in livers of CV and GF mice, but were oppositely regulated in CV (down-regulation) and GF (up-regulation) mice by BDE-99. **(D)** PCGs that were oppositely regulated in CV (up-regulation) and GF (down-regulation) mice by both BDE-47 and BDE-99. Asterisks (*) indicate statistically significant differences as compared to vehicle-treated groups of the same enterotypes of mice ($p < 0.05$).

Figure 4

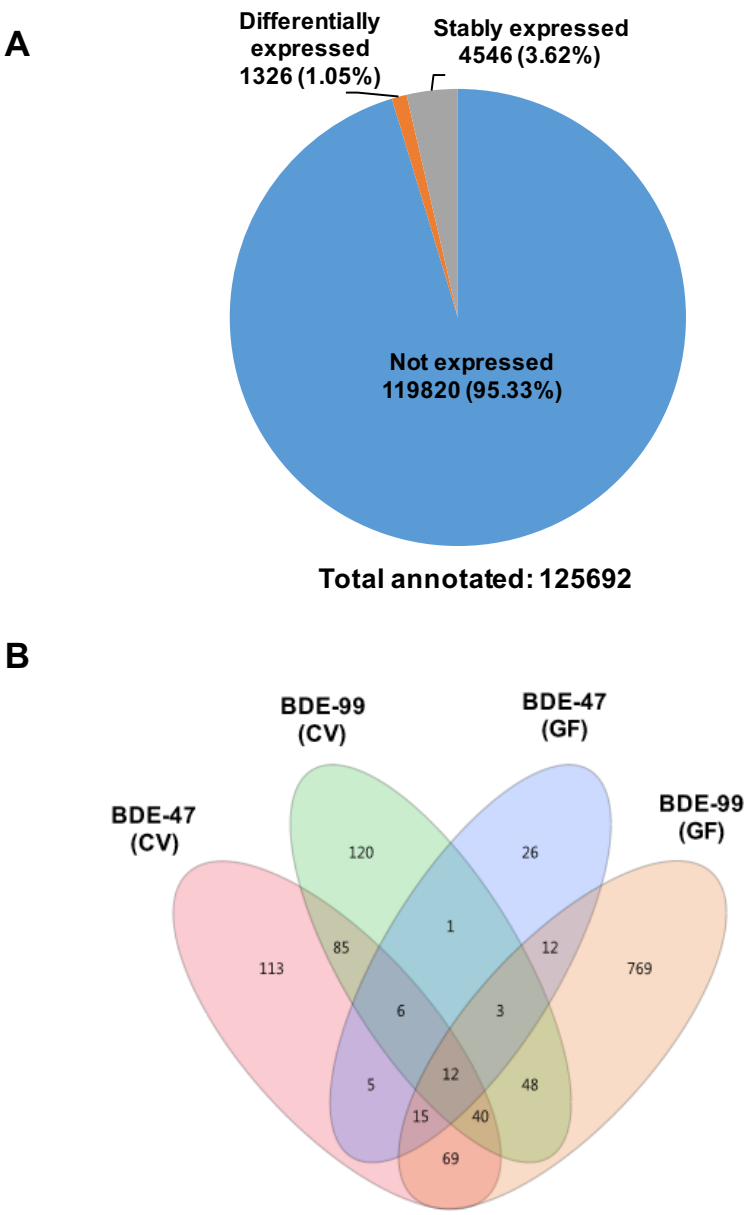

Figure 4. Regulation of long noncoding RNAs (lncRNAs) in livers of CV and GF mice treated with corn oil, BDE-47 (100 µmol/kg), or BDE-99 (100 µmol/kg). (A) A pie chart showing lncRNAs that were not expressed in any groups (blue), stably expressed in all groups (grey), and differentially expressed by PBDE treatment in at least one of the four comparisons (orange). These four comparisons are: CV_CO (corn oil) vs CV_BDE-47; CV_CO vs CV_BDE-99; GF_CO vs GF_BDE-47; and GF_CO vs GF_BDE-99, FDR adjusted p-value <0.05). **(B)** A Venn diagram showing the differentially expressed lncRNAs that were commonly or uniquely regulated by PBDEs among the four comparisons as described in Fig. 4A. Venn diagram was generated using JMP Genomics.

Figure 5

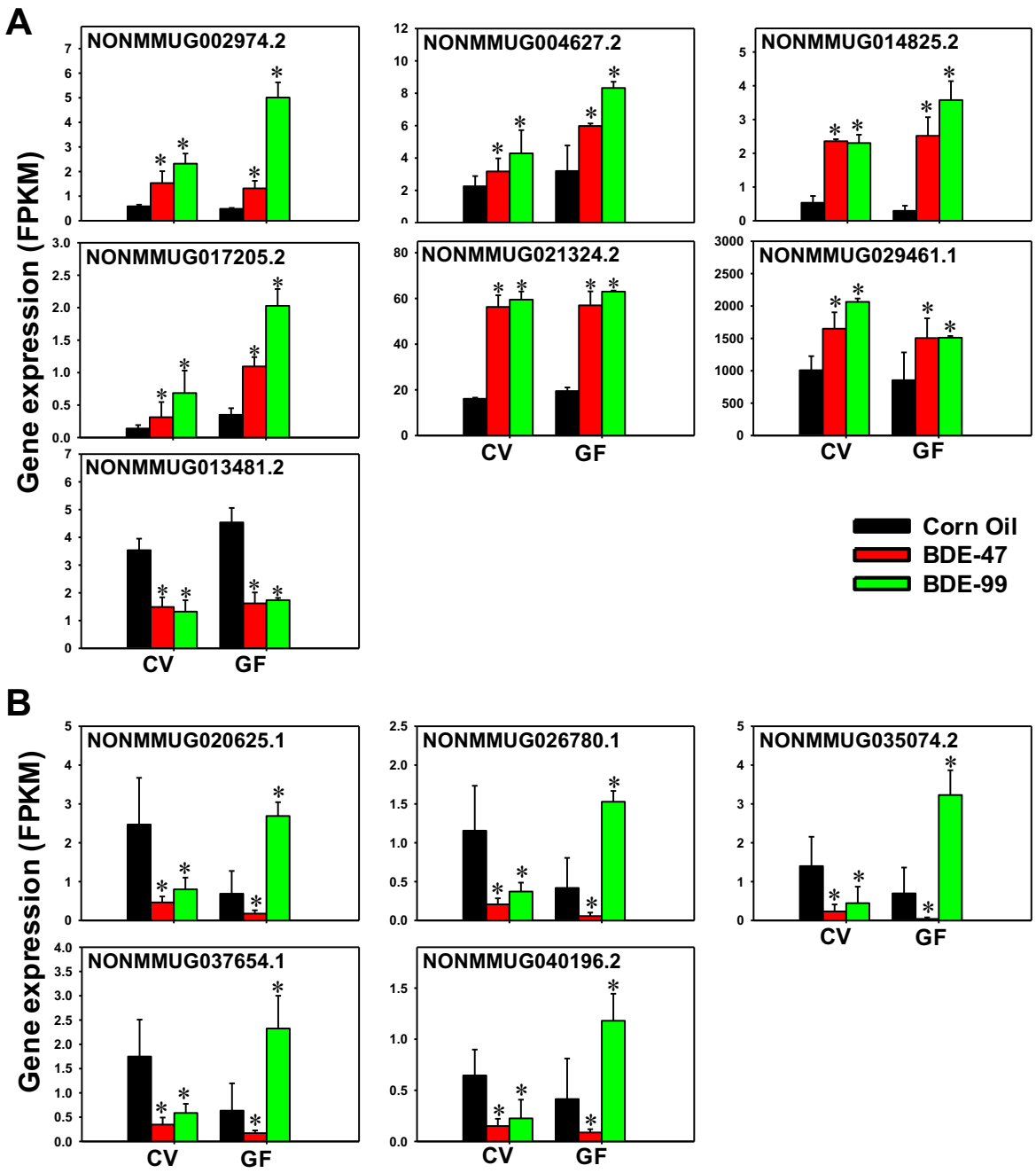

Figure 5. lncRNAs that were differentially regulated by both PBDEs in livers of CV and GF mice. **(A)** lncRNAs that were commonly up-regulated or down-regulated by BDE-47 and BDE-99 in livers of both CV and GF mice. **(B)** lncRNAs that were consistently down-regulated by BDE-47 in livers of CV and GF mice, but were oppositely regulated in CV (down-regulation) and GF (up-regulation) mice by BDE-99. Asterisks (*) indicate statistically significant differences as compared to vehicle-treated groups of the same enterotypes of mice ($p < 0.05$).

Figure 6

A. CO vs BDE-47

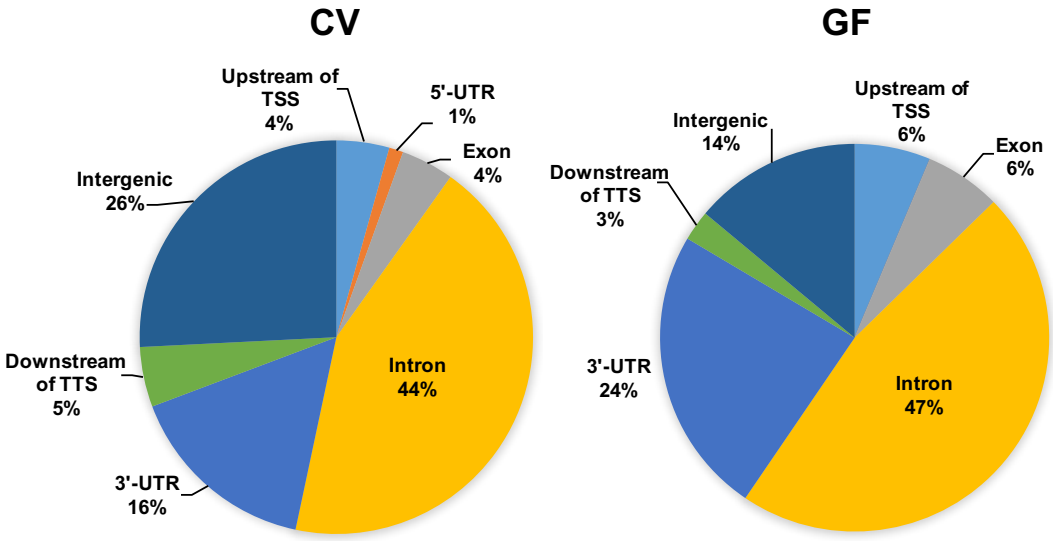

B. CO vs BDE-99

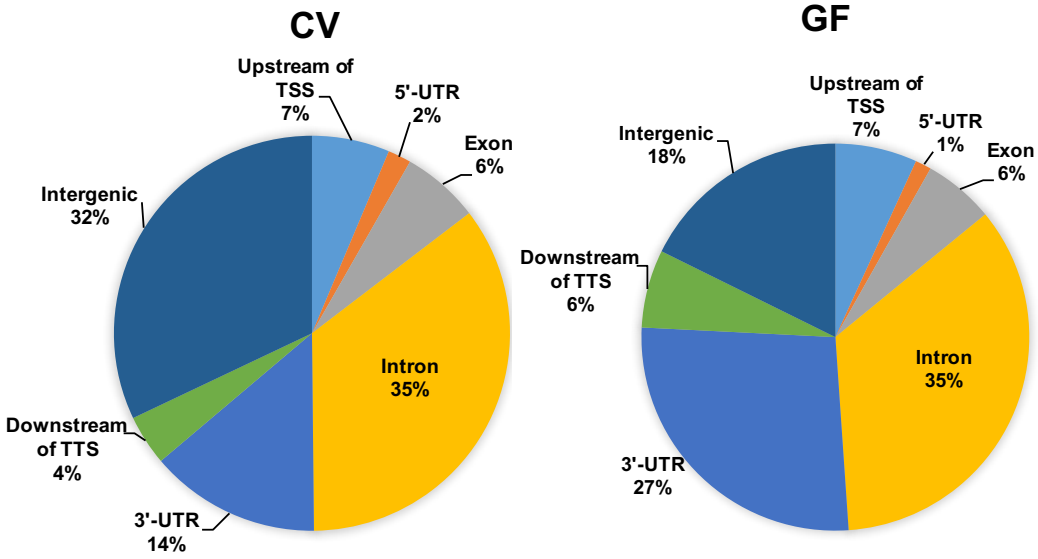

Figure 6. Genomic annotation of differentially regulated lncRNAs relative to the closest PCGs, including up to 5 kb upstream of transcription start site (TSS), intronic, exonic, 5'-untranslated region (UTR), 3'-UTR, and up to 1 kb downstream of transcriptional termination site (TTS). **(A)** lncRNAs that were differentially regulated by BDE-47 in livers of CV (left) and GF (right) mice, compared to the vehicle-treated control group of the same enterotypes of mice. **(B)** lncRNAs that were differentially regulated by BDE-99 in livers of CV (left) and GF (right) mice, compared to the vehicle-treated control group of the same enterotypes of mice.

Figure 7 CV_BDE47

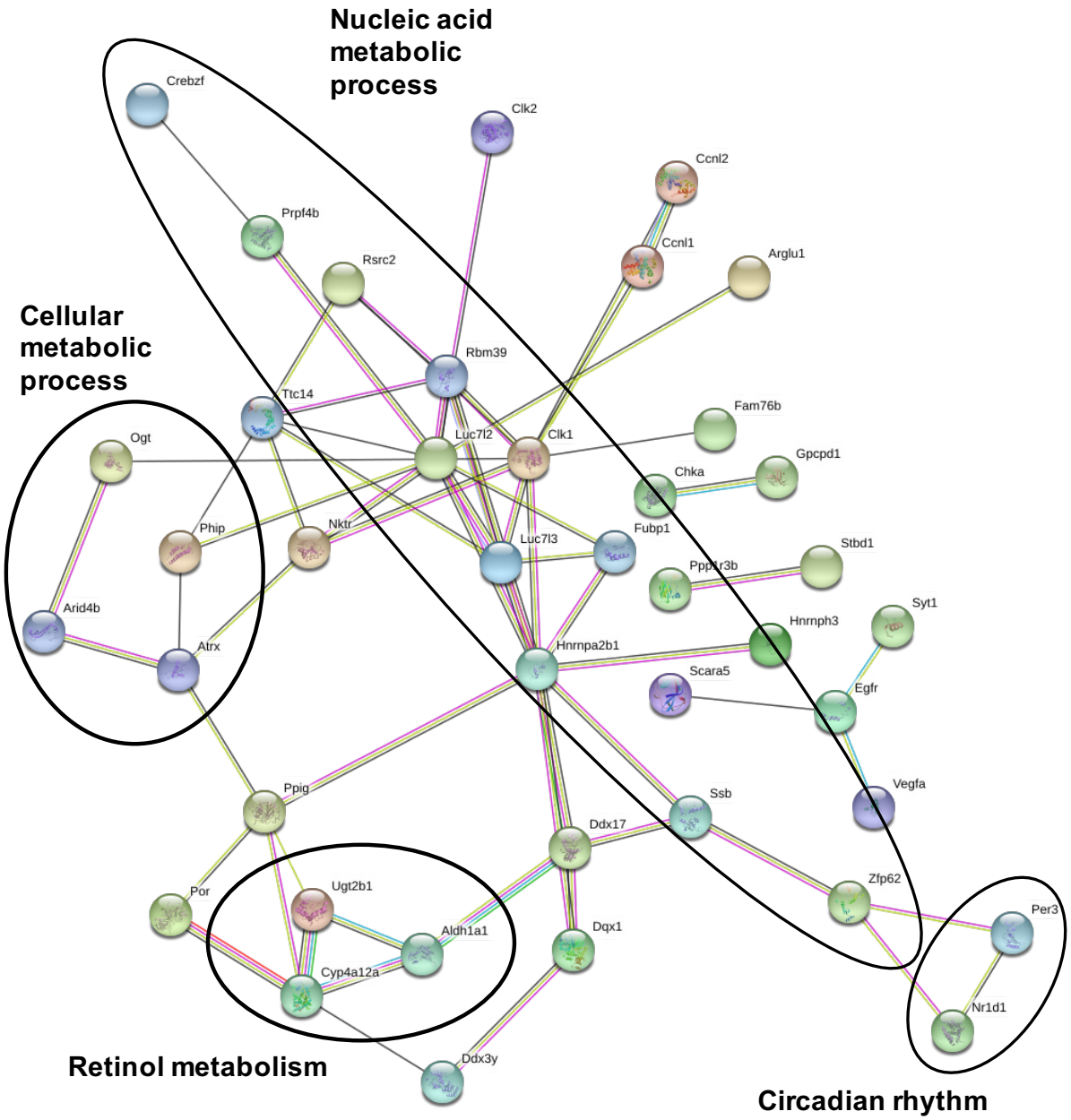

Figure 7. Pathway analysis of lncRNA-PCG pairs that were differentially regulated by BDE-47 in livers of CV mice compared to corn oil-treated CV group. The lncRNA-PCG pairs between CV_CO and CV_BDE-47 were subjected to STRING analysis using the default settings. The top network is shown.

Figure 8 CV_BDE47

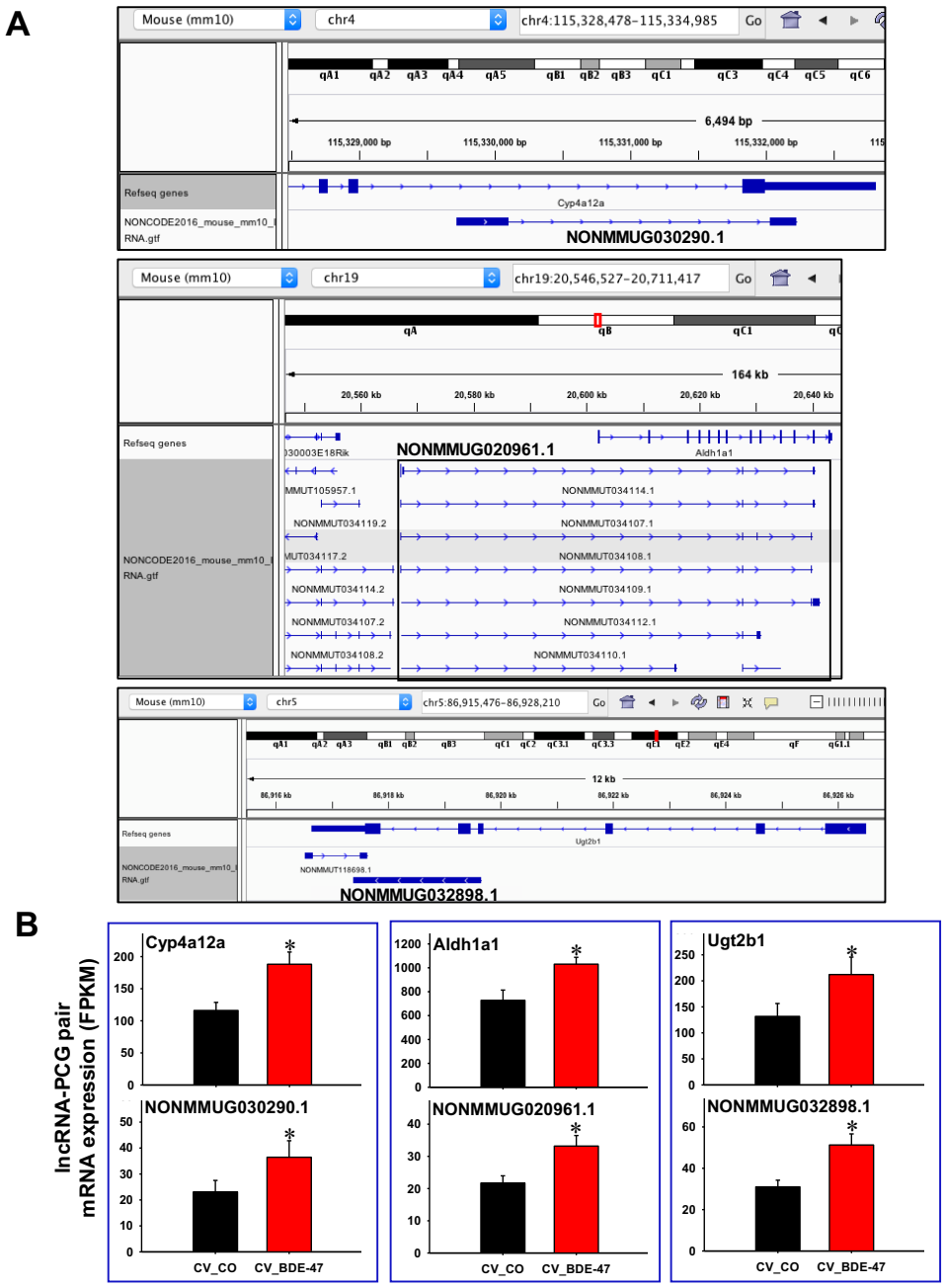

Figure 8. Genomic location (A) and gene expression (B) of lncRNA-PCG pairs that were differentially regulated by BDE-47 in livers of CV mice compared to corn oil-treated CV mice. Drug-metabolizing enzymes Cyp4a12a and aldehyde dehydrogenase (Aldh) 1a1 (phase I), as well as UDP-glucuronosyltransferase (Ugt) 2b1 (phase II) are shown. Expression of lncRNAs and paired PCGs were plotted using mean FPKM ± S.E. Asterisks (*) indicate statistically significant differences as compared to vehicle-treated groups of the same enterotypes of mice ($p < 0.05$).

Figure 9 CV_BDE47

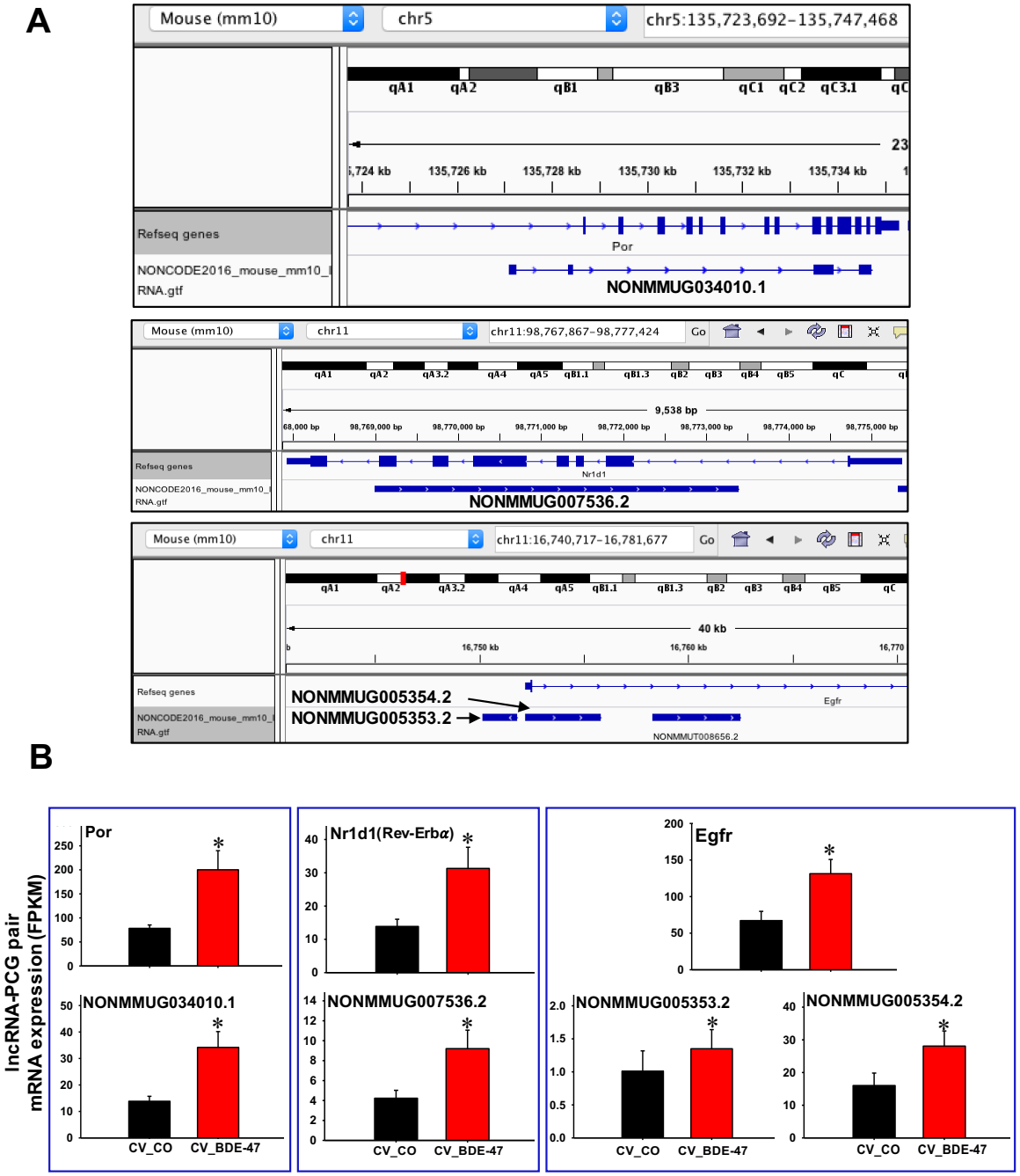

Figure 9. Genomic location (A) and gene expression (B) of lncRNA-PCG pairs that were differentially regulated by BDE-47 in livers of CV mice compared to corn oil-treated CV mice. The P450-reductase (Por), nuclear receptor Nr1d1 (also known as Rev-Erbα), and epidermal growth factor receptor (Egfr) are shown. Expression of lncRNAs and paired PCGs were plotted using mean FPKM ± S.E. Asterisks (*) indicate statistically significant differences as compared to vehicle-treated groups of the same enterotypes of mice ($p < 0.05$).

Figure 10 CV_BDE99

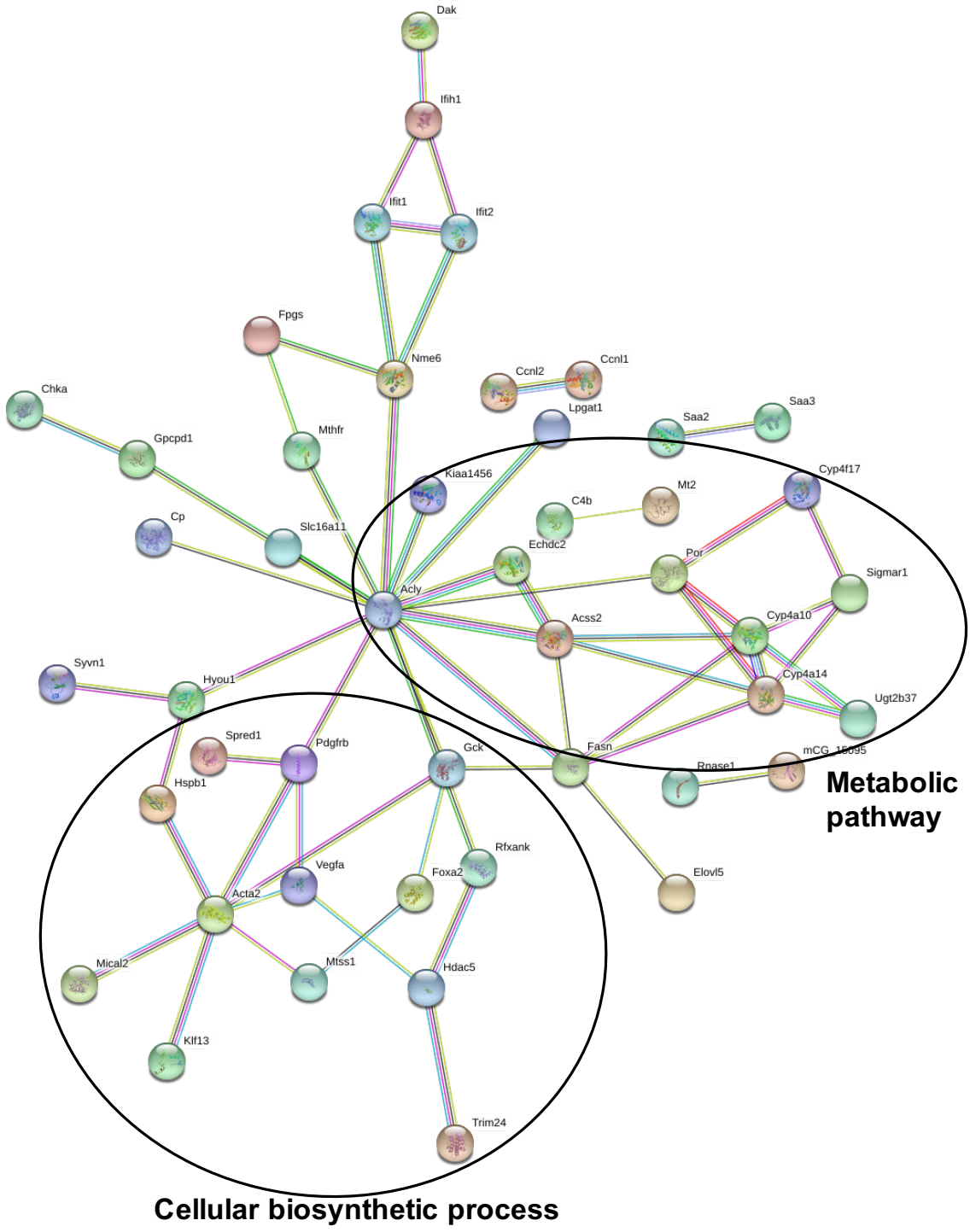

Figure 10. Pathway analysis of lncRNA-PCG pairs that were differentially regulated by BDE-99 in livers of CV mice compared to corn oil-treated CV group. The lncRNA-PCG pairs between CV_CO and CV_BDE-99 were subjected to STRING analysis using the default settings. The top network is shown.

Figure 11 CV_BDE99

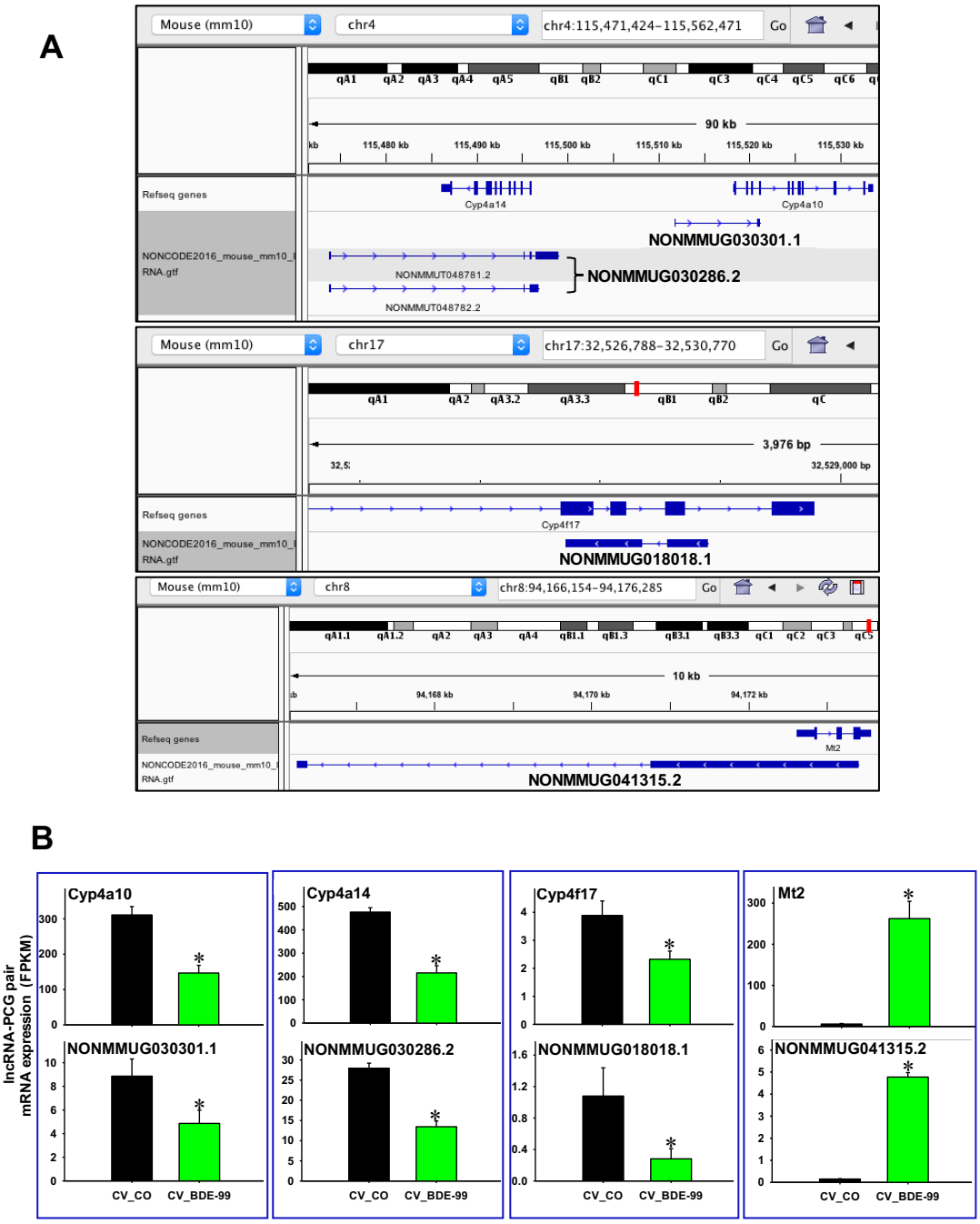

Figure 11. Genomic location (A) and gene expression (B) of lncRNA-PCG pairs that were differentially regulated by BDE-99 in livers of CV mice compared to corn oil-treated CV mice. The drug-metabolizing enzymes Cyp4a10, Cyp4a14, Cyp4f17, as well as the cysteine-rich metal-binding protein metallothionein 2 (Mt2) are shown. Expression of lncRNAs and paired PCGs were plotted using mean FPKM ± S.E. Asterisks (*) indicate statistically significant differences as compared to vehicle-treated groups of the same enterotypes of mice ($p < 0.05$).

Figure 12 CV_BDE99

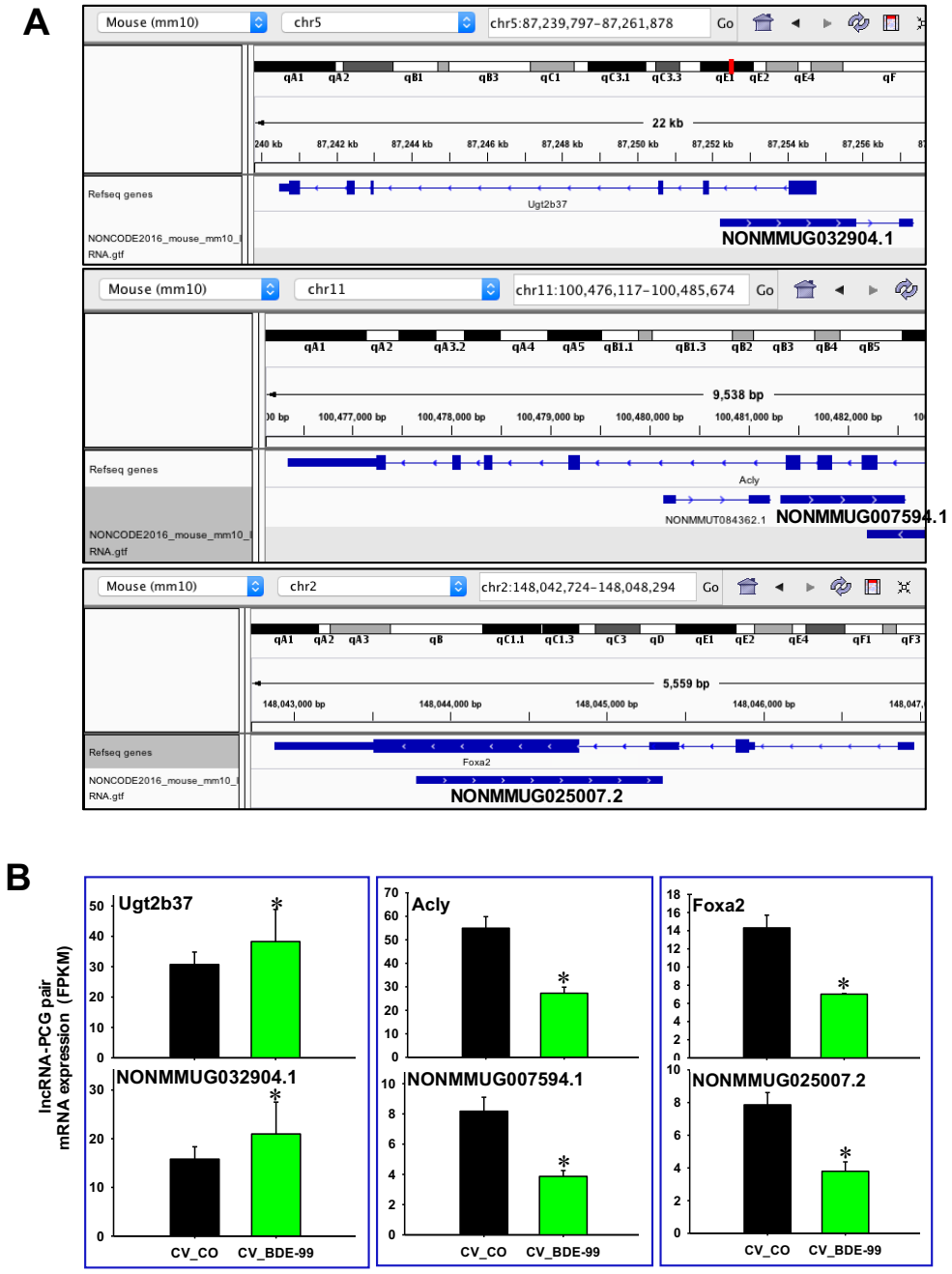

Figure 12. Genomic location (A) and gene expression (B) of lncRNA-PCG pairs that were differentially regulated by BDE-99 in livers of CV mice compared to corn oil-treated CV mice. The drug-metabolizing enzyme Ugt2b37, fatty acid synthesizing enzyme ATP citrate lyase (Acly), and the transcription factor forkhead box A2 (foxA2; also known as HNF3β) are shown. Expression of lncRNAs and paired PCGs were plotted using mean FPKM ± S.E. Asterisks (*) indicate statistically significant differences as compared to vehicle-treated groups of the same enterotypes of mice ($p < 0.05$).

Figure 13 GF_BDE47

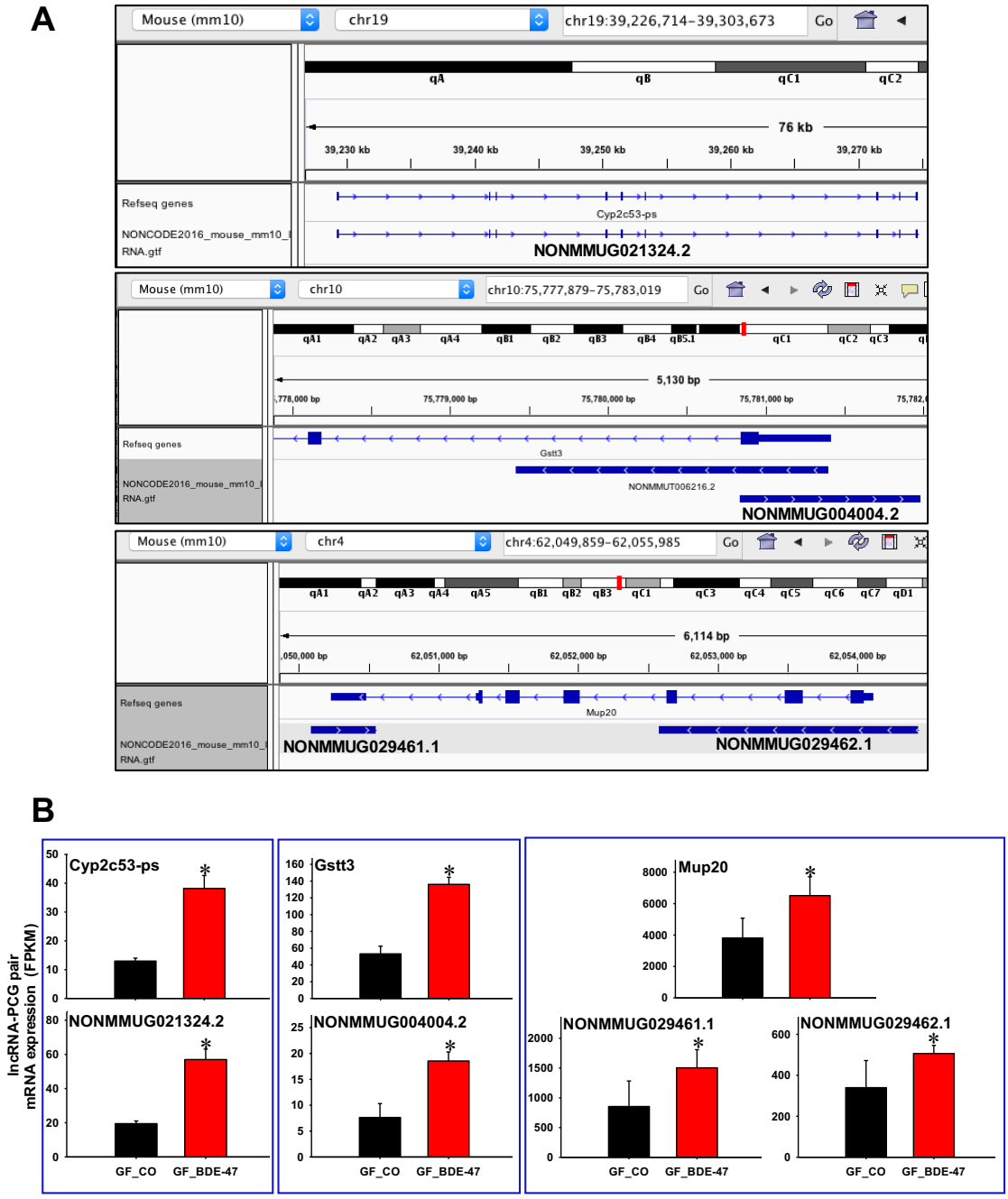

Figure 13. Genomic location (A) and gene expression (B) of lncRNA-PCG pairs that were differentially regulated by BDE-47 in livers of GF mice compared to corn oil-treated GF mice. Cyp2c53-ps (pseudogene in the P450 family), drug metabolizing enzyme glutathione *S*-transferase (Gst) t3, and major urinary protein (Mup) 20 are shown. Expression of lncRNAs and paired PCGs were plotted using mean FPKM ± S.E. Asterisks (*) indicate statistically significant differences as compared to vehicle-treated groups of the same enterotypes of mice ($p < 0.05$).

Figure 14

A. PPARα-signaling pathway

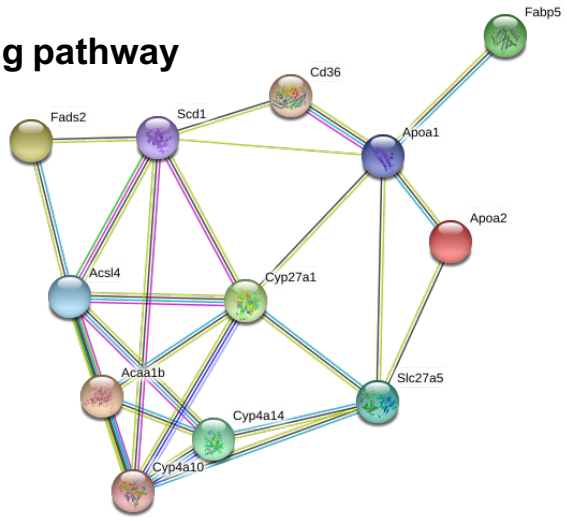

B. Metabolic signaling

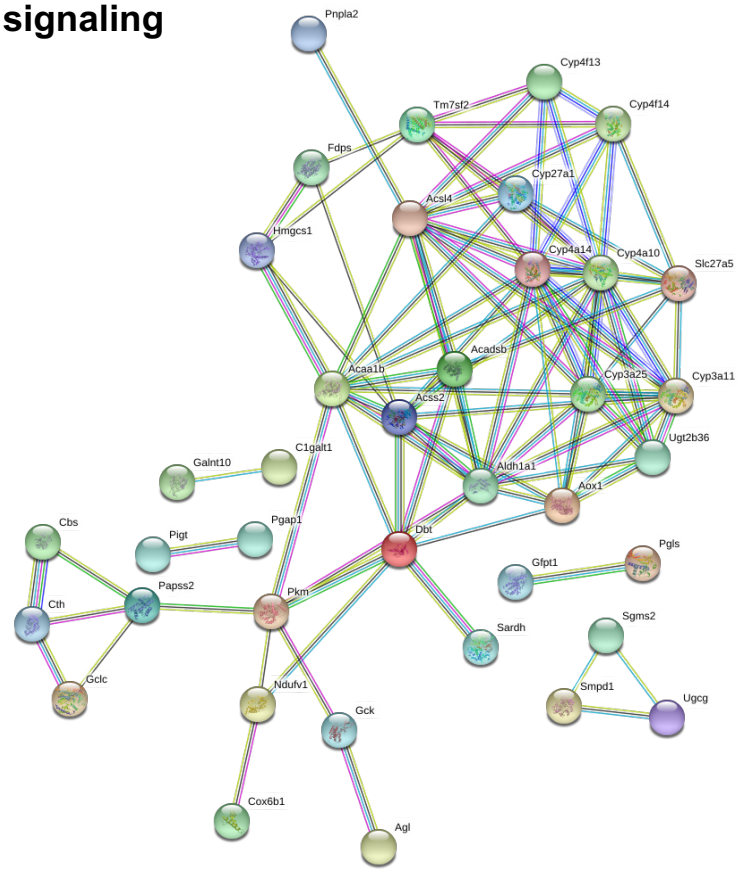

Figure 14. lncRNA-PCG pairs that were differentially regulated by BDE-99 in GF condition were enriched in PPARα-signaling (A) and metabolic signaling (B) pathways. The lncRNA-PCG pairs between GF_CO and GF_BDE-99 were subjected to STRING analysis using the default settings. The top network is shown.

Figure 15 GF_BDE99

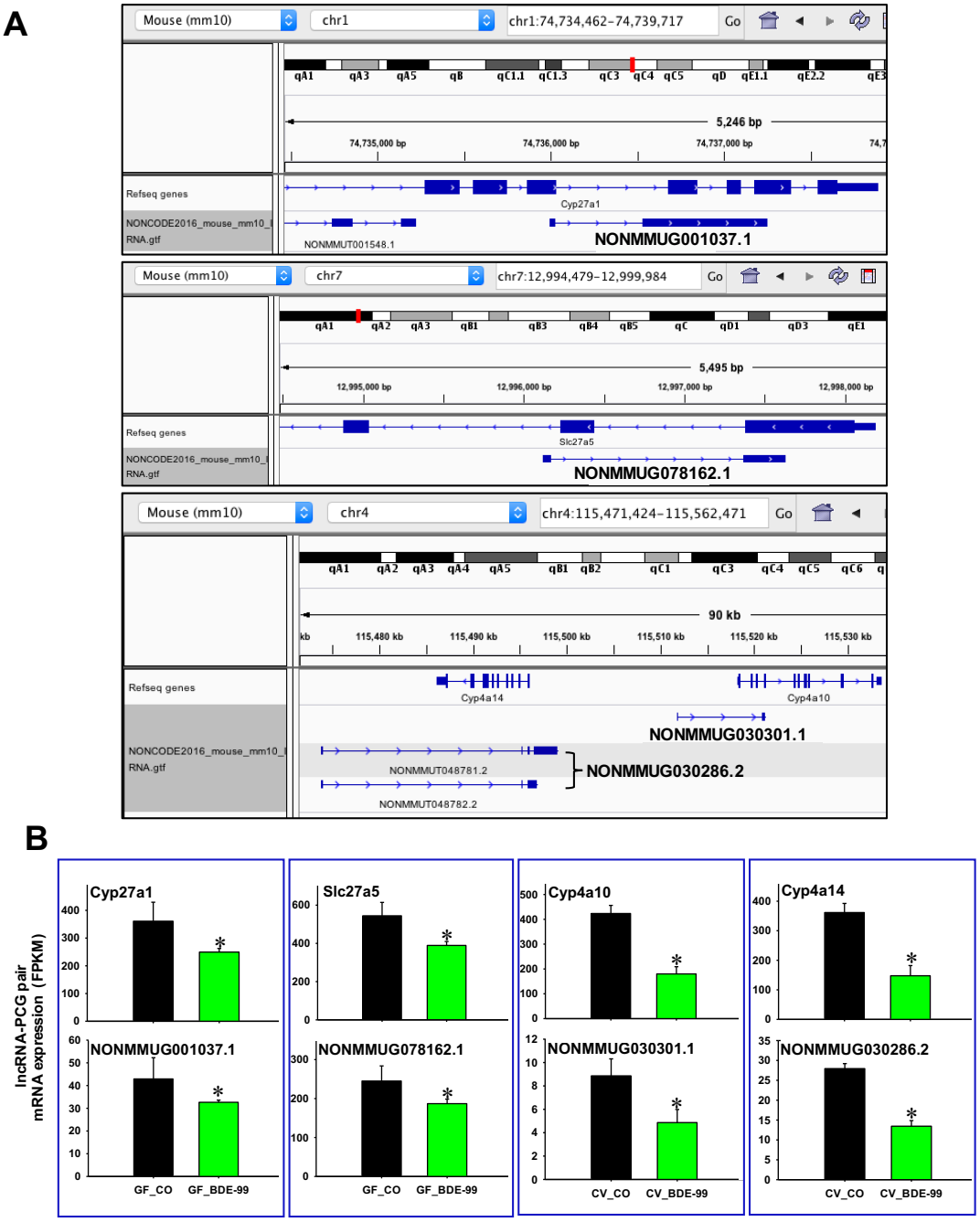

Figure 15. Genomic location (A) and gene expression (B) of lncRNA-PCG pairs that were differentially regulated by BDE-99 in livers of GF mice compared to corn oil-treated GF mice. Cyp27a1 (bile acid synthetic enzyme in alternative pathway), solute carrier (Slc) 27a5 (also known as bile acid ligase), Cyp4a10, and Cyp4a14 are shown. Expression of lncRNAs and paired PCGs were plotted using mean FPKM ± S.E. Asterisks (*) indicate statistically significant differences as compared to vehicle-treated groups of the same enterotypes of mice ($p < 0.05$).

Figure 16 GF_BDE99

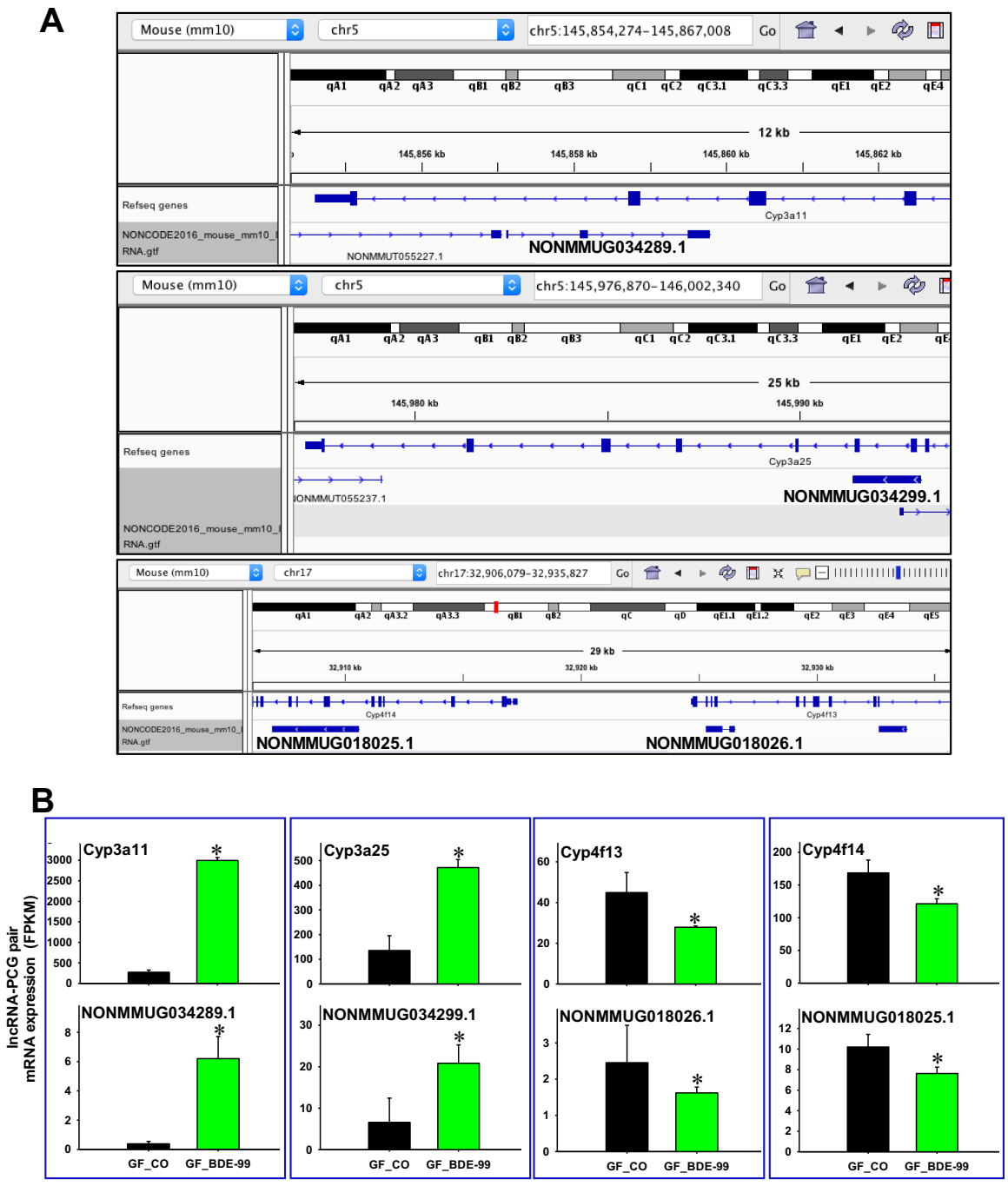

Figure 16. Genomic location (A) and gene expression (B) of lncRNA-PCG pairs that were differentially regulated by BDE-99 in livers of GF mice compared to corn oil-treated GF mice. The P450s Cyp3a11, Cyp3a25, Cyp4f13, and Cyp4f14 are shown. Expression of lncRNAs and paired PCGs were plotted using mean FPKM ± S.E. Asterisks (*) indicate statistically significant differences as compared to vehicle-treated groups of the same enterotypes of mice ($p < 0.05$).

Supplemental Figure 1. Top network of PCGs that were differentially regulated by BDE-47 in livers of CV mice compared to corn oil-treated CV group as analyzed by Ingenuity Pathway Analysis (IPA, *p<0.05*).

Lipid metabolism, small molecule biochemistry, drug metabolism (Network 14)

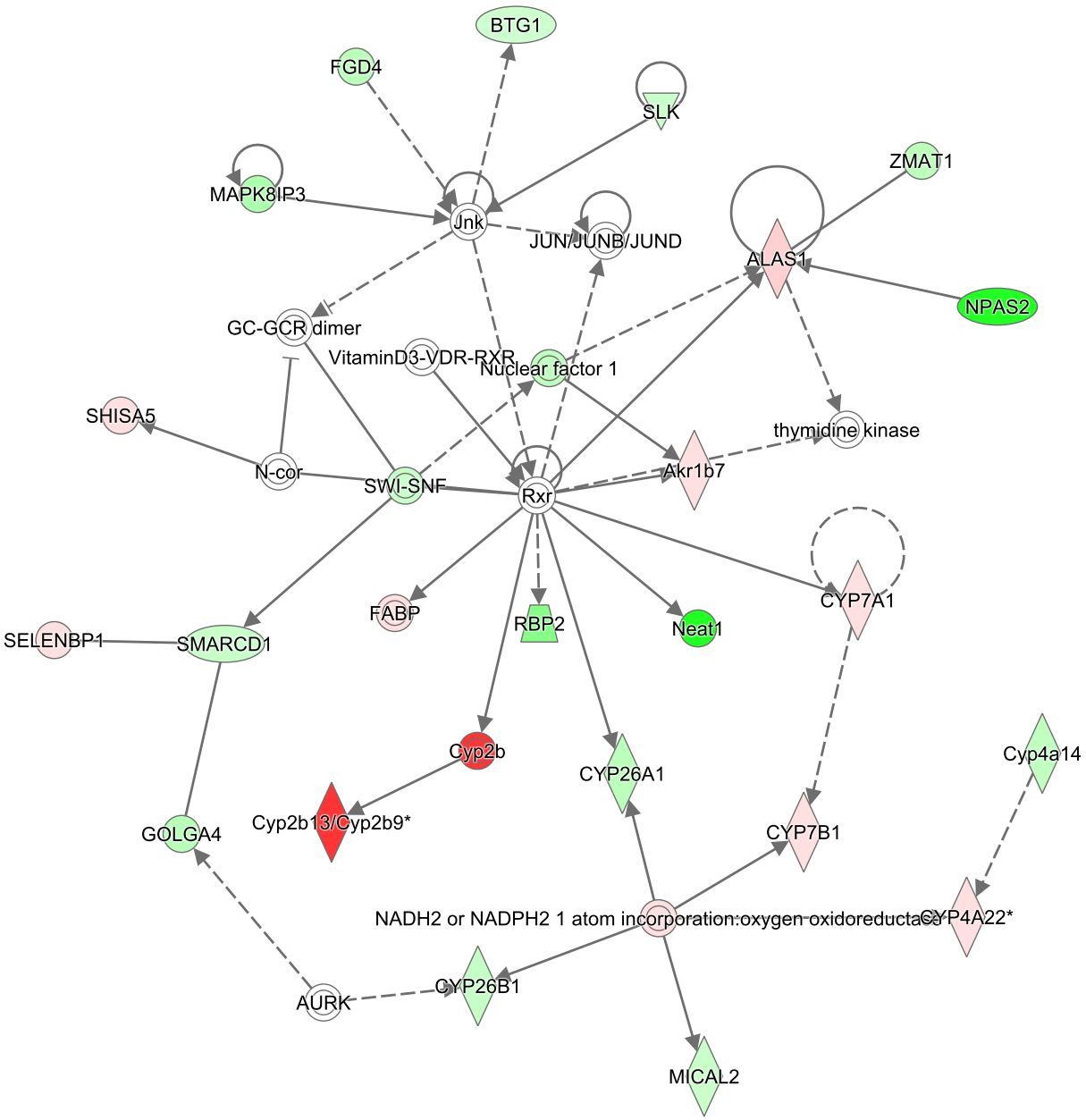

Supplemental Figure 2. Top network of PCGs that were differentially regulated by BDE-99 in livers of CV mice compared to corn oil-treated CV group as analyzed by Ingenuity Pathway Analysis (IPA, *p<0.05*).

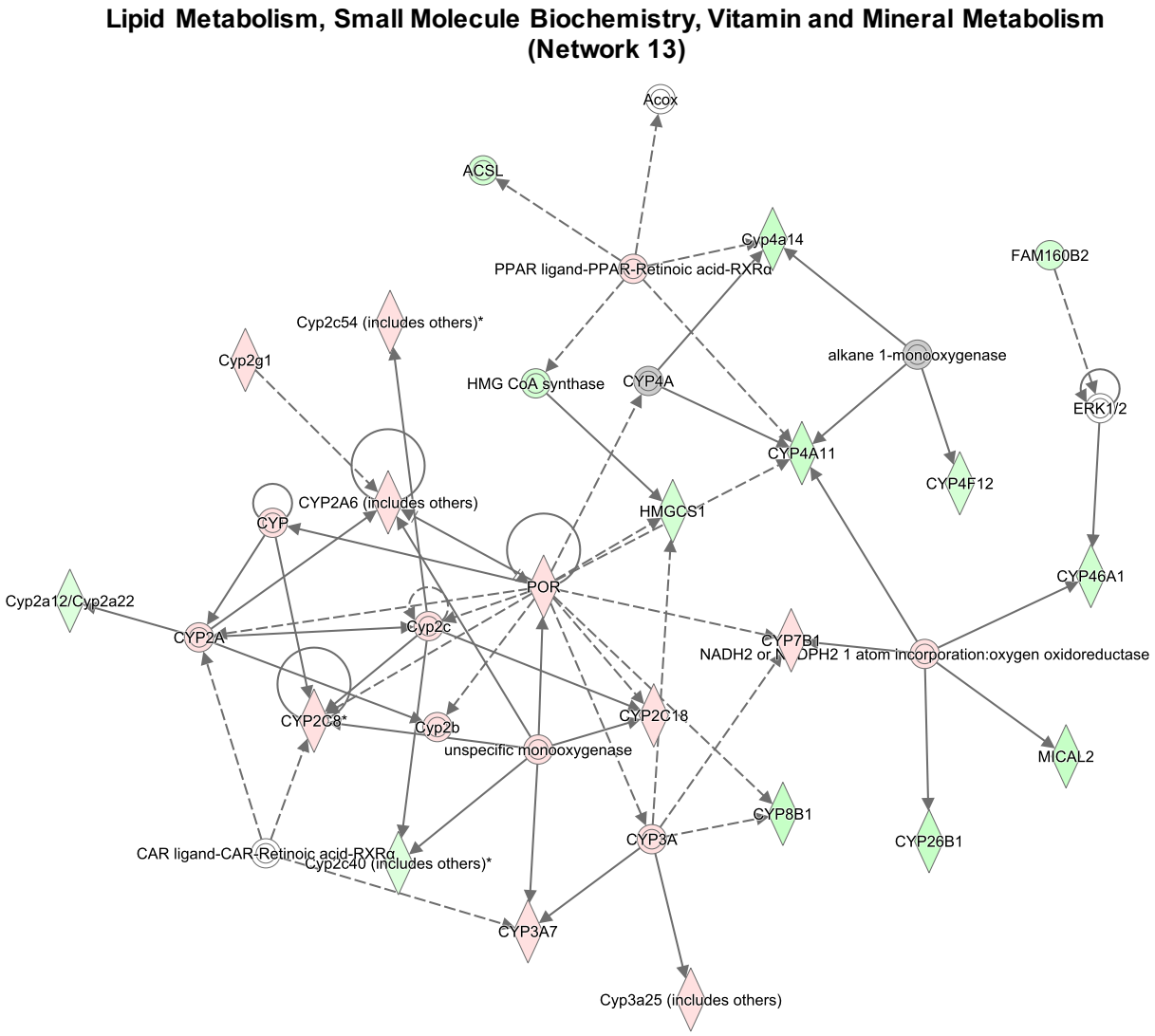

Supplemental Figure 3. Top network of PCGs that were differentially regulated by BDE-47 in livers of GF mice compared to corn oil-treated GF group as analyzed by Ingenuity Pathway Analysis (IPA, *p<0.05*).

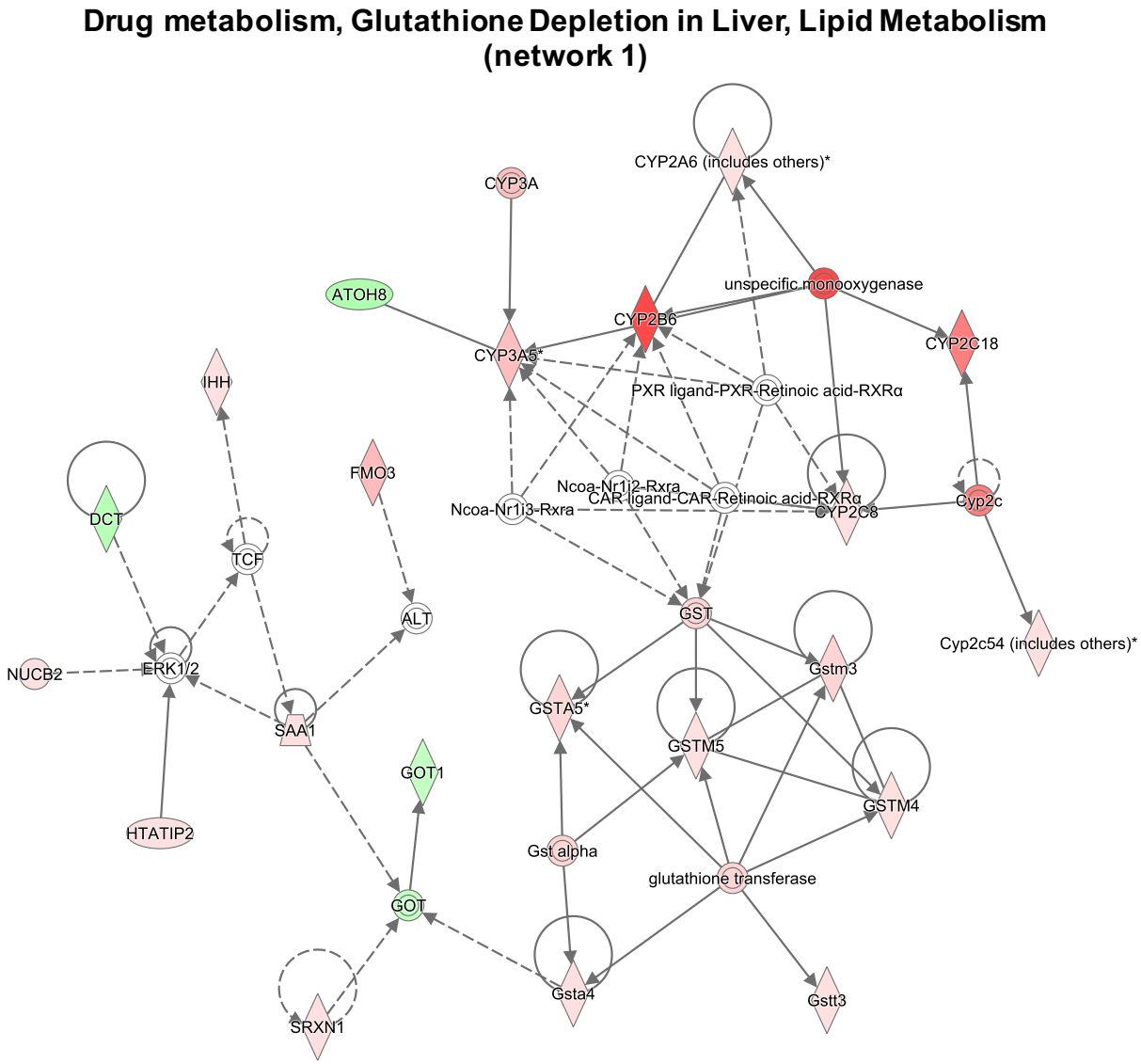

Supplemental Figure 4. Top network of PCGs that were differentially regulated by BDE-99 in livers of GF mice compared to corn oil-treated GF group as analyzed by Ingenuity Pathway Analysis (IPA, *p<0.05*).

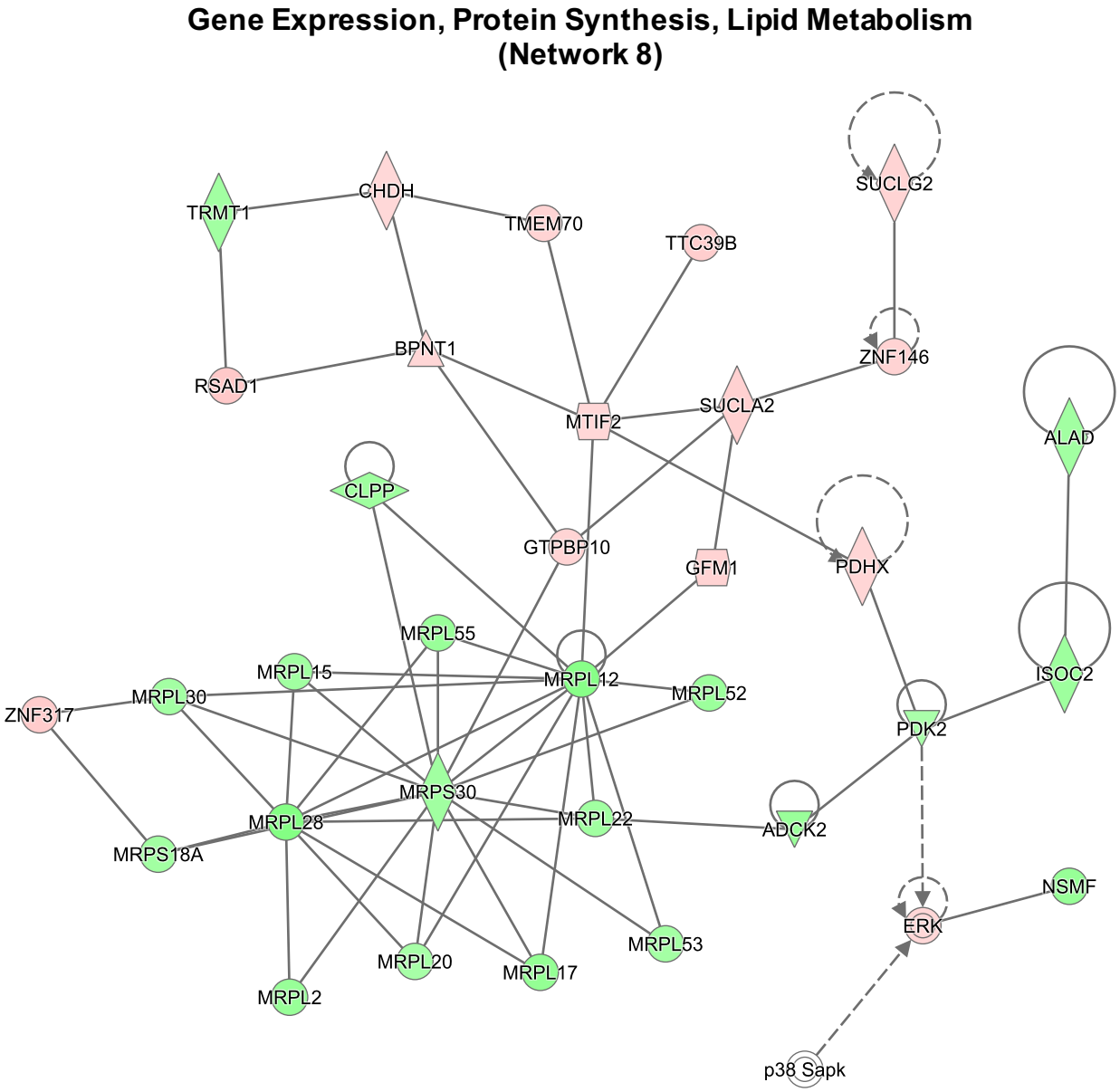

Supplemental Figure 5. KEGG pathway of PCGs that were commonly regulated by both BDE-47 and BDE-99 in livers of CV and GF mice as analyzed by STRING Analysis (*p<0.05*).

KEGG Pathways			
pathway ID	*pathway description*	*count in gene set*	*false discovery rate*
01100	Metabolic pathways	12	6.7e-05
05204	Chemical carcinogenesis	11	2.66e-15
00830	Retinol metabolism	9	4.89e-12
00140	Steroid hormone biosynthesis	8	2.56e-10
00590	Arachidonic acid metabolism	6	9.66e-07

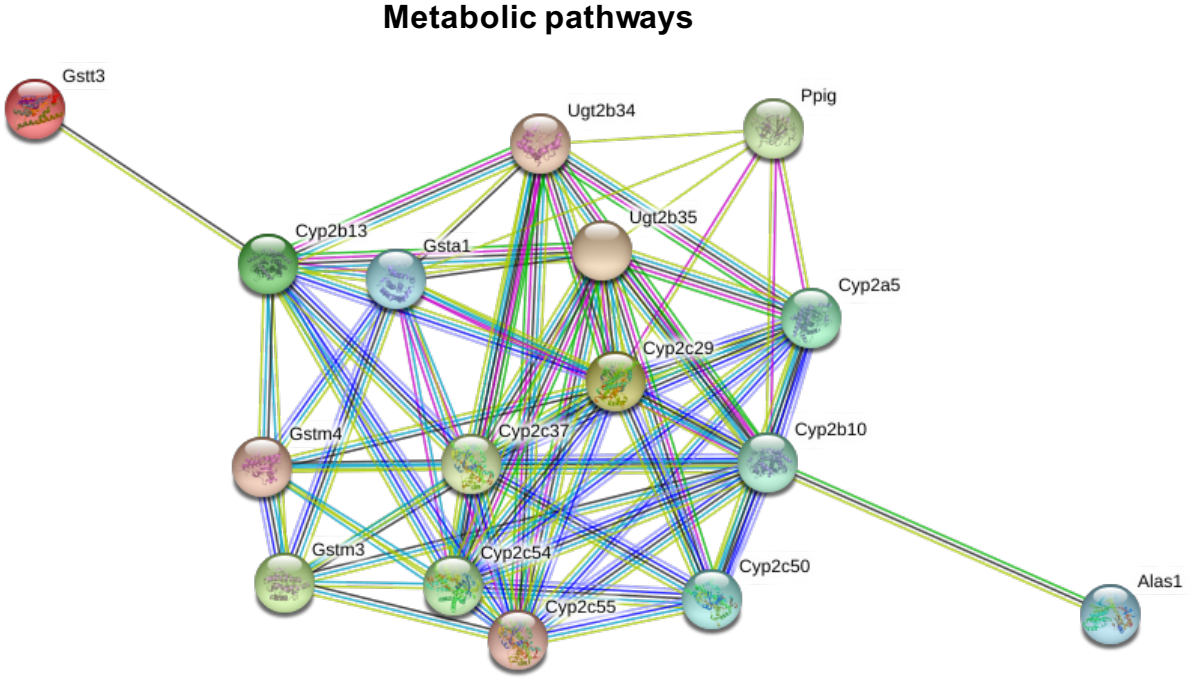

Supplemental Figure 6. Top network of PCGs that were uniquely regulated by BDE-47 in livers of CV mice compared to corn oil-treated CV group as analyzed by Ingenuity Pathway Analysis (IPA, *p<0.05*).

Top Networks

ID	Associated Network Functions	Score
1	Cellular Development, Cancer, Cell Death and Survival	41
2	Carbohydrate Metabolism, Molecular Transport, Cell Morphology	38
3	Cardiovascular Disease, Lipid Metabolism, Small Molecule Biochemistry	26
4	Lipid Metabolism, Small Molecule Biochemistry, Cell Death and Survival	26
5	Antimicrobial Response, Inflammatory Response, Connective Tissue Disorders	24

Cellular Development, Cancer, Cell Death and Survival (network 1)

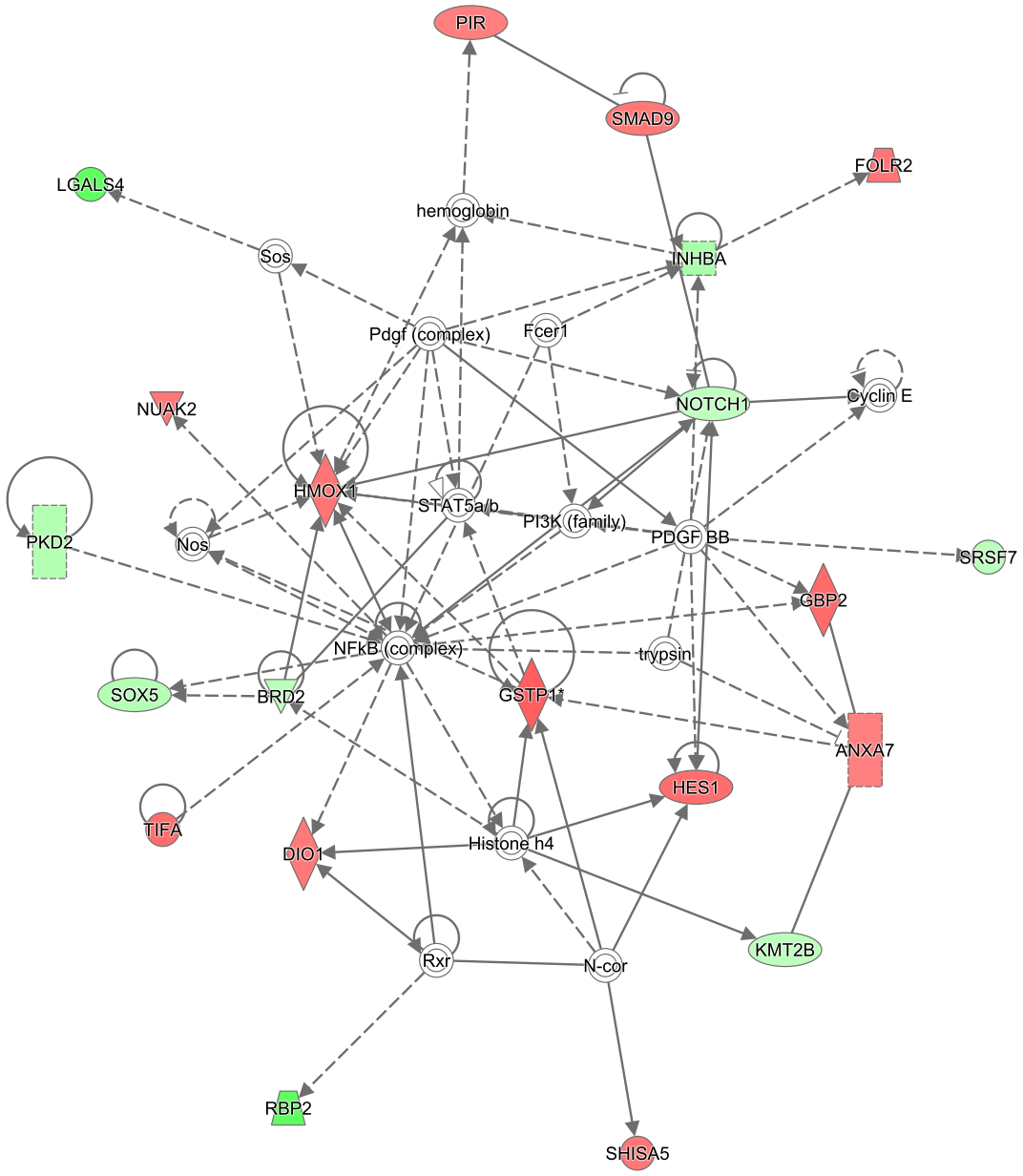

Supplemental Figure 7. Top networks of PCGs that were uniquely regulated by BDE-99 in livers of CV mice compared to corn oil-treated CV group as analyzed by Ingenuity Pathway Analysis (IPA, *p<0.05*).

Top Networks		
ID	Associated Network Functions	Score
1	Carbohydrate Metabolism, Lipid Metabolism, Small Molecule Biochemistry	38
2	Post-Translational Modification, Protein Degradation, Protein Synthesis	36
3	Cancer, Organismal Injury and Abnormalities, Reproductive System Disease	34
4	Hematological System Development and Function, Tissue Morphology, Cellular Movement	29
5	Cellular Assembly and Organization, Lipid Metabolism, Small Molecule Biochemistry	25

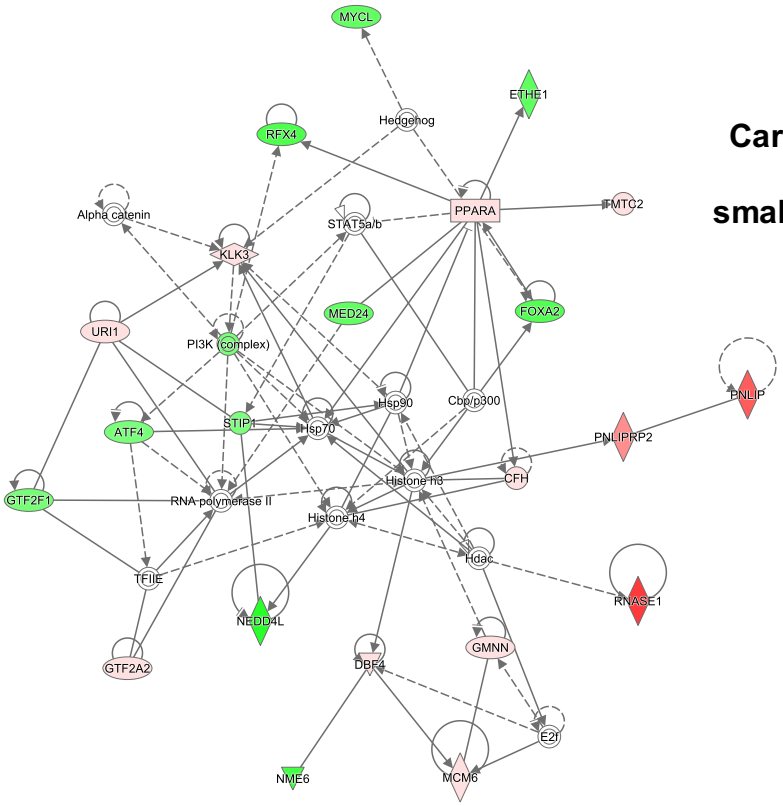

Carbohydrate metabolism, lipid metabolism, small molecule biochemistry (network 1)

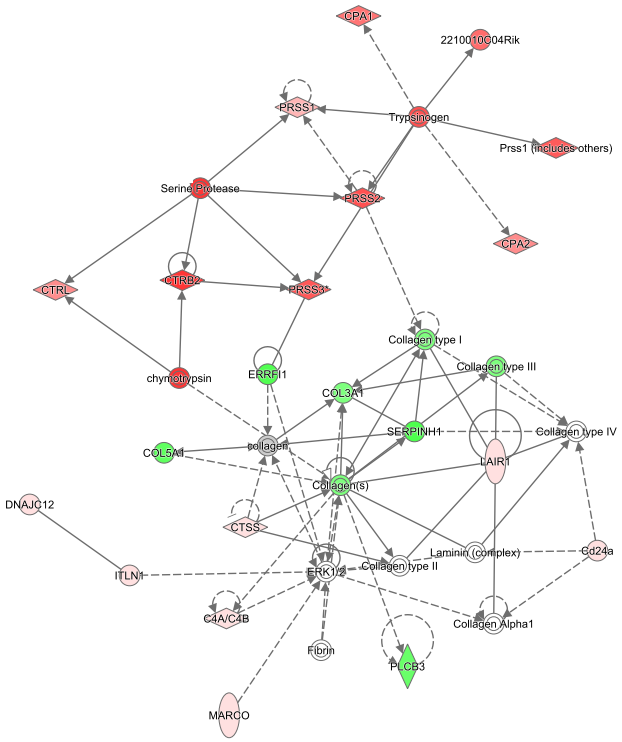

Post-translational modification, protein degradation, protein synthesis (network 2)

Supplemental Figure 8. Top network of PCGs that were uniquely regulated by BDE-99 in livers of GF mice compared to corn oil-treated GF group as analyzed by Ingenuity Pathway Analysis (IPA, *p<0.05*).

Top Networks		
ID	Associated Network Functions	Score
1	Auditory Disease, Developmental Disorder, Hereditary Disorder	38
2	Gene Expression, Protein Synthesis, Cellular Assembly and Organization	38
3	Cellular Development, Cellular Growth and Proliferation, Cell Cycle	35
4	Tissue Morphology, Cellular Assembly and Organization, DNA Replication, Recombination, and Repair	33
5	Cancer, Endocrine System Disorders, Hereditary Disorder	33

Gene expression, protein synthesis, cellular assembly and organization (network 2)

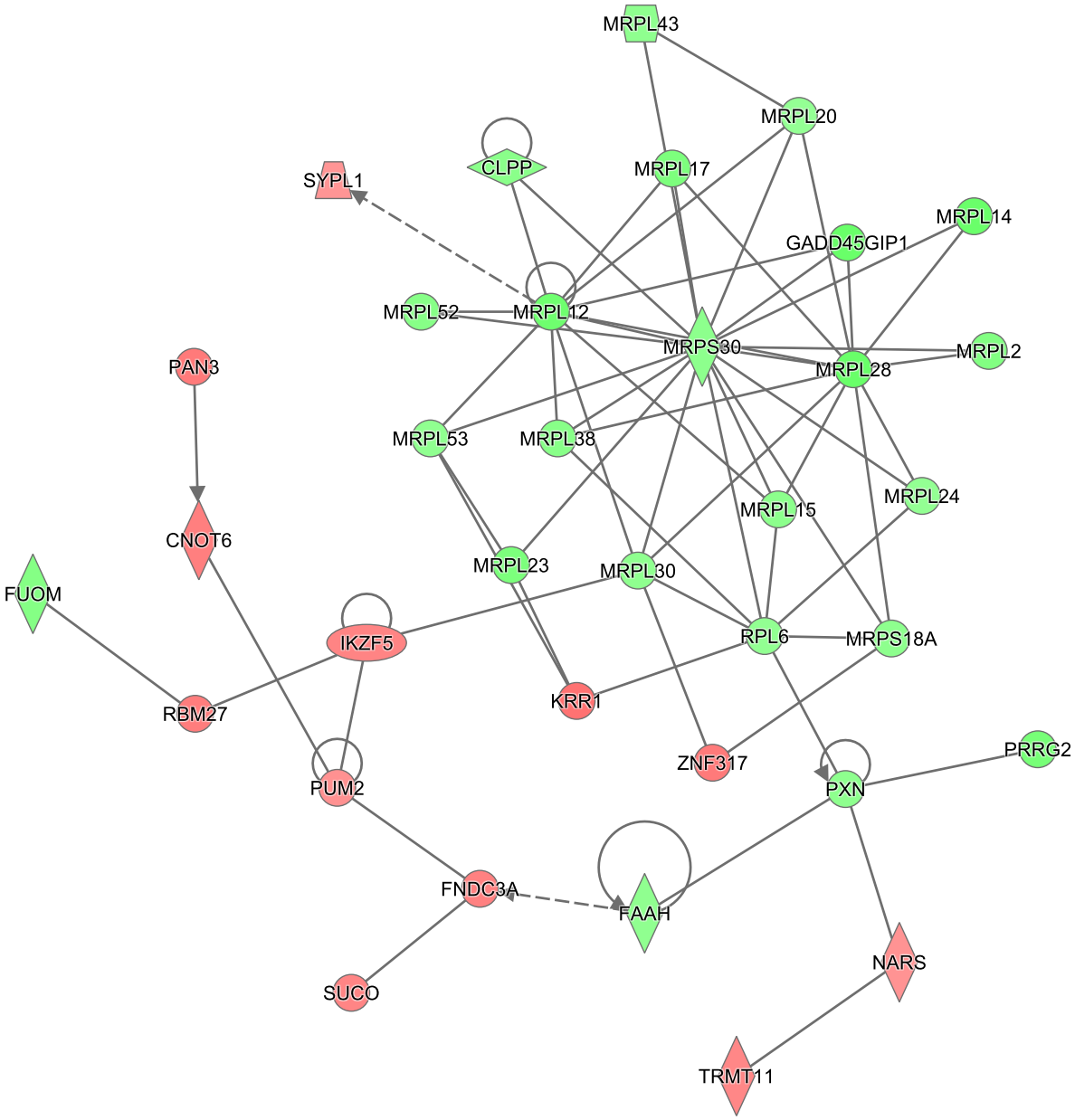

Supplemental Figure 9. Genomic annotations of lncRNAs that were differentially regulated between control CV and control GF mice ($p<0.05$) in relative to the closest PCGs.

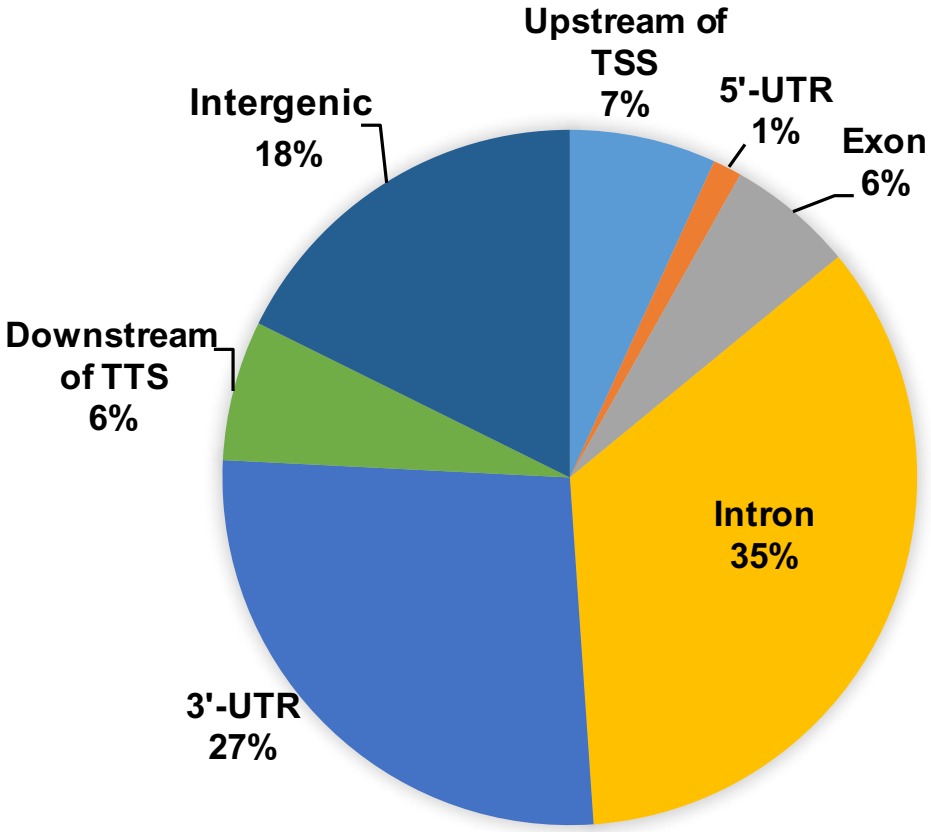

Supplemental Figure 10. Other examples of lncRNA-PCG pairs that were differentially regulated by BDE-99 in livers of CV mice compared to corn oil-treated CV group. The epigenetic enzyme histone deacetylase (Hdac) 5 and P450-reductase (Por) are shown.

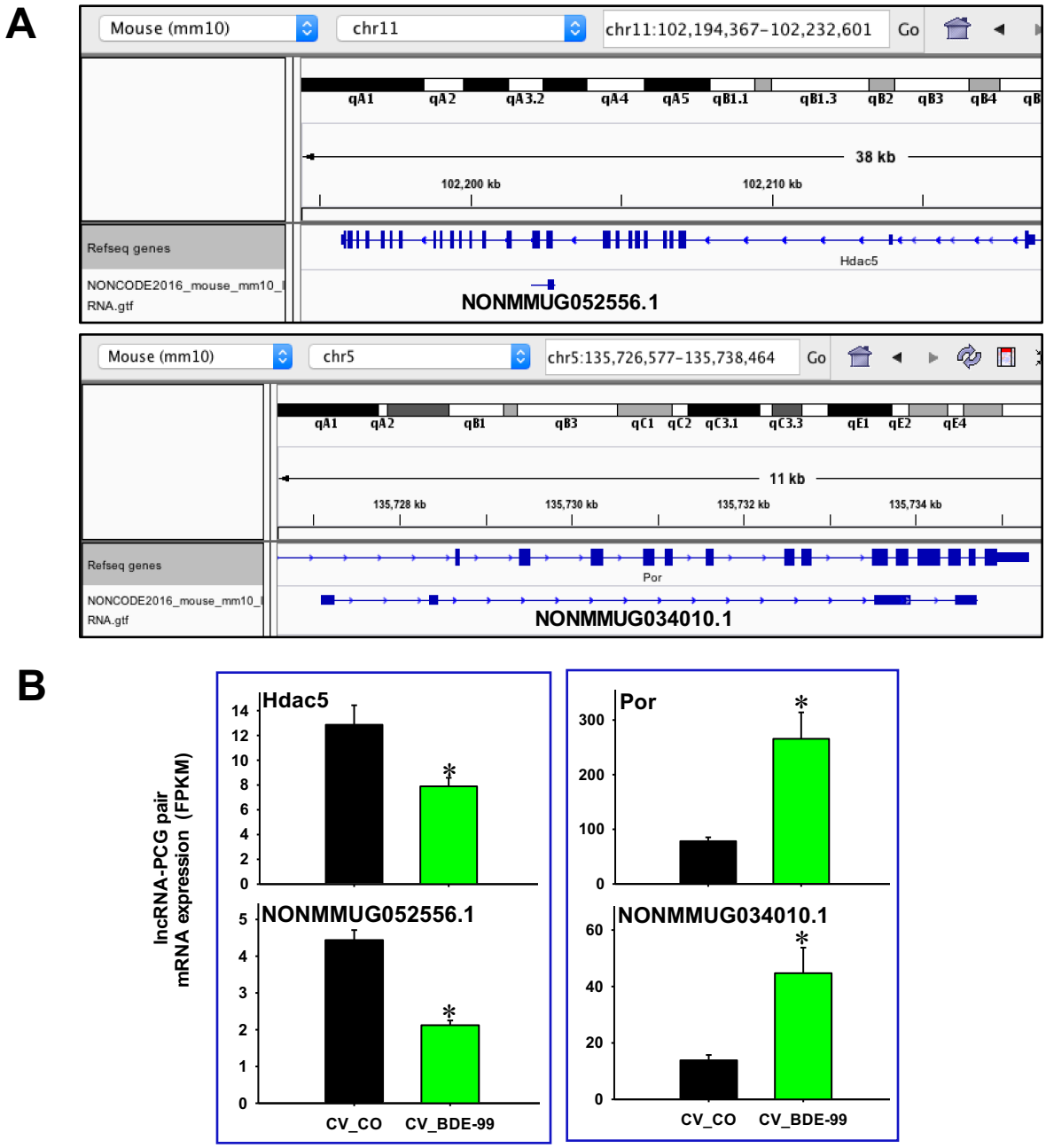

Supplemental Figure 11. Other examples of lncRNA-PCG pairs that were differentially regulated by BDE-47 in livers of GF mice ($p<0.05$) compared to corn oil-treated GF group. RIKEN-derived gene (1700067K01Rik), Family with sequence similarity 213 member B (Fam213b), and tetratricopeptide repeat domain 39C (Ttc39c) are shown.

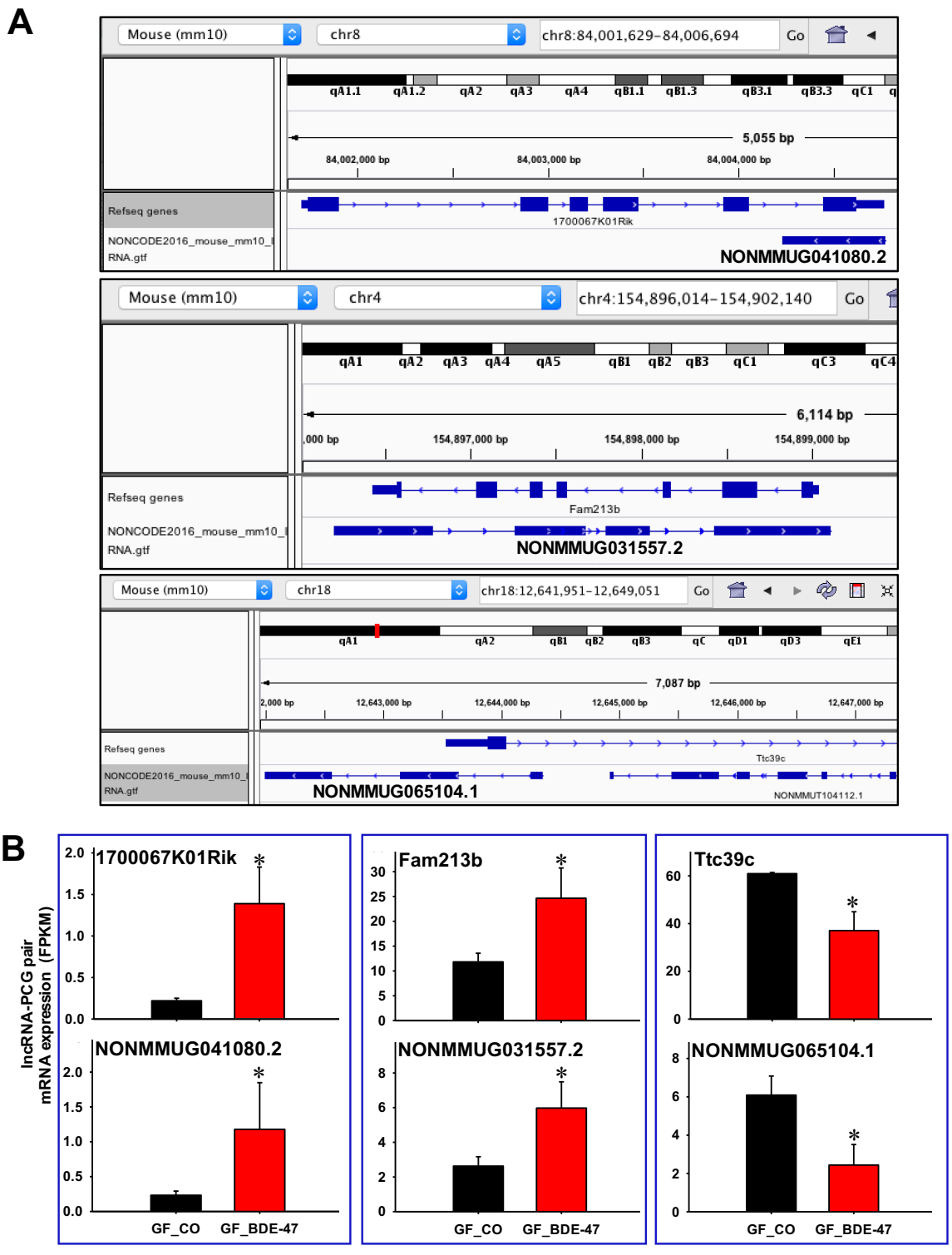

Supplemental Figure 12. Other examples of lncRNA-PCG pairs that were differentially regulated by BDE-47 in livers of GF mice ($p<0.05$) compared to vehicle-treated GF group. Major urinary protein (Gm2083) and two cholesterol metabolism-related genes, namely transforming growth factor beta-stimulated clone 22 homolog (Tsc22d1) and transmembrane 7 superfamily member 2 (Tm7sf2, also known as delta(14)-sterol reductase) are shown here.

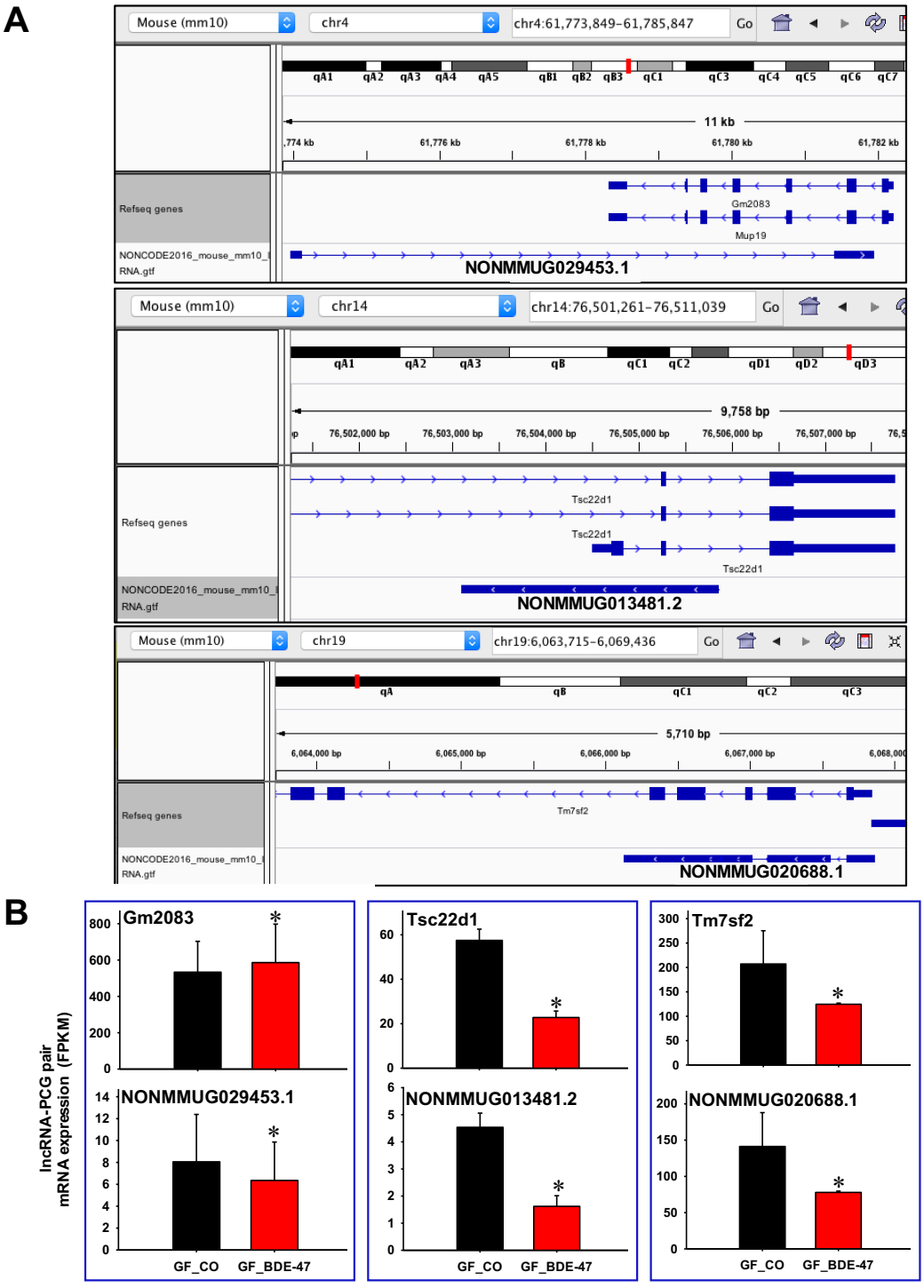

Supplemental Figure 13. KEGG pathways of lncRNA-PCG pairs that were differentially regulated by BDE-99 in livers of GF mice compared to corn oil-treated GF group ($p<0.05$).

KEGG Pathways			
pathway ID	*pathway description*	*count in gene set*	*false discovery rate*
03320	PPAR signaling pathway	12	3.36e-05
01100	Metabolic pathways	47	0.0107
04622	RIG-I-like receptor signaling pathway	8	0.0107
05160	Hepatitis C	11	0.0124
05212	Pancreatic cancer	7	0.027

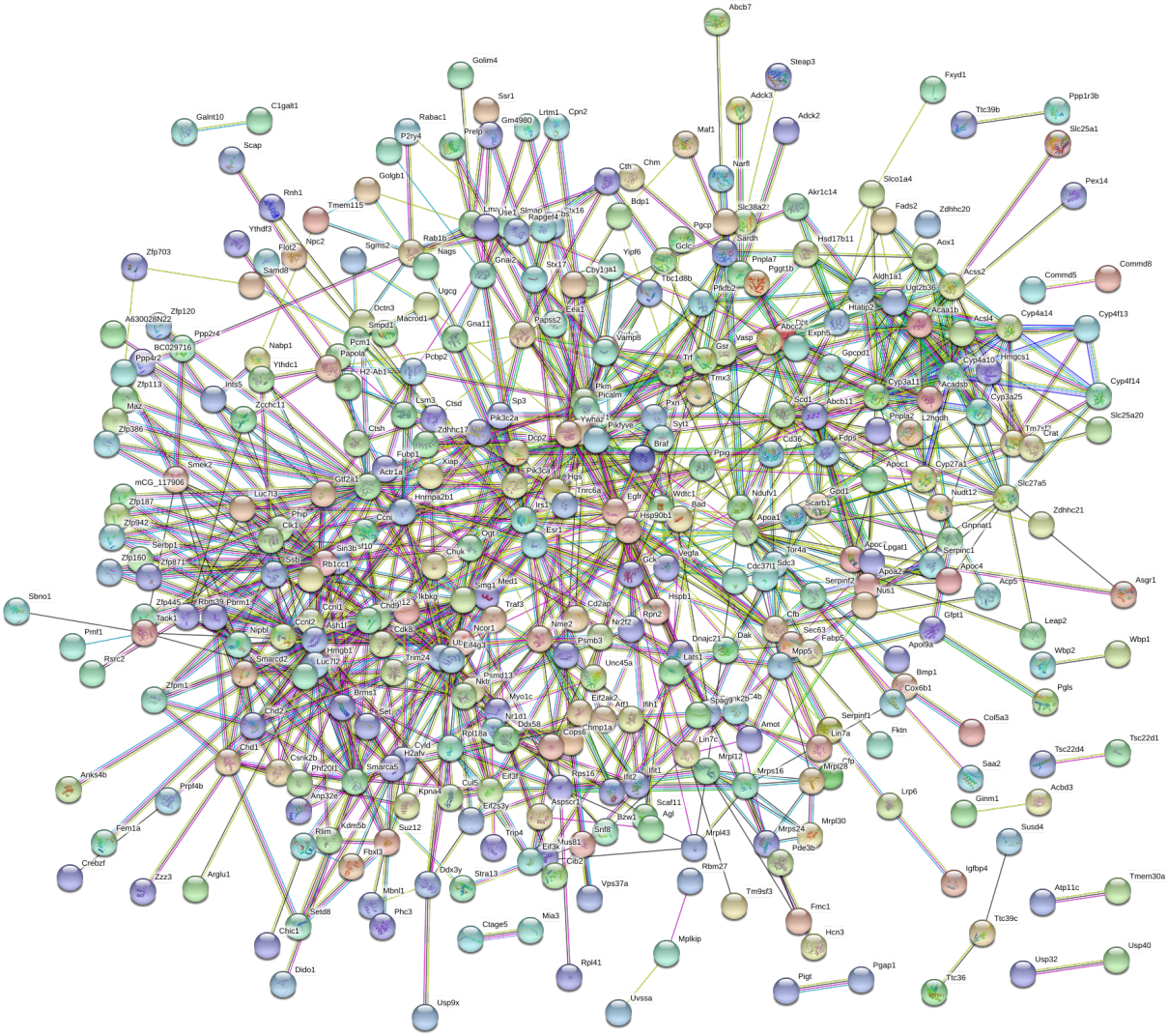

Supplemental Figure 14. Other examples of lncRNA-PCG pairs that were differentially regulated by BDE-99 in livers of GF mice compared to corn oil-treated GF group. Fatty acid desaturase 2 (Fads2), glycoprotein (Cd36), and apolipoprotein (Apo)a1 are shown here.

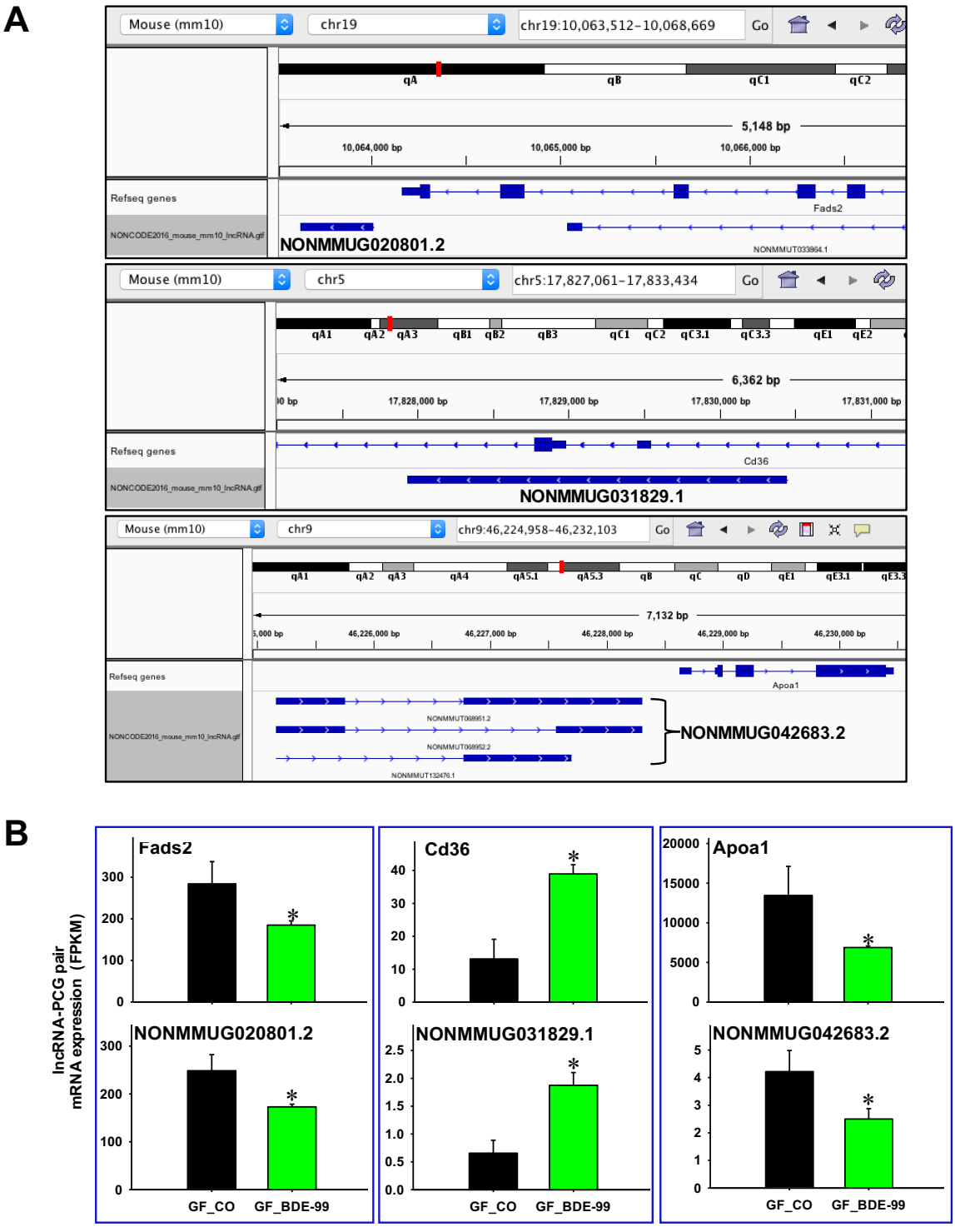

Supplemental Figure 15. More lncRNA-PCG pairs that were differentially regulated by BDE-99 in livers of GF mice compared to corn oil-treated GF group ($p<0.05$). Data were analyzed using STRING Analysis. Apolipoprotein A2 (Apoa2), fatty acid binding protein (Fabp5), and acetyl-CoA acyltransferase 1(Acaa1b) are shown here.

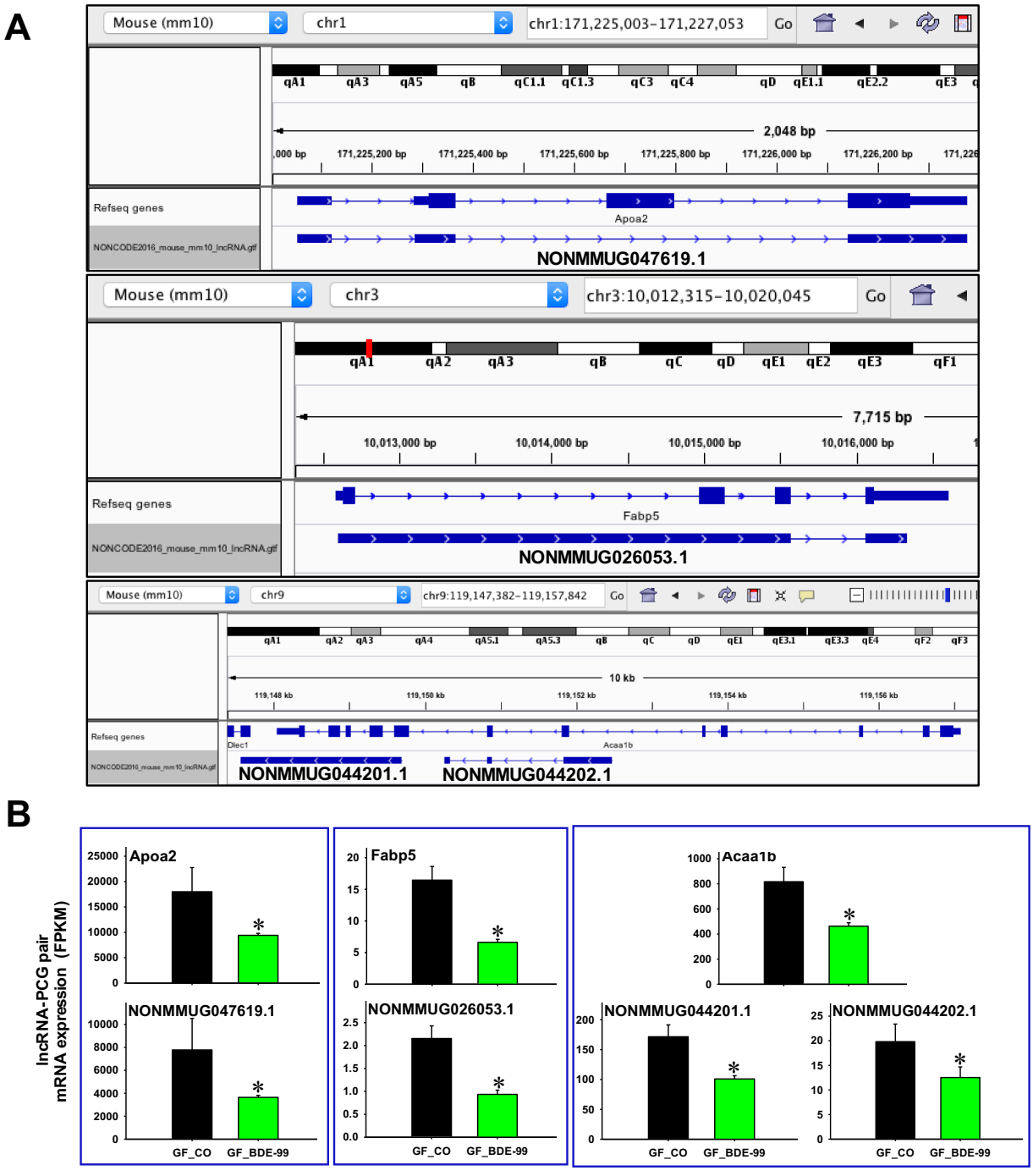

Supplemental Figure 16. More lncRNA-PCG pairs that were differentially regulated by BDE-99 in livers of GF mice compared to corn oil-treated GF group ($p<0.05$). The phase II drug metabolizing enzyme UDP-glucuronosyltransferase (Ugt) 2b36, 3-hydroxymethylglutaryl-CoA synthase (Hmgcs1), and Glutamate-cysteine ligase catalytic subunit (Gclc), which is the rate-limiting enzyme of glutathione synthesis against oxidative stress, are shown here.

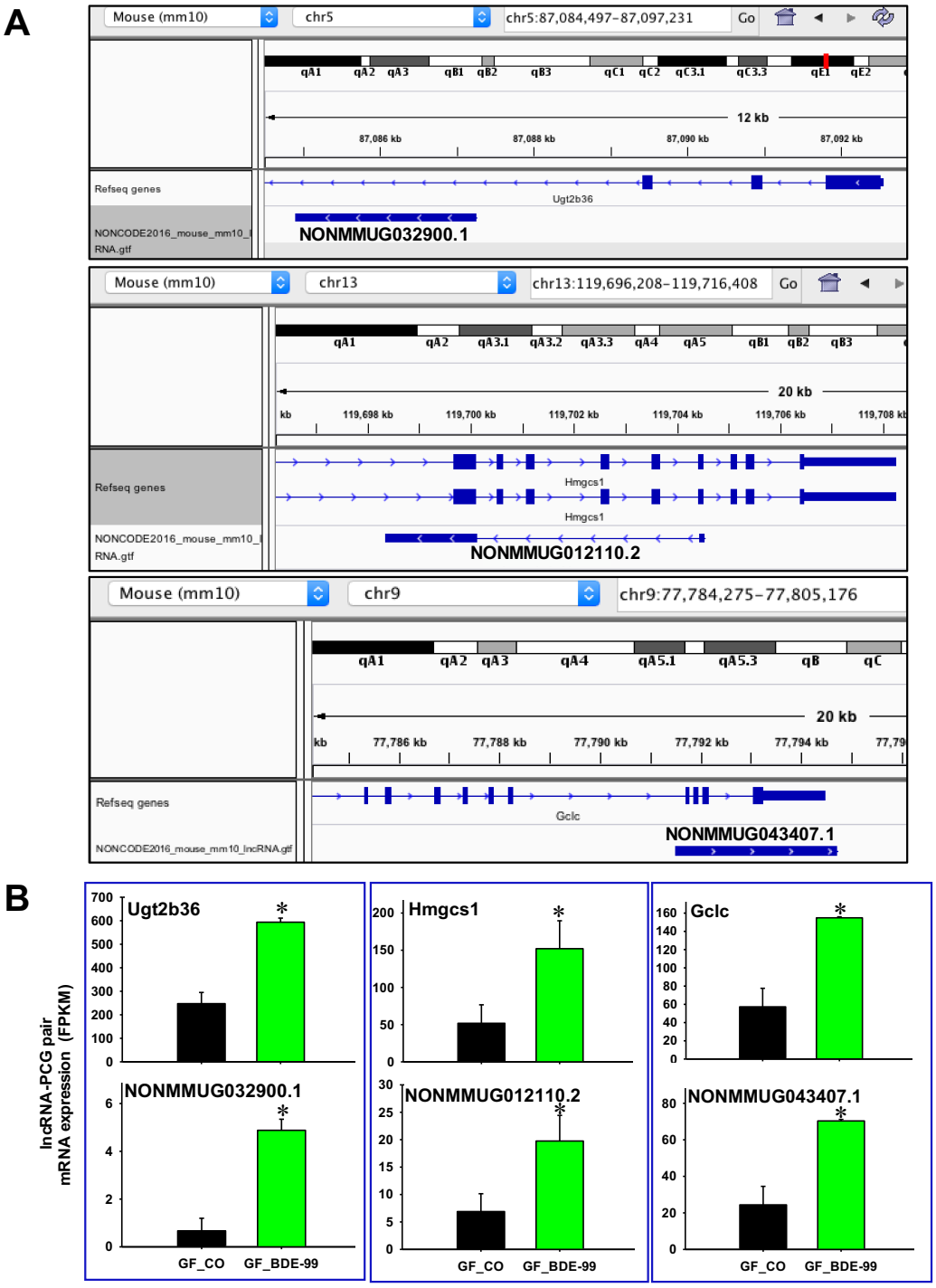

Table 1. Top molecules that were differentially regulated by PBDEs in livers of CV and GF mice compared to the vehicle-treated control group of the same enterotype of mice.

Treatment	Up-regulated		Down-regulated	
	Gene	**Fold-increase**	**Gene**	**% decrease**
CV_CO vs CV_BDE-47	Mt2	37.29	Gadd45g	18%
	Cyp2b10	18.84	Tff2	18%
	Dbp	14.68	Reg3b	17%
	Cyp2b13	14.38	Prap1	17%
	Cyp2c55	13.45	F830016B08Rik	14%
	Rgs16	11.67	Firre	13%
	Saa2	11.17	Neat1	12%
	Lcn2	10.65	Spink3	10%
	Ciart	10.16	Npas2	6%
	Mt1	9.34	Dmbt1	5%
CV_CO vs CV_BDE-99	Cel	533.16	Cdkn1a	16%
	Saa2	389.22	Loxl4	16%
	Ctrb1	334.83	Hcn3	15%
	Rnase1	322.47	Chka	14%
	Cpb1	320.53	Elovl3	14%
	Prss2	284.89	Clic3	13%
	Try5	274.07	Serpina4-ps1	11%
	Prss3	268.69	Gadd45g	8%
	Pnlip	266.54	Arntl	6%
	Lcn2	253.64	Npas2	1%
GFCO vs GF_BDE-47	Sult2a2	25.39	Serpina9	36%
	Sult2a1	24.13	Atrx	36%
	Cyp2b10	22.41	Phip	33%
	Cyp2c55	15.88	F830016B08Rik	32%
	Cyp2b13	12.71	D930016D06Rik	31%
	Akr1b7	9.66	Igip	31%
	A1bg	8.50	Rock1	28%
	Fmo3	8.38	Malat1	25%
	Cyp3a16	7.87	Bcl6	21%
	Pnliprp1	7.66	Snora7a	18%
GFCO vs GF_BDE-99	Cyp2b10	53.56	Tff3	28%
	Cyp2c55	52.83	H2-Ab1	27%
	Meig1	21.79	Flywch2	26%
	Gsta1	19.15	Hbb-bt	25%
	Gstm3	18.41	Serpina3c	24%
	Sult1e1	15.48	Cyp46a1	23%
	Vtcn1	15.42	Rad51b	21%
	Pnliprp1	15.39	Serpina12	18%
	Snhg11	12.46	Acot1	17%
	Akr1b7	12.08	Sult2a1	0%

Table 2. Top molecules that were uniquely regulated by BDE-47 in CV condition, by BDE-99 in CV condition, by BDE-47 in GF condition, and by BDE-99 in GF condition.

Treatment	Up-regulated		Down-regulated	
	Gene	**Fold-increase**	**Gene**	**% decrease**
CV_CO vs CV_BDE-47	Gm7694	2.20	Zfp935	62%
	Mup12	2.07	Snhg5	63%
	Oas1g	2.04	Mapk8ip3	65%
	2010003K11Rik	1.96	Rab26os	66%
	Mup8	1.96	Arid4b	69%
	Oas1a	1.84	Lypd8	70%
	Cib3	1.84	Lgals4	75%
	Plscr1	1.81	Rbp2	76%
	Ms4a6d	1.75	Prpf39	78%
	Cyp4a12b	1.74	Prap1	83%
CV_CO vs CV_BDE-99	Cel	533.16	Fpgs	56%
	Ctrb1	334.83	Ndrg1	56%
	Rnase1	322.47	Szt2	56%
	Cpb1	320.53	Id3	58%
	Prss2	284.89	Elovl5	58%
	Try5	274.07	Phospho1	59%
	Prss3	268.69	Nedd4l	60%
	Pnlip	266.55	Mypop	60%
	2210010C04Rik	240.82	Ngfr	62%
	Cpa1	227.64	Tubb2b	83%
GFCO vs GF_BDE-47	Sult2a2	25.39	Got1	69%
	A1bg	8.50	Sesn2	62%
	Ptgds	5.64	Epha2	59%
	Gmds	3.41	Dct	57%
	Mup4	2.65	Snora7a	18%
	Acot3	2.11		
	Fam213b	2.08		
	Eif4ebp3	2.04		
	Cyp39a1	1.96		
	Mup19	1.88		
GFCO vs GF_BDE-99	Sult1e1	15.48	Ccl5	37%
	Gm11974	8.62	Camk2b	36%
	Mmd2	5.86	Map1lc3a	36%
	Gm14403	5.70	Caln1	33%
	Hsp90aa1	4.52	Ces4a	31%
	Zfp445	4.40	Wfdc2	30%
	Samd9l	4.37	Guca1a	28%
	Aox1	4.24	H2-Eb1	28%
	Robo1	4.01	Flywch2	26%
	Slc10a2	3.90	Serpina3c	24%

Table 3. Differentially regulated lncRNAs paired with neighboring PCGs by PAVIS. lncRNA-PCG pair was defined as lncRNAs overlapped with or within 5 kb upstream and 1 kb downstream of closest PCGs.

Transcripts	**CV_BDE-47**	**CV_BDE-99**	**GF_BDE-47**	**GF_BDE-99**
lncRNAs differentially regulated	345	315	80	968
Annotated lncRNAs	255	214	68	794
lncRNA-PCG pairs	132	130	19	544

Supplemental Table 1. Mapping statistics of RNA-Seq.

Sample	**Total reads**	**reads mapped**	**% mapped**
CV_CO1	127166234	114920125	90.37%
CV_CO2	72155698	52298449	72.48%
CV_CO3	65480436	55736947	85.12%
CV_BDE47_1	115222113	91751368	79.63%
CV_BDE47_2	65093299	56155989	86.27%
CV_BDE47_3	48123870	43165414	89.70%
CV_BDE99_1	105371498	97936933	92.94%
CV_BDE99_2	46057295	42014130	91.22%
GF_CO1	92574095	87136316	94.13%
GF_CO2	84704938	53528596	63.19%
GF_CO3	47418827	43114075	90.92%
GF_BDE47_1	82417373	76999864	93.43%
GF_BDE47_2	38614284	35522885	91.99%
GF_BDE47_3	49942704	38686913	77.46%
GF_BDE99_1	48804600	44545654	91.27%
GF_BDE99_2	50005307	46728929	93.45%
GF_BDE99_3	44559087	41316843	92.72%

Supplemental Table 2. Top 15 networks for PCGs that were differentially regulated by PBDEs in livers of CV and GF mice compared to corn oil-treated control group of the same enterotype of mice. The network in red color was shown in Supplemental Figures.

CV_CO vs CV_BDE-47:

	Top Diseases and Functions	**Focus Molecules**
1	RNA Post-Transcriptional Modification, Developmental Disorder, Hereditary Disorder	34
2	Cellular Development, Cellular Growth and Proliferation, Cell Cycle	32
3	Cancer, Gastrointestinal Disease, Organismal Injury and Abnormalities	30
4	Behavior, Nervous System Development and Function, Antimicrobial Response	27
5	Cancer, Organismal Injury and Abnormalities, Renal and Urological Disease	27
6	Cell Cycle, Gene Expression, Cellular Growth and Proliferation	26

7	Cancer, Cellular Movement, Organismal Injury and Abnormalities	26
8	Lipid Metabolism, Small Molecule Biochemistry, Endocrine System Development and Function	25
9	Dermatological Diseases and Conditions, Organismal Injury and Abnormalities, DNA Replication, Recombination, and Repair	24
10	Carbohydrate Metabolism, Molecular Transport, Cell-To-Cell Signaling and Interaction	24
11	Immunological Disease, Antimicrobial Response, Inflammatory Response	24
12	RNA Damage and Repair, Respiratory System Development and Function, Cancer	23
13	Carbohydrate Metabolism, Cell Morphology, Cellular Assembly and Organization	23
14	Lipid Metabolism, Small Molecule Biochemistry, Drug Metabolism	22
15	Cell Cycle, Cellular Assembly and Organization, DNA Replication, Recombination, and Repair	21

CV_CO vs CV_BDE-99:

	Top Diseases and Functions	Focus Molecules
1	Lipid Metabolism, Small Molecule Biochemistry, Molecular Transport	28
2	Behavior, Nervous System Development and Function, Gene Expression	26
3	Drug Metabolism, Protein Synthesis, Glutathione Depletion In Liver	26
4	RNA Post-Transcriptional Modification, Cell Cycle, Connective Tissue Development and Function	26
5	Endocrine System Disorders, Gastrointestinal Disease, Immunological Disease	26
6	Lipid Metabolism, Small Molecule Biochemistry, Vitamin and Mineral Metabolism	25
7	Gene Expression, Lipid Metabolism, Molecular Transport	24
8	Carbohydrate Metabolism, Cellular Development, Cellular Growth and Proliferation	24
9	Cancer, Connective Tissue Disorders, Endocrine System Disorders	23
10	Endocrine System Disorders, Gastrointestinal Disease, Immunological Disease	22
11	Cardiovascular System Development and Function, Cardiovascular Disease, Cancer	22
12	Cancer, Connective Tissue Disorders, Organismal Injury and Abnormalities	21
13	Lipid Metabolism, Small Molecule Biochemistry, Vitamin and Mineral Metabolism	20
14	Immunological Disease, Endocrine System Disorders, Gastrointestinal Disease	20
15	Cellular Compromise, Cellular Development, Embryonic Development	20

GF_CO vs GF_BDE-47:

	Top Diseases and Functions	Focus Molecules

1	Drug Metabolism, Glutathione Depletion In Liver, Lipid Metabolism	21
2	Lipid Metabolism, Liver Cholestasis, Molecular Transport	21
3	Drug Metabolism, Small Molecule Biochemistry, Cell-To-Cell Signaling and Interaction	19
4	Endocrine System Development and Function, Small Molecule Biochemistry, Drug Metabolism	15
5	Carbohydrate Metabolism, Digestive System Development and Function, Cardiovascular Disease	14
6	Cell-To-Cell Signaling and Interaction, Cell-mediated Immune Response, Cellular Movement	14
7	Organ Development, Reproductive System Development and Function, Developmental Disorder	13
8	Cellular Growth and Proliferation, Lymphoid Tissue Structure and Development, Cellular Development	12
9	Cell-To-Cell Signaling and Interaction, Molecular Transport, Small Molecule Biochemistry	11
10	Cell-To-Cell Signaling and Interaction, Nervous System Development and Function, Cellular Growth and Proliferation	10
11	Embryonic Development, Organismal Development, Tissue Development	10
12	Cell Cycle, Cellular Assembly and Organization, Cancer	1

GF_CO vs GF_BDE-99:

	Top Diseases and Functions	Focus Molecules
1	Cancer, Organismal Injury and Abnormalities, Hereditary Disorder	35
2	Developmental Disorder, Hereditary Disorder, Metabolic Disease	35
3	RNA Post-Transcriptional Modification, Cell Cycle, Developmental Disorder	34
4	Hereditary Disorder, Metabolic Disease, Neurological Disease	34
5	Carbohydrate Metabolism, Drug Metabolism, Molecular Transport	34
6	RNA Post-Transcriptional Modification, Embryonic Development, Organismal Development	34
7	RNA Post-Transcriptional Modification, Carbohydrate Metabolism, Lipid Metabolism	34
8	Gene Expression, Protein Synthesis, Lipid Metabolism	33
9	Cellular Assembly and Organization, Hereditary Disorder, Nephrosis	33
10	Connective Tissue Disorders, Dermatological Diseases and Conditions, Developmental Disorder	33
11	RNA Post-Transcriptional Modification, Cellular Assembly and Organization, Cell Cycle	33
12	Cell Morphology, Cellular Function and Maintenance, Connective Tissue Development and Function	33
13	Cell Morphology, Organ Morphology, Organismal Injury and Abnormalities	33
14	Small Molecule Biochemistry, Dermatological Diseases and Conditions, Hair and Skin Development and Function	32
15	Developmental Disorder, Hereditary Disorder, Organismal Functions	32

References

Abdallah MA and Harrad S (2011) Tetrabromobisphenol-A, hexabromocyclododecane and its degradation products in UK human milk: relationship to external exposure. *Environ Int* **37:**443-448.

Abrego J, Gunda V, Vernucci E, Shukla SK, King RJ, Dasgupta A, Goode G, Murthy D, Yu F, and Singh PK (2017) GOT1-mediated anaplerotic glutamine metabolism regulates chronic acidosis stress in pancreatic cancer cells. *Cancer Lett* **400:**37-46.

Ahn J, Sinha R, Pei Z, Dominianni C, Wu J, Shi J, Goedert JJ, Hayes RB, and Yang L (2013) Human gut microbiome and risk for colorectal cancer. *J Natl Cancer Inst* **105:**1907-1911.

Ainger SA, Yong XL, Wong SS, Skalamera D, Gabrielli B, Leonard JH, and Sturm RA (2014) DCT protects human melanocytic cells from UVR and ROS damage and increases cell viability. *Exp Dermatol* **23:**916-921.

Aleksunes LM and Klaassen CD (2012) Coordinated regulation of hepatic phase I and II drug-metabolizing genes and transporters using AhR-, CAR-, PXR-, PPARalpha-, and Nrf2-null mice. *Drug Metab Dispos* **40:**1366-1379.

Annayev Y, Adar S, Chiou YY, Lieb JD, Sancar A, and Ye R (2014) Gene model 129 (Gm129) encodes a novel transcriptional repressor that modulates circadian gene expression. *J Biol Chem* **289:**5013-5024.

Arnould T, Sellin L, Benzing T, Tsiokas L, Cohen HT, Kim E, and Walz G (1999) Cellular activation triggered by the autosomal dominant polycystic kidney disease gene product PKD2. *Mol Cell Biol* **19:**3423-3434.

Arumugam M, Raes J, Pelletier E, Le Paslier D, Yamada T, Mende DR, Fernandes GR, Tap J, Bruls T, Batto JM, Bertalan M, Borruel N, Casellas F, Fernandez L, Gautier L, Hansen T, Hattori M, Hayashi T, Kleerebezem M, Kurokawa K, Leclerc M, Levenez F, Manichanh C, Nielsen HB, Nielsen T, Pons N, Poulain J, Qin J, Sicheritz-Ponten T, Tims S, Torrents D, Ugarte E, Zoetendal EG, Wang J, Guarner F, Pedersen O, de Vos WM, Brunak S, Dore J, Meta HITC, Antolin M, Artiguenave F, Blottiere HM, Almeida M, Brechot C, Cara C, Chervaux C, Cultrone A, Delorme C, Denariaz G, Dervyn R, Foerstner KU, Friss C, van de Guchte M, Guedon E, Haimet F, Huber W, van Hylckama-Vlieg J, Jamet A, Juste C, Kaci G, Knol J, Lakhdari O, Layec S, Le Roux K, Maguin E, Merieux A, Melo Minardi R, M'Rini C, Muller J, Oozeer R, Parkhill J, Renault P, Rescigno M, Sanchez N, Sunagawa S, Torrejon A, Turner K, Vandemeulebrouck G, Varela E, Winogradsky Y, Zeller G, Weissenbach J, Ehrlich SD, and Bork P (2011) Enterotypes of the human gut microbiome. *Nature* **473:**174-180.

Bai W, Yang J, Yang G, Niu P, Tian L, and Gao A (2014) Long non-coding RNA NR_045623 and NR_028291 involved in benzene hematotoxicity in occupationally benzene-exposed workers. *Exp Mol Pathol* **96:**354-360.

Balasubramanian S, Messmer-Blust AF, Jeyaratnam JA, and Vestal DJ (2011) Role of GTP binding, isoprenylation, and the C-terminal alpha-helices in the inhibition of cell spreading by the interferon-induced GTPase, mouse guanylate-binding protein-2. *J Interferon Cytokine Res* **31:**291-298.

Bechmann LP, Hannivoort RA, Gerken G, Hotamisligil GS, Trauner M, and Canbay A (2012) The interaction of hepatic lipid and glucose metabolism in liver diseases. *J Hepatol* **56:**952-964.

Bellezza I, Roberti R, Gatticchi L, Del Sordo R, Rambotti MG, Marchetti MC, Sidoni A, and Minelli A (2013) A novel role for Tm7sf2 gene in regulating TNFalpha expression. *PLoS One* **8:**e68017.

Bhan A and Mandal SS (2014) Long noncoding RNAs: emerging stars in gene regulation, epigenetics and human disease. *ChemMedChem* **9:**1932-1956.

Bhatt DK and Prasad B (2017) Critical Issues and Optimized Practices in Quantification of Protein Abundance Level to Determine Interindividual Variability in DMET Proteins by LC-MS/MS Proteomics. *Clin Pharmacol Ther*.

Bjorkholm B, Bok CM, Lundin A, Rafter J, Hibberd ML, and Pettersson S (2009) Intestinal microbiota regulate xenobiotic metabolism in the liver. *PLoS One* **4:**e6958.

Boussicault L, Alves S, Lamaziere A, Planques A, Heck N, Moumne L, Despres G, Bolte S, Hu A, Pages C, Galvan L, Piguet F, Aubourg P, Cartier N, Caboche J, and Betuing S (2016) CYP46A1, the rate-limiting enzyme for cholesterol degradation, is neuroprotective in Huntington's disease. *Brain* **139:**953-970.

Brzoska K, Stepkowski TM, and Kruszewski M (2011) Putative proto-oncogene Pir expression is significantly up-regulated in the spleen and kidney of cytosolic superoxide dismutase-deficient mice. *Redox Rep* **16:**129-133.

Bugge A, Feng D, Everett LJ, Briggs ER, Mullican SE, Wang F, Jager J, and Lazar MA (2012) Rev-erbalpha and Rev-erbbeta coordinately protect the circadian clock and normal metabolic function. *Genes Dev* **26:**657-667.

Bumpus NN and Johnson EF (2011) 5-Aminoimidazole-4-carboxyamide-ribonucleoside (AICAR)-stimulated hepatic expression of Cyp4a10, Cyp4a14, Cyp4a31, and other peroxisome proliferator-activated receptor alpha-responsive mouse genes is AICAR 5'-monophosphate-dependent and AMP-activated protein kinase-independent. *J Pharmacol Exp Ther* **339:**886-895.

Cali JJ, Ma D, Sobol M, Simpson DJ, Frackman S, Good TD, Daily WJ, and Liu D (2006) Luminogenic cytochrome P450 assays. *Expert Opin Drug Metab Toxicol* **2:**629-645.

Cali JJ, Ma D, Wood MG, Meisenheimer PL, and Klaubert DH (2012) Bioluminescent assays for ADME evaluation: dialing in CYP selectivity with luminogenic substrates. *Expert Opin Drug Metab Toxicol* **8:**1115-1130.

Canton RF, Sanderson JT, Letcher RJ, Bergman A, and van den Berg M (2005) Inhibition and induction of aromatase (CYP19) activity by brominated flame retardants in H295R human adrenocortical carcinoma cells. *Toxicol Sci* **88:**447-455.

Cao-Ehlker X, Zong X, Hammelmann V, Gruner C, Fenske S, Michalakis S, Wahl-Schott C, and Biel M (2013) Up-regulation of hyperpolarization-activated cyclic nucleotide-gated channel 3 (HCN3) by specific interaction with K+ channel tetramerization domain-containing protein 3 (KCTD3). *J Biol Chem* **288:**7580-7589.

Caporaso JG, Kuczynski J, Stombaugh J, Bittinger K, Bushman FD, Costello EK, Fierer N, Pena AG, Goodrich JK, Gordon JI, Huttley GA, Kelley ST, Knights D, Koenig

JE, Ley RE, Lozupone CA, McDonald D, Muegge BD, Pirrung M, Reeder J, Sevinsky JR, Turnbaugh PJ, Walters WA, Widmann J, Yatsunenko T, Zaneveld J, and Knight R (2010) QIIME allows analysis of high-throughput community sequencing data. *Nat Methods* **7:**335-336.

Chen LJ, Lebetkin EH, Sanders JM, and Burka LT (2006) Metabolism and disposition of 2,2',4,4',5-pentabromodiphenyl ether (BDE99) following a single or repeated administration to rats or mice. *Xenobiotica* **36:**515-534.

Chen S, Shao C, Xu M, Ji J, Xie Y, Lei Y, and Wang X (2015) Macrophage infiltration promotes invasiveness of breast cancer cells via activating long non-coding RNA UCA1. *Int J Clin Exp Pathol* **8:**9052-9061.

Cheng J, Kapranov P, Drenkow J, Dike S, Brubaker S, Patel S, Long J, Stern D, Tammana H, Helt G, Sementchenko V, Piccolboni A, Bekiranov S, Bailey DK, Ganesh M, Ghosh S, Bell I, Gerhard DS, and Gingeras TR (2005) Transcriptional maps of 10 human chromosomes at 5-nucleotide resolution. *Science* **308:**1149-1154.

Chevrier J, Harley KG, Bradman A, Gharbi M, Sjodin A, and Eskenazi B (2010) Polybrominated diphenyl ether (PBDE) flame retardants and thyroid hormone during pregnancy. *Environ Health Perspect* **118:**1444-1449.

Chiang JY (2002) Bile acid regulation of gene expression: roles of nuclear hormone receptors. *Endocr Rev* **23:**443-463.

Chiang JY (2003) Bile acid regulation of hepatic physiology: III. Bile acids and nuclear receptors. *Am J Physiol Gastrointest Liver Physiol* **284:**G349-356.

Chiang JY (2004) Regulation of bile acid synthesis: pathways, nuclear receptors, and mechanisms. *J Hepatol* **40:**539-551.

Chiang JY (2009) Bile acids: regulation of synthesis. *J Lipid Res* **50:**1955-1966.

Choi UY, Kang JS, Hwang YS, and Kim YJ (2015) Oligoadenylate synthase-like (OASL) proteins: dual functions and associations with diseases. *Exp Mol Med* **47:**e144.

Chu Y, Gomez Rosso L, Huang P, Wang Z, Xu Y, Yao X, Bao M, Yan J, Song H, and Wang G (2014) Liver Med23 ablation improves glucose and lipid metabolism through modulating FOXO1 activity. *Cell Res* **24:**1250-1265.

Costa LG and Giordano G (2007) Developmental neurotoxicity of polybrominated diphenyl ether (PBDE) flame retardants. *Neurotoxicology* **28:**1047-1067.

Costa LG, Pellacani C, Dao K, Kavanagh TJ, and Roque PJ (2015) The brominated flame retardant BDE-47 causes oxidative stress and apoptotic cell death in vitro and in vivo in mice. *Neurotoxicology* **48:**68-76.

Cui JY and Klaassen CD (2016) RNA-Seq reveals common and unique PXR- and CAR-target gene signatures in the mouse liver transcriptome. *Biochim Biophys Acta* **1859:**1198-1217.

Cui YJ, Cheng X, Weaver YM, and Klaassen CD (2009) Tissue distribution, gender-divergent expression, ontogeny, and chemical induction of multidrug resistance transporter genes (Mdr1a, Mdr1b, Mdr2) in mice. *Drug Metab Dispos* **37:**203-210.

Damas ND, Marcatti M, Come C, Christensen LL, Nielsen MM, Baumgartner R, Gylling HM, Maglieri G, Rundsten CF, Seemann SE, Rapin N, Thezenas S, Vang S, Orntoft T, Andersen CL, Pedersen JS, and Lund AH (2016) SNHG5 promotes

colorectal cancer cell survival by counteracting STAU1-mediated mRNA destabilization. *Nat Commun* **7:**13875.
Darnerud PO (2003) Toxic effects of brominated flame retardants in man and in wildlife. *Environ Int* **29:**841-853.
Darnerud PO, Eriksen GS, Johannesson T, Larsen PB, and Viluksela M (2001) Polybrominated diphenyl ethers: occurrence, dietary exposure, and toxicology. *Environ Health Perspect* **109 Suppl 1:**49-68.
Darnerud PO and Risberg S (2006) Tissue localisation of tetra- and pentabromodiphenyl ether congeners (BDE-47, -85 and -99) in perinatal and adult C57BL mice. *Chemosphere* **62:**485-493.
Dawson PA, Lan T, and Rao A (2009) Bile acid transporters. *J Lipid Res* **50:**2340-2357.
de Wit CA (2002) An overview of brominated flame retardants in the environment. *Chemosphere* **46:**583-624.
DeBruyne JP, Weaver DR, and Reppert SM (2007) CLOCK and NPAS2 have overlapping roles in the suprachiasmatic circadian clock. *Nat Neurosci* **10:**543-545.
Dempsey JL and Cui JY (2016) Long Non-Coding RNAs: A Novel Paradigm for Toxicology. *Toxicological sciences : an official journal of the Society of Toxicology*.
Derrien M, Belzer C, and de Vos WM (2017) Akkermansia muciniphila and its role in regulating host functions. *Microb Pathog* **106:**171-181.
Diao W, Lu L, Li S, Chen J, Zen K, and Li L (2017) MicroRNA-125b-5p modulates the inflammatory state of macrophages via targeting B7-H4. *Biochem Biophys Res Commun* **491:**912-918.
Ding M, Lu L, and Toth LA (2008) Gene expression in lung and basal forebrain during influenza infection in mice. *Genes Brain Behav* **7:**173-183.
Dingemans MM, van den Berg M, and Westerink RH (2011) Neurotoxicity of brominated flame retardants: (in)direct effects of parent and hydroxylated polybrominated diphenyl ethers on the (developing) nervous system. *Environ Health Perspect* **119:**900-907.
Doldo E, Costanza G, Agostinelli S, Tarquini C, Ferlosio A, Arcuri G, Passeri D, Scioli MG, and Orlandi A (2015) Vitamin A, cancer treatment and prevention: the new role of cellular retinol binding proteins. *Biomed Res Int* **2015:**624627.
Dong B, Zhou Q, Zhao J, Zhou A, Harty RN, Bose S, Banerjee A, Slee R, Guenther J, Williams BR, Wiedmer T, Sims PJ, and Silverman RH (2004) Phospholipid scramblase 1 potentiates the antiviral activity of interferon. *J Virol* **78:**8983-8993.
Dong H, Li Z, Man X, Zhou J, Lu H, and Wang S (2010) Identification of the metabolites of polybrominated diphenyl ether 99 and its related cytochrome P450s. *J Biomed Res* **24:**223-232.
Dumas ME, Barton RH, Toye A, Cloarec O, Blancher C, Rothwell A, Fearnside J, Tatoud R, Blanc V, Lindon JC, Mitchell SC, Holmes E, McCarthy MI, Scott J, Gauguier D, and Nicholson JK (2006) Metabolic profiling reveals a contribution of gut microbiota to fatty liver phenotype in insulin-resistant mice. *Proc Natl Acad Sci U S A* **103:**12511-12516.

Duncan SH, Lobley GE, Holtrop G, Ince J, Johnstone AM, Louis P, and Flint HJ (2008) Human colonic microbiota associated with diet, obesity and weight loss. *Int J Obes (Lond)* **32:**1720-1724.

Dunn LL, Midwinter RG, Ni J, Hamid HA, Parish CR, and Stocker R (2014) New insights into intracellular locations and functions of heme oxygenase-1. *Antioxid Redox Signal* **20:**1723-1742.

Ellen TP, Ke Q, Zhang P, and Costa M (2008) NDRG1, a growth and cancer related gene: regulation of gene expression and function in normal and disease states. *Carcinogenesis* **29:**2-8.

Endsley MA, Njongmeta LM, Shell E, Ryan MW, Indrikovs AJ, Ulualp S, Goldblum RM, Mwangi W, and Estes DM (2009) Human IgA-inducing protein from dendritic cells induces IgA production by naive IgD+ B cells. *J Immunol* **182:**1854-1859.

Engreitz JM, Haines JE, Perez EM, Munson G, Chen J, Kane M, McDonel PE, Guttman M, and Lander ES (2016) Local regulation of gene expression by lncRNA promoters, transcription and splicing. *Nature* **539:**452-455.

Eriksson P, Jakobsson E, and Fredriksson A (2001) Brominated flame retardants: a novel class of developmental neurotoxicants in our environment? *Environ Health Perspect* **109:**903-908.

Erratico C, Zheng X, Ryden A, Marsh G, Maho W, and Covaci A (2015) Human hydroxylated metabolites of BDE-47 and BDE-99 are glucuronidated and sulfated in vitro. *Toxicol Lett* **236:**98-109.

Erratico CA, Moffatt SC, and Bandiera SM (2011) Comparative oxidative metabolism of BDE-47 and BDE-99 by rat hepatic microsomes. *Toxicol Sci* **123:**37-47.

Erratico CA, Szeitz A, and Bandiera SM (2010) Validation of a novel in vitro assay using ultra performance liquid chromatography-mass spectrometry (UPLC/MS) to detect and quantify hydroxylated metabolites of BDE-99 in rat liver microsomes. *J Chromatogr B Analyt Technol Biomed Life Sci* **878:**1562-1568.

Erratico CA, Szeitz A, and Bandiera SM (2012) Oxidative metabolism of BDE-99 by human liver microsomes: predominant role of CYP2B6. *Toxicol Sci* **129:**280-292.

Erratico CA, Szeitz A, and Bandiera SM (2013) Biotransformation of 2,2',4,4'-tetrabromodiphenyl ether (BDE-47) by human liver microsomes: identification of cytochrome P450 2B6 as the major enzyme involved. *Chem Res Toxicol* **26:**721-731.

Farhang-Fallah J, Yin X, Trentin G, Cheng AM, and Rozakis-Adcock M (2000) Cloning and characterization of PHIP, a novel insulin receptor substrate-1 pleckstrin homology domain interacting protein. *J Biol Chem* **275:**40492-40497.

Farrell JJ, Taupin D, Koh TJ, Chen D, Zhao CM, Podolsky DK, and Wang TC (2002) TFF2/SP-deficient mice show decreased gastric proliferation, increased acid secretion, and increased susceptibility to NSAID injury. *J Clin Invest* **109:**193-204.

Feo ML, Gross MS, McGarrigle BP, Eljarrat E, Barcelo D, Aga DS, and Olson JR (2013) Biotransformation of BDE-47 to potentially toxic metabolites is predominantly mediated by human CYP2B6. *Environ Health Perspect* **121:**440-446.

Fernie KJ, Shutt JL, Mayne G, Hoffman D, Letcher RJ, Drouillard KG, and Ritchie IJ (2005) Exposure to polybrominated diphenyl ethers (PBDEs): changes in thyroid,

vitamin A, glutathione homeostasis, and oxidative stress in American kestrels (Falco sparverius). *Toxicol Sci* **88:**375-383.
Fogg PC, O'Neill JS, Dobrzycki T, Calvert S, Lord EC, McIntosh RL, Elliott CJ, Sweeney ST, Hastings MH, and Chawla S (2014) Class IIa histone deacetylases are conserved regulators of circadian function. *J Biol Chem* **289:**34341-34348.
Fraguas S, Barberan S, and Cebria F (2011) EGFR signaling regulates cell proliferation, differentiation and morphogenesis during planarian regeneration and homeostasis. *Dev Biol* **354:**87-101.
Franklin MP, Sathyanarayan A, and Mashek DG (2017) Acyl-CoA Thioesterase 1 (ACOT1) Regulates PPARalpha to Couple Fatty Acid Flux With Oxidative Capacity During Fasting. *Diabetes* **66:**2112-2123.
Fraser DJ, Zumsteg A, and Meyer UA (2003) Nuclear receptors constitutive androstane receptor and pregnane X receptor activate a drug-responsive enhancer of the murine 5-aminolevulinic acid synthase gene. *J Biol Chem* **278:**39392-39401.
Frederiksen M, Vorkamp K, Thomsen M, and Knudsen LE (2009) Human internal and external exposure to PBDEs--a review of levels and sources. *Int J Hyg Environ Health* **212:**109-134.
Fu ZD and Cui JY (2017) Remote Sensing between Liver and Intestine: Importance of Microbial Metabolites. *Curr Pharmacol Rep* **3:**101-113.
Fu ZD, Selwyn FP, Cui JY, and Klaassen CD (2017) RNA-Seq Profiling of Intestinal Expression of Xenobiotic Processing Genes in Germ-Free Mice. *Drug Metab Dispos*.
Gao C, He Z, Li J, Li X, Bai Q, Zhang Z, Zhang X, Wang S, Xiao X, Wang F, Yan Y, Li D, Chen L, Zeng X, Xiao Y, Dong G, Zheng Y, Wang Q, and Chen W (2016) Specific long non-coding RNAs response to occupational PAHs exposure in coke oven workers. *Toxicology Reports* **3:**160-166.
Gascon M, Vrijheid M, Martinez D, Forns J, Grimalt JO, Torrent M, and Sunyer J (2011) Effects of pre and postnatal exposure to low levels of polybromodiphenyl ethers on neurodevelopment and thyroid hormone levels at 4 years of age. *Environ Int* **37:**605-611.
Ge H, Gardner J, Wu X, Rulifson I, Wang J, Xiong Y, Ye J, Belouski E, Cao P, Tang J, Lee KJ, Coberly S, Wu X, Gupte J, Miao L, Yang L, Nguyen N, Shan B, Yeh WC, Veniant MM, Li Y, and Baribault H (2015) Trefoil Factor 3 (TFF3) Is Regulated by Food Intake, Improves Glucose Tolerance and Induces Mucinous Metaplasia. *PLoS One* **10:**e0126924.
Ge X, Yin L, Ma H, Li T, Chiang JY, and Zhang Y (2011) Aldo-keto reductase 1B7 is a target gene of FXR and regulates lipid and glucose homeostasis. *J Lipid Res* **52:**1561-1568.
Geenes V, Chambers J, Khurana R, Shemer EW, Sia W, Mandair D, Elias E, Marschall HU, Hague W, and Williamson C (2015) Rifampicin in the treatment of severe intrahepatic cholestasis of pregnancy. *Eur J Obstet Gynecol Reprod Biol* **189:**59-63.
Gerecke AC, Giger W, Hartmann PC, Heeb NV, Kohler HP, Schmid P, Zennegg M, and Kohler M (2006) Anaerobic degradation of brominated flame retardants in sewage sludge. *Chemosphere* **64:**311-317.

Giordano G, Kavanagh TJ, and Costa LG (2008) Neurotoxicity of a polybrominated diphenyl ether mixture (DE-71) in mouse neurons and astrocytes is modulated by intracellular glutathione levels. *Toxicol Appl Pharmacol* **232:**161-168.

Goodrich JK, Davenport ER, Beaumont M, Jackson MA, Knight R, Ober C, Spector TD, Bell JT, Clark AG, and Ley RE (2016) Genetic Determinants of the Gut Microbiome in UK Twins. *Cell Host Microbe* **19:**731-743.

Goodwin B, Jones SA, Price RR, Watson MA, McKee DD, Moore LB, Galardi C, Wilson JG, Lewis MC, Roth ME, Maloney PR, Willson TM, and Kliewer SA (2000) A regulatory cascade of the nuclear receptors FXR, SHP-1, and LRH-1 represses bile acid biosynthesis. *Mol Cell* **6:**517-526.

Grechez-Cassiau A, Feillet C, Guerin S, and Delaunay F (2015) The hepatic circadian clock regulates the choline kinase alpha gene through the BMAL1-REV-ERBalpha axis. *Chronobiol Int* **32:**774-784.

Gross MS, Butryn DM, McGarrigle BP, Aga DS, and Olson JR (2015) Primary role of cytochrome P450 2B6 in the oxidative metabolism of 2,2',4,4',6-pentabromodiphenyl ether (BDE-100) to hydroxylated BDEs. *Chem Res Toxicol* **28:**672-681.

Gupta RA, Shah N, Wang KC, Kim J, Horlings HM, Wong DJ, Tsai MC, Hung T, Argani P, Rinn JL, Wang Y, Brzoska P, Kong B, Li R, West RB, van de Vijver MJ, Sukumar S, and Chang HY (2010) Long non-coding RNA HOTAIR reprograms chromatin state to promote cancer metastasis. *Nature* **464:**1071-1076.

Guttman M, Amit I, Garber M, French C, Lin MF, Feldser D, Huarte M, Zuk O, Carey BW, Cassady JP, Cabili MN, Jaenisch R, Mikkelsen TS, Jacks T, Hacohen N, Bernstein BE, Kellis M, Regev A, Rinn JL, and Lander ES (2009) Chromatin signature reveals over a thousand highly conserved large non-coding RNAs in mammals. *Nature* **458:**223-227.

Guttman M, Donaghey J, Carey BW, Garber M, Grenier JK, Munson G, Young G, Lucas AB, Ach R, Bruhn L, Yang X, Amit I, Meissner A, Regev A, Rinn JL, Root DE, and Lander ES (2011) lincRNAs act in the circuitry controlling pluripotency and differentiation. *Nature* **477:**295-300.

Guvenius DM, Aronsson A, Ekman-Ordeberg G, Bergman A, and Noren K (2003) Human prenatal and postnatal exposure to polybrominated diphenyl ethers, polychlorinated biphenyls, polychlorobiphenylols, and pentachlorophenol. *Environ Health Perspect* **111:**1235-1241.

Hakk H, Larsen G, and Klasson-Wehler E (2002) Tissue disposition, excretion and metabolism of 2,2',4,4',5-pentabromodiphenyl ether (BDE-99) in the male Sprague-Dawley rat. *Xenobiotica* **32:**369-382.

Hallgren S, Sinjari T, Hakansson H, and Darnerud PO (2001) Effects of polybrominated diphenyl ethers (PBDEs) and polychlorinated biphenyls (PCBs) on thyroid hormone and vitamin A levels in rats and mice. *Arch Toxicol* **75:**200-208.

Hamers T, Kamstra JH, Sonneveld E, Murk AJ, Kester MH, Andersson PL, Legler J, and Brouwer A (2006) In vitro profiling of the endocrine-disrupting potency of brominated flame retardants. *Toxicol Sci* **92:**157-173.

Hamers T, Kamstra JH, Sonneveld E, Murk AJ, Visser TJ, Van Velzen MJ, Brouwer A, and Bergman A (2008) Biotransformation of brominated flame retardants into

potentially endocrine-disrupting metabolites, with special attention to 2,2',4,4'-tetrabromodiphenyl ether (BDE-47). *Mol Nutr Food Res* **52:**284-298.

Hardbower DM, Singh K, Asim M, Verriere TG, Olivares-Villagomez D, Barry DP, Allaman MM, Washington MK, Peek RM, Jr., Piazuelo MB, and Wilson KT (2016) EGFR regulates macrophage activation and function in bacterial infection. *J Clin Invest* **126:**3296-3312.

Harris IR, Hoppner H, Siefken W, Farrell AM, and Wittern KP (2000) Regulation of HMG-CoA synthase and HMG-CoA reductase by insulin and epidermal growth factor in HaCaT keratinocytes. *J Invest Dermatol* **114:**83-87.

Hartmann S, Ridley AJ, and Lutz S (2015) The Function of Rho-Associated Kinases ROCK1 and ROCK2 in the Pathogenesis of Cardiovascular Disease. *Front Pharmacol* **6:**276.

He J, Robrock KR, and Alvarez-Cohen L (2006) Microbial reductive debromination of polybrominated diphenyl ethers (PBDEs). *Environ Sci Technol* **40:**4429-4434.

He P, He W, Wang A, Xia T, Xu B, Zhang M, and Chen X (2008) PBDE-47-induced oxidative stress, DNA damage and apoptosis in primary cultured rat hippocampal neurons. *Neurotoxicology* **29:**124-129.

Hellstrom I, Raycraft J, Hayden-Ledbetter M, Ledbetter JA, Schummer M, McIntosh M, Drescher C, Urban N, and Hellstrom KE (2003) The HE4 (WFDC2) protein is a biomarker for ovarian carcinoma. *Cancer Res* **63:**3695-3700.

Hildebrandt TM, Di Meo I, Zeviani M, Viscomi C, and Braun HP (2013) Proteome adaptations in Ethe1-deficient mice indicate a role in lipid catabolism and cytoskeleton organization via post-translational protein modifications. *Biosci Rep* **33**.

Hites RA (2004) Polybrominated diphenyl ethers in the environment and in people: a meta-analysis of concentrations. *Environ Sci Technol* **38:**945-956.

Hoekstra M, Li Z, Kruijt JK, Van Eck M, Van Berkel TJ, and Kuiper J (2010) The expression level of non-alcoholic fatty liver disease-related gene PNPLA3 in hepatocytes is highly influenced by hepatic lipid status. *J Hepatol* **52:**244-251.

Holmes RS, Wright MW, Laulederkind SJ, Cox LA, Hosokawa M, Imai T, Ishibashi S, Lehner R, Miyazaki M, Perkins EJ, Potter PM, Redinbo MR, Robert J, Satoh T, Yamashita T, Yan B, Yokoi T, Zechner R, and Maltais LJ (2010) Recommended nomenclature for five mammalian carboxylesterase gene families: human, mouse, and rat genes and proteins. *Mamm Genome* **21:**427-441.

Hong S, Moreno-Navarrete JM, Wei X, Kikukawa Y, Tzameli I, Prasad D, Lee Y, Asara JM, Fernandez-Real JM, Maratos-Flier E, and Pissios P (2015) Nicotinamide N-methyltransferase regulates hepatic nutrient metabolism through Sirt1 protein stabilization. *Nat Med* **21:**887-894.

Hooper K, She J, Sharp M, Chow J, Jewell N, Gephart R, and Holden A (2007) Depuration of polybrominated diphenyl ethers (PBDEs) and polychlorinated biphenyls (PCBs) in breast milk from California first-time mothers (primiparae). *Environ Health Perspect* **115:**1271-1275.

Hovander L, Athanasiadou M, Asplund L, Jensen S, and Wehler EK (2000) Extraction and cleanup methods for analysis of phenolic and neutral organohalogens in plasma. *J Anal Toxicol* **24:**696-703.

Hrycay EG and Bandiera SM (2009) Expression, function and regulation of mouse cytochrome P450 enzymes: comparison with human P450 enzymes. *Curr Drug Metab* **10:**1151-1183.

Hu X, Bonde Y, Eggertsen G, and Rudling M (2014) Muricholic bile acids are potent regulators of bile acid synthesis via a positive feedback mechanism. *J Intern Med* **275:**27-38.

Huang H, Bogstie JN, and Vogel HJ (2012) Biophysical and structural studies of the human calcium- and integrin-binding protein family: understanding their functional similarities and differences. *Biochem Cell Biol* **90:**646-656.

Huang W, Loganantharaj R, Schroeder B, Fargo D, and Li L (2013) PAVIS: a tool for Peak Annotation and Visualization. *Bioinformatics* **29:**3097-3099.

Hui DY and Howles PN (2002) Carboxyl ester lipase: structure-function relationship and physiological role in lipoprotein metabolism and atherosclerosis. *J Lipid Res* **43:**2017-2030.

Hung T, Wang Y, Lin MF, Koegel AK, Kotake Y, Grant GD, Horlings HM, Shah N, Umbricht C, Wang P, Wang Y, Kong B, Langerod A, Borresen-Dale AL, Kim SK, van de Vijver M, Sukumar S, Whitfield ML, Kellis M, Xiong Y, Wong DJ, and Chang HY (2011) Extensive and coordinated transcription of noncoding RNAs within cell-cycle promoters. *Nat Genet* **43:**621-629.

Hunt MC, Siponen MI, and Alexson SE (2012) The emerging role of acyl-CoA thioesterases and acyltransferases in regulating peroxisomal lipid metabolism. *Biochim Biophys Acta* **1822:**1397-1410.

Ikeda H, Ueda M, Ikeda M, Kobayashi H, and Honda Y (2003) Oxysterol 7alpha-hydroxylase (CYP39A1) in the ciliary nonpigmented epithelium of bovine eye. *Lab Invest* **83:**349-355.

Inagaki T, Choi M, Moschetta A, Peng L, Cummins CL, McDonald JG, Luo G, Jones SA, Goodwin B, Richardson JA, Gerard RD, Repa JJ, Mangelsdorf DJ, and Kliewer SA (2005) Fibroblast growth factor 15 functions as an enterohepatic signal to regulate bile acid homeostasis. *Cell Metab* **2:**217-225.

Jager J, Greiner V, Strzoda D, Seibert O, Niopek K, Sijmonsma TP, Schafer M, Jones A, De Guia R, Martignoni M, Dallinga-Thie GM, Diaz MB, Hofmann TG, and Herzig S (2014) Hepatic transforming growth factor-beta 1 stimulated clone-22 D1 controls systemic cholesterol metabolism. *Mol Metab* **3:**155-166.

Jaglin XH, Poirier K, Saillour Y, Buhler E, Tian G, Bahi-Buisson N, Fallet-Bianco C, Phan-Dinh-Tuy F, Kong XP, Bomont P, Castelnau-Ptakhine L, Odent S, Loget P, Kossorotoff M, Snoeck I, Plessis G, Parent P, Beldjord C, Cardoso C, Represa A, Flint J, Keays DA, Cowan NJ, and Chelly J (2009) Mutations in the beta-tubulin gene TUBB2B result in asymmetrical polymicrogyria. *Nat Genet* **41:**746-752.

Jiang S, Heller B, Tagliabracci VS, Zhai L, Irimia JM, DePaoli-Roach AA, Wells CD, Skurat AV, and Roach PJ (2010) Starch binding domain-containing protein 1/genethonin 1 is a novel participant in glycogen metabolism. *J Biol Chem* **285:**34960-34971.

Jumpertz R, Le DS, Turnbaugh PJ, Trinidad C, Bogardus C, Gordon JI, and Krakoff J (2011) Energy-balance studies reveal associations between gut microbes, caloric load, and nutrient absorption in humans. *Am J Clin Nutr* **94:**58-65.

Kageyama R, Ohtsuka T, and Kobayashi T (2007) The Hes gene family: repressors and oscillators that orchestrate embryogenesis. *Development* **134:**1243-1251.
Kamizono S, Duncan GS, Seidel MG, Morimoto A, Hamada K, Grosveld G, Akashi K, Lind EF, Haight JP, Ohashi PS, Look AT, and Mak TW (2009) Nfil3/E4bp4 is required for the development and maturation of NK cells in vivo. *J Exp Med* **206:**2977-2986.
Karlsson O and Baccarelli AA (2016) Environmental Health and Long Non-coding RNAs. *Curr Environ Health Rep* **3:**178-187.
Kido H, Fukusen N, and Katunuma N (1985) Chymotrypsin- and trypsin-type serine proteases in rat mast cells: properties and functions. *Arch Biochem Biophys* **239:**436-443.
Kim D, Langmead B, and Salzberg SL (2015) HISAT: a fast spliced aligner with low memory requirements. *Nat Methods* **12:**357-360.
Kim MS, Kim SS, Jung ST, Park JY, Yoo HW, Ko J, Csiszar K, Choi SY, and Kim Y (2003) Expression and purification of enzymatically active forms of the human lysyl oxidase-like protein 4. *J Biol Chem* **278:**52071-52074.
Kitiratschky VB, Behnen P, Kellner U, Heckenlively JR, Zrenner E, Jagle H, Kohl S, Wissinger B, and Koch KW (2009) Mutations in the GUCA1A gene involved in hereditary cone dystrophies impair calcium-mediated regulation of guanylate cyclase. *Hum Mutat* **30:**E782-796.
Klaassen CD and Aleksunes LM (2010) Xenobiotic, bile acid, and cholesterol transporters: function and regulation. *Pharmacol Rev* **62:**1-96.
Klaassen CD and Cui JY (2015) Review: Mechanisms of How the Intestinal Microbiota Alters the Effects of Drugs and Bile Acids. *Drug Metab Dispos* **43:**1505-1521.
Klaassen CD and Slitt AL (2005) Regulation of hepatic transporters by xenobiotic receptors. *Curr Drug Metab* **6:**309-328.
Kliewer SA, Goodwin B, and Willson TM (2002) The nuclear pregnane X receptor: a key regulator of xenobiotic metabolism. *Endocr Rev* **23:**687-702.
Knights D, Ward TL, McKinlay CE, Miller H, Gonzalez A, McDonald D, and Knight R (2014) Rethinking "enterotypes". *Cell Host Microbe* **16:**433-437.
Kong B, Wang L, Chiang JY, Zhang Y, Klaassen CD, and Guo GL (2012) Mechanism of tissue-specific farnesoid X receptor in suppressing the expression of genes in bile-acid synthesis in mice. *Hepatology* **56:**1034-1043.
Kool MJ, van de Bree JE, Bodde HE, Elgersma Y, and van Woerden GM (2016) The molecular, temporal and region-specific requirements of the beta isoform of Calcium/Calmodulin-dependent protein kinase type 2 (CAMK2B) in mouse locomotion. *Sci Rep* **6:**26989.
Kubota Y, Nomura K, Katoh Y, Yamashita R, Kaneko K, and Furuyama K (2016) Novel Mechanisms for Heme-dependent Degradation of ALAS1 Protein as a Component of Negative Feedback Regulation of Heme Biosynthesis. *J Biol Chem* **291:**20516-20529.
Kumamoto T and Oshio S (2013) Effect of fetal exposure to bisphenol A on brain mediated by X-chromosome inactivation. *J Toxicol Sci* **38:**485-494.
Lan X, Yan J, Ren J, Zhong B, Li J, Li Y, Liu L, Yi J, Sun Q, Yang X, Sun J, Meng L, Zhu W, Holmdahl R, Li D, and Lu S (2016) A novel long noncoding RNA Lnc-HC

binds hnRNPA2B1 to regulate expressions of Cyp7a1 and Abca1 in hepatocytic cholesterol metabolism. *Hepatology* **64:**58-72.

Langille MG, Zaneveld J, Caporaso JG, McDonald D, Knights D, Reyes JA, Clemente JC, Burkepile DE, Vega Thurber RL, Knight R, Beiko RG, and Huttenhower C (2013) Predictive functional profiling of microbial communities using 16S rRNA marker gene sequences. *Nat Biotechnol* **31:**814-821.

Lasorella A, Benezra R, and Iavarone A (2014) The ID proteins: master regulators of cancer stem cells and tumour aggressiveness. *Nat Rev Cancer* **14:**77-91.

Lee C, Ding X, and Riddick DS (2013) The role of cytochrome P450-dependent metabolism in the regulation of mouse hepatic growth hormone signaling components and target genes by 3-methylcholanthrene. *Drug Metab Dispos* **41:**457-465.

Lee JH, Bodmer R, Bier E, and Karin M (2010) Sestrins at the crossroad between stress and aging. *Aging (Albany NY)* **2:**369-374.

Lee JS, Lee S, Lim BC, Kim KJ, Hwang YS, Choi M, and Chae JH (2015) Alpha-thalassemia X-linked intellectual disability syndrome identified by whole exome sequencing in two boys with white matter changes and developmental retardation. *Gene* **569:**318-322.

Ley RE, Backhed F, Turnbaugh P, Lozupone CA, Knight RD, and Gordon JI (2005) Obesity alters gut microbial ecology. *Proc Natl Acad Sci U S A* **102:**11070-11075.

Li C, Fan Y, Lan TH, Lambert NA, and Wu G (2012) Rab26 modulates the cell surface transport of alpha2-adrenergic receptors from the Golgi. *J Biol Chem* **287:**42784-42794.

Li CY, Cheng SL, Bammler TK, and Cui JY (2016a) Editor's Highlight: Neonatal Activation of the Xenobiotic-Sensors PXR and CAR Results in Acute and Persistent Down-regulation of PPARalpha-Signaling in Mouse Liver. *Toxicol Sci* **153:**282-302.

Li CY, Lee S, Cade S, Kuo LJ, Schultz IR, Bhatt DK, Prasad B, Bammler TK, and Cui JY (2017) Novel Interactions between Gut Microbiome and Host Drug-Processing Genes Modify the Hepatic Metabolism of the Environmental Chemicals Polybrominated Diphenyl Ethers. *Drug Metab Dispos* **45:**1197-1214.

Li CY, Renaud HJ, Klaassen CD, and Cui JY (2016b) Age-Specific Regulation of Drug-Processing Genes in Mouse Liver by Ligands of Xenobiotic-Sensing Transcription Factors. *Drug Metab Dispos* **44:**1038-1049.

Li H, Handsaker B, Wysoker A, Fennell T, Ruan J, Homer N, Marth G, Abecasis G, Durbin R, and Genome Project Data Processing S (2009a) The Sequence Alignment/Map format and SAMtools. *Bioinformatics* **25:**2078-2079.

Li LO, Ellis JM, Paich HA, Wang S, Gong N, Altshuller G, Thresher RJ, Koves TR, Watkins SM, Muoio DM, Cline GW, Shulman GI, and Coleman RA (2009b) Liver-specific loss of long chain acyl-CoA synthetase-1 decreases triacylglycerol synthesis and beta-oxidation and alters phospholipid fatty acid composition. *J Biol Chem* **284:**27816-27826.

Li P, Ruan X, Yang L, Kiesewetter K, Zhao Y, Luo H, Chen Y, Gucek M, Zhu J, and Cao H (2015) A liver-enriched long non-coding RNA, lncLSTR, regulates systemic lipid metabolism in mice. *Cell Metab* **21:**455-467.

Li T and Chiang JY (2009) Regulation of bile acid and cholesterol metabolism by PPARs. *PPAR Res* **2009:**501739.

Lickteig AJ, Csanaky IL, Pratt-Hyatt M, and Klaassen CD (2016) Activation of Constitutive Androstane Receptor (CAR) in Mice Results in Maintained Biliary Excretion of Bile Acids Despite a Marked Decrease of Bile Acids in Liver. *Toxicol Sci*.

Lim KT, Lee SC, Gao Y, Kim KP, Song G, An SY, Adachi K, Jang YJ, Kim J, Oh KJ, Kwak TH, Hwang SI, You JS, Ko K, Koo SH, Sharma AD, Kim JH, Hui L, Cantz T, Scholer HR, and Han DW (2016) Small Molecules Facilitate Single Factor-Mediated Hepatic Reprogramming. *Cell Rep*.

Linares V, Belles M, and Domingo JL (2015) Human exposure to PBDE and critical evaluation of health hazards. *Arch Toxicol* **89:**335-356.

Lind Y, Darnerud PO, Atuma S, Aune M, Becker W, Bjerselius R, Cnattingius S, and Glynn A (2003) Polybrominated diphenyl ethers in breast milk from Uppsala County, Sweden. *Environ Res* **93:**186-194.

Lindahl U, Pejler G, Bogwald J, and Seljelid R (1989) A prothrombinase complex of mouse peritoneal macrophages. *Arch Biochem Biophys* **273:**180-188.

Lio YC, Mazin AV, Kowalczykowski SC, and Chen DJ (2003) Complex formation by the human Rad51B and Rad51C DNA repair proteins and their activities in vitro. *J Biol Chem* **278:**2469-2478.

Liu MJ, Takahashi Y, Wada T, He J, Gao J, Tian Y, Li S, and Xie W (2009) The aldo-keto reductase Akr1b7 gene is a common transcriptional target of xenobiotic receptors pregnane X receptor and constitutive androstane receptor. *Mol Pharmacol* **76:**604-611.

Loewer S, Cabili MN, Guttman M, Loh YH, Thomas K, Park IH, Garber M, Curran M, Onder T, Agarwal S, Manos PD, Datta S, Lander ES, Schlaeger TM, Daley GQ, and Rinn JL (2010) Large intergenic non-coding RNA-RoR modulates reprogramming of human induced pluripotent stem cells. *Nat Genet* **42:**1113-1117.

Lorber M (2008) Exposure of Americans to polybrominated diphenyl ethers. *J Expo Sci Environ Epidemiol* **18:**2-19.

Lossos IS, Akasaka T, Martinez-Climent JA, Siebert R, and Levy R (2003) The BCL6 gene in B-cell lymphomas with 3q27 translocations is expressed mainly from the rearranged allele irrespective of the partner gene. *Leukemia* **17:**1390-1397.

Lu SC (2009) Regulation of glutathione synthesis. *Mol Aspects Med* **30:**42-59.

Lupton SJ, McGarrigle BP, Olson JR, Wood TD, and Aga DS (2009) Human liver microsome-mediated metabolism of brominated diphenyl ethers 47, 99, and 153 and identification of their major metabolites. *Chem Res Toxicol* **22:**1802-1809.

Madia F, Giordano G, Fattori V, Vitalone A, Branchi I, Capone F, and Costa LG (2004) Differential in vitro neurotoxicity of the flame retardant PBDE-99 and of the PCB Aroclor 1254 in human astrocytoma cells. *Toxicol Lett* **154:**11-21.

Maghazachi AA, Al-Aoukaty A, and Schall TJ (1996) CC chemokines induce the generation of killer cells from CD56+ cells. *Eur J Immunol* **26:**315-319.

Malmberg T, Athanasiadou M, Marsh G, Brandt I, and Bergman A (2005) Identification of hydroxylated polybrominated diphenyl ether metabolites in blood plasma from polybrominated diphenyl ether exposed rats. *Environ Sci Technol* **39:**5342-5348.

Mann SS and Hammarback JA (1996) Gene localization and developmental expression of light chain 3: a common subunit of microtubule-associated protein 1A(MAP1A) and MAP1B. *J Neurosci Res* **43:**535-544.

Marsh G, Athanasiadou M, Athanassiadis I, and Sandholm A (2006) Identification of hydroxylated metabolites in 2,2',4,4'-tetrabromodiphenyl ether exposed rats. *Chemosphere* **63:**690-697.

Meerts IA, van Zanden JJ, Luijks EA, van Leeuwen-Bol I, Marsh G, Jakobsson E, Bergman A, and Brouwer A (2000) Potent competitive interactions of some brominated flame retardants and related compounds with human transthyretin in vitro. *Toxicol Sci* **56:**95-104.

Meijer L, Hafkamp AM, Bosman WE, Havinga R, Bergman A, Sauer PJ, and Verkade HJ (2006) Nonabsorbable dietary fat enhances disposal of 2,2',4,4'-tetrabromodiphenyl ether in rats through interruption of enterohepatic circulation. *J Agric Food Chem* **54:**6440-6444.

Ming X and Thakker DR (2010) Role of basolateral efflux transporter MRP4 in the intestinal absorption of the antiviral drug adefovir dipivoxil. *Biochem Pharmacol* **79:**455-462.

Miyata M, Hayashi K, Yamakawa H, Yamazoe Y, and Yoshinari K (2015) Antibacterial drug treatment increases intestinal bile acid absorption via elevated levels of ileal apical sodium-dependent bile acid transporter but not organic solute transporter alpha protein. *Biol Pharm Bull* **38:**493-496.

Molotkov A and Duester G (2003) Genetic evidence that retinaldehyde dehydrogenase Raldh1 (Aldh1a1) functions downstream of alcohol dehydrogenase Adh1 in metabolism of retinol to retinoic acid. *J Biol Chem* **278:**36085-36090.

Moreau A, Vilarem MJ, Maurel P, and Pascussi JM (2008) Xenoreceptors CAR and PXR activation and consequences on lipid metabolism, glucose homeostasis, and inflammatory response. *Mol Pharm* **5:**35-41.

Motohashi H and Yamamoto M (2004) Nrf2-Keap1 defines a physiologically important stress response mechanism. *Trends Mol Med* **10:**549-557.

Muller DN, Schmidt C, Barbosa-Sicard E, Wellner M, Gross V, Hercule H, Markovic M, Honeck H, Luft FC, and Schunck WH (2007) Mouse Cyp4a isoforms: enzymatic properties, gender- and strain-specific expression, and role in renal 20-hydroxyeicosatetraenoic acid formation. *Biochem J* **403:**109-118.

National Toxicology P (1986) NTP Toxicology and Carcinogenesis Studies of Decabromodiphenyl Oxide (CAS No. 1163-19-5) In F344/N Rats and B6C3F1 Mice (Feed Studies). *Natl Toxicol Program Tech Rep Ser* **309:**1-242.

Nayak RR and Turnbaugh PJ (2016) Mirror, mirror on the wall: which microbiomes will help heal them all? *BMC Med* **14:**72.

O'Brien TW, Liu J, Sylvester JE, Mougey EB, Fischel-Ghodsian N, Thiede B, Wittmann-Liebold B, and Graack HR (2000) Mammalian mitochondrial ribosomal proteins (4). Amino acid sequencing, characterization, and identification of corresponding gene sequences. *J Biol Chem* **275:**18153-18159.

Okumura R, Kurakawa T, Nakano T, Kayama H, Kinoshita M, Motooka D, Gotoh K, Kimura T, Kamiyama N, Kusu T, Ueda Y, Wu H, Iijima H, Barman S, Osawa H, Matsuno H, Nishimura J, Ohba Y, Nakamura S, Iida T, Yamamoto M, Umemoto

E, Sano K, and Takeda K (2016) Lypd8 promotes the segregation of flagellated microbiota and colonic epithelia. *Nature* **532:**117-121.
Orn U and Klasson-Wehler E (1998) Metabolism of 2,2',4,4'-tetrabromodiphenyl ether in rat and mouse. *Xenobiotica* **28:**199-211.
Pacyniak E, Hagenbuch B, Klaassen CD, Lehman-McKeeman L, and Guo GL (2011) Organic anion transporting polypeptides in the hepatic uptake of PBDE congeners in mice. *Toxicol Appl Pharmacol* **257:**23-31.
Pacyniak E, Roth M, Hagenbuch B, and Guo GL (2010) Mechanism of polybrominated diphenyl ether uptake into the liver: PBDE congeners are substrates of human hepatic OATP transporters. *Toxicol Sci* **115:**344-353.
Pacyniak EK, Cheng X, Cunningham ML, Crofton K, Klaassen CD, and Guo GL (2007) The flame retardants, polybrominated diphenyl ethers, are pregnane X receptor activators. *Toxicol Sci* **97:**94-102.
Padda MS, Sanchez M, Akhtar AJ, and Boyer JL (2011) Drug-induced cholestasis. *Hepatology* **53:**1377-1387.
Parasramka MA, Maji S, Matsuda A, Yan IK, and Patel T (2016) Long non-coding RNAs as novel targets for therapy in hepatocellular carcinoma. *Pharmacol Ther* **161:**67-78.
Park HR and Loch-Caruso R (2014) Protective effect of nuclear factor E2-related factor 2 on inflammatory cytokine response to brominated diphenyl ether-47 in the HTR-8/SVneo human first trimester extravillous trophoblast cell line. *Toxicol Appl Pharmacol* **281:**67-77.
Park JE, Son AI, and Zhou R (2013) Roles of EphA2 in Development and Disease. *Genes (Basel)* **4:**334-357.
Park S, Cheng SL, and Cui JY (2016) Characterizing drug-metabolizing enzymes and transporters that are bona fide CAR-target genes in mouse intestine. *Acta Pharm Sin B* **6:**475-491.
Pashkov V, Huang J, Parameswara VK, Kedzierski W, Kurrasch DM, Tall GG, Esser V, Gerard RD, Uyeda K, Towle HC, and Wilkie TM (2011) Regulator of G protein signaling (RGS16) inhibits hepatic fatty acid oxidation in a carbohydrate response element-binding protein (ChREBP)-dependent manner. *J Biol Chem* **286:**15116-15125.
Peng L, Paulson A, Li H, Piekos S, He X, Li L, and Zhong XB (2014) Developmental programming of long non-coding RNAs during postnatal liver maturation in mice. *PLoS One* **9:**e114917.
Peng M, Yin N, and Li MO (2017) SZT2 dictates GATOR control of mTORC1 signalling. *Nature* **543:**433-437.
Perez MJ and Briz O (2009) Bile-acid-induced cell injury and protection. *World J Gastroenterol* **15:**1677-1689.
Petreas M, She J, Brown FR, Winkler J, Windham G, Rogers E, Zhao G, Bhatia R, and Charles MJ (2003) High body burdens of 2,2',4,4'-tetrabromodiphenyl ether (BDE-47) in California women. *Environ Health Perspect* **111:**1175-1179.
Peyer AK, Jung D, Beer M, Gnerre C, Keogh A, Stroka D, Zavolan M, and Meyer UA (2007) Regulation of human liver delta-aminolevulinic acid synthase by bile acids. *Hepatology* **46:**1960-1970.

Pierre JF, Martinez KB, Ye H, Nadimpalli A, Morton TC, Yang J, Wang Q, Patno N, Chang EB, and Yin DP (2016) Activation of bile acid signaling improves metabolic phenotypes in high-fat diet-induced obese mice. *Am J Physiol Gastrointest Liver Physiol* **311:**G286-304.

Png CW, Linden SK, Gilshenan KS, Zoetendal EG, McSweeney CS, Sly LI, McGuckin MA, and Florin TH (2010) Mucolytic bacteria with increased prevalence in IBD mucosa augment in vitro utilization of mucin by other bacteria. *Am J Gastroenterol* **105:**2420-2428.

Podvinec M, Handschin C, Looser R, and Meyer UA (2004) Identification of the xenosensors regulating human 5-aminolevulinate synthase. *Proc Natl Acad Sci U S A* **101:**9127-9132.

Porez G, Gross B, Prawitt J, Gheeraert C, Berrabah W, Alexandre J, Staels B, and Lefebvre P (2013) The hepatic orosomucoid/alpha1-acid glycoprotein gene cluster is regulated by the nuclear bile acid receptor FXR. *Endocrinology* **154:**3690-3701.

Prasad B and Unadkat JD (2014) Optimized approaches for quantification of drug transporters in tissues and cells by MRM proteomics. *AAPS J* **16:**634-648.

Qin X, Xie X, Fan Y, Tian J, Guan Y, Wang X, Zhu Y, and Wang N (2008) Peroxisome proliferator-activated receptor-delta induces insulin-induced gene-1 and suppresses hepatic lipogenesis in obese diabetic mice. *Hepatology* **48:**432-441.

Qiu M, Chen X, Deng D, Guo J, Sun G, Mai B, and Xu M (2012) Effects of electron donors on anaerobic microbial debromination of polybrominated diphenyl ethers (PBDEs). *Biodegradation* **23:**351-361.

Qiu X, Bigsby RM, and Hites RA (2009) Hydroxylated metabolites of polybrominated diphenyl ethers in human blood samples from the United States. *Environ Health Perspect* **117:**93-98.

Rabot S, Membrez M, Bruneau A, Gerard P, Harach T, Moser M, Raymond F, Mansourian R, and Chou CJ (2010) Germ-free C57BL/6J mice are resistant to high-fat-diet-induced insulin resistance and have altered cholesterol metabolism. *FASEB J* **24:**4948-4959.

Radominska A, Little JM, Lehman PA, Samokyszyn V, Rios GR, King CD, Green MD, and Tephly TR (1997) Glucuronidation of retinoids by rat recombinant UDP: glucuronosyltransferase 1.1 (bilirubin UGT). *Drug Metab Dispos* **25:**889-892.

Rao XJ, Wu YM, Wang Y, and Shi SW (2017) WITHDRAWN: JIP3 deficiency protects mice from high fat diet-induced liver injury. *Biochem Biophys Res Commun*.

Ravussin Y, Koren O, Spor A, LeDuc C, Gutman R, Stombaugh J, Knight R, Ley RE, and Leibel RL (2012) Responses of gut microbiota to diet composition and weight loss in lean and obese mice. *Obesity (Silver Spring)* **20:**738-747.

Reichold A, Brenner SA, Forster-Fromme K, Bergheim I, Mollenhauer J, and Bischoff SC (2013) Dmbt1 does not affect a Western style diet-induced liver damage in mice. *J Clin Biochem Nutr* **53:**145-149.

Reistad T and Mariussen E (2005) A commercial mixture of the brominated flame retardant pentabrominated diphenyl ether (DE-71) induces respiratory burst in human neutrophil granulocytes in vitro. *Toxicol Sci* **87:**57-65.

Ridaura VK, Faith JJ, Rey FE, Cheng J, Duncan AE, Kau AL, Griffin NW, Lombard V, Henrissat B, Bain JR, Muehlbauer MJ, Ilkayeva O, Semenkovich CF, Funai K,

Hayashi DK, Lyle BJ, Martini MC, Ursell LK, Clemente JC, Van Treuren W, Walters WA, Knight R, Newgard CB, Heath AC, and Gordon JI (2013) Gut microbiota from twins discordant for obesity modulate metabolism in mice. *Science* **341:**1241214.

Ridlon JM, Kang DJ, and Hylemon PB (2006) Bile salt biotransformations by human intestinal bacteria. *J Lipid Res* **47:**241-259.

Rion N and Ruegg MA (2017) LncRNA-encoded peptides: More than translational noise? *Cell Res* **27:**604-605.

Robrock KR, Korytar P, and Alvarez-Cohen L (2008) Pathways for the anaerobic microbial debromination of polybrominated diphenyl ethers. *Environ Sci Technol* **42:**2845-2852.

Ross AC and Zolfaghari R (2011) Cytochrome P450s in the regulation of cellular retinoic acid metabolism. *Annu Rev Nutr* **31:**65-87.

Rui L (2014) Energy metabolism in the liver. *Compr Physiol* **4:**177-197.

Runge-Morris M, Kocarek TA, and Falany CN (2013) Regulation of the cytosolic sulfotransferases by nuclear receptors. *Drug Metab Rev* **45:**15-33.

Russell DW (2003) The enzymes, regulation, and genetics of bile acid synthesis. *Annu Rev Biochem* **72:**137-174.

Ruttkay-Nedecky B, Nejdl L, Gumulec J, Zitka O, Masarik M, Eckschlager T, Stiborova M, Adam V, and Kizek R (2013) The role of metallothionein in oxidative stress. *Int J Mol Sci* **14:**6044-6066.

Sajner J and Krizek V (1984) [Vaclav Payer from Loket. 1488-1537]. *Cas Lek Cesk* **123:**1481-1484.

Satelli A, Rao PS, Thirumala S, and Rao US (2011) Galectin-4 functions as a tumor suppressor of human colorectal cancer. *Int J Cancer* **129:**799-809.

Sayin SI, Wahlstrom A, Felin J, Jantti S, Marschall HU, Bamberg K, Angelin B, Hyotylainen T, Oresic M, and Backhed F (2013) Gut microbiota regulates bile acid metabolism by reducing the levels of tauro-beta-muricholic acid, a naturally occurring FXR antagonist. *Cell Metab* **17:**225-235.

Sberna AL, Assem M, Gautier T, Grober J, Guiu B, Jeannin A, Pais de Barros JP, Athias A, Lagrost L, and Masson D (2011) Constitutive androstane receptor activation stimulates faecal bile acid excretion and reverse cholesterol transport in mice. *J Hepatol* **55:**154-161.

Schecter A, Papke O, Tung KC, Staskal D, and Birnbaum L (2004) Polybrominated diphenyl ethers contamination of United States food. *Environ Sci Technol* **38:**5306-5311.

Schecter A, Pavuk M, Papke O, Ryan JJ, Birnbaum L, and Rosen R (2003) Polybrominated diphenyl ethers (PBDEs) in U.S. mothers' milk. *Environ Health Perspect* **111:**1723-1729.

Sekiya S and Suzuki A (2011) Direct conversion of mouse fibroblasts to hepatocyte-like cells by defined factors. *Nature* **475:**390-393.

Selwyn FP, Cheng SL, Bammler TK, Prasad B, Vrana M, Klaassen C, and Cui JY (2015a) Developmental Regulation of Drug-Processing Genes in Livers of Germ-Free Mice. *Toxicol Sci* **147:**84-103.

Selwyn FP, Cheng SL, Klaassen CD, and Cui JY (2015b) Regulation of Hepatic Drug-metabolizing Enzymes in Germ-free mice by Conventionalization and Probiotics. *Drug Metab Dispos*.

Selwyn FP, Csanaky IL, Zhang Y, and Klaassen CD (2015c) Importance of Large Intestine in Regulating Bile Acids and Glucagon-Like Peptide-1 in Germ-Free Mice. *Drug Metab Dispos* **43:**1544-1556.

Selwyn FP, Cui JY, and Klaassen CD (2015d) RNA-Seq Quantification of Hepatic Drug Processing Genes in Germ-Free Mice. *Drug Metab Dispos* **43:**1572-1580.

Shane B (1989) Folylpolyglutamate synthesis and role in the regulation of one-carbon metabolism. *Vitam Horm* **45:**263-335.

Shao J, White CC, Dabrowski MJ, Kavanagh TJ, Eckert ML, and Gallagher EP (2008) The role of mitochondrial and oxidative injury in BDE 47 toxicity to human fetal liver hematopoietic stem cells. *Toxicol Sci* **101:**81-90.

Shen G and Kong AN (2009) Nrf2 plays an important role in coordinated regulation of Phase II drug metabolism enzymes and Phase III drug transporters. *Biopharm Drug Dispos* **30:**345-355.

Shreiner AB, Kao JY, and Young VB (2015) The gut microbiome in health and in disease. *Curr Opin Gastroenterol* **31:**69-75.

Sjodin A, Patterson DG, Jr., and Bergman A (2001) Brominated flame retardants in serum from U.S. blood donors. *Environ Sci Technol* **35:**3830-3833.

Sjodin A, Wong LY, Jones RS, Park A, Zhang Y, Hodge C, Dipietro E, McClure C, Turner W, Needham LL, and Patterson DG, Jr. (2008) Serum concentrations of polybrominated diphenyl ethers (PBDEs) and polybrominated biphenyl (PBB) in the United States population: 2003-2004. *Environ Sci Technol* **42:**1377-1384.

Srinivasan G, Aitken JD, Zhang B, Carvalho FA, Chassaing B, Shashidharamurthy R, Borregaard N, Jones DP, Gewirtz AT, and Vijay-Kumar M (2012) Lipocalin 2 deficiency dysregulates iron homeostasis and exacerbates endotoxin-induced sepsis. *J Immunol* **189:**1911-1919.

Stapleton HM, Kelly SM, Pei R, Letcher RJ, and Gunsch C (2009) Metabolism of polybrominated diphenyl ethers (PBDEs) by human hepatocytes in vitro. *Environ Health Perspect* **117:**197-202.

Stark AL, Delaney SM, Wheeler HE, Im HK, and Dolan ME (2012) Functional consequences of PRPF39 on distant genes and cisplatin sensitivity. *Hum Mol Genet* **21:**4348-4355.

Staskal DF, Hakk H, Bauer D, Diliberto JJ, and Birnbaum LS (2006) Toxicokinetics of polybrominated diphenyl ether congeners 47, 99, 100, and 153 in mice. *Toxicol Sci* **94:**28-37.

Staudinger JL, Goodwin B, Jones SA, Hawkins-Brown D, MacKenzie KI, LaTour A, Liu Y, Klaassen CD, Brown KK, Reinhard J, Willson TM, Koller BH, and Kliewer SA (2001) The nuclear receptor PXR is a lithocholic acid sensor that protects against liver toxicity. *Proc Natl Acad Sci U S A* **98:**3369-3374.

Steinberg SJ, Mihalik SJ, Kim DG, Cuebas DA, and Watkins PA (2000) The human liver-specific homolog of very long-chain acyl-CoA synthetase is cholate:CoA ligase. *J Biol Chem* **275:**15605-15608.

Stoffel W, Jenke B, Block B, Zumbansen M, and Koebke J (2005) Neutral sphingomyelinase 2 (smpd3) in the control of postnatal growth and development. *Proc Natl Acad Sci U S A* **102:**4554-4559.

Sueyoshi T, Li L, Wang H, Moore R, Kodavanti PR, Lehmler HJ, Negishi M, and Birnbaum LS (2014) Flame retardant BDE-47 effectively activates nuclear receptor CAR in human primary hepatocytes. *Toxicol Sci* **137:**292-302.

Swanson HI (2015) Drug Metabolism by the Host and Gut Microbiota: A Partnership or Rivalry? *Drug Metab Dispos* **43:**1499-1504.

Sylvester JE, Fischel-Ghodsian N, Mougey EB, and O'Brien TW (2004) Mitochondrial ribosomal proteins: candidate genes for mitochondrial disease. *Genet Med* **6:**73-80.

Szabo A, Xiao X, Haughney M, Spector A, Sahin-Toth M, and Lowe ME (2015) A novel mutation in PNLIP causes pancreatic triglyceride lipase deficiency through protein misfolding. *Biochim Biophys Acta* **1852:**1372-1379.

Tang J and Zhai JX (2017) Distribution of polybrominated diphenyl ethers in breast milk, cord blood and placentas: a systematic review. *Environ Sci Pollut Res Int* **24:**21548-21573.

Tanikawa C, Zhang YZ, Yamamoto R, Tsuda Y, Tanaka M, Funauchi Y, Mori J, Imoto S, Yamaguchi R, Nakamura Y, Miyano S, Nakagawa H, and Matsuda K (2017) The Transcriptional Landscape of p53 Signalling Pathway. *EBioMedicine* **20:**109-119.

Tesi B, Davidsson J, Voss M, Rahikkala E, Holmes TD, Chiang SCC, Komulainen-Ebrahim J, Gorcenco S, Rundberg Nilsson A, Ripperger T, Kokkonen H, Bryder D, Fioretos T, Henter JI, Mottonen M, Niinimaki R, Nilsson L, Pronk CJ, Puschmann A, Qian H, Uusimaa J, Moilanen J, Tedgard U, Cammenga J, and Bryceson YT (2017) Gain-of-function SAMD9L mutations cause a syndrome of cytopenia, immunodeficiency, MDS, and neurological symptoms. *Blood* **129:**2266-2279.

Thomas C, Pellicciari R, Pruzanski M, Auwerx J, and Schoonjans K (2008) Targeting bile-acid signalling for metabolic diseases. *Nat Rev Drug Discov* **7:**678-693.

Toda T, Saito N, Ikarashi N, Ito K, Yamamoto M, Ishige A, Watanabe K, and Sugiyama K (2009) Intestinal flora induces the expression of Cyp3a in the mouse liver. *Xenobiotica* **39:**323-334.

Tokarz JA, 3rd, Ahn MY, Leng J, Filley TR, and Nies L (2008) Reductive debromination of polybrominated diphenyl ethers in anaerobic sediment and a biomimetic system. *Environ Sci Technol* **42:**1157-1164.

Trapnell C, Williams BA, Pertea G, Mortazavi A, Kwan G, van Baren MJ, Salzberg SL, Wold BJ, and Pachter L (2010) Transcript assembly and quantification by RNA-Seq reveals unannotated transcripts and isoform switching during cell differentiation. *Nat Biotechnol* **28:**511-515.

Tsai WC, Hueng DY, Nieh S, and Gao HW (2017) ARID4B is a good biomarker to predict tumour behaviour and decide WHO grades in gliomas and meningiomas. *J Clin Pathol* **70:**162-167.

Turnbaugh PJ and Gordon JI (2009) The core gut microbiome, energy balance and obesity. *J Physiol* **587:**4153-4158.

Turnbaugh PJ, Ley RE, Mahowald MA, Magrini V, Mardis ER, and Gordon JI (2006) An obesity-associated gut microbiome with increased capacity for energy harvest. *Nature* **444:**1027-1031.

Turnbaugh PJ, Ridaura VK, Faith JJ, Rey FE, Knight R, and Gordon JI (2009) The effect of diet on the human gut microbiome: a metagenomic analysis in humanized gnotobiotic mice. *Sci Transl Med* **1:**6ra14.

van Ampting MT, Loonen LM, Schonewille AJ, Konings I, Vink C, Iovanna J, Chamaillard M, Dekker J, van der Meer R, Wells JM, and Bovee-Oudenhoven IM (2012) Intestinally secreted C-type lectin Reg3b attenuates salmonellosis but not listeriosis in mice. *Infect Immun* **80:**1115-1120.

van Passel MW, Kant R, Zoetendal EG, Plugge CM, Derrien M, Malfatti SA, Chain PS, Woyke T, Palva A, de Vos WM, and Smidt H (2011) The genome of Akkermansia muciniphila, a dedicated intestinal mucin degrader, and its use in exploring intestinal metagenomes. *PLoS One* **6:**e16876.

Vargova K, Curik N, Burda P, Basova P, Kulvait V, Pospisil V, Savvulidi F, Kokavec J, Necas E, Berkova A, Obrtlikova P, Karban J, Mraz M, Pospisilova S, Mayer J, Trneny M, Zavadil J, and Stopka T (2011) MYB transcriptionally regulates the miR-155 host gene in chronic lymphocytic leukemia. *Blood* **117:**3816-3825.

Venkatesh M, Mukherjee S, Wang H, Li H, Sun K, Benechet AP, Qiu Z, Maher L, Redinbo MR, Phillips RS, Fleet JC, Kortagere S, Mukherjee P, Fasano A, Le Ven J, Nicholson JK, Dumas ME, Khanna KM, and Mani S (2014) Symbiotic bacterial metabolites regulate gastrointestinal barrier function via the xenobiotic sensor PXR and Toll-like receptor 4. *Immunity* **41:**296-310.

Verbeure B, Lescrinier E, Wang J, and Herdewijn P (2001) RNase H mediated cleavage of RNA by cyclohexene nucleic acid (CeNA). *Nucleic Acids Res* **29:**4941-4947.

Viberg H, Fredriksson A, and Eriksson P (2004) Neonatal exposure to the brominated flame-retardant, 2,2',4,4',5-pentabromodiphenyl ether, decreases cholinergic nicotinic receptors in hippocampus and affects spontaneous behaviour in the adult mouse. *Environ Toxicol Pharmacol* **17:**61-65.

von Meyerinck L, Hufnagel B, Schmoldt A, and Benthe HF (1990) Induction of rat liver microsomal cytochrome P-450 by the pentabromo diphenyl ether Bromkal 70 and half-lives of its components in the adipose tissue. *Toxicology* **61:**259-274.

Vrana M, Whittington D, Nautiyal V, and Prasad B (2017) Database of Optimized Proteomic Quantitative Methods for Human Drug Disposition-Related Proteins for Applications in Physiologically Based Pharmacokinetic Modeling. *CPT Pharmacometrics Syst Pharmacol* **6:**267-276.

Wang KC and Chang HY (2011) Molecular mechanisms of long noncoding RNAs. *Mol Cell* **43:**904-914.

Wang Q, Jiang L, Wang J, Li S, Yu Y, You J, Zeng R, Gao X, Rui L, Li W, and Liu Y (2009) Abrogation of hepatic ATP-citrate lyase protects against fatty liver and ameliorates hyperglycemia in leptin receptor-deficient mice. *Hepatology* **49:**1166-1175.

Wang Y, Ma C, Sun Y, Li Y, Kang L, and Jiang Y (2017) Dynamic transcriptome and DNA methylome analyses on longissimus dorsi to identify genes underlying intramuscular fat content in pigs. *BMC Genomics* **18:**780.

Wang Y, Xu Z, Jiang J, Xu C, Kang J, Xiao L, Wu M, Xiong J, Guo X, and Liu H (2013a) Endogenous miRNA sponge lincRNA-RoR regulates Oct4, Nanog, and Sox2 in human embryonic stem cell self-renewal. *Dev Cell* **25:**69-80.

Wang YL, Liang HY, Gao YH, Wu XJ, Chen X, Pan BY, Yang XX, and Liu HZ (2013b) A functional variant of NEDD4L is associated with obesity and related phenotypes in a Han population of Southern China. *Int J Mol Sci* **14:**7433-7444.

Wapinski O and Chang HY (2011) Long noncoding RNAs and human disease. *Trends Cell Biol* **21:**354-361.

Watanabe TK, Suzuki M, Omori Y, Hishigaki H, Horie M, Kanemoto N, Fujiwara T, Nakamura Y, and Takahashi E (1997) Cloning and characterization of a novel member of the human Mad gene family (MADH6). *Genomics* **42:**446-451.

Wederell ED, Bilenky M, Cullum R, Thiessen N, Dagpinar M, Delaney A, Varhol R, Zhao Y, Zeng T, Bernier B, Ingham M, Hirst M, Robertson G, Marra MA, Jones S, and Hoodless PA (2008) Global analysis of in vivo Foxa2-binding sites in mouse adult liver using massively parallel sequencing. *Nucleic Acids Res* **36:**4549-4564.

Wehrbein H and Diedrich P (1992) [Progressive pneumatization of the basal maxillary sinus after extraction and space closure]. *Fortschr Kieferorthop* **53:**77-83.

Wikoff WR, Anfora AT, Liu J, Schultz PG, Lesley SA, Peters EC, and Siuzdak G (2009) Metabolomics analysis reveals large effects of gut microflora on mammalian blood metabolites. *Proc Natl Acad Sci U S A* **106:**3698-3703.

Wilson ID and Nicholson JK (2017) Gut microbiome interactions with drug metabolism, efficacy, and toxicity. *Transl Res* **179:**204-222.

Wolfrum C, Asilmaz E, Luca E, Friedman JM, and Stoffel M (2004) Foxa2 regulates lipid metabolism and ketogenesis in the liver during fasting and in diabetes. *Nature* **432:**1027-1032.

Wright MW and Bruford EA (2011) Naming 'junk': human non-protein coding RNA (ncRNA) gene nomenclature. *Hum Genomics* **5:**90-98.

Xu G, Wang J, and Lu M (2014) Complete debromination of decabromodiphenyl ether using the integration of Dehalococcoides sp. strain CBDB1 and zero-valent iron. *Chemosphere* **117:**455-461.

Xu M, Chen X, Qiu M, Zeng X, Xu J, Deng D, Sun G, Li X, and Guo J (2012) Bar-coded pyrosequencing reveals the responses of PBDE-degrading microbial communities to electron donor amendments. *PLoS One* **7:**e30439.

Xu MJ, Feng D, Wu H, Wang H, Chan Y, Kolls J, Borregaard N, Porse B, Berger T, Mak TW, Cowland JB, Kong X, and Gao B (2015a) Liver is the major source of elevated serum lipocalin-2 levels after bacterial infection or partial hepatectomy: a critical role for IL-6/STAT3. *Hepatology* **61:**692-702.

Xu Y, Cao J, Huang S, Feng D, Zhang W, Zhu X, and Yan X (2015b) Characterization of tetratricopeptide repeat-containing proteins critical for cilia formation and function. *PLoS One* **10:**e0124378.

Yamaguchi S, Mitsui S, Yan L, Yagita K, Miyake S, and Okamura H (2000) Role of DBP in the circadian oscillatory mechanism. *Mol Cell Biol* **20:**4773-4781.

Yan J, Chen B, Lu J, and Xie W (2015) Deciphering the roles of the constitutive androstane receptor in energy metabolism. *Acta Pharmacol Sin* **36:**62-70.

Yang CW, Huang HW, and Chang BV (2017a) Microbial communities associated with anaerobic degradation of polybrominated diphenyl ethers in river sediment. *J Microbiol Immunol Infect* **50:**32-39.

Yang CW, Lee CC, Ku H, and Chang BV (2017b) Bacterial communities associated with anaerobic debromination of decabromodiphenyl ether from mangrove sediment. *Environ Sci Pollut Res Int* **24:**5391-5403.

Yang H, Huang X, Fang S, Xin W, Huang L, and Chen C (2016a) Uncovering the composition of microbial community structure and metagenomics among three gut locations in pigs with distinct fatness. *Sci Rep* **6:**27427.

Yang J, Zhu J, and Chan KM (2016b) BDE-99, but not BDE-47, is a transient aryl hydrocarbon receptor agonist in zebrafish liver cells. *Toxicol Appl Pharmacol* **305:**203-215.

Yoon JH, Abdelmohsen K, and Gorospe M (2014) Functional interactions among microRNAs and long noncoding RNAs. *Semin Cell Dev Biol* **34:**9-14.

Zadjali F, Santana-Farre R, Vesterlund M, Carow B, Mirecki-Garrido M, Hernandez-Hernandez I, Flodstrom-Tullberg M, Parini P, Rottenberg M, Norstedt G, Fernandez-Perez L, and Flores-Morales A (2012) SOCS2 deletion protects against hepatic steatosis but worsens insulin resistance in high-fat-diet-fed mice. *FASEB J* **26:**3282-3291.

Zechner R, Zimmermann R, Eichmann TO, Kohlwein SD, Haemmerle G, Lass A, and Madeo F (2012) FAT SIGNALS--lipases and lipolysis in lipid metabolism and signaling. *Cell Metab* **15:**279-291.

Zhang J, Wong H, Ramanan S, Cheong D, Leong A, and Hooi SC (2003) The proline-rich acidic protein is epigenetically regulated and inhibits growth of cancer cell lines. *Cancer Res* **63:**6658-6665.

Zhang L, Yang Z, Ma A, Qu Y, Xia S, Xu D, Ge C, Qiu B, Xia Q, Li J, and Liu Y (2014) Growth arrest and DNA damage 45G down-regulation contributes to Janus kinase/signal transducer and activator of transcription 3 activation and cellular senescence evasion in hepatocellular carcinoma. *Hepatology* **59:**178-189.

Zhang N, Ahsan MH, Purchio AF, and West DB (2005) Serum amyloid A-luciferase transgenic mice: response to sepsis, acute arthritis, and contact hypersensitivity and the effects of proteasome inhibition. *J Immunol* **174:**8125-8134.

Zhang S, Franco G, Li XB, Lu XX, Hou Z, and Yang JJ (2013) [Aerobic microbial degradation of 2,2',4,4'-tetrabrominated diphenyl ether]. *Huan Jing Ke Xue* **34:**1945-1950.

Zhang X, Li S, Zhou Y, Su W, Ruan X, Wang B, Zheng F, Warner M, Gustafsson JA, and Guan Y (2017a) Ablation of cytochrome P450 omega-hydroxylase 4A14 gene attenuates hepatic steatosis and fibrosis. *Proc Natl Acad Sci U S A* **114:**3181-3185.

Zhang Y and Klaassen CD (2010) Effects of feeding bile acids and a bile acid sequestrant on hepatic bile acid composition in mice. *J Lipid Res* **51:**3230-3242.

Zhang Y, Xu C, Gu D, Wu M, Yan B, Xu Z, Wang Y, and Liu H (2017b) H/ACA Box Small Nucleolar RNA 7A Promotes the Self-Renewal of Human Umbilical Cord Mesenchymal Stem Cells. *Stem Cells* **35:**222-235.

Zhao S, Liu W, Wang J, Shi J, Sun Y, Wang W, Ning G, Liu R, and Hong J (2017) Akkermansia muciniphila improves metabolic profiles by reducing inflammation in chow diet-fed mice. *J Mol Endocrinol* **58:**1-14.

Zhou T, Taylor MM, DeVito MJ, and Crofton KM (2002) Developmental exposure to brominated diphenyl ethers results in thyroid hormone disruption. *Toxicol Sci* **66:**105-116.

Zhou Y, Jiang L, and Rui L (2009) Identification of MUP1 as a regulator for glucose and lipid metabolism in mice. *J Biol Chem* **284:**11152-11159.

Zhou Z, Liu H, Wang C, Lu Q, Huang Q, Zheng C, and Lei Y (2015) Long non-coding RNAs as novel expression signatures modulate DNA damage and repair in cadmium toxicology. *Sci Rep* **5:**15293.

Zuehlke AD, Beebe K, Neckers L, and Prince T (2015) Regulation and function of the human HSP90AA1 gene. *Gene* **570:**8-16.